MULTIPLE-TIMESCALE ADAPTIVE CONTROL FOR UNCERTAIN NONLINEAR DYNAMICAL SYSTEMS

A Dissertation

by

KAMERON J. EVES

Submitted to the Graduate and Professional School of
Texas A&M University
in partial fulfillment of the requirements for the degree of

DOCTOR OF PHILOSOPHY

Chair of Committee,	John Valasek
Committee Members,	Mark Balas
	Aniruddha Datta
	John E. Hurtado
	Manoranjan Majji
Head of Department,	Ivett Leyva

May 2023

Major Subject: Aerospace Engineering

ABSTRACT

Adaptive control is a field of control theory dedicated to addressing uncertain and time-varying system models. Multiple-timescale control is dedicated to addressing systems with some states evolving quickly and others evolving slowly. Multiple-timescale control has been shown to have difficulty with uncertain systems and adaptive control has been shown to have difficulty with multiple-timescale systems. This dissertation describes a novel control methodology called [K]control of Adaptive Multiple-timescale Systems (KAMS). KAMS seeks to address systems that simultaneously exhibit uncertain and multiple-timescale behaviors. Unlike traditional multiple-timescale control literature, KAMS uses adaptive control to stabilize the subsystems. The reference models and adapting parameters used in adaptive control significantly complicate the stability analysis. KAMS is a flexible theory and framework. The stability proofs apply to a wide array of adaptive algorithms and multiple-timescale fusion techniques. The examples in this dissertation include the adaptive control methods Model Reference Adaptive Control and Adaptive Nonlinear Dynamic Inversion. The multiple-timescale fusion techniques of Composite Control, Sequential Control, and Simultaneous Slow and Fast Tracking are all used. The primary novel contributions of this dissertation are 1.) a formal development and analysis of KAMS theory and its design methodology; 2.) a set of theoretical tools for stability analyses of KAMS including proofs of sufficient conditions for asymptotic stability; 3.) demonstration of the benefits of KAMS, including formal and numerical validation of how KAMS can relax the minimum phase assumption for a multitude of common adaptive control methods. KAMS is demonstrated and evaluated on examples consisting of stabilization and attitude control of a quadrotor Unmanned Air System; fuel-efficient orbital transfer maneuvers; and preventing inlet unstart on hypersonic aircraft. Results presented in the dissertation demonstrate that KAMS has better performance overall, and improved robustness to uncertainty in the time scale separation parameter than traditional approaches like adaptive control alone, or multiple-timescale control alone.

DEDICATION

To Ali

My wonderful wife and best freind. She has earned at least two doctoral degrees in the time it has taken me to earn one. Her first one is in motherhood for her work raising our two kids, and her second one is in aerospace engineering for listening to my never ending crazy ideas.

The graduation ceremonies are for you, just as much as they are for me.

ACKNOWLEDGMENTS

I would like to thank my parents for their moral, emotional, and financial support throughout the years. I never would have made it here without you. I would like to thank Dr. John Valasek for his patience in mentoring me over the past four years. You've taught me more than I ever thought I could learn, and I hope I've been able to give back to the lab in some small way. Thank you for giving me a chance. I would like to thank my committee. In alphabetical order, they are Dr. Mark Balas, Dr. Aniruddha Datta, Dr. John E. Hurtado, and Dr. Manoranjan Majji. I admire each of you individually for your professional and personal accomplishments. I have learned something different from each of you, and I'm glad to have people I respect so much as my committee members. I'm honored to have you on my committee. Finally, I'd like to thank my coworkers in the Vehicle Systems and Control Laboratory. Your friendship and support have helped me survive the past four years. Thanks for catching my mistakes when I needed it and having my back regardless. We will forever be bonded by the dust and heat we endured at a classified location. I wish I could thank each of you individually, but I would like to especially thank Dr. Garrett Jares who has been with me the whole way. Again I couldn't have made it without you. I can't tell you how much it meant to have a friend to commiserate and celebrate with. I wish you the best in your career, and I hope we cross paths again. There are many others whom I should thank, but suffice it to be said that I am grateful for the many people who have knowingly and unknowingly sacrificed so much to help me get here. I may have written this dissertation independently, but it is only the tip of a large iceberg of technical and personal effort. Thank you.

CONTRIBUTORS AND FUNDING SOURCES

Contributors

This work was supported by a dissertation committee consisting of:

- Dr. John Valasek (advisor) - Professor, Aerospace Engineering
- Dr. Mark Balas - Professor, Mechanical Engineering
- Dr. Aniruddha Datta - Professor, Electrical & Computer Engineering
- Dr. John E. Hurtado - Professor of Aerospace Engineering
- Dr. Manoranjan Majji - Associate Professor, Aerospace Engineering

All other work conducted for the dissertation was completed by the student independently.

Funding Sources

Graduate study was gratefully supported by research and teaching assistantships with the Department of Aerospace Engineering at Texas A&M University.

TABLE OF CONTENTS

Page

ABSTRACT ii

DEDICATION iii

ACKNOWLEDGMENTS iv

CONTRIBUTORS AND FUNDING SOURCES v

TABLE OF CONTENTS vi

LIST OF FIGURES ix

LIST OF TABLES xiii

1. INTRODUCTION 1

1.1 Multiple-Timescale Control 2
1.2 Adaptive Control 7
1.3 [K]control of Adaptive Multiple-Timescale Systems Architecture 9
1.3.1 Methodology 9
1.3.2 Benefits 10
1.3.3 Research Questions 11
1.3.4 Scope 13
1.3.5 Contributions of This Dissertation 14
1.4 Literature Review 15
1.4.1 Adaptive Control with Elements of Multiple-Timescale Control 15
1.4.1.1 Assumed Model Reduction 16
1.4.1.2 Tikhonov's Theorem 17
1.4.1.3 Singular Perturbation Control 18
1.4.2 Multiple-Timescale Control with Elements of Adaptive Control 20

2. TOOLS FOR STABILITY ANALYSES 23

2.1 Control Synthesis 24
2.1.1 System Description 24
2.1.2 Singular Perturbation Analysis 25
2.1.3 Adaptive Control 25
2.1.4 Multiple-Timescale Fusion 27
2.1.4.1 Composite Control 28

2.1.4.2 Sequential Control 28
2.1.4.3 Simultaneous Slow and Fast Tracking 28
2.2 Stability Analysis 28
2.2.1 Augmented Error Dynamics 29
2.2.2 Differential Geometry 34
2.2.3 The Manifold and The Reference Model 34
2.2.4 Full-Order System Stability 37
2.2.4.1 Foundation Of Reduced-Order Stability 38
2.2.4.2 Case 1 39
2.2.4.3 Case 2 43
2.2.4.4 Case 3 44
2.3 Validation 46
2.3.1 Control Synthesis 47
2.3.2 Confirmation of Full-Order Stability 48
2.3.3 Numerical Results 49
2.3.4 Alternate Approach 51
2.4 Chapter Summary 54

3. RELAXING THE NON-MINIMUM PHASE ASSUMPTION 56

3.1 Problem Formulation 56
3.2 Diffeomorphism 57
3.3 Numerical Demonstration 61
3.4 Chapter Summary 64

4. COMPARISONS WITH OTHER APPROACHES 67

4.1 Full-Order Adaptive Control 67
4.2 Reduced-Order Adaptive Control 71
4.3 [K]control of Adaptive Multiple-Timescale Systems 74
4.4 Numerical Comparision 75
4.4.1 Control Synthesis 77
4.4.1.1 Full-Order Adaptive Control 77
4.4.1.2 Reduced-Order Adaptive Control 78
4.4.1.3 KAMS 80
4.4.1.4 Summary of Control Laws 83
4.4.2 Numerical Results 83
4.4.3 Robustness Test 89
4.5 Chapter Summary 91

5. QUADROTOR ATTITUDE STABILIZATION USING ADAPTIVE REGULATION OF A LINEAR MULTIPLE-TIMESCALE MODEL 93

5.1 Multiple-Timescale Model 93
5.2 Control Synthesis 97
5.2.1 Control and Adaptation Laws 98

5.2.2 Stability Analysis 99
5.3 Numerical Results 105
5.4 Chapter Summary 114

6. ORBITAL TRANSFER MANEUVERS USING ADAPTIVE CONTROL OF A MULTIPLE-TIMESCALE MODEL 116

6.1 Multiple-Timescale Model 117
6.2 Control Synthesis 119
6.2.1 Control and Adaptation Laws 120
6.2.2 Guidance 121
6.2.3 Stability Analysis 122
6.3 Numerical Results 128
6.3.1 Geostationary Transfer 131
6.3.2 Geostationary Orbit Insertion 135
6.3.3 Efficiency Analysis 139
6.4 Chapter Summary 139

7. INLET UNSTART PREVENTION BY ADAPTIVE REGULATION USING A NON-LINEAR LONGITUDINAL TIMESCALE MODEL 141

7.1 Multiple-Timescale Model 142
7.2 Control Synthesis 146
7.2.1 Zero Dynamics 146
7.2.2 Control Synthesis 148
7.2.3 Full-Order Stability Analysis 149
7.2.3.1 Differentiation of the Manifold 150
7.2.3.2 Application of Theorem 2.1 153
7.3 Numerical Results 155
7.4 Chapter Summary 162

8. CONCLUSIONS 163

9. RECOMMENDATIONS 165

REFERENCES 167

APPENDIX A. PROOF OF LEMMAS 184

A.1 Lemma 1 184
A.2 Lemma 2 184

LIST OF FIGURES

FIGURE Page

1.1 A block diagram of multiple-timescale control. 6

1.2 A block diagram of KAMS. 11

1.3 A block diagram of KAMS with adaptive control only used for the slow subsystem. 12

1.4 A block diagram of KAMS with adaptive control only used for the fast subsystem... 13

2.1 The primary feedback loop of KAMS..... 35

2.2 The unconventional feedback loop of KAMS. 36

2.3 Evolution of the slow state..... 50

2.4 Evolution of the fast state. 50

2.5 Evolution of the adapting gain..... 51

2.6 Effects of varying ϵ and d on the applicablility of Corollary 2.1..... 53

2.7 Evolution of the slow state for the alternate approach..... 53

2.8 Evolution of the fast state for the alternate approach. 54

2.9 Evolution of the adapting gain for the alternate approach..... 54

3.1 Evolution of the external dynamics for a non-minimum phase system..... 64

3.2 Evolution of the internal dynamics for a non-minimum phase system. 65

3.3 Evolution of the adapting parameters for a non-minimum phase system..... 65

4.1 A block diagram of FOAC. 68

4.2 Evolution of a simple linear system under FOAC for several different timescale separation parameters. 70

4.3 A block diagram of ROAC..... 72

4.4 Slow state evolution comparison of FOAC, ROAC, and KAMS..... 86

4.5 Fast state evolution comparison of FOAC, ROAC, and KAMS. 86
4.6 First adapting gain evolution comparison of FOAC, ROAC, and KAMS. 87
4.7 Second adapting gain evolution comparison of FOAC, ROAC, and KAMS. 87
4.8 Third adapting gain evolution comparison of FOAC, ROAC, and KAMS. 87
4.9 Fourth adapting gain evolution comparison of FOAC, ROAC, and KAMS. 87
4.10 Slow state evolution of Composite Control on a parametrically uncertain plant. 88
4.11 Fast state evolution of Composite Control on a parametrically uncertain plant. 88
4.12 Slow state evolution comparison with large timescale uncertainty. 89
4.13 Fast state evolution comparison of FOAC, ROAC, and KAMS. 90
4.14 First adapting gain evolution comparison of FOAC, ROAC, and KAMS. 90
4.15 Second adapting gain evolution comparison of FOAC, ROAC, and KAMS. 90
4.16 Third adapting gain evolution comparison of FOAC, ROAC, and KAMS. 90
4.17 Fourth adapting gain evolution comparison of FOAC, ROAC, and KAMS. 91
5.1 LPM over a range of possible d. 108
5.2 Evolution of the altitude. 109
5.3 Evolution of the roll attitude angle. 110
5.4 Evolution of the pitch attitude angle. 110
5.5 Evolution of the yaw attitude angle. 111
5.6 Evolution of body axis down velocity. 111
5.7 Evolution of body axis roll rate. 112
5.8 Evolution of body axis pitch rate. 112
5.9 Evolution of body axis yaw rate. 113
5.10 Evolution of the components of the adapting parameters' error. 113
5.11 Evolution of the motor angular velocities. 114
6.1 Numerical simulation of the system trajectory. 129

6.2 Evolution of the angular velocity during the Hohmann transfer. 132

6.3 Evolution of the radius during the Hohmann transfer. 132

6.4 Evolution of the tangential thrust during the TGI burn. 133

6.5 Evolution of the radial thrust during the TGI burn. 133

6.6 Evolution of the radial control effectiveness parameter during the Hohmann transfer. 133

6.7 Evolution of the tangential control effectiveness parameter during the Hohmann transfer. 134

6.8 Evolution of the true anomaly during the Hohmann transfer. 134

6.9 Evolution of the angular velocity after reaching geostationary orbit. 136

6.10 Evolution of the radius after reaching geostationary orbit. 136

6.11 Evolution of the tangential thrust during the GOI burn. 137

6.12 Evolution of the radial thrust during the GOI burn. 137

6.13 Evolution of the radial control effectiveness parameter after reaching geostationary orbit. 137

6.14 Evolution of the tangential control effectiveness parameter after reaching geostationary orbit. 138

6.15 Evolution of the true anomaly after reaching geostationary orbit. 138

7.1 Phase diagram of the slow subsystem zero dynamics. 147

7.2 Evolution of the angle-of-attack. 158

7.3 Evolution of the body axis pitch rate for a hypersonic aircraft. 159

7.4 Evolution of the lift curve slope stability derivative estimate. 159

7.5 Evolution of the lift static longitudinal stability derivative estimate. 159

7.6 Evolution of the second order angle-of-attack stability derivative estimate. 159

7.7 Evolution of the elevator effectiveness control derivative estimate. 160

7.8 Evolution of the elevator control inputs. 160

7.9 Evolution of the pitch attitude angle for a hypersonic aircraft. 161

7.10 Evolution of the vehicle's Mach number. 162

LIST OF TABLES

TABLE Page

2.1 Proof that the conditions of Barbalat's Lemma are met. 42

4.1 Comparison of ROAC, FOAC, and KAMS control methodologies. 84

5.1 Reference model steady state error. 105

5.2 Quadrotor vehicle parameters. 106

5.3 Quadrotor vehicle control gains. 107

7.1 Hypersonic vehicle parameters adapted from [142]. 156

7.2 Hypersonic vehicle control gains. 157

7.3 Hypersonic vehicle initial conditions. 158

1. INTRODUCTION

Two control techniques, adaptive control and multiple-timescale control, are active areas of research and address the complexities of physical systems. Multiple-timescale control is intended for systems that have both fast and slow modes. The controller must be able to simultaneously stabilize the fast and slow modes of the system. Adaptive control was developed for systems with uncertain and time-varying parameters. For such systems, the control objective must be achieved despite imperfections in the model. However, relatively little research has addressed multiple-timescale systems and uncertain models simultaneously. This dissertation introduces a novel control methodology that addresses uncertain multiple-timescale systems. This methodology is called [K]control of Adaptive multiple-timescale Systems (KAMS). KAMS builds upon the first principles of adaptive control and multiple-timescale control. KAMS expands the set of systems to which adaptive control and multiple-timescale control can apply. Prior work has used elements of each of these methods, but it has stopped short of fully and rigorously combining them. KAMS is more extensible, simpler, and leads to greater insight into the physics of the system.

This dissertation is organized as follows. The remainder of this chapter introduces multiple-timescale control and adaptive control individually, defines the KAMS methodology, and contextualizes this dissertation within the prior literature. Chapter 2 develops several theoretical tools (i.e. theorems) for stability analysis when KAMS is used including sufficient conditions for asymptotic stability. Chapter 3 briefly describes how KAMS can be used to relax the non-minimum phase assumption. Chapter 4 Discusses two potential alternatives to KAMS and directly compares the three methods with a simple numerical example. Chapters 5, 6, and 7 give examples of KAMS on aerospace systems and explore the various fascists of the theorems from Chapter 2. Chapter 5 performs attitude stabilization and control on a linearized model of a quadrotor Uncrewed Air Vehicle (UAV). Chapter 6 performs an orbital transfer maneuver of a satellite by tracking a Hohmann transfer trajectory. Chapter 7 performs inlet unstart prevention by adaptive regulation of a hypersonic vehicle angle-of-attack. Finally, Chapter 8 describes the conclusions from this dissertation,

and Chapter 9 describes the recommendations from this dissertation.

1.1 Multiple-Timescale Control

Many systems have coupled fast and slow modes which occur simultaneously. Examples exist in nearly every engineering field. For example, multiple-timescale models have been published for robotic arms [1], electric circuits [2], chemical processes [3], factory logistics [4], and even pandemics [5]. Many aerospace systems are multiple-timescale systems. For example fixed wing aicraft [6], hypersoinc vehicles [7], satalites [8], rotorcraft [9], UAV [10], and trajectory optimization [11]. For more examples see [12]. A general two-timescale system can be represented as the following system of dynamic equations.

$$\acute{\boldsymbol{x}} = f_x(\boldsymbol{x}, \boldsymbol{z}, \boldsymbol{u}) \tag{1.1a}$$

$$\epsilon\acute{\boldsymbol{z}} = f_z(\boldsymbol{x}, \boldsymbol{z}, \boldsymbol{u}, \epsilon) \tag{1.1b}$$

In this system of equations $\boldsymbol{x}$ is the slow state, $\boldsymbol{z}$ is the fast state, $\boldsymbol{u}$ is the system input, and f_x and f_z can be any nonlinear function as long as they are the same order of magnitude. The variable ϵ is called the timescale separation parameter. It represents the ratio between the timescale of the slow states (t_s) and the fast states (t_f) such that $0 < \epsilon \triangleq {}^{t_s}\!/_{t_f} \ll 1$. This can be thought of as a unit conversion. For example, if $t_s = 1$ minute and $t_f = 60$ seconds then $\epsilon = {}^{1}\!/_{60}$. Applying this to Eq. (1.1) it is found that typically $\acute{\boldsymbol{z}} \gg \acute{\boldsymbol{x}}$. The accent above $\boldsymbol{x}$ and $\boldsymbol{z}$ is the time derivative with respect to the slow timescale $\acute{(\cdot)} \triangleq {}^{d(\cdot)}\!/_{dt_s}$.

Singular perturbation theory is a branch of mathematics dedicated to functions with limits that do not equal the value of the function [13]. The system in Eq. (1.1) is an example of such a system [14]. Setting $\epsilon = 0$ gives

$$\acute{\boldsymbol{x}} = f_x(\boldsymbol{x}, \boldsymbol{z}_s, \boldsymbol{u}) \tag{1.2a}$$

$$0 = f_z(\boldsymbol{x}, \boldsymbol{z}_s, \boldsymbol{u}, 0) \tag{1.2b}$$

This is known by multiple-timescale control theorists as the *reduced slow system* or the *outer system*. It is called this because it describes how the slow states evolve after the fast states have reached steady state. Using the definition of $\acute{\boldsymbol{x}}$ a new derivative of time $\grave{(\cdot)} \triangleq {}^{1}\!/\!_{\epsilon}\acute{(\cdot)}$ can be defined such that

$$\grave{\boldsymbol{x}} = \epsilon f_x(\boldsymbol{x}, \boldsymbol{z}, \boldsymbol{u}) \tag{1.3a}$$

$$\grave{\boldsymbol{z}} = f_z(\boldsymbol{x}, \boldsymbol{z}, \boldsymbol{u}, \epsilon) \tag{1.3b}$$

Once again setting $\epsilon = 0$ reveals a new reduced system

$$\grave{\boldsymbol{x}} = 0 \tag{1.4a}$$

$$\grave{\boldsymbol{z}} = f_z(\boldsymbol{x}, \boldsymbol{z}, \boldsymbol{u}, 0) \tag{1.4b}$$

This is known as the *reduced fast system* or the *boundary system* because it describes how the fast states evolve before the slow states begin to change. The true system is somewhere between the reduced fast system and the reduced slow system. Taking the limit as ϵ goes to zero necessarily discounts some aspects of the dynamics. Sometimes, Eq. (1.2b) can be solved for $\boldsymbol{z}$ so that the steady-state trajectory of the fast states is known. Let this steady-state trajectory be $\boldsymbol{z}_s$. This trajectory is called the *fast state manifold*. In this dissertation, the error between the manifold and the fast states is denoted $\tilde{\boldsymbol{z}} \triangleq \boldsymbol{z} - \boldsymbol{z}_s$. If the manifold can be found algebraically then the system is called *standard*. Physically, nonstandard systems are more common. Aircraft are a good example of a nonstandard system because coupling in the fast dynamics makes f_z intractable.

In multiple-timescale control literature, the current state of the art is Composite Control [15, p. 94-102], Sequential Control [9], and Simultaneous Slow and Fast Tracking [16]. In Composite Control the input is selected to be $\boldsymbol{u} = \boldsymbol{u}_s(\boldsymbol{x}) + \boldsymbol{u}_f(\boldsymbol{x}, \boldsymbol{z})$ where $\boldsymbol{u}_s(\boldsymbol{x})$ is a control signal that is used to stabilize the reduced slow system, and $\boldsymbol{u}_f(\boldsymbol{x}, \boldsymbol{z})$ is a control signal that is used to stabilize the reduced fast system. Importantly, $\boldsymbol{u}_f$ is chosen such that $\boldsymbol{u}_f(\boldsymbol{x}, \boldsymbol{z}_s) = 0$. This allows the slow input to be the only influence on the system when the fast state has converged to its manifold.

Notably, this requires knowledge of the manifold. The literature describes three ways to obtain the manifold. For standard systems the manifold can be derived from the system dynamics [9, p. 42-54]. For a nonstandard system, the manifold can be approximated [17]. In Sequential Control, the manifold is specified [9, p. 78-91]. The manifold is used as an input for the slow subsystem. Then the control input is used to drive the fast states to the manifold. This is very related to Cascaded Control. However, Sequential Control is slightly more rigorous because the timescale separation is formally defined as ϵ, and Sequential Control theory allows the engineers to calculate exactly how much timescale separation is required for the approach to be successful. Finally, Simultaneous Slow and Fast Tracking are best suited for fully actuated systems. The inputs can then be selected so that the slow and fast states simultaneously converge to an arbitrary trajectory. For this method, the manifold is again specified because the steady state trajectory of the fast states is arbitrary. All three of these control approaches are frameworks for fusing the control signals for the reduced subsystems. The control for the subsystems is typically selected via a Lyapunov analysis of the reduced-order systems [18, p. 97-154]. However, other approaches (e.g. Feedback Linearization) is perfectly allowable [9] (to foreshadow slightly, KAMS uses adaptive control).

The control fusion techniques described above ensure that the reduced-order models are stable under $\boldsymbol{u}$. However, the true full-order system is a coupled version of the slow and fast subsystems. It is possible for this coupling to incite instability [9, p. 46]. Thus, the closed-loop behavior of the full-order model would still be unknown. Saberi and Khalil showed full-order stability for a multiple-timescale system via a third Lyapunov analysis [19] (i.e. one for each reduced subsystem and one for the full-order model). They then extended that result to a system under Composite Control [20]. Saberi and Khalil's result is highly general and essential in multiple-timescale control. It is restated here because it is foundational to this dissertation

Theorem 1.1 - *[20] Using the variable definitions above. Let $V(\boldsymbol{x})$ and $W(\boldsymbol{x}, \tilde{\boldsymbol{z}})$ be Lyapunov functions. Choose the input to be Composite Control. Let $0 < \alpha_1, \alpha_2, \beta_1, \beta_2, \beta_3, \gamma_1, \gamma_2 \in \mathbb{R}$ be arbitrary. Let $\Psi(\boldsymbol{x})$ and $\Phi(\tilde{\boldsymbol{z}})$ be arbitrary continuous scalar functions such that $\Psi(0) = \Phi(0) = 0$.*

IF *the following conditions are met:*

$$\frac{\partial V}{\partial \boldsymbol{x}} f(\boldsymbol{x}, \boldsymbol{z}_s, \boldsymbol{u}_s) \leq -\alpha_1 \Psi^2(\boldsymbol{x}) \tag{1.5}$$

$$\frac{\partial W}{\partial \tilde{\boldsymbol{z}}} g(\boldsymbol{x}, \boldsymbol{z}, \boldsymbol{u}, 0) \leq -\alpha_2 \Phi^2(\tilde{\boldsymbol{z}}) \tag{1.6}$$

$$\frac{\partial V}{\partial \boldsymbol{x}} \left[f(\boldsymbol{x}, \boldsymbol{z}, \boldsymbol{u}) - f(\boldsymbol{x}, \boldsymbol{z}_s, \boldsymbol{u}_s) \right] \leq \beta_1 \Psi(\boldsymbol{x}) \Phi(\tilde{\boldsymbol{z}}) \tag{1.7}$$

$$\frac{\partial W}{\partial \tilde{\boldsymbol{z}}} \left[g(\boldsymbol{x}, \boldsymbol{z}, \boldsymbol{u}, \epsilon) - g(\boldsymbol{x}, \boldsymbol{z}, \boldsymbol{u}, 0) \right] \leq \epsilon \beta_2 \Psi(\boldsymbol{x}) \Phi(\tilde{\boldsymbol{z}}) + \epsilon \gamma_1 \Phi^2(\tilde{\boldsymbol{z}}) \tag{1.8}$$

$$\left[\frac{\partial W}{\partial \boldsymbol{x}} - \frac{\partial W}{\partial \tilde{\boldsymbol{z}}} \frac{\partial \boldsymbol{z}_s}{\partial \boldsymbol{x}} \right] f(\boldsymbol{x}, \boldsymbol{z}, \boldsymbol{u}) \leq \beta_3 \Psi(\boldsymbol{x}) \Phi(\tilde{\boldsymbol{z}}) + \gamma_2 \Phi^2(\tilde{\boldsymbol{z}}) \tag{1.9}$$

$$\epsilon < \frac{\alpha_1 \alpha_2}{(\gamma_1 + \gamma_2)\alpha_1 + \beta_1(\beta_2 + \beta_3)} \tag{1.10}$$

THEN *the full-order closed-loop system is asymptotically stable about the origin.*

Proof. Proof of Theorem 1.1 can be found in [20]. □

Condition (1.7)-(1.9) are called the *interconnection conditions*. Each condition in Theorem 1.1 has a physical meaning. Condition (1.5) stipulates that the reduced slow system be stable. Condition (1.6) stipulates that the reduced fast system be stable. Condition (1.7) is a bound on the effect of the manifold on the slow subsystem. Condition (1.8) is a bound on the effect of the reduced slow system on the reduced fast system. Condition (1.9) is a bound on the effect of the reduced slow system on the reduced fast system. Multiple-timescale control breaks down for single-timescale systems because the timescale separation parameter can no longer be approximated as 0. Hence, condition (1.10) is an acceptable range for the timescale separation parameter. Often, the timescale separation parameter is difficult to determine exactly. It is much more common for control engineers to have a rough estimate of the timescale separation parameter. Therefore, an important aspect of most multiple-timescale control stability proofs is deriving an acceptable range for this parameter. Multiple-timescale control methods have been extended to allow output feedback [21], state observers [22], and an arbitrary number of timescales [9, p. 109-127].

A block diagram for multiple-timescale control (including all three fusion methods described above) is given in Fig. 1.1. The empty spaces in this diagram are reserved for blocks that will

be added later. Notably, the multiple-timescale control stability proofs discussed above are all developed under the assumption that the system model is exactly known. In the literature, standard practice when deriving multiple-timescale control for an uncertain system is to assume that any errors in the system model are negligible [23]. Static estimates of the uncertain parameters are required. Steady-state error can occur if the system model is incorrect. Relatively little research has addressed multiple-timescale systems with uncertain parameters. The research in this dissertation does so.

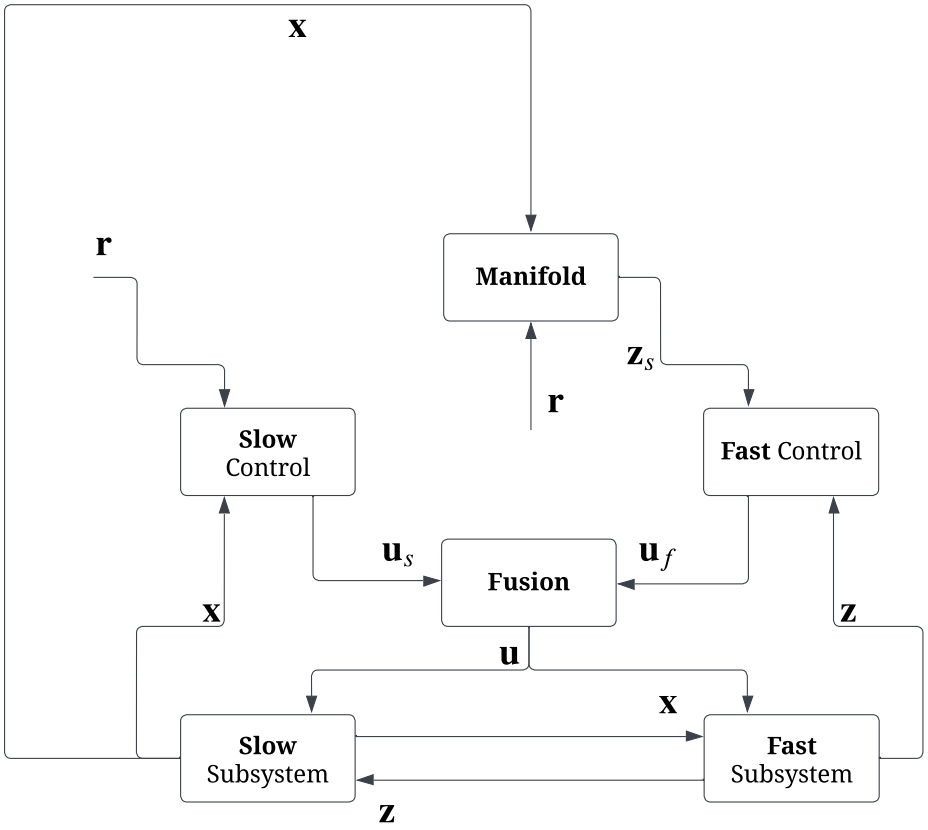

Figure 1.1: A block diagram of multiple-timescale control.

1.2 Adaptive Control

Adaptive control is an effective method of accounting for time-varying parameters and uncertain models [24, p. 4]. Adaptive control has particular application to aircraft which are frequently uncertain and nonlinear [25, 26, 27, 28]. The inertias and control derivatives are the two biggest sources of parametric uncertainty in aircraft dynamic modeling. Measuring these parameters can be an expensive and time-consuming process. Adaptive control can address several different types of uncertainty. This uncertainty is divided into structured uncertainty, unstructured uncertainty, and unmodeled dynamics. *Structured uncertainty*, also known as *parametric uncertainty*, applies to systems where individual parameters are unknown [29]. *Unstructured uncertainty* applies to systems where an entire section of the dynamics is an unknown [30]. This creates an unspecified function in the differential equations. *Unmodled dynamics* applies to systems when there is a coupled differential equation in the dynamics that is either unknown or discounted [31]. The types of uncertainties can further be divided into three more categories: Matched uncertainty, unmatched uncertainty, and control input uncertainty. *Matched uncertainty* can be completely canceled out by the control if it is known [32]. *Unmatched uncertainty* cannot be directly canceled out because of singularities encountered while inverting the dynamics [33]. *Control input uncertainty* is an uncertain parameter that is directly multiplied by the input [34]. Examples of each type of uncertainty can be found in [35, p. 86-88]. Finally, adaptive control can also apply to time-varying parameters [36]. Each of these applications of adaptive control has extensive research in the literature.

Adaptive control techniques are typically divided into two broad categories: *direct* and *indirect*. *Indirect adaptive control* uses the adaptive laws to estimate the uncertain or time-varying values [37]. The control gains are then calculated using the estimated values. On the other hand, *direct adaptive control* estimates the control gains directly without ever obtaining the uncertain or time-varying parameters [38]. Because the control gains are functions of the uncertain or time-varying values, the difference between direct and indirect adaptive control can often be thought of as a change of variables.

Implementation of adaptive control typically proceeds by selecting a suitable control law that

stabilizes the idealized model. Then, parameter estimators are chosen which ensure stability for the uncertain systems. These parameter estimators are typically dynamic equations that are functions of the system's states and inputs. Conceptually the parameter estimates converge to the true parameter value. However, in practice, parameter estimators are not required (or desired) to drive the estimation error to zero. It is usually sufficient to ensure that the estimation error is bounded and the control objective is achieved. Stability and convergence are often proved using a Lyapunov analysis and Barbalat's Lemma [39].

There are several methods of choosing adaptive laws and control laws. The control laws must be chosen such that the control objective would be achieved if the parameters were known perfectly. A common method is dynamic inversion because it can be applied to nonlinear systems [40]. However, more traditional methods such as proportional, integral, derivative (PID) control [41] or full state feedback are possible [42, Section 4]. A common consideration when choosing a control law is to ensure the uncertain or time-varying values appear in the closed-loop system such that the system fits one of the parametric models that are used in the derivation of adaptive laws. In other words, the system must be formatted such that it fits a generic model (called a parametric model) used by standard adaptive laws. The adaptive laws can then be chosen from the list of adaptive laws that fit that parametric model. Some common standard adaptive laws include Strictly Positive Real (SPR) Lyapunov [43], Gradient Descent [44], and Least Squares [45]. Alterations such as normalization [46] or projection [47] can be used to ensure the parameter estimates are bounded.

Model Reference Adaptive Control (MRAC) is the most common version of adaptive control [48, p 221-222]. MRAC chooses adaptive laws and control laws such that the system tracks a theoretical reference system. Many other "flavors" of adaptive control have been studied throughout the years including L_1 Adaptive Control [49], Structured Adaptive Model Inversion (SAMI) Control [50], and Intelligent Adaptive Control [51]. A comprehensive review of adaptive techniques is beyond the scope of this work. The reader is referred to a survey paper such as [52] for an in-depth summary.

While adaptive control is advantageous for uncertain systems, it has been shown to struggle

with multiple-timescale systems [24, p. 549-552] [35, p. 5]. All of the adaptive control research described above is applied solely to single-timescale systems. In the literature, there are two primary ways to apply adaptive control to a multiple-timescale system. They are Full-Order Adaptive Control (FOAC) and Reduced Order Adaptive Control (ROAC) [53]. This dissertation proposes a novel third method - KAMS. FOAC and ROAC will be discussed in more detail in Chapter 4.

1.3 [K]control of Adaptive Multiple-Timescale Systems Architecture

This section details this dissertation's research from a high-level perspective. It describes the KAMS methodology and lists the expected benefits. Then several research questions are listed which his dissertation answers. Finally, the scope of this dissertation is discussed.

1.3.1 Methodology

The multiple-timescale control fusion techniques described previously are characterized by selecting a controller for both of the reduced systems and then fusing them. For Composite Control, as long as the assumptions and conditions of Theorem 1.1 are met any method can be used to select the control for the reduced subsystems. KAMS uses adaptive control on the reduced subsystem. The problem definition and assumptions of Theorem 1.1 do not hold for adaptive control. The reason for this is the complex interactions between the fast reference model and manifold. This will be discussed in more detail in Chapter 2. A major contribution of this dissertation is a novel theorem that is equivalent to Theorem 1.1 but for KAMS. Using this novel theorem, the design procedure for KAMS is

1. Derive the reduced fast and reduced slow subsystems.

2. Select a multiple-timescale fusion technique and obtain the system manifold(s) using the reduced slow system or by specifying it. Which method is used depends upon the control objective and the system type (standard or nonstandard).

3. Select an adaptive control or traditional control to drive the reduced slow system to the control objective. Which type of control is used depends upon the location of uncertainties

and time-varying parameters.

4. Select an adaptive control or traditional control to drive the reduced fast system to the control objective. Which type of control is used depends on the location of uncertainties and time-varying parameters.

5. Confirm full-order stability by checking the sufficient conditions of the novel theorem.

Figure 1.2 shows a block diagram for KAMS. As will be seen in Chapter 2 the fast adaptive control is allowed to be a function of the slow states. This uncommon case is excluded from the block diagram for readability. If the uncertain parameters do not appear in one of the subsystems then a traditional (i.e. non-adaptive) form of control can be used for that subsystem. This still fits within the framework of KAMS. Figures 1.3 and 1.4 show block diagrams for KAMS with adaptive control in only the slow and fast subsystems respectively. If adaptive control is not necessary for either subsystem then the system is reduced to traditional multiple-timescale control and theroem 1.1 is sufficient.

1.3.2 Benefits

KAMS expands the applicability of multiple-timescale control and adaptive control to uncertain multiple-timescale systems. It also provides several important benefits over prior methodologies. For example, KAMS is generalized and simplified when compared to [54]. This and other related research are discussed in the literature review to follow. KAMS is also agnostic to the type of adaptive control used. This allows KAMS to take advantage of the most recent research in adaptive control and multiple-timescale control. In summary, KAMS provides the following benefits:

1. Extends both adaptive control and multiple-timescale control to a wider class of systems.

2. Method is generalized.

3. Underlying physics inherent in the timescale separation are evident in the control law. This allows for improved analysis.

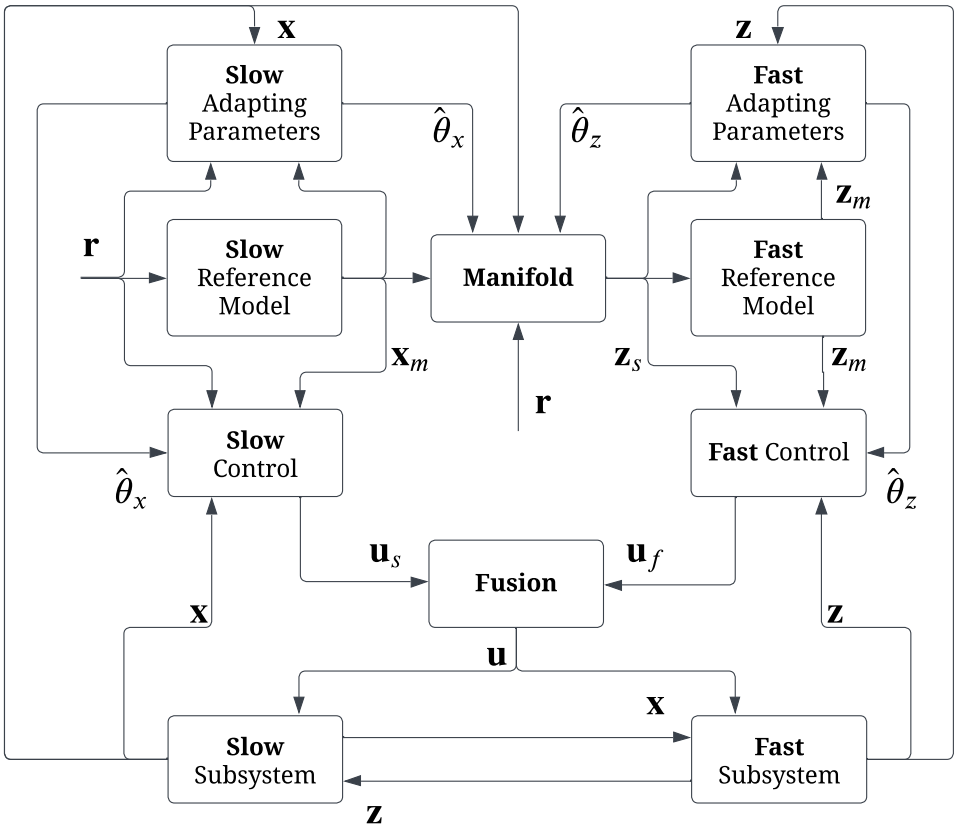

Figure 1.2: A block diagram of KAMS.

4. Derivation and implementation are simplified.

5. KAMS is agnostic to the type of adaptive control and multiple-timescale control used. This means the new technique can take advantage of the most recent research.

These fascets make KAMS an attractive choice when working with uncertain systems with timescale separation. However, if the system is deterministic then traditional multiple-timescale control should be used. If the timescale separation is small then traditional adaptive control should be used.

1.3.3 Research Questions

There are several important research questions that this dissertation addresses.

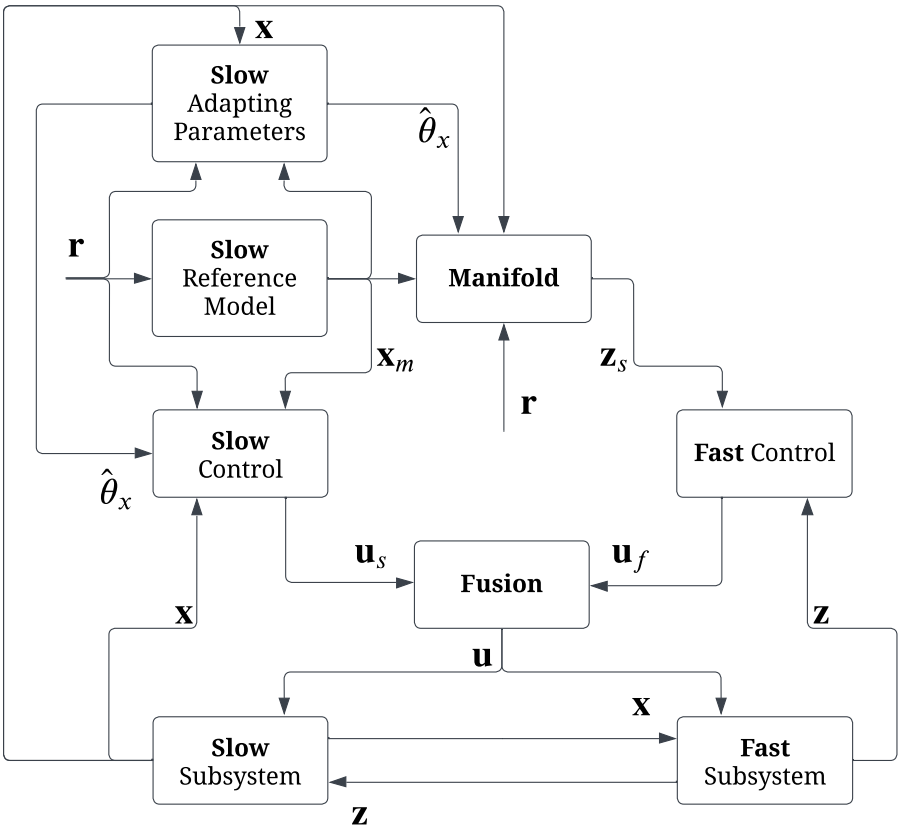

Figure 1.3: A block diagram of KAMS with adaptive control only used for the slow subsystem.

1. What is a generalized method for control of multi-input multi-output (MIMO), uncertain, nonlinear, nonstandard, adaptive multiple-timescale systems?

2. How can stability and convergence be proved for this generalized method? What is the acceptable range for the timescale separation parameter?

3. How does this method and the associated stability proof change when the adaptive control is used for only one subsystem as opposed to both?

4. What timescale do the adaptive parameters adapt in? Is it the fast timescale, the slow timescale, or a new timescale?

5. How does this method perform on aerospace systems?

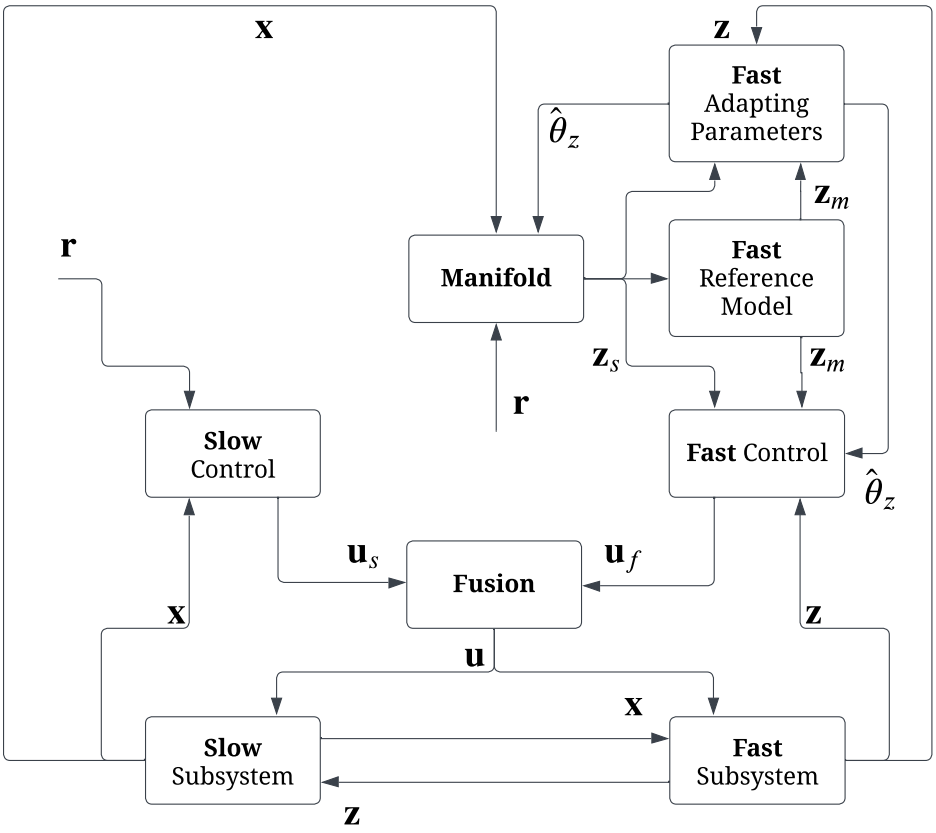

Figure 1.4: A block diagram of KAMS with adaptive control only used for the fast subsystem.

1.3.4 Scope

This dissertation primarily addresses slow state tracking of a reference signal for two-timescale systems using full state feedback, although Simultaneous Slow and Fast Tracking is investigated in Chapter 6. The multiple-timescale control fusion techniques considered are Composite Control, Sequential Control, and Simultaneous Slow and Fast Tracking. The methodology proposed herein applies to many adaptive methodologies and types of uncertainty that currently exist in the literature. However, exhaustive testing of all adaptive control methods is beyond the scope of this dissertation. Traditional MRAC and Adaptive Nonlinear Dynamic Inversion (ANDI) are chosen to demonstrate the approach and results. Direct adaptive control is used and the adaptive laws are selected via a Lyapunov analysis. Parametric uncertainty is assumed and certain assumptions

about the uncertain parameters are imposed. Collectively, these techniques are chosen because their simplicity elucidates the advantages and disadvantages of the approach.

1.3.5 Contributions of This Dissertation

This dissertation develops and analyses a generalized method of adaptive control for uncertain, nonlinear, nonstandard, multiple-input multiple-output, multiple-timescale systems. As discussed in the next section, several researchers have addressed subsets of this problem, but this is the first work that addresses all of these components simultaneously. The KAMS methodology itself is novel; as are the related theories that are proven and studied in Chapter 2. These theories give proof of conditions that are sufficient for the asymptotic stability of the full-order system under KAMS. The stability proof was significantly complicated by complex interactions between the fast-state reference model and the manifold. These proofs show that if the conditions are met then the coupling which is eliminated during the model reduction is insufficient to destabilize the system. This work also contributes analysis of KAMS. This analysis includes a direct comparison of performance and robustness with a few notable alternative approaches. The analysis also includes evidence for the versatility of KAMS through several first-of-kind demonstrations with a variety of

1. Adaptive control methods
    (a) MRAC
    (b) ANDI
2. Multiple-timescale fusion techniques
    (a) Composite Control
    (b) Sequential Control
    (c) Simultaneous Slow and Fast Tracking
3. Plants

(a) Linear and nonlinear

(b) Small and large timescale separation

(c) Single-Input Single-Output (SISO) and Multiple-Input Multiple-Output (MIMO)

(d) With and without the timescale separation parameter appearing on the right-hand side of the fast states' equations of motion

This dissertation also includes the first demonstration of how KAMS can be used to relax the minimum phase assumption. This contribution is particularly significant because the minimum phase assumption has been a notable drawback to adaptive control since its inception. Finally, the practical examples at the end of this dissertation use KAMS to develop new approaches for quadrotor attitude stabilization, orbital transfer maneuvers, and inlet unstart prevention for hypersonic aircraft. The approaches used in these practical examples are novel. Each of these contributions individually and collectively represent significant novel additions to societal knowledge.

1.4 Literature Review

There is some prior work that addresses the issues of uncertain multiple-timescale systems. Prior work begins with either adaptive control *or* multiple-timescale control and then applies elements of the other method. KAMS approaches the problem from a more fundamental first principles approach. Thus, the following literature review is divided into two sections: adaptive control with elements of multiple-timescale control and multiple-timescale control with elements of adaptive control.

1.4.1 Adaptive Control with Elements of Multiple-Timescale Control

The literature reports three ways to incorporate multiple-timescale methods into adaptive control. They are assumed model reduction, Tikhonov's Theorem, and singular perturbation in the control.

1.4.1.1 Assumed Model Reduction

One common method to apply adaptive control to a multiple-timescale system is to apply the adaptive control to the reduced slow model and assume the neglected dynamics are stable (e.g. [9, p. 41-42]). This method is called Reduced-Order Adaptive Control (ROAC) herein. Under ROAC, if the input accidentally excites the dynamic modes in the discounted dynamics then the full-order system can be driven unstable [55]. For a deterministic linear time-invariant (LTI) system this problem has been solved [56], but the proposed research addresses uncertain and nonlinear systems. Wahdan and Tawfik said, "*It has been established that standard adaptive control algorithms would likely become unstable, in the presence of unmodeled plant dynamics and external sinusoidal disturbances*" [57]. Wahdan and Tawfik attempted to reduce the effects of this problem by regularly resetting the adaptive parameters to their initial conditions, but they stopped short of proving full-order stability. Rohrs *et al.* acknowledged the difficulty of applying adaptive control to a subsystem of the dynamics. They said, "*...sinusoidal reference inputs at specific frequencies... can cause the loop gain to increase without bound, thereby exciting the unmodeled high-frequency dynamics, and yielding an unstable control system*" [58]. Rohrs *et al.* concluded that "*existing adaptive control algorithms as they are presented in the literature referenced in this paper, cannot be used with confidence in practical designs where the plant contains unmodeled dynamics because instability is likely to result*" [58]. Later Rohrs said, "*These theoretical assumptions are too restrictive from an engineering point of view. Real plants always contain unmodeled high-frequency dynamics...*" [59]. Some researchers have disputed Rohrs' claim [60] and demonstrated adaptive controllers which are robust to unmodeled dynamics (e.g. [61]). Another common approach is to treat the unmodeled fast dynamics as a time delay (e.g. [62]). However, the class of systems discussed in this research implicitly assume that at least some subset of the fast dynamics are known. If these dynamics are known then discounting them only puts the engineer at a greater disadvantage. Stability guarantees and robustness can only be strengthened by including all known dynamics. KAMS improves upon ROAC by considering both reduced subsystems. KAMS is directly compared to ROAC in chapter 4.

A related approach is to use Cascaded Control (also known as Sequential Loop Closure) [63, p. 58-60]. Cascaded Control segments the system into a slow and fast subsystem and then uses the fast states as an input to the slow states. As previously mentioned, this is related to the multiple-timescale control fusion technique of Sequential Control. Indeed, the control signals for Cascaded Control and Sequential Control are often identical. However, Sequential Control carries with it additional tools from singular perturbation theory. A common rule of thumb for Cascaded Control is that the fast dynamics must be about ten times faster than the slow dynamics and the coupling between subsystems is ignored in stability proofs. On the other hand, singular perturbation theory allows Sequential Control to provide an analytical bound on the allowable timescale separation. This bound is derived from the system dynamics. Additionally, singular perturbation theory allows Sequential Control to rigorously account for the coupling between subsystems in the stability proof. Rollins, Famularo, and Valasek gave several examples of adaptive control within the framework of Cascaded Control [30, 34, 64, 65, 66, 67]. They applied their work to a hypersonic aircraft. Chapter 7 of this dissertation gives a comparison between their work and KAMS. The comparison demonstrates how KAMS can be used to obtain more rigorous stability guarantees. Further, KAMS also allows for more exotic fusion techniques like sequential control and simultaneous fast and slow tracking.

1.4.1.2 Tikhonov's Theorem

Vasil'eva built upon Tikhonov's work [68] and showed that after finite time the full-order system approximates the reduced slow system [69]. This is known as Tikhonov's Theorem and can be found in English in [18, Theorem 9.1]. Via Tikhonov's Theorem, the full-order model can sometimes be shown to be stable when a reduced subsystem is under adaptive control. However, Tikhonov's theorem requires several restrictive assumptions. For example, the system must be standard. The several examples below discuss systems that are structured such that Tikhonov's Theorem is sufficient to prove stability, but a more general method such as KAMS is needed.

Al-Radhawi *et al.* modeled the progression of the COVID-19 pandemic as a multiple-timescale system [5]. The input to the system was the public's perception of the danger of the disease. Al-

Radhawi demonstrated that the efforts to suppress the contagion can be modeled as an adaptive control law. Using Tikhonov's Theorem, Al-Radhawi showed both stability and that the model correctly matched ground truth data from the pandemic. Macchelli *et al.* modeled a leaking hydraulic press as a multiple-timescale system [70]. Using singular perturbation theory, Macchelli was able to demonstrate that the adaptive controller selected for the fast dynamics, was still able to track the reference model despite the unmodeled slow dynamics of leaking hydraulic fluid.

Nguyen *et al.* studied a particularly interesting case. Nguyen used Tikhonov's Theorem to apply adaptive control to a general linear system with matched uncertainty. Nguyen's work builds upon a modification of adaptive control that is derived from optimal control [71]. Nguyen then derived a controller for a system with actuator dynamics using this modified adaptive control [72]. Interestingly, Nguyen assumed the actuator dynamics were significantly slower than the system dynamics. The actuator dynamics and system dynamics were together modeled as a multiple-timescale system. Nguyen used the reduced-order model to obtain the manifold. Nguyen then differentiated the manifold and used it to supplement the slow dynamics. In other words, only the transient response of the fast dynamics is discounted. Finally, Nguyen performed two validating numerical examples including a simulation of the pitch dynamics of an aircraft. These numerical examples showed that Nguyen's technique can achieve better performance than MRAC for this class of system. This is a promising result because Nguyen showed that adaptive control can be improved by considering the steady-state response of the fast dynamics. This implies that also including the transient response will improve performance even more. KAMS considers both the transient and steady-state dynamics of the full-order model.

1.4.1.3 Singular Perturbation Control

Singular perturbation theory applies to any system with states that evolve in different timescales. The adaptive laws convert the control law into a differential equation. The adaptive gains have a large influence on the timescale of control input. Thus, depending on the control structure the input equation can augment the dynamics of a single-timescale system to create a two-timescale system. Singular perturbation theory applies to this augmented two-timescale system just

as it does to a system that is inherently multiple-timescale. In this case, singular perturbation theory can be useful to enforce convergence criteria on the control and adaptation. This methodology is related to KAMS through its use of singular perturbation theory. However, research using singular perturbation theory in the control has only been applied to single-timescale dynamic systems. Thus, using singular perturbation in the control does not address the class of problems addressed by KAMS. For completeness, research papers using singular perturbation in the control are discussed below.

Hovakimyan *et al.* derived a control law that numerically converges to a dynamic inversion controller for a nonlinear system that is algebraically intractable [73]. Lavretsky *et al.* merged traditional adaptive control techniques into this method [74]. Hovakimyan *et al.* extended this technique to multivariable systems [75] and added a state estimator [76]. All of this research used singular perturbation theory to ensure the control law converges faster than the system dynamics. This research also used adaptive control to account for uncertainties in the system dynamics.

Early adaptive control researchers used averaging theory to address periodic signals. Averaging theory postulates that the convergence of a function $f(t, x)$ can be proven by showing that an *average* function $f_{av}(x)$ is stable. Here, $f_{av}(x)$ is defined as

$$f_{av}(x) \equiv \lim_{t\to\infty} \frac{1}{t} \int_0^t f(\tau, x) d\tau \tag{1.11}$$

It is relevant to the present discussion that adaptive control with averaging theory requires the adaptive parameters to change slowly. This essentially filters out the oscillations. The slow adaption is modeled by a timescale separation parameter and singular perturbation theory can be applied. A tutorial and literature review on averaging techniques can be found in [77, p. 158-208].

Timescale separation in adaptive control can also cause problems when the control is in a slow timescale. Extremum Seeking (ES) is a method of adaptive control that regularly applies very small changes to the control and then checks for improved performance. If performance improves then the control law is updated. Deese and Vermillion said, "*Although rigorous convergence guarantees*

exist for ES, convergence times can be slow due to the assumptions of timescale separation between system dynamics and the ES perturbation period" [78].

Several other researchers have used singular perturbation theory in conjunction with adaptive control. Sun *et al.* applied singular perturbation to adaptive control on a subset of underactuated Euler-Lagrange systems [79]. Rayguru *et al.* [80] and Yang *et al.* [81] both used singular perturbation in adaptive control to ensure closed-loop stability despite input saturation. Krishnamurthy and Khorrami generalized the use of singular perturbation in adaptive control for a class of systems with nonlinear input uncertainty [82]. Asadi and Khayatian [83] as well as Chakrabortty and Arcak [84] examined different methods where singular perturbation in the adaptive control leads to provable stability for a generalized class of systems with matched and unmatched uncertainty.

The work described in this section only applies to single-timescale systems and does not address multiple-timescale systems. Instead, timescales are imposed on the control, not the system, to meet stability criteria. Thus, the research in this section does not apply to the class of systems for which KAMS is tailored.

1.4.2 Multiple-Timescale Control with Elements of Adaptive Control

Several multiple-timescale control researchers have postulated the benefits of a KAMS-like approach. For example, when analyzing a multiple-timescale controller Li *et al.* said, "*It is worth noting that the more accurate system model will yield the higher control accuracy... For future work, we will introduce adaptive mechanisms to further improve the control performance*" [23]. Some researchers have approached the multiple-timescale adaptive control problem by applying elements of adaptive control to multiple-timescale control. These methods are described here. First observers for multiple-timescale systems are related to KAMS. Then a few foundational works which used adaptive control in multiple-timescale control are described. These works are the most related to this dissertation but have several important differences.

Adaptive control has its origins in state estimators for systems with uncertain parameters [46]. The uncertain parameters were needed for the observers. Astrom and Wittenmark [85] discovered that it was possible to use the parameter estimates directly in the control. Estimation and adaptive

control have since diverged, but there remain some marked similarities. Saha *et al.* applied a nonlinear observer to their control of a multiple-timescale spring-mass-damper [86]. The work by Jing *et al.* [87] is similar in form to the multiple-timescale adaptive control example in Chapter 4 except that state estimation is the goal. Ren *et al.* derived a nonlinear observer for a multiple-timescale model of a hypersonic aircraft [7]. In each of these examples, the estimator is estimating the states. The control is not robust to uncertainty in the model, so KAMS is needed to address multiple-timescale systems with uncertain models.

After the initial discovery of Composite Control Ioannou and Kokotovic demonstrated a method of using adaptive control within the context of Composite Control [88]. Ioannou and Kokotovic used adaptive control in the control for the subsystems. Their method is an example of KAMS. However, they assumed that each subsystem had a separate input, and their work only considered linear systems. Similarly, Li and Sun integrated an adaptive controller into a control algorithm for fuzzy logic systems using a method based upon Composite Control [89]. In contrast to both of these works, this dissertation applies to generalized highly coupled nonlinear systems and applies to a wide class of adaptive control methods and multiple-timescale fusion techniques.

Saha *et al.* encountered structured uncertainty while deriving multiple-timescale controllers for several systems including an F-16 aircraft [90, 91], a spring-mass-damper [92], and a satellite [8]. Later work added state observers [86] and output feedback [54]. To resolve the problems created by uncertain parameters Saha derived adaptive estimators from the full-order Lyapunov analysis. Saha's method is inherently a multiple-timescale control method developed from sequential multiple-timescale control. It is also an adaptive control method because the uncertain parameter estimates are used in the multiple-timescale control laws. Therefore, this technique is adaptive multiple-timescale control. However, KAMS is different from Saha's methodology in two important ways.

1. Because Saha's adaptive laws are derived from the full-order stability analysis, they are necessarily separated from the reduced-order model control laws to which they are applied. The implications of this are that the adaptive laws can be very different from the generalized

adaptive laws that are commonly found in adaptive control research. This separates Saha's work from the most recent adaptive control research. KAMS is agnostic to the adaptive control technique chosen thus allowing it to take advantage of state-of-the-art research.

2. Saha's method is not generalized and must be re-derived for each unique system considered. As mentioned above, Saha considered several specific dynamic systems. Each system considered produced different control and adaptive laws. KAMS has a generalized and simplified procedure.

Collectively these two differences mean that KAMS has a greatly simplified implementation and analysis compared to Saha's method.

2. TOOLS FOR STABILITY ANALYSES

Singularly perturbed differential equations can be used to model systems with elements that evolve at different rates. Singular perturbation theory is a more precise method of dealing with timescale behavior, but adaptive control research lacks a rigorous analytical method to check for stability in the presence of singularly perturbed plants. Singular perturbation theory is a broad mathematical field. The singularly perturbed nature of the plant causes a subset of the states to evolve significantly faster than the other states. The general premise of KAMS is that the fast states converge to the fast state reference model much faster than the slow states converge to their reference model. This difference in speed implies that the coupling between the fast and slow states is minor. As is done in multiple-timescale control, geometric singular perturbation theory is used to fully decouple the fast and slow states [9]. Two different adaptive controllers can then be designed for these two independent subsystems in isolation. The independent control signals are fused using a wide class of methods from the field of multiple-timescale control. These multiple-timescale control fusion techniques have not been studied in the presence of adaptive control. This dissertation addresses that gap in the literature.

The novel contribution of this chapter is a formal proof that under certain sufficient conditions, the coupling present in the more accurate full-order model is insufficient to destabilize these adaptive controllers even though they are designed in isolation. This chapter considers systems that require adaptive control in both the fast and the slow subsystems. Allowing adaptive control in both the fast and slow subsystem is a challenging problem because of complex interactions between the manifold and the fast state reference model.

Section 2.1 mathematically defines the KAMS control method and associated singular perturbation analysis that is used to decouple the subsystems. In section 2.2, a set of conditions are derived that are sufficient to show that the states converge to their reference models. Finally, in section 2.3 an example of KAMS on a nonlinear nonstandard system is given. This example demonstrates how methods common in the literature - Sequential Control and Adaptive Nonlinear Dynamic Inversion

(ANDI) - can be used on singularly perturbed systems within the framework of KAMS.

2.1 Control Synthesis

This section introduces KAMS, explains the assumptions, and describes the notation. For more details, the reader is referred to [24, 48, 35] for adaptive control, [9, 15] for multiple-timescale control, [93] for singular perturbation theory, and [94] for differential geometry in the context of control theory.

2.1.1 System Description

This work addresses singularly perturbed systems that model multiple-timescale plants. A *singularly perturbed system* is a system that is a function of a small scalar ϵ but not well approximated by the limit as that scalar approaches zero. This scalar is called the singular perturbation parameter. The *timescale* of a system is a measure of how quickly a system's states evolve. The systems considered in this dissertation have two timescales. The slow states ($\boldsymbol{x} \in \mathbb{D}_x^{n_x} \subseteq \mathbb{R}^{n_z}$) evolve on the slow timescale (t_s) and the fast states ($\boldsymbol{z} \in \mathbb{D}_z^{n_z} \subseteq \mathbb{R}^{n_z}$) evolve on the fast timescale (t_f). Conversion between fast time and slow time is a change of units. Let the timescale separation parameter be the ratio of the two timescales $\epsilon \triangleq {}^{t_s}\!/_{t_f}$. It can be shown that $0 < \epsilon \ll 1$. The derivative with respect to the fast timescale is denoted ${}^{d(\cdot)}\!/_{dt_f} \triangleq \grave{(\cdot)}$ and the derivative with respect to the slow timescale is denoted ${}^{d(\cdot)}\!/_{dt_s} \triangleq \acute{(\cdot)}$. Using the above definitions it can be shown that $\grave{(\cdot)} = \epsilon\acute{(\cdot)}$. As a general rule $\acute{z} \gg \acute{x}$ and $\epsilon\acute{z} \approx \acute{x}$. Whereas these relationships are not always true, they provide good intuition behind the meaning of the timescale separation parameter. Multiple-timescale plants can be modeled using singular perturbation theory by making the timescale separation parameter a singular perturbation parameter.

This work is generalized to uncertain, nonlinear, multiple-input multiple-output (MIMO) plants of the form

$$\acute{\boldsymbol{x}} = f_x(\boldsymbol{x}, \boldsymbol{z}, \boldsymbol{u}) \tag{1.1a revisited}$$

$$\epsilon\acute{\boldsymbol{z}} = f_z(\boldsymbol{x}, \boldsymbol{z}, \boldsymbol{u}, \epsilon) \tag{1.1b revisited}$$

where $\boldsymbol{u} \in \mathbb{R}^{n_u}$ is the system input. This system is singularly perturbed because the functions f_x and f_z are defined such that $\mathcal{O}(f_x) = \mathcal{O}(f_z) = \mathcal{O}(1)$. The order of a function (i.e. the output of the $\mathcal{O}$ operator) is a measure of the rate of change of that function as $\epsilon \to 0$. See [9, Appendix A.2] for a more formal definition. The system in Eq. (1.1) is singularly perturbed because $0 < \epsilon \ll 1$.

2.1.2 Singular Perturbation Analysis

Geometric singular perturbation theory suggests that the system can be approximated by two different asymptotic solutions. The first system is found by taking the limit as $\epsilon \to 0$

$$\acute{\boldsymbol{x}} = f_x(\boldsymbol{x}, \boldsymbol{z}_s, \boldsymbol{u}) \tag{1.2a revisited}$$

$$0 = f_z(\boldsymbol{x}, \boldsymbol{z}_s, \boldsymbol{u}, 0) \tag{1.2b revisited}$$

This is called the *reduced slow subsystem* and is only a valid approximation when $t \gg 0$. Note that the fast states are constrained to a subset of their domain $\boldsymbol{z}_s \in \mathbb{D}_{z_s}^{n_z} \subseteq \mathbb{D}_z^{n_z}$ where $\boldsymbol{z}_s$ is the root of Eq. (1.2b). In multiple-timescale control, $\boldsymbol{z}_s$ is called the *manifold*. Notably $\boldsymbol{z}_s$ is also the equilibrium of Eq. (1.1b). If Eq. (1.1b) can be solved for $\boldsymbol{z}_s$ then the system is called *standard*. The second asymptotic solution for Eq. (1.1) is found by performing a change of timescales (recall that $\grave{(\cdot)} = \epsilon\acute{(\cdot)}$) and again taking the limit as $\epsilon \to 0$

$$\grave{\boldsymbol{x}} = 0 \tag{1.4a revisited}$$

$$\grave{\boldsymbol{z}} = f_z(\boldsymbol{x}, \boldsymbol{z}, \boldsymbol{u}, 0) \tag{1.4b revisited}$$

This is called the *reduced fast subsystem* and is only a valid approximation when t is very close to 0.

2.1.3 Adaptive Control

The control objective of this dissertation is to choose the input as a function of the states so that the full-order system asymptotically tracks a reference model. The first step in this process is to design two separate adaptive control algorithms which individually stabilize the reduced subsystems.

The input to the slow subsystem is $\boldsymbol{u}_s \in \mathbb{R}^{n_u}$ and the input to the fast subsystems is $\boldsymbol{u}_f \in \mathbb{R}^{n_u}$. The variables $\boldsymbol{x}_m \in \mathbb{D}_x^{n_x}$ and $\boldsymbol{z}_m \in \mathbb{D}_z^{n_z}$ are reference model states. The parameters $\hat{\boldsymbol{\theta}}_x \in \mathbb{P}_{\theta_x}^{n_{\theta_x}} \subseteq \mathbb{R}^{n_{\theta_x}}$ and $\hat{\boldsymbol{\theta}}_z \in \mathbb{P}_{\theta_z}^{n_{\theta_z}} \subseteq \mathbb{R}^{n_{\theta_z}}$ are adaptive estimates of the true parameters $\boldsymbol{\theta}_x$ and $\boldsymbol{\theta}_z$ respectively. The true parameters are allowed to be time-varying. Let

$$\boldsymbol{\theta}_x = g_{\theta_x}(t_s) \tag{2.4a}$$

$$\boldsymbol{\theta}_z = g_{\theta_z}(t_f) \tag{2.4b}$$

$$\acute{\boldsymbol{\theta}}_x = f_{\theta_x}(t_s) \tag{2.4c}$$

$$\grave{\boldsymbol{\theta}}_z = f_{\theta_z}(t_f) \tag{2.4d}$$

Define $\boldsymbol{r}_x \in \mathbb{R}^{n_{r_x}}$ to be the bounded input to the slow state reference model. $\boldsymbol{r}_x$ is a function of time. This function and its derivative are

$$\boldsymbol{r}_x = g_{r_x}(t_s) \tag{2.5a}$$

$$\acute{\boldsymbol{r}}_x = f_{r_x}(t_s) \tag{2.5b}$$

The reference models and adaptation laws must be selected in tandem with the control input so that the control objective is achieved. The differential equations describing the motion of the reference models and parameter estimates are of the form

$$\acute{\boldsymbol{x}}_m = f_{x_m}(\boldsymbol{x}, \boldsymbol{x}_m, \hat{\boldsymbol{\theta}}_x, t_s) \tag{2.6a}$$

$$\acute{\hat{\boldsymbol{\theta}}}_x = f_{\hat{\theta}_x}(\boldsymbol{x}, \boldsymbol{x}_m, \hat{\boldsymbol{\theta}}_x, t_s) \tag{2.6b}$$

$$\grave{\boldsymbol{z}}_m = f_{z_m}(\boldsymbol{x}, \boldsymbol{x}_m, \hat{\boldsymbol{\theta}}_x, \boldsymbol{z}, \boldsymbol{z}_m, \hat{\boldsymbol{\theta}}_z, t_f) \tag{2.6c}$$

$$\grave{\hat{\boldsymbol{\theta}}}_z = f_{\hat{\theta}_z}(\boldsymbol{x}, \boldsymbol{x}_m, \hat{\boldsymbol{\theta}}_x, \boldsymbol{z}, \boldsymbol{z}_m, \hat{\boldsymbol{\theta}}_z, t_f) \tag{2.6d}$$

Keep in mind that $\boldsymbol{r}_x$ is implicitly included as a possible input to these functions because it is fully described by time. A wide array of adaptive methods fit this format (e.g. [24, 65]). The role of the

timescale separation parameter is important in these equations. If the control input is incorrectly designed then the timescale analysis in the previous section could be invalidated. The following two assumptions are made to ensure that doesn't happen.

Assumption 2.1 - *The manifold is an asymptotically stable equilibrium of the fast reference model in the reduced fast subsystem.*

Assumption 2.2 - *The timescale of the reference models, the slow state reference model input, and the adaptation laws all match the timescale of the subsystem to which they are applied. Mathematically this means that* $\mathcal{O}(f_{x_m}) = \mathcal{O}(f_{\hat{\theta}_x}) = \mathcal{O}(f_{\theta_x}) = \mathcal{O}(f_{z_m}) = \mathcal{O}(f_{\hat{\theta}_z}) = \mathcal{O}(f_{\theta_z}) = \mathcal{O}(f_{r_x}) = \mathcal{O}(1)$

These assumptions are intuitive. For example, if the reference model for the slow states evolved on the fast timescale then the slow states would not be able to keep up - or, more precisely, their evolution could not be decoupled from the fast states.

2.1.4 Multiple-Timescale Fusion

The inputs to the reduced subsystems have been chosen, but the reduced subsystems only exist on paper. The inputs to the reduced-order subsystems will form the building blocks of the full-order system input. Let the full-order input take the form

$$\boldsymbol{u} = g_u(\boldsymbol{x}, \boldsymbol{x}_m, \hat{\boldsymbol{\theta}}_x, \boldsymbol{z}, \boldsymbol{z}_m, \hat{\boldsymbol{\theta}}_z, t_s) \tag{2.7}$$

The stability analysis in the next section depends on the reduced-order models being stabilized by their inputs $\boldsymbol{u}_s$ and $\boldsymbol{u}_f$. The control objective is to select $\boldsymbol{u}$ so that both reduced-order systems are simultaneously stabilized. Several different multiple-timescale control techniques accomplish this objective by fusing the control signals for the two reduced subsystems. In this section, three possible methods are summarized. See [9] for more information on each of these methods.

2.1.4.1 *Composite Control*

Composite Control [15, p. 94-102] selects the control input to be $\boldsymbol{u} = \boldsymbol{u}_s + \boldsymbol{u}_f$ where $\boldsymbol{u}_f = 0$ when $\boldsymbol{z} = \boldsymbol{z}_s$. The engineer first selects $\boldsymbol{u}_s$ so that the reduced slow model is stable. Then the engineer selects $\boldsymbol{u}_f$ so that $\boldsymbol{u}_s + \boldsymbol{u}_f$ drives the fast states to $\boldsymbol{z} = \boldsymbol{z}_s$. This requires prior knowledge of the system's open-loop manifold so the system must be standard.

2.1.4.2 *Sequential Control*

In Sequential Control [9] the fast states are used as the input to the slow subsystem. The manifold is selected such that the slow states converge to their reference model. Then the input $\boldsymbol{u}$ can be selected to drive the fast states to the manifold. Thus Sequential Control uses $\boldsymbol{u} = \boldsymbol{u}_f$.

2.1.4.3 *Simultaneous Slow and Fast Tracking*

Simultaneous Slow and Fast Tracking [16] uses the input $\boldsymbol{u} = \boldsymbol{u}_s = \boldsymbol{u}_f$. The control is chosen to stabilize both reduced-order systems simultaneously. As such this method is not suitable for underactuated systems. The advantage of this method is that the slow states and the fast states can both be commanded to any arbitrary trajectory within the state space (constrained only by smoothness). Unlike Composite Control and Sequential Control, Simultaneous Slow and Fast Tracking allows an arbitrary manifold.

2.2 Stability Analysis

Whereas the adaptive controllers have been designed so that the reduced-order systems are well-behaved, these properties might not extend to the coupled full-order system. This section develops tools for the stability analysis of the full-order system. The system of equations is rewritten as a single augmented system in terms of the error coordinates. This is primarily done for notational simplicity. Examining the differential geometric nature of the augmented system leads to important insights into the behavior of the full-order system.

2.2.1 Augmented Error Dynamics

Adaptive control adds additional states (i.e. the reference model and adapting parameters) to the closed-loop system. These states evolve over time (see Eq. (2.6)) and effectively create a coupled augmented closed-loop system with control states and system states. The augmented closed-loop system is defined in this section.

The variables which describe the state of the system are $\boldsymbol{x}$, $\boldsymbol{x}_m$, $\hat{\boldsymbol{\theta}}_x$, $\boldsymbol{z}$, $\boldsymbol{z}_m$, and $\hat{\boldsymbol{\theta}}_z$. For notational simplicity, these states are concatenated together. Let

$$\boldsymbol{\xi} \triangleq \begin{bmatrix} \boldsymbol{x}^T & \boldsymbol{x}_m^T & \hat{\boldsymbol{\theta}}_x^T \end{bmatrix}^T \qquad \in \mathbb{D}_{\xi}^{n_\xi} \tag{2.8a}$$

$$\boldsymbol{\eta} \triangleq \begin{bmatrix} \boldsymbol{z}^T & \boldsymbol{z}_m^T & \hat{\boldsymbol{\theta}}_z^T \end{bmatrix}^T \qquad \in \mathbb{D}_{\eta}^{n_\eta} \tag{2.8b}$$

$$\boldsymbol{\phi} \triangleq \begin{bmatrix} \boldsymbol{\xi}^T & \boldsymbol{\eta}^T \end{bmatrix}^T \qquad \in \mathbb{D}_{\phi}^{n_\phi} \tag{2.8c}$$

The differential equations describing the evolution of $\boldsymbol{\phi}$ are found in Eqs. (1.1) and (2.6). These differential equations are dependent upon the system state variables, the input, and time. However, the input is also a function of the system state variables and time (see Eq. (2.7)). Therefore, the system's dynamics are entirely described by the system's state and time. Similarly, the manifold is a function of the slow states and the input (see Eq. (1.2b)). So it too can be described by a function of the system state and time. Let that function and its time derivative be

$$\boldsymbol{z}_s = g_{z_s}(\boldsymbol{x}, \boldsymbol{x}_m, \hat{\boldsymbol{\theta}}_x, \hat{\boldsymbol{\theta}}_z, t_s) \tag{2.9a}$$

$$\acute{\boldsymbol{z}}_s = f_{z_s}(\boldsymbol{x}, \boldsymbol{x}_m, \hat{\boldsymbol{\theta}}_x, \boldsymbol{z}, \boldsymbol{z}_m, \hat{\boldsymbol{\theta}}_z, t_s) \tag{2.9b}$$

Section 2.2.3 discusses the manifold in detail, but for now, the following assumption is made:

Assumption 2.3 - *g_{z_s} is a diffeomorphism and the manifold evolves in the slow timescale. Mathematically this means that $\mathcal{O}(f_{z_s}) = \mathcal{O}(1)$.*

If the control objective for the full-order system is successfully achieved then three things occur

as $\boldsymbol{t} \to \infty$. First $\boldsymbol{z} \to \boldsymbol{z}_m \to \boldsymbol{z}_s$. This is followed by $\boldsymbol{x} \to \boldsymbol{x}_m$. Additionally, if the subsystems are persitantly exciting then $\hat{\boldsymbol{\theta}}_x \to \boldsymbol{\theta}_x$ and $\hat{\boldsymbol{\theta}}_z \to \boldsymbol{\theta}_z$. These goals imply a set of error variables. Let

$$\boldsymbol{e}_x \triangleq \boldsymbol{x} - \boldsymbol{x}_m \qquad \in \mathbb{B}^{n_x}(r_{e_x}) \tag{2.10a}$$

$$\tilde{\boldsymbol{x}}_m \triangleq \boldsymbol{x}_m - \boldsymbol{r}_x \qquad \in \mathbb{B}^{n_x}(r_{x_m}) \tag{2.10b}$$

$$\tilde{\boldsymbol{\theta}}_x \triangleq \hat{\boldsymbol{\theta}}_x - \boldsymbol{\theta}_x \qquad \in \mathbb{B}^{n_{\theta_x}}(r_{\tilde{\theta}_x}) \tag{2.10c}$$

$$\tilde{\boldsymbol{z}} \triangleq \boldsymbol{z} - \boldsymbol{z}_s \qquad \in \mathbb{B}^{n_z}(r_{\tilde{z}}) \tag{2.10d}$$

$$\tilde{\boldsymbol{z}}_m \triangleq \boldsymbol{z}_m - \boldsymbol{z}_s \qquad \in \mathbb{B}^{n_z}(r_{\tilde{z}_m}) \tag{2.10e}$$

$$\boldsymbol{e}_z \triangleq \boldsymbol{z} - \boldsymbol{z}_m \qquad \in \mathbb{B}^{n_z}(r_{e_z}) \tag{2.10f}$$

$$\tilde{\boldsymbol{\theta}}_z \triangleq \hat{\boldsymbol{\theta}}_z - \boldsymbol{\theta}_z \qquad \in \mathbb{B}^{n_{\theta_z}}(r_{\tilde{\theta}_z}) \tag{2.10g}$$

where $r_{e_x}, r_{x_m}, r_{\tilde{\theta}_x}, r_{\tilde{z}}, r_{\tilde{z}_m}, r_{e_z}, r_{\tilde{\theta}_z} \in \mathbb{R}_+$. Whereas $\boldsymbol{x}_m$ doesn't necessarily converge to $\boldsymbol{r}_x$ their relationship is nonetheless important. Note that

$$\boldsymbol{e}_z = \tilde{\boldsymbol{z}} - \tilde{\boldsymbol{z}}_m \tag{2.11}$$

A change of variables is now performed to describe the system in terms of the error variables. The new system state variables are

$$\boldsymbol{e}_\xi \triangleq \begin{bmatrix} \boldsymbol{e}_x^T & \tilde{\boldsymbol{x}}_m^T & \tilde{\boldsymbol{\theta}}_x^T \end{bmatrix}^T \qquad \in \mathbb{B}^{n_\xi}(r_{e_\xi}) \tag{2.12a}$$

$$\boldsymbol{e}_\eta \triangleq \begin{bmatrix} \boldsymbol{e}_z^T & \tilde{\boldsymbol{z}}_m^T & \tilde{\boldsymbol{\theta}}_z^T \end{bmatrix}^T \qquad \in \mathbb{B}^{n_\eta}(r_{e_\eta}) \tag{2.12b}$$

$$\boldsymbol{e}_\phi \triangleq \begin{bmatrix} \boldsymbol{e}_\xi^T & \boldsymbol{e}_\eta^T \end{bmatrix}^T \qquad \in \mathbb{B}^{n_\phi}(r_{e_\phi}) \tag{2.12c}$$

where $r_{e_\xi} \triangleq \max(\{r_{e_x}, r_{x_m}, r_{\tilde{\theta}_x}\})$, $r_{e_\eta} \triangleq \max(\{r_{e_z}, r_{\tilde{z}_m}, r_{\tilde{\theta}_z}\})$, and $r_{e_\phi} \triangleq \max(\{r_{e_\xi}, r_{e_\eta}\})$. Let the mapping $h : \mathbb{B}^{n_\phi}(r_{e_\phi}) \times \mathbb{R}_+ \to \mathbb{D}_\phi^{n_\phi} \times \mathbb{R}_+$ be the diffeomorphism between the two sets of state

variables

$$(\boldsymbol{\phi}, t_s) = h(\boldsymbol{e}_\phi, t_s) \tag{2.13}$$

where $\boldsymbol{\phi}$ is

$$\boldsymbol{\phi} = \begin{bmatrix} \boldsymbol{e}_x + \tilde{\boldsymbol{x}}_m + g_{r_x}(t_s) \\ \tilde{\boldsymbol{x}}_m + g_{r_x}(t_s) \\ \tilde{\boldsymbol{\theta}}_x + g_{\theta_x}(t_s) \\ \boldsymbol{e}_z + \tilde{\boldsymbol{z}}_m + g_{z_s}(\cdot) \\ \tilde{\boldsymbol{z}}_m + g_{z_s}(\cdot) \\ \tilde{\boldsymbol{\theta}}_z + g_{\theta_z}(t_s/\epsilon) \end{bmatrix} \tag{2.14}$$

and

$$g_{z_s}(\cdot) = g_{z_s}(\boldsymbol{e}_x + \tilde{\boldsymbol{x}}_m + g_{r_x}(t_s),\ \tilde{\boldsymbol{x}}_m + g_{r_x}(t_s),\ \tilde{\boldsymbol{\theta}}_x + g_{\theta_x}(t_s),\ \tilde{\boldsymbol{\theta}}_z + g_{\theta_z}(t_s/\epsilon),\ t_s) \tag{2.15}$$

Eqs. (1.1) and (2.6) can be rewritten in terms of the new state variables

$$\acute{\boldsymbol{e}}_x = f_x \circ h(\boldsymbol{e}_\xi, \boldsymbol{e}_\eta, t_s) - f_{x_m} \circ h(\boldsymbol{e}_\xi, t_s) \tag{2.16a}$$

$$\acute{\tilde{\boldsymbol{x}}}_m = f_{x_m} \circ h(\boldsymbol{e}_\xi, t_s) - f_{r_x}(t_s) \tag{2.16b}$$

$$\acute{\tilde{\boldsymbol{\theta}}}_x = f_{\hat{\theta}_x} \circ h(\boldsymbol{e}_\xi, t_s) - f_{\theta_x}(t_s) \tag{2.16c}$$

$$\epsilon\acute{\boldsymbol{e}}_z = f_z \circ h(\boldsymbol{e}_\xi, \boldsymbol{e}_\eta, t_s, \epsilon) - f_{z_m} \circ h(\boldsymbol{e}_\xi, \boldsymbol{e}_\eta, t_s) \tag{2.16d}$$

$$\epsilon\acute{\tilde{\boldsymbol{z}}}_m = f_{z_m} \circ h(\boldsymbol{e}_\xi, \boldsymbol{e}_\eta, t_s) - \epsilon f_{z_s} \circ h(\boldsymbol{e}_\xi, \boldsymbol{e}_\eta, t_s) \tag{2.16e}$$

$$\epsilon\acute{\tilde{\boldsymbol{\theta}}}_z = f_{\hat{\theta}_z} \circ h(\boldsymbol{e}_\xi, \boldsymbol{e}_\eta, t_s) - f_{\theta_z}(t_f) \tag{2.16f}$$

This system can be written simply as

$$\acute{\boldsymbol{e}}_\xi = f_{e_\xi}(\boldsymbol{e}_\xi, \boldsymbol{e}_\eta, t_s) \tag{2.17a}$$

$$\epsilon\acute{\boldsymbol{e}}_\eta = f_{e_\eta}(\boldsymbol{e}_\xi, \boldsymbol{e}_\eta, t_s, \epsilon) \tag{2.17b}$$

or even simpler

$$\acute{\boldsymbol{e}}_{\phi} = f_{e_{\phi}}(\boldsymbol{e}_{\phi}, t_s, \epsilon) \tag{2.18}$$

where f_{e_ξ}, f_{e_η}, and $f_{\boldsymbol{e}_\phi}$ are defined such that Eqs. (2.17) and (2.18) are identitically equal to the vector field in Eq. (2.16). This last option obscures the timescale behavior because $\mathcal{O}(f_{\boldsymbol{e}_\phi}) \neq \mathcal{O}(1)$. Equation (2.17) is recognizable as a singularly perturbed system of the type typically studied by multiple-timescale control researchers. Traditional analysis tools are applicable. However, because the form of Eq. (2.16) is available, additional insights are available.

Let the subscript s be used to denote a variable or vector field on the slow subsystem manifold. For example $\boldsymbol{e}_{\eta,s}$ represents $\boldsymbol{e}_\eta$ when $\boldsymbol{z} = \boldsymbol{z}_m = \boldsymbol{z}_s$. Similarly, let the subscript f represent a variable or vector field on the fast subsystem manifold.

The augmented reduced slow subsystem in error coordinates can be found by setting $\epsilon = 0$ and $\boldsymbol{z} = \boldsymbol{z}_m = \boldsymbol{z}_s$

$$\acute{\boldsymbol{e}}_x = f_x \circ h(\boldsymbol{e}_\xi, \boldsymbol{e}_{\eta,s}, t_s) - f_{x_m} \circ h(\boldsymbol{e}_\xi, t_s) \tag{2.19a}$$

$$\acute{\hat{\boldsymbol{x}}}_m = f_{x_m} \circ h(\boldsymbol{e}_\xi, t_s) - f_{r_x}(t_s) \tag{2.19b}$$

$$\acute{\hat{\boldsymbol{\theta}}}_x = f_{\hat{\theta}_x} \circ h(\boldsymbol{e}_\xi, t_s) - f_{\theta_x}(t_s) \tag{2.19c}$$

This reduced slow subsystem can be written simply as

$$\acute{\boldsymbol{e}}_\xi = f_{e_\xi,s}(\boldsymbol{e}_\xi, \boldsymbol{e}_{\eta,s}, t_s) \tag{2.20}$$

where $f_{e_\xi,s}$ is defined such that Eq. (2.20) is identitically equal to the vector field in Eq. (2.19). Equation (2.20) looks very similar to Eqs. (2.17) and (2.18), but it represents a fundamentally different vector field. This vector field is only defined on a subset of the full-order domain (i.e where $\boldsymbol{z} = \boldsymbol{z}_m = \boldsymbol{z}_s$).

The augmented reduced fast subsystem in error coordinates is

$$\grave{\boldsymbol{e}}_x = 0 \tag{2.21a}$$

$$\grave{\tilde{\boldsymbol{x}}}_m = 0 \tag{2.21b}$$

$$\grave{\tilde{\boldsymbol{\theta}}}_x = 0$$

$$\grave{\boldsymbol{e}}_z = f_z \circ h(\boldsymbol{e}_\xi, \boldsymbol{e}_\eta, t_s, 0) - f_{z_m} \circ h(\boldsymbol{e}_\xi, \boldsymbol{e}_\eta, t_s) \tag{2.21c}$$

$$\grave{\tilde{\boldsymbol{z}}}_m = f_{z_m} \circ h(\boldsymbol{e}_\xi, \boldsymbol{e}_\eta, t_s) - 0 \tag{2.21d}$$

$$\grave{\tilde{\boldsymbol{\theta}}}_z = f_{\hat{\theta}_z} \circ h(\boldsymbol{e}_\xi, \boldsymbol{e}_\eta, t_s) - f_{\theta_z}(t_f) \tag{2.21e}$$

This reduced fast subsystem can be written simply as

$$\grave{\boldsymbol{e}}_\xi = f_{e_\xi, f}(\boldsymbol{e}_\xi, \boldsymbol{e}_\eta, t_f) \tag{2.22a}$$

$$\grave{\boldsymbol{e}}_\eta = f_{e_\eta, f}(\boldsymbol{e}_\xi, \boldsymbol{e}_\eta, t_f) \tag{2.22b}$$

or even simpler

$$\acute{\boldsymbol{e}}_\phi = f_{e_\phi, f}(\boldsymbol{e}_\phi, t_f) \tag{2.23}$$

where $f_{e_\xi, f}$, $f_{e_\eta, f}$, and $f_{\boldsymbol{e}_\phi, f}$ are defined such that Eqs. (2.22) and (2.23) are identitically equal to the vector field in Eq. (2.21). Finally, in the reduced fast subsystem

$$\grave{\boldsymbol{r}}_x = 0 \tag{2.24a}$$

$$\grave{\boldsymbol{\theta}}_x = 0 \tag{2.24b}$$

$$\grave{\boldsymbol{z}}_s = 0 \tag{2.24c}$$

by assumptions 2.2 and 2.3

2.2.2 Differential Geometry

Differential geometry is a natural fit for the analysis of singularly perturbed systems. The differential equations which describe these systems form nonautonomous vector fields on a topological manifold. To this point, the term manifold has been used somewhat informally. The term *manifold* will continue to be used to refer to $\boldsymbol{z}_s$, but it is worth noting that the reduced subsystems form differential submanifolds embedded within the full-order system manifold in the topological sense. In this light, it is clear that g_s is a diffeomorphic chart between the full-order manifold ($\mathcal{M}$) and the reduced slow manifold ($\mathcal{M}_s$). The chart between the full-order manifold and the reduced fast manifold ($\mathcal{M}_f$) is the trivial automorphism. The stability analysis to follow will involve the time derivative of Lyapunov functions along a vector field that is a subset of the tangent bundle of one of these topological manifolds. The notation $\mathcal{L}(\cdot)$ is used to represent the Lie derivative along the vector field given in the parentheses (the traditional subscript notation is not used to ensure the subscripts on the functions are readable). Let $|(\cdot)|_p$ be the l_p norm of a vector or the induced l_p norm of a matrix and let $\|(\cdot)\|_p$ be the L_p norm over time where $p \in [1, \infty]$. If the L_p norm is applied to a vector then it means the L_p norm of each component of the vector. Unless otherwise specified, all sets are subsets of the Euclidean Hilbert space with the dimension given in the superscript. An integer subscript $(\cdot)_i$ on a variable (not to be confused with the subscript on the p-norms) represents the i^{th} element of the vector.

2.2.3 The Manifold and The Reference Model

The stability proofs in the next section are significantly complicated by the relationship between the manifold and the fast reference model. Traditional multiple-timescale control and adaptive control both use a feedback loop to ensure closed-loop stability. These feedback loops still exist in the KAMS control architecture. Figure 2.1 is a copy of the block diagram for KAMS from Fig. 1.2 except the traditional feedback loop has been highlighted. All paths which contribute to this loop are bolded but the primary loop is blue. However, KAMS has a second unconventional feedback loop. This occurs because the fast reference model uses the manifold as an input (see

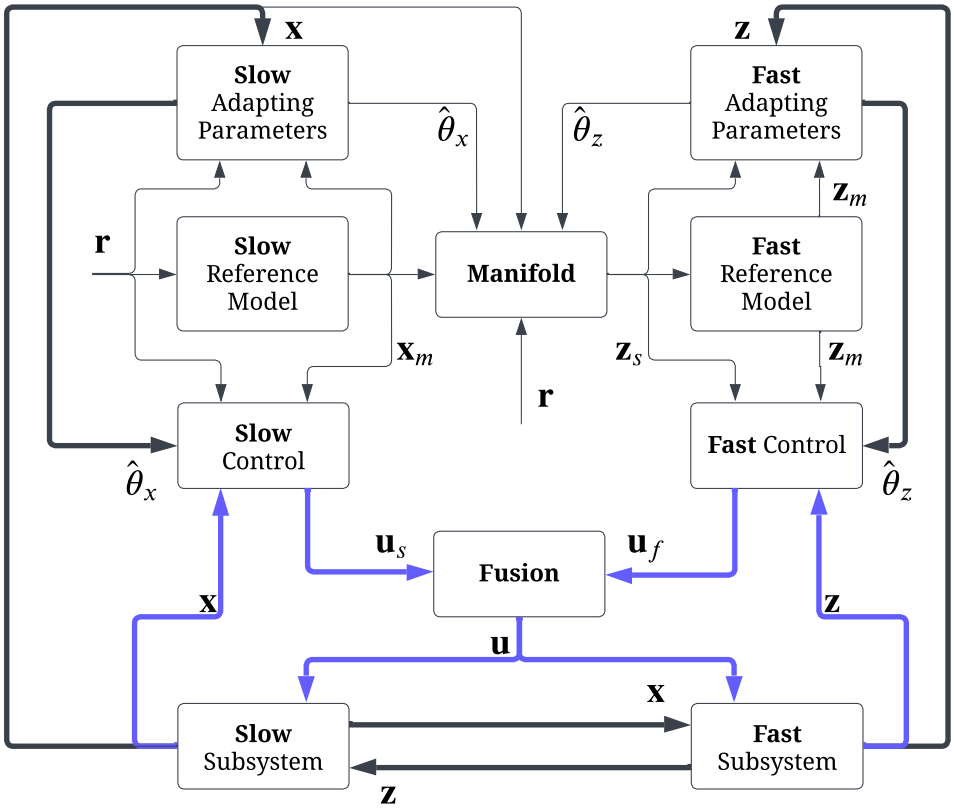

Figure 2.1: The primary feedback loop of KAMS.

Fig. 1.2), the manifold is a function of the slow states (see Eq. (2.9)), the slow states are coupled with the fast states, and the control objective is for the fast states to track the fast reference model which is itself a function of the manifold. This creates a feedback loop that is typically not seen in adaptive control. Figure 2.2 highlights this feedback loop. Again, all paths which contribute to this loop are bolded but the primary unconventional loop is red.

The reference model adds a complication that is not observed in multiple-timescale control. If the fast reference model is not asymptotically stable then the steady state trajectory for the slow states may not be the slow subsystem. This calls into question the validity of the slow subsystem and means that the multple timescale fusion stability proofs in prior work are not applicable (e.g. Theorem 1.1). These effects are unavoidable because the full-order stability analysis works by extending the stability of the reduced subsystems to the full-order system. The slow subsystem

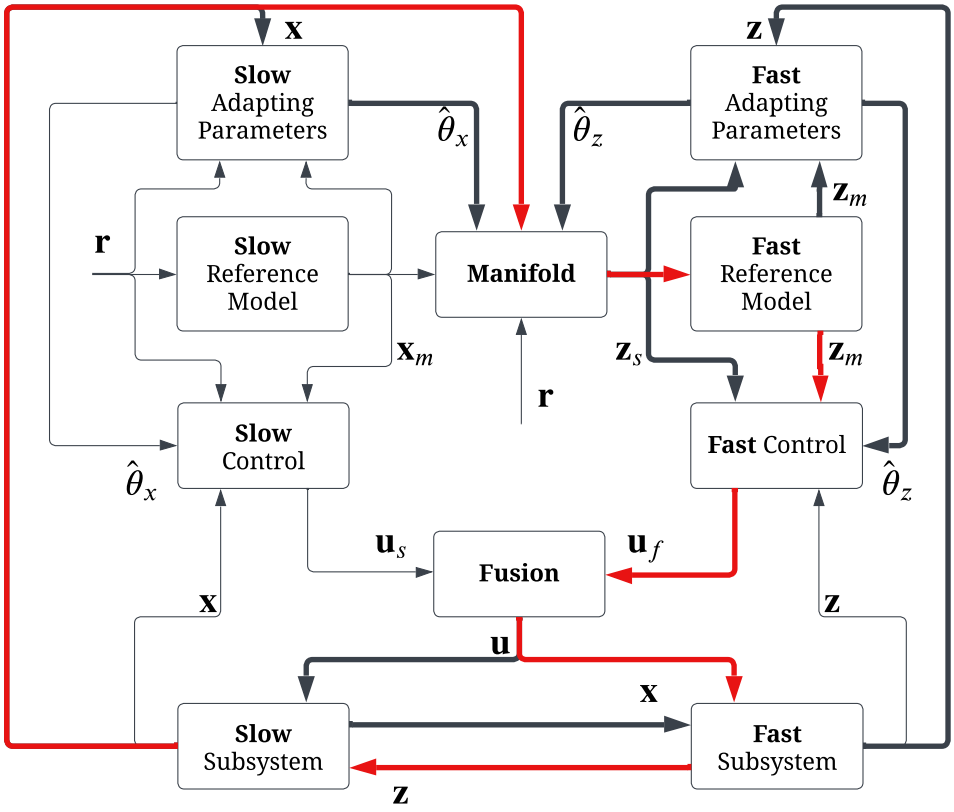

Figure 2.2: The unconventional feedback loop of KAMS.

assumes that the fast states have reached their manifold. Therefore, if the stability of the reduced slow subsystem is to have any bearing on the full-order system then the fast reference model must converge to that manifold. This is the purpose of Assumption 2.1. Reference models are rarely asymptotically stable when their input is time-varying. (Reference models are typically type 1 linear systems so they are only capable of tracking a step input with zero steady-state error.) However, closer examination reveals that Assumption 2.1 is not as restrictive as it seems. Recall that the manifold is assumed to evolve on the slow timescale. Equation (2.24c) shows that in the fast timescale $\dot{z}_s = 0$. Thus the manifold is stationary in the reduced fast subsystem, and even a type 1 reference model can be asymptotically stable. Assumption 2.1 is usually satisfied. The full-order system does not benefit from this simplification. The steady-state value of $\tilde{z}_m$ influences the form and function of the full-order stability proofs in section 2.2.4. Three cases are studied:

Case 1: *No prior assumptions about the stability of the fast reference model in relation to the full-order manifold.* This is the most general case considered, but also has the most restrictive conditions. This case often requires the control objective to be downgraded to a regulation problem.

Case 2: *The fast reference model is always on the manifold.* This case most commonly occurs when adaptive control is not necessary for the fast subsystem. In this case, the fast control drives the fast states directly to the manifold. This type of control can be modeled by setting $\tilde{\boldsymbol{z}}_m = 0$ and $\dot{\hat{\boldsymbol{\theta}}}_z = 0$. (A parallel simplification exists where there the slow control is non-adaptive, $\tilde{\boldsymbol{x}}_m = 0$, and $\dot{\hat{\boldsymbol{\theta}}}_x = 0$ but this still falls within Case 1 above.)

Case 3: *The manifold is an asymptotically stable equilibrium of the fast state reference model in the context of the full-order system.* This is possible but requires an unusual reference model. This case is a slightly stricter version of Assumption 2.1 which only requires asymptotic stability in a subset of the domain.

Remark 2.1 - *In this dissertation, stating that the slow subsystem does not require adaptive control will be equivalent to saying $\tilde{\boldsymbol{x}}_m = 0$ and $\dot{\hat{\boldsymbol{\theta}}}_x = 0$. Similarly, stating that the fast subsystem does not require adaptive control will be equivalent to saying $\tilde{\boldsymbol{z}}_m = 0$ and $\dot{\hat{\boldsymbol{\theta}}}_z = 0$. This terminology may be slightly misleading because there exists model-free adaptive control algorithms (e.g. [78]) and there exists non-adaptive control methods which require reference models (e.g. Feedback Linearization [18]). However, the intricacies of these methods are not in the scope of this work.*

2.2.4 Full-Order System Stability

In this section, the stability of KAMS is analyzed in the context of the full-order system. The goal is to develop conditions that, if met, extend the stability of the reduced subsystems to the full-order system. To that end, four related theorems are proven in this section. Each theory falls into one of the three cases described in the previous section. All of the theorems in this work will

make use of the vector $\boldsymbol{v} \in \mathbb{R}^4_{\geq 0}$ which is defined as

$$\boldsymbol{v} \triangleq \begin{bmatrix} |\boldsymbol{e}_x|_2 & |\tilde{\boldsymbol{x}}_m|_2 & |\boldsymbol{e}_z|_2 & |\tilde{\boldsymbol{z}}_m|_2 \end{bmatrix}^T \tag{2.25}$$

2.2.4.1 Foundation Of Reduced-Order Stability

The proofs in this section are similar to the proof proposed by [19, 20]. However, they have been significantly altered to account for adaptive control. The general process begins by generating a composite Lyapunov function using Lyapunov functions for the reduced-order subsystems. This composite Lyapunov function is then differentiated along the vector field describing the evolution of the full-order subsystem. Using the stability of the reduced subsystems it is shown that the differences between reduced subsystems and the full-order system are insufficient to violate the negative definiteness. This implies that $\boldsymbol{e}_x, \boldsymbol{e}_z \in L_\infty$ by Lyapunov's direct's method [24, Theorem 3.4.1]. The following four Lyapunov functions form the basis of this approach

$$V_{e_x}(\boldsymbol{e}_x, \tilde{\boldsymbol{\theta}}_x, t_s) : \mathbb{B}^{n_x}(r_{e_x}) \times \mathbb{B}^{n_{\theta_x}}(r_{\tilde{\theta}_x}) \times \mathbb{R}_+ \to \mathbb{R}_{\geq 0} \tag{2.26a}$$

$$V_{\tilde{x}_m}(\tilde{\boldsymbol{x}}_m, t_s) : \mathbb{B}^{n_x}(r_{x_m}) \times \mathbb{R}_+ \to \mathbb{R}_{\geq 0} \tag{2.26b}$$

$$V_{e_z}(\boldsymbol{e}_z, \tilde{\boldsymbol{\theta}}_z, t_f) : \mathbb{B}^{n_z}(r_{e_z}) \times \mathbb{B}^{n_{\theta_z}}(r_{\tilde{\theta}_z}) \times \mathbb{R}_+ \to \mathbb{R}_{\geq 0} \tag{2.26c}$$

$$V_{\tilde{z}_m}(\tilde{\boldsymbol{z}}_m, t_f) : \mathbb{B}^{n_z}(r_{\tilde{z}_m}) \times \mathbb{R}_+ \to \mathbb{R}_{\geq 0} \tag{2.26d}$$

These Lyapunov functions are positive definite functions of class C^1 (i.e. the function and its derivative are continuous) where $V_{e_x}(0, 0, t_s) = V_{\tilde{x}_m}(0, t_s) = V_{e_z}(0, 0, t_f) = V_{\tilde{z}_m}(0, t_f) = 0$. Let the adaptive control for the reduced subsystems be defined such that

$$\frac{\partial V_{e_x}}{\partial t_s} + \mathcal{L}(f_{e_\xi, s}) V_{e_x} \leq -\alpha_1 |\boldsymbol{e}_x|_2^2 \tag{2.27a}$$

$$\frac{\partial V_{e_z}}{\partial t_f} + \mathcal{L}(f_{e_\eta, f}) V_{e_z} \leq -\alpha_3 |\boldsymbol{e}_z|_2^2 \tag{2.27b}$$

$$\frac{\partial V_{\tilde{z}_m}}{\partial t_f} + \mathcal{L}(f_{z_m, f}) V_{\tilde{z}_m} \leq -\alpha_4 |\tilde{\boldsymbol{z}}_m|_2^2 \tag{2.27c}$$

for some $\alpha_1, \alpha_3, \alpha_4 \in \mathbb{R}_+$. The following assumption is now made:

Assumption 2.4 - *The Lyapunov functions V_{e_x}, V_{e_z}, and as needed $V_{\tilde{z}_m}$ are known and exist such that Eq.* (2.27) *is satisfied.*

Note that the existence of $V_{\tilde{z}_m}$ such that Eq. (2.27c) holds is sufficient to guarantee that Assumption 2.1 is satisfied. After the Lyapunov analysis, Barbalet's Lemma is used to prove convergence [24, Lemma 3.2.5]. To that end, the following assumption is made to ensure that the conditions of Barbalet's Lemma are satisfied:

Assumption 2.5 - *The functions defined in this chapter are sufficiently smooth and bounded. Sufficiently smooth means that the function is continuously differentiable as many times as necessary. Sufficiently bounded means that, as necessary, the domain of a function being in L_∞ is sufficient to imply that the function's range is also in L_∞.*

The definitions above are a formal way of saying, and indeed imply that the adaptive control for the reduced subsystems is well designed. This conclusion only applies to the reduced subsystems.

2.2.4.2 Case 1

No prior assumptions about the stability of the fast reference model in relation to the full-order manifold.

Theorem 2.1 - *Assume $\exists \alpha_2 \in \mathbb{R}_+$, $\exists \beta \in \mathbb{R}_{\geq 0}$, and $\exists \boldsymbol{\gamma}, \boldsymbol{\delta} \in \mathbb{R}^4_{\geq 0}$ such that*

$$\frac{\partial V_{\tilde{x}_m}}{\partial t_s} + \mathcal{L}(f_{\tilde{x}_m}) V_{\tilde{x}_m} \leq -\alpha_2 |\tilde{\boldsymbol{x}}_m|_2^2 \tag{2.28a}$$

$$\mathcal{L}(f_x - f_{x,s}) V_{e_x} \leq \beta |\boldsymbol{e}_x|_2 |\tilde{\boldsymbol{z}}|_2 \tag{2.28b}$$

$$\mathcal{L}(f_z - f_{z,f}) V_{e_z} \leq \epsilon \boldsymbol{\gamma}^T \boldsymbol{v} |\boldsymbol{e}_z|_2 \tag{2.28c}$$

$$-\mathcal{L}(f_{z_s}) V_{\tilde{z}_m} \leq \boldsymbol{\delta}^T \boldsymbol{v} |\tilde{\boldsymbol{z}}_m|_2 \tag{2.28d}$$

Let the matrix $K = K^T$ be defined as

$$K \triangleq \begin{bmatrix} d^*\alpha_1 & 0 & -\frac{1}{2}(d^*\beta + d\gamma_1) & -\frac{1}{2}(d^*\beta + d\delta_1) \\ & d^*\alpha_2 & -\frac{1}{2}d\gamma_2 & -\frac{1}{2}d\delta_2 \\ & & \frac{d}{\epsilon}\alpha_3 - d\gamma_3 & -\frac{1}{2}(d\delta_3 + d\gamma_4) \\ \textit{Symmetric} & & & \frac{d}{\epsilon}\alpha_4 - d\delta_4 \end{bmatrix} \tag{2.29}$$

If $\exists d \in (0,1)$ and $d^* \triangleq (1-d)$ such that K is positive definite, then $\boldsymbol{e}_x, \boldsymbol{e}_z \to 0$ as $t \to \infty$.

Proof. Define a composite Lyapunov function

$$V \triangleq d^*(V_{e_x} + V_{\tilde{x}_m}) + d(V_{e_z} + V_{\tilde{z}_m}) \tag{2.30}$$

Differentiate along the full-order system

$$\acute{V} = d^* \left(\frac{\partial V_{e_x}}{\partial t_s} + \frac{\partial V_{\tilde{x}_m}}{\partial t_s} \right) + d \left(\frac{\partial V_{e_z}}{\partial t_s} + \frac{\partial V_{\tilde{z}_m}}{\partial t_s} \right) \tag{2.31a}$$

$$+ d^*\mathcal{L}(f_{e_\phi})(V_{e_x} + V_{\tilde{x}_m}) + d\mathcal{L}(f_{e_\phi})(V_{e_z} + V_{\tilde{z}_m}) \tag{2.31b}$$

Add and subtract $d^*\mathcal{L}(f_{e_\phi,s})(V_{e_x} + V_{\tilde{x}_m}) + d\mathcal{L}(f_{e_\phi,f})(V_{e_z} + V_{\tilde{z}_m})$

$$\begin{aligned} \acute{V} = {} & d^* \left(\frac{\partial V_{e_x}}{\partial t_s} + \frac{\partial V_{\tilde{x}_m}}{\partial t_s} \right) + d \left(\frac{\partial V_{e_z}}{\partial t_s} + \frac{\partial V_{\tilde{z}_m}}{\partial t_s} \right) \\ & + d^*\mathcal{L}(f_{e_\phi,s})(V_{e_x} + V_{\tilde{x}_m}) \\ & + d^*\mathcal{L}(f_{e_\phi} - f_{e_\phi,s})(V_{e_x} + V_{\tilde{x}_m}) \\ & + d\mathcal{L}(f_{e_\phi,f})(V_{e_z} + V_{\tilde{z}_m}) \\ & + d\mathcal{L}(f_{e_\phi} - f_{e_\phi,f})(V_{e_z} + V_{\tilde{z}_m}) \end{aligned} \tag{2.32}$$

Conceptually this is the derivative in the subsystems plus some errors due to inaccuracies in the

model reduction. Rearranging gives

$$\begin{aligned}\acute{V} = & d^* \left(\frac{\partial V_{e_x}}{\partial t_s} + \mathcal{L}(f_{e_\phi,s}) V_{e_x} + \frac{\partial V_{\tilde{x}_m}}{\partial t_s} + \mathcal{L}(f_{e_\phi,s}) V_{\tilde{x}_m} \right) \\ & + d^* \mathcal{L}(f_{e_\phi} - f_{e_\phi,s}) V_{e_x} + d^* \mathcal{L}(f_{e_\phi} - f_{e_\phi,s}) V_{\tilde{x}_m} \\ & + d \left(\frac{\partial V_{e_z}}{\partial t_s} + \mathcal{L}(f_{e_\phi,f}) V_{e_z} + \frac{\partial V_{\tilde{z}_m}}{\partial t_s} + \mathcal{L}(f_{e_\phi,f}) V_{\tilde{z}_m} \right) \\ & + d \mathcal{L}(f_{e_\phi} - f_{e_\phi,f}) V_{e_z} + d \mathcal{L}(f_{e_\phi} - f_{e_\phi,f}) V_{\tilde{z}_m} \end{aligned} \tag{2.33}$$

Some of these terms can be simplified because each Lyapunov function is not a function of all state variables (i.e. its partial derivative is zero). In doing so, ϵ must be carefully accounted for.

$$\begin{aligned}\acute{V} = & d^* \left(\frac{\partial V_{e_x}}{\partial t_s} + \mathcal{L}(f_{e_\xi,s}) V_{e_x} + \frac{\partial V_{\tilde{x}_m}}{\partial t_s} + \mathcal{L}(f_{\tilde{x}_m,s}) V_{\tilde{x}_m} \right) \\ & + d^* \mathcal{L}(f_{e_\xi} - f_{e_\xi,s}) V_{e_x} + d^* \mathcal{L}(f_{\tilde{x}_m} - f_{\tilde{x}_m,s}) V_{\tilde{x}_m} \\ & + \frac{d}{\epsilon} \left(\frac{\partial V_{\tilde{z}_m}}{\partial t_f} + \mathcal{L}(f_{e_\eta,f}) V_{e_z} + \frac{\partial V_{\tilde{z}_m}}{\partial t_f} + \mathcal{L}(f_{\tilde{z}_m,f}) V_{\tilde{z}_m} \right) \\ & + \frac{d}{\epsilon} \mathcal{L}(f_{e_\eta} - f_{e_\eta,f}) V_{e_z} + \frac{d}{\epsilon} \mathcal{L}(f_{\tilde{z}_m} - f_{\tilde{z}_m,f}) V_{\tilde{z}_m} \end{aligned} \tag{2.34}$$

Some of the vector fields are the same in the reduced subsystem and the full-order subsystem. This allows further simplification

$$\begin{aligned}\acute{V} = & d^* \left(\frac{\partial V_{e_x}}{\partial t_s} + \mathcal{L}(f_{e_\xi,s}) V_{e_x} + \frac{\partial V_{\tilde{x}_m}}{\partial t_s} + \mathcal{L}(f_{\tilde{x}_m}) V_{\tilde{x}_m} \right) \\ & + d^* \mathcal{L}(f_x - f_{x,s}) V_{e_x} \\ & + \frac{d}{\epsilon} \left(\frac{\partial V_{\tilde{z}_m}}{\partial t_f} + \mathcal{L}(f_{e_\eta,f}) V_{e_z} + \frac{\partial V_{\tilde{z}_m}}{\partial t_f} + \mathcal{L}(f_{\tilde{z}_m,f}) V_{\tilde{z}_m} \right) \\ & + \frac{d}{\epsilon} \mathcal{L}(f_z - f_{z,f}) V_{e_z} - d \mathcal{L}(f_{z_s}) V_{\tilde{z}_m} \end{aligned} \tag{2.35}$$

Table 2.1: Proof that the conditions of Barbalat's Lemma are met.

Condition	Argument
$\boldsymbol{e}_\phi, \acute{V} \in L_\infty$	Lyapunov's Direct Method
$\acute{\boldsymbol{e}}_\phi \in L_\infty$	Assumption 2.5
$\exists \lambda \in \mathbb{R}_+$ s.t. $\acute{\nu} \leq -\lambda \lvert \boldsymbol{v} \rvert_2^2$	K is positive definite
$\lvert \boldsymbol{e}_x \rvert_2, \lvert \tilde{\boldsymbol{x}}_m \rvert_2, \lvert \boldsymbol{e}_z \rvert_2, \lvert \tilde{\boldsymbol{z}}_m \rvert_2 \in L_2$	Lemma A.1
$\lvert \boldsymbol{e}_x \rvert_2, \lvert \tilde{\boldsymbol{x}}_m \rvert_2, \lvert \boldsymbol{e}_z \rvert_2, \lvert \tilde{\boldsymbol{z}}_m \rvert_2 \in L_1$	Lemma A.2
$\boldsymbol{e}_x, \boldsymbol{x}_m, \boldsymbol{e}_z, \tilde{\boldsymbol{z}}_m \in L_2$	Lemma A.2
$\boldsymbol{e}_x, \boldsymbol{x}_m, \boldsymbol{e}_z, \tilde{\boldsymbol{z}}_m \to 0$ as $t \to \infty$	Barbalat's Lemma

Substituting the conditions from Eqs. (2.27) and (2.28) gives:

$$\begin{aligned}
\acute{V} \leq & -d^* \alpha_1 \lvert \boldsymbol{e}_x \rvert_2^2 - d^* \alpha_2 \lvert \tilde{\boldsymbol{x}}_m \rvert_2^2 \\
& + d^* \beta \lvert \boldsymbol{e}_x \rvert_2 \lvert \tilde{\boldsymbol{z}} \rvert_2 \\
& - \frac{d}{\epsilon} \alpha_3 \lvert \boldsymbol{e}_z \rvert_2^2 - \frac{d}{\epsilon} \alpha_4 \lvert \tilde{\boldsymbol{z}}_m \rvert_2^2 \\
& + \frac{d}{\epsilon} \epsilon \boldsymbol{\gamma}^T \boldsymbol{v} \lvert \boldsymbol{e}_z \rvert_2 + d \boldsymbol{\delta}^T \boldsymbol{v} \lvert \tilde{\boldsymbol{z}}_m \rvert_2
\end{aligned} \tag{2.36}$$

The triangle inequality shows that $\lvert \tilde{\boldsymbol{z}} \rvert_2 \leq \lvert \boldsymbol{e}_z \rvert_2 + \lvert \tilde{\boldsymbol{z}}_m \rvert_2$. Using this and rearranging gives

$$\acute{V} \leq -\boldsymbol{v}^T K \boldsymbol{v} \tag{2.37}$$

Thus, by Lyapunov's direct method, $\boldsymbol{e}_\phi \in L_\infty$ The goal now is to show that the conditions of Barbalat's Lemma are satisfied. This is done by showing that $\boldsymbol{e}_x, \boldsymbol{e}_z, \acute{\boldsymbol{e}}_x, \acute{\boldsymbol{e}}_z \in L_\infty$ and $\boldsymbol{e}_x, \boldsymbol{e}_z \in L_2$. By the arguments in table 2.1 it can be concluded that these conditions are met. Note that the order of the lines in this table is significant. See the appendix for proof of Lemmas A.1 and A.2. Thus, via Barbalat's Lemma, it is known that $\boldsymbol{e}_x, \boldsymbol{e}_z \to 0$ as $t \to \infty$. □

Corollary 2.1 - *Let the plant exist such that the reduced slow subsystem does not require adaptive*

control (i.e. $\tilde{\boldsymbol{x}}_m = 0$ *and* $\dot{\tilde{\boldsymbol{\theta}}}_x = 0$*). Assume that conditions* (2.28b)*,* (2.28c)*, and* (2.28d) *of Theorem 2.1 are true. Let the matrix* $K = K^T$ *be defined as*

$$K \triangleq \begin{bmatrix} d^*\alpha_1 & -\frac{1}{2}(d^*\beta + d\gamma_1) & -\frac{1}{2}(d^*\beta + d\delta_1) \\ & \frac{d}{\epsilon}\alpha_3 - d\gamma_3 & -\frac{1}{2}(d\delta_3 + d\gamma_4) \\ \textit{Symmetric} & & \frac{d}{\epsilon}\alpha_4 - d\delta_4 \end{bmatrix} \tag{2.38}$$

If $\exists d \in (0,1)$ *and* $d^* \triangleq (1-d)$ *such that* K *is positive definite, then* $\boldsymbol{e}_x, \boldsymbol{e}_z \to 0$ *as* $t \to \infty$*.*

Proof. The proof proceeds exactly as Theorem 2.1 except $V_{\tilde{x}_m} = 0$. Also, because $\tilde{\boldsymbol{x}}_m = 0$ it follows that $\gamma_2 = 0$ and $\delta_2 = 0$. □

Each of the following proofs assumes that $f_z - f_{z,f} = 0$ which occurs when ϵ does not appear on the right side of Equation (1.1b). This is very common and making this assumption will aid in interpreting the results.

2.2.4.3 Case 2

The fast reference model is always on the manifold.

Corollary 2.2 - *Let the plant exist such that the reduced fast subsystem does not require adaptive control (*$\tilde{\boldsymbol{z}}_m = 0$ *and* $\dot{\tilde{\boldsymbol{\theta}}}_z = 0$*) and* ϵ *does not appear on the right side of Equation* (1.1b)*. Assume that condition* (2.28b) *of Theorem 2.1 is true. Then* $\forall \epsilon$ *it is true that* $\boldsymbol{e}_x, \boldsymbol{e}_z \to 0$ *as* $t \to \infty$*.*

Proof. The proof proceeds exactly as Theorem 2.1 except $\boldsymbol{\gamma} = 0$ and $\tilde{\boldsymbol{z}}_m = 0$. This reduces the matrix $K = K^T$ to

$$K \triangleq \begin{bmatrix} d^*\alpha_1 & -\frac{1}{2}d^*\beta \\ -\frac{1}{2}d^*\beta & \frac{d}{\epsilon}\alpha_3 \end{bmatrix} \tag{2.39}$$

where $V_{\tilde{x}_m}$ has been dropped because all of the cross terms of $\tilde{\boldsymbol{x}}_m$ have been removed. This is simple enough for additional conclusions. By Sylvester's Criterion K is positive definite if and only if the leading principle minors (LPM) are positive [95]. This gives rise to the following two

inequalities which, if satisfied, imply that K is positive definite.

$$0 < d^* \alpha_1 \tag{2.40a}$$

$$0 < \frac{d(1-d)\alpha_1 \alpha_3}{\epsilon} - \frac{1}{4}(1-d)^2 \beta^2 \tag{2.40b}$$

Inequality Eq. (2.40a) is satisfied by definition. Rearranging inequality Eq. (2.40b) gives

$$\epsilon < \frac{4d\alpha_1 \alpha_3}{(1-d)\beta^2} \tag{2.41}$$

when $\beta \neq 0$. When $\beta = 0$ then inequality Eq. (2.40b) is satisfied by definition. Recall that d is arbitrary. So, $\forall \epsilon \; \exists d$ such that inequality Eq. (2.41) is satisfied. Continuing with Barbalet's Lemma as in Theorem 2.1 gives that $\boldsymbol{e}_x, \boldsymbol{e}_z \to 0$ as $t \to \infty$. □

2.2.4.4 Case 3

> *The manifold is an asymptotically stable equilibrium of the fast state reference model in the context of the full-order system.*

Corollary 2.3 - *Assume that ϵ does not appear on the right side of Equation* (1.1b)*. Assume that condition* (2.28b) *of Theorem 2.1 is true. If $\exists \alpha_4 \in \mathbb{R}_+$ such that*

$$\mathcal{L}(f_{\tilde{z}_m}) V_{\tilde{z}_m} \leq -\alpha_4 |\tilde{\boldsymbol{z}}_m|_2^2 \tag{2.42}$$

Then $\forall \epsilon$ it is true that $\boldsymbol{e}_x, \boldsymbol{e}_z \to 0$ as $t \to \infty$.

Proof. The proof largely follows Theorem 2.1 except $V_{\tilde{x}_m}$ is removed from the composite Lyapunov function. Before reaching Eq. (2.35), Eq. (2.34) can be rewritten using $\mathcal{L}(f_{\tilde{z}_m} - f_{\tilde{z}_m,f}) V_{\tilde{z}_m} +$

$\mathcal{L}(f_{\tilde{z}_m,f})V_{\tilde{z}_m} = \mathcal{L}(f_{\tilde{z}_m})V_{\tilde{z}_m}$. Continuing to follow the proof of Theorem 2.1 gives

$$K \triangleq \begin{bmatrix} d^*\alpha_1 & -\frac{1}{2}d^*\beta & -\frac{1}{2}d^*\beta \\ -\frac{1}{2}d^*\beta & \frac{d}{\epsilon}\alpha_3 & 0 \\ -\frac{1}{2}d^*\beta & 0 & \frac{d}{\epsilon}\alpha_4 \end{bmatrix} \tag{2.43}$$

This is simple enough for additional conclusions. By Sylvester's Criterion K is positive definite if and only if the LPMs are positive. This gives rise to the following three inequalities which, if satisfied, imply that K is positive definite.

$$0 < d^*\alpha_1 \tag{2.44a}$$

$$0 < \frac{d(1-d)\alpha_1\alpha_3}{\epsilon} - \frac{1}{4}(1-d)^2\beta^2 \tag{2.44b}$$

$$0 < \frac{d^2(1-d)}{\epsilon^2}\alpha_1\alpha_3\alpha_4 - \frac{d(1-d)^2}{4\epsilon}(\alpha_3+\alpha_4)\beta^2 \tag{2.44c}$$

Inequality Eq. (2.40a) is satisfied by definition. Rearranging the other two inequalities gives

$$\epsilon < \frac{4d\alpha_1\alpha_3}{(1-d)\beta^2} \tag{2.45a}$$

$$\epsilon < \frac{4d\alpha_1\alpha_3\alpha_4}{(1-d)(\alpha_3+\alpha_4)\beta^2} \tag{2.45b}$$

when $\beta \neq 0$. When $\beta = 0$ then inequalities (2.44b) and (2.44c) are satisfied by definition. Recall that d is arbitrary. So, $\forall\epsilon\ \exists d$ such that the inequalities in Eq. (2.45) are satisfied. Continuing with Barbalet's Lemma as in Theorem 2.1 gives that $\boldsymbol{e}_x, \boldsymbol{e}_z \to 0$ as $t \to \infty$. □

Remark 2.2 - *Assumption 2.2 places bounds on the acceptable range of the adaptation gains. Note that ϵ is not required to implement the control. This is advantageous because ϵ can be difficult to determine. However, a rough approximation of ϵ allows the engineer to design the adaptive laws and reference models so that they evolve on the correct timescale. Beyond these conditions, ϵ is allowed to be uncertain.*

Remark 2.3 - *The condition that K be positive definite limits the range of acceptable timescale separation parameters (e.g. see [19]). However, for Theorem 2.1 and Corollary 2.1 the analytical solution would be complex.*

Remark 2.4 - *Corillaries 2.1 and 2.2 study the case where only one subsystem requires adaptive control. If neither subsystem requires adaptive control then Theorem 2.1 reduces to Theorem 1.1.*

Remark 2.5 - *Systems which use adaptive control are likely to be nonstandard because adaptive control is specifically designed for systems with model uncertainties. Thus it is common for the open-loop manifold to be uncertain even if the system is standard in the traditional sense. Let the term* uncertain nonstandard *refer to this condition. Recent multiple-timescale control research has addressed nonstandard systems [9]. Both Sequential Control and Simultaneous Slow and Fast Tracking are nonstandard methods because the manifold is specified. Composite Control, on the other hand, requires that the open-loop manifold be known apriori. The manifold must be measured or analytically available. Thus Composite Control is well suited for systems that do not require adaptive control in the fast subsystem.*

2.3 Validation

An example demonstrates and validates this method. Consider the following nonlinear nonstandard uncertain dynamical system

$$\acute{x} = -(x^2 + 1)z \tag{2.46a}$$

$$\epsilon\acute{z} = \theta x z + u \tag{2.46b}$$

where $\theta \in \mathbb{R}_+$ is an uncertain parameter. The control objective is for x to track the following reference model

$$\acute{x}_m = -a_x(x_m - r_x) \tag{2.47}$$

where $a_x \in \mathbb{R}_+$.

2.3.1 Control Synthesis

The reduced slow subsystem is

$$\acute{x} = -(x^2 + 1)z_s \tag{2.48a}$$

and the reduced fast subsystem is

$$\grave{x} = 0 \tag{2.49a}$$

$$\grave{z} = \theta x z + u \tag{2.49b}$$

This system is uncertain nonstandard. Sequential Control is used to fuse the control signals [9]. The slow subsystem is deterministic. Using z_s as the input to the slow subsystem the manifold is chosen using Nonlinear Dynamic Inversion (NDI).

$$z_s = -(x^2 + 1)^{-1}(\acute{x}_m - k_x e_x) \tag{2.50}$$

where $k_x \in \mathbb{R}_+$ is a constant control gain. The closed-loop dynamics of the reduced slow subsystem are

$$\acute{x} = \acute{x}_m - k_x e_x \tag{2.51}$$

or equivalently

$$\acute{e}_x = -k_x e_x \tag{2.52}$$

The input can now be chosen so that it drives the fast states to this manifold. The fast subsystem is parametrically uncertain. ANDI is chosen to stabilize the fast subsystem

$$u = \grave{z}_m - \hat{\theta} x z - k_z e_z \tag{2.53}$$

where $k_z \in \mathbb{R}_+$ is a constant control gain. The adaptive law for $\hat{\theta}$ is

$$\dot{\hat{\theta}} = \gamma \, \text{Proj}(\hat{\theta}, xze_z) \tag{2.54}$$

where $\gamma \in \mathbb{R}_+$ is an adaptation rate gain. For more information on ANDI see [65, p. 6-12]. The fast state reference model is chosen to be asymptotically stable about the manifold

$$\dot{\tilde{z}}_m = -a_z \tilde{z}_m \tag{2.55}$$

or equivalently

$$\dot{z}_m = -a_z \tilde{z}_m + \dot{z}_s \tag{2.56}$$

where $a_z \in \mathbb{R}_+$. The time derivative of the manifold is

$$\dot{z}_s = \frac{2xz\epsilon}{x^2+1}(a_x \tilde{x}_m + k_x e_x) + \frac{\epsilon}{x^2+1}(-a_x(a_x \tilde{x}_m + \acute{r}_x) + k_x(-(x^2+1)z + a_x \tilde{x}_m)) \tag{2.57}$$

2.3.2 Confirmation of Full-Order Stability

Consider the candidate Lyapunov functions

$$V_{e_x} = \frac{1}{2} e_x^2 \tag{2.58a}$$

$$V_{e_z} = \frac{1}{2} e_z^2 + \frac{1}{2\gamma} \tilde{\theta}^2 \tag{2.58b}$$

$$V_{\tilde{z}_m} = \frac{1}{2} \tilde{z}_m^2 \tag{2.58c}$$

Differentiating gives

$$\mathcal{L}(f_{e_\xi,s})V_{e_x} = -k_x e_x^2 \qquad \leq -\alpha_1 |e_x|_2^2 \tag{2.59a}$$

$$\mathcal{L}(f_{e_\eta,f})V_{e_z} \leq -k_z e_z^2 \qquad \leq -\alpha_3 |e_z|_2^2 \tag{2.59b}$$

$$\mathcal{L}(f_{\tilde{z}_m})V_{\tilde{z}_m} = -a_z \tilde{z}_m \qquad \leq -\alpha_4 |\tilde{z}_m|_2^2 \tag{2.59c}$$

$$\mathcal{L}(f_x - f_{x,s})V_{e_x} = -(x^2+1)e_x \tilde{z} \qquad \leq \beta |e_x|_2 |\tilde{z}|_2 \tag{2.59d}$$

where $\alpha_1 = k_x$, $\alpha_3 = k_z$, $\alpha_4 = a_z$, and $\beta = 1$. See [65, Eqs. 1.20 to 1.23] for a derivation of Eq. (2.59b). By Corollary 2.3, $\boldsymbol{e}_x, \boldsymbol{e}_z \to 0$ as $t \to \infty$.

2.3.3 Numerical Results

A numerical simulation validates the control. The following system parameters are used

$$\theta = 0.5 \tag{2.60a}$$

$$\epsilon = 0.1 \tag{2.60b}$$

The control parameters are

$$r_x = \sin(t_s) \tag{2.61a}$$

$$a_x = k_x = a_z = k_z = \gamma = 1 \tag{2.61b}$$

The initial conditions are

$$x = z = 0.5 \tag{2.62a}$$

$$x_m = z_m = 0 \tag{2.62b}$$

$$\hat{\theta} = 0.44 \tag{2.62c}$$

The time evolution of the slow state is shown in Fig. 2.3 and the fast state is shown in Fig. 2.4. The time evolution of the adapting gain is shown in Fig. 2.5. The states and gain evolve on the proper

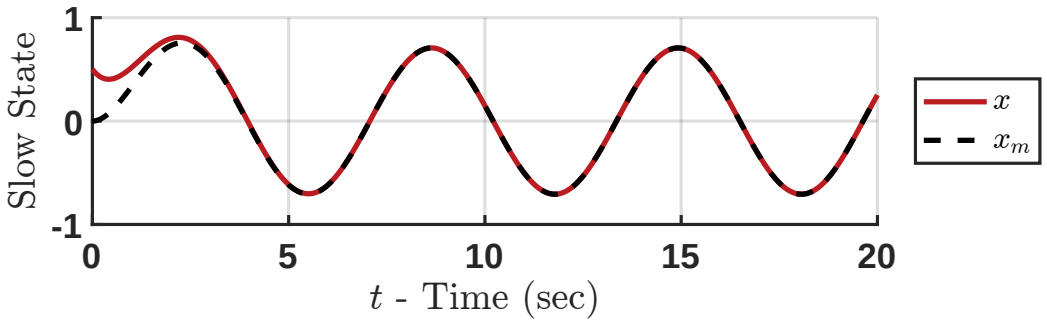

Figure 2.3: Evolution of the slow state.

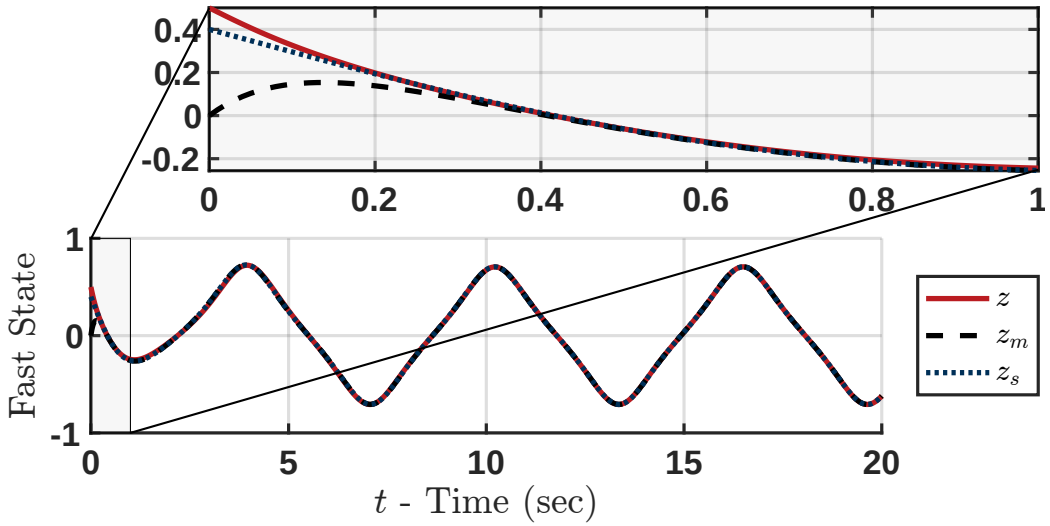

Figure 2.4: Evolution of the fast state.

timescales and the system converges asymptotically with zero steady-state error. The adapting gain also converges to the true value because the reference input is chosen to be persistently exciting, but KAMS does not require this. When implementing KAMS it is important to keep track of the timescale. For example, if the numerical integration is occurring in the slow timescale then Eqs. (2.54) and (2.56) must be scaled by a factor of ϵ^{-1}. This effectively scales the adaptation gain and reference model parameters.

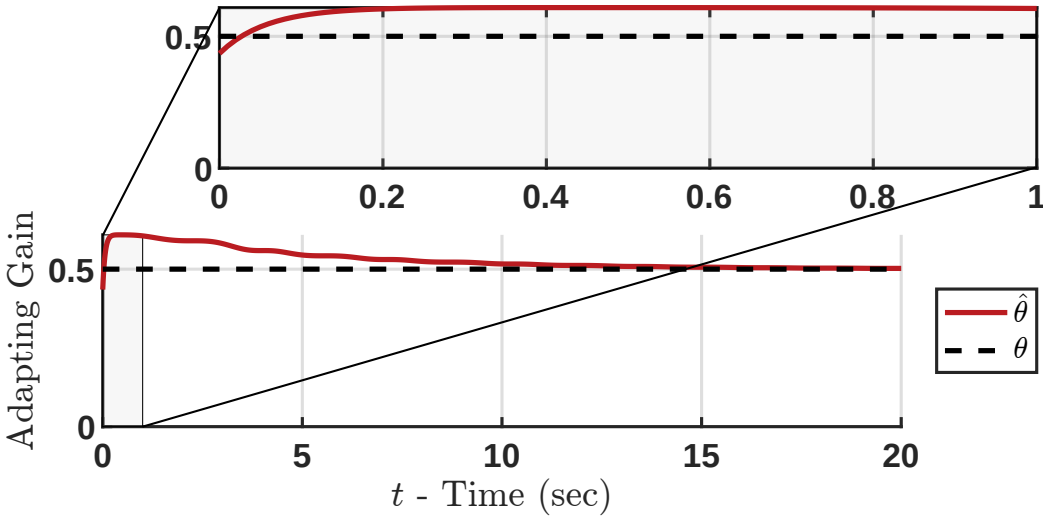

Figure 2.5: Evolution of the adapting gain.

2.3.4 Alternate Approach

Corollary 2.1 is also applicable because adaptive control is only required for the fast subsystem. To demonstrate this the problem is downgraded to a regulation problem and the fast reference model is redefined so that it is no longer *asymptotically* stable about the manifold

$$\dot{\tilde{z}}_m = -a_z \tilde{z}_m \tag{2.63}$$

Note that the manifold is still a stable equilibrium. It is even asymptotically stable when the manifold is constant with respect to time. However, it is not *asymptotically* stable in the context of the full-order system. Reference models such as this are useful if $\acute{\boldsymbol{r}}_x$ is not known apriori or the

manifold is difficult to differentiate. From Eq. (2.57) it can be shown that

$$-\mathcal{L}(f_{z_s})V_{\tilde{z}_m} = \left(-\frac{2xz}{x^2+1}k_x e_x + k_x z\right)\tilde{z}_m \tag{2.64a}$$

$$\leq (2k_x|e_x|_2 + k_x|z|_2)\,|\tilde{\boldsymbol{z}}_m|_2 \tag{2.64b}$$

$$\leq \begin{bmatrix} 2k_x + k_x^2 & 0 & k_x & k_x \end{bmatrix} \boldsymbol{v}|\tilde{z}_m|_2 \tag{2.64c}$$

$$\leq \boldsymbol{\delta}^T \boldsymbol{v}|\tilde{z}_m|_2 \tag{2.64d}$$

where the domain has been restricted to $x < 1$ and $z < 1$. Note that $\delta_1 = 2k_x + k_x^2$, $\delta_2 = 0$, $\delta_3 = k_x$, and $\delta_4 = k_x$. Substituting the values from the previous numerical example gives

$$K \triangleq \begin{bmatrix} d^* & -\frac{1}{2}d^* & -\frac{1}{2}(d^*+3d) \\ -\frac{1}{2}d^* & \frac{d}{\epsilon} & -\frac{1}{2}d \\ -\frac{1}{2}(d^*+3d) & -\frac{1}{2}d & \frac{d}{\epsilon} - d \end{bmatrix} \tag{2.65}$$

From Corollary 2.1 it is known that if $\exists d \in (0,1)$ and $d^* \triangleq (1-d)$ such that K is positive definite then $\boldsymbol{e}_x, \boldsymbol{e}_z \to 0$ as $t \to \infty$. By Sylvester's Criterion K is positive definite if and only if the LPMs are positive. The first LPM is positive by definition. The second and third LPMs depend upon ϵ and d. Fig. 2.6 plots this relationship. If both LPMs are positive for a given ϵ then the conditions of Corollary 2.1 are satisfied. In Fig. 2.6, note that as ϵ increases there is a point after which $\nexists d$ such that both LPMs are positive simultaneously. At this point, the timescale separation is insufficient for Corollary 2.1 to guarantee convergence.

From Fig. 2.6 it can be seen that when $\epsilon = 0.1$ (as in the previous example) $\exists d$ such that all of the LPMs are positive. Thus by Corollary 2.1 it is known that $\boldsymbol{e}_x, \boldsymbol{e}_z \to 0$ as $t \to \infty$. The time evolution of the slow state for this alternate approach is shown in Fig. 2.7. The fast state is shown in Fig. 2.8. The time evolution of the adapting gain is shown in Fig. 2.9. This example demonstrates how the manifold evolves on the slow timescale per Assumption 2.3.

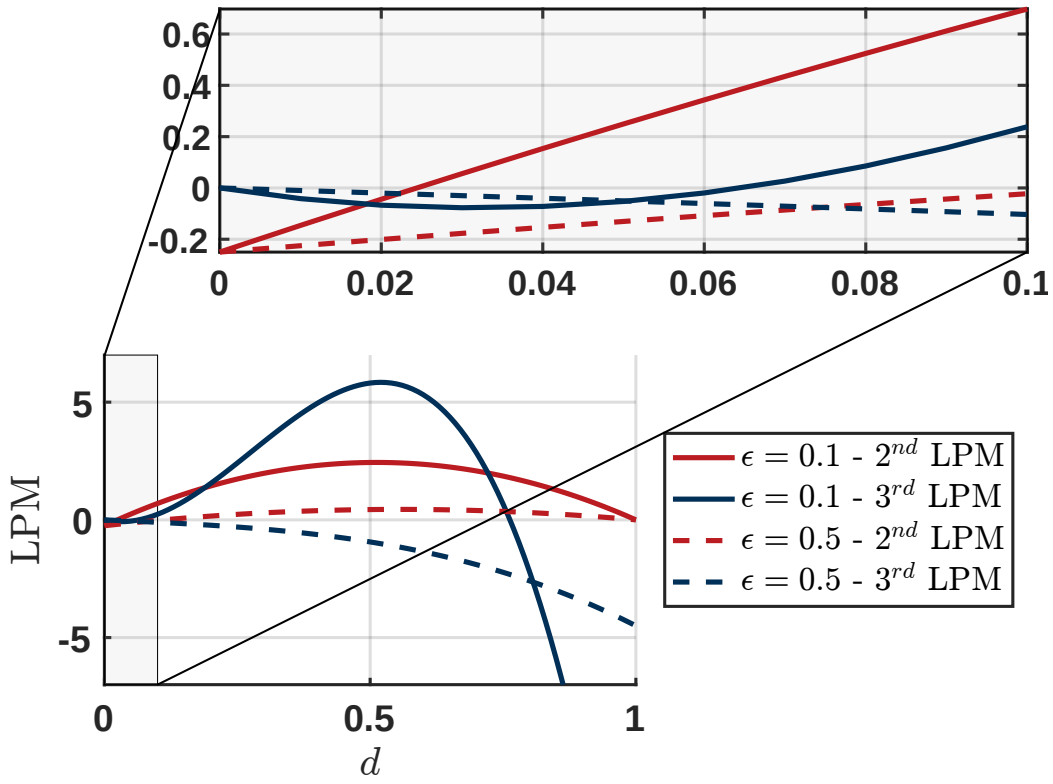

Figure 2.6: Effects of varying ϵ and d on the applicablility of Corollary 2.1.

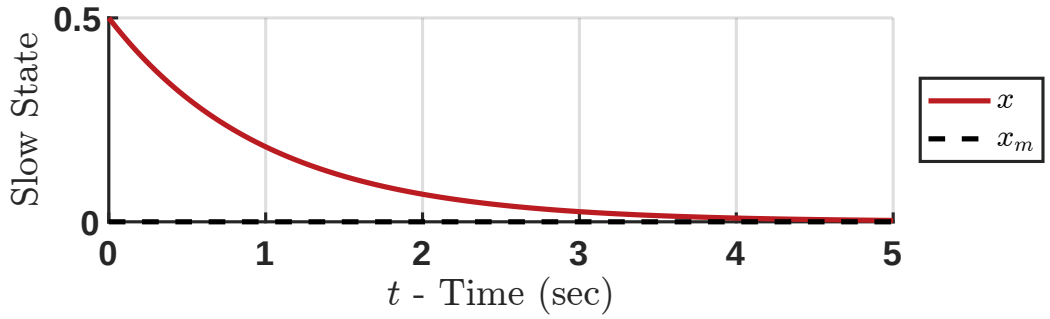

Figure 2.7: Evolution of the slow state for the alternate approach.

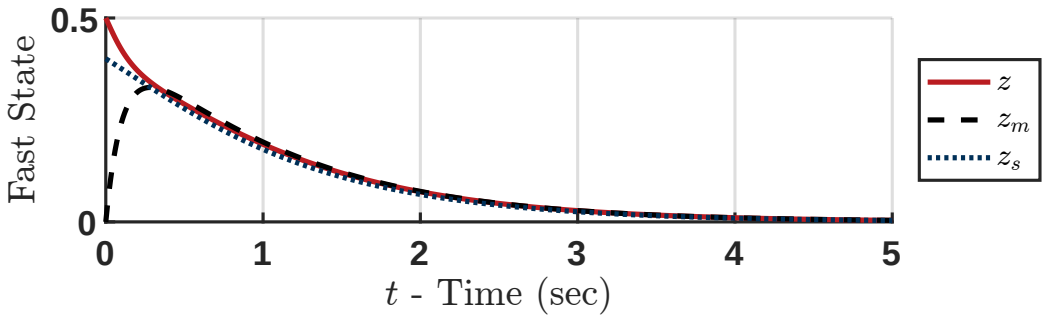

Figure 2.8: Evolution of the fast state for the alternate approach.

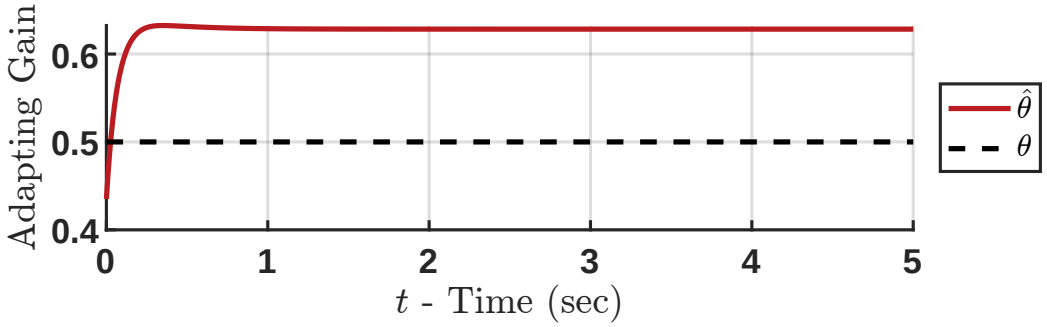

Figure 2.9: Evolution of the adapting gain for the alternate approach.

2.4 Chapter Summary

In this chapter sufficient conditions for asymptotic stability were proven. A wide class of adaptive control and multiple-timescale control methods fit within this framework. Coupling effects between the manifold and the fast reference model were identified. The stability of the full-order system was connected to the stability of the reduced-order systems through Theorem 2.1 and its corollaries. Finally, a nonlinear nonstandard system was used to demonstrate KAMS. The following conclusions are drawn from the results presented in this chapter:

1. Complex interactions between the fast reference model and the manifold significantly complicate the stability analysis when adaptive control is used to stabilize the fast subsystem. The theorems proven in this chapter account for these interactions.

2. KAMS is judged to be a feasible control approach for uncertain nonstandard singularly perturbed systems.

When designing a KAMS controller the following criteria can be used to determine which of the theorems in this chapter are applicable:

1. Theorem 2.1 requires that the slow reference model be asymptotically stable to the reference model input. Three special cases of Theorem 2.1 were studied which do not have this limitation.

   (a) Corollary 2.1 is applicable when adaptive control is only used for the fast subsystem.

   (b) Corollary 2.2 is applicable when adaptive control is only used for the slow subsystem.

   (c) Corollary 2.3 allows adaptive control in both subsystems, but the manifold must be an asymptotically stable equilibrium of the fast reference model in the context of the full-order system.

Theorem 2.1 and Corollary 2.1 both allow the timescale separation parameter to appear on the right side of the fast states' equations of motion and require checking the positive definiteness of a matrix. Corollaries 2.2 and 2.3 do not. KAMS typically requires differentiation of the manifold. In Theorem 2.1 and Corollary 2.1 the derivative of the manifold is used to ensure that condition (2.28d) is satisfied. The derivative of the manifold is not explicitly required for Corollary 2.3, but it is required to ensure the manifold is an asymptotically stable equilibrium of the fast reference model. It is therefore significant that Corollary 2.2 does not require differentiating the manifold.

3. RELAXING THE NON-MINIMUM PHASE ASSUMPTION *

One advantage of KAMS is that it allows adaptive control to be used on some non-minimum phase systems even though many adaptive algorithms assume the system is minimum phase. Ioannou and Sun illustrated the significance of the non-minimum phase adaptive control problem. "*The assumption of minimum phase... has often been considered as one of the limitations of adaptive control in general...*" Further, "*The minimum phase assumption is one of the main drawbacks of* [MRAC] *for the simple reason that the corresponding discrete-time plant of a sampled minimum phase continuous-time plant is often nonminimum* [sic] *phase*" [24, p. 412-413]. Goodwin and Sin showed local stability for MRAC on a class of discrete non-minimum phase systems [97]. Johnstone, Shah, and Fisher used control weighting to overcome the non-minimum phase problem [98]. Previously researchers have shown that feedforward terms can make the problem minimum phase [99, 100]. Some model-free adaptive control methods do not require the non-minimum phase assumption [101, 102, 103, 104, 105, 106]. For a general treatise on adaptive methods for non-minimum phase systems sees [107]. Unlike related work, the method demonstrated in this chapter utilizes model reduction to simplify implementation and provide insights into the dynamics of the plant.

3.1 Problem Formulation

Consider nonlinear MIMO systems of the form

$$\dot{\boldsymbol{\chi}} = f_\chi(\boldsymbol{\chi}, \boldsymbol{\mu}) \tag{3.1a}$$

$$\boldsymbol{y} = g_y(\boldsymbol{\chi}) \tag{3.1b}$$

where $f_\chi : \mathbb{D}_\chi^{n_\chi} \times \mathbb{R}^{n_\mu} \to \mathbb{R}^{n_\chi}$ and $h : \mathbb{D}_\chi^{n_\chi} \to \mathbb{R}^{n_y}$ are sufficiently smooth (i.e. continuously differentiable as many times as needed) on the domain $\mathbb{D}_\chi^{n_\chi}$. $\boldsymbol{\chi}$ is the system state, $\boldsymbol{\mu}$ is the system

*Portions of this chapter are reprinted with permission from "Adaptive Control for Non-Minimum Phase Systems Via Time Scale Separation" by Kameron Eves and John Valasek, 2023. American Control Conference, Copyright 2023 by American Automatic Control Council [96].

input, and $\boldsymbol{y}$ is the system output.

This work is specifically applicable to systems with unstable *zero dynamics*. The zero dynamics of a system can be determined by setting the output and its time derivatives (of orders up to the relative degree) equal to zero and solving for the remaining dynamics. The relative degree is the number of times the output must be differentiated before the input appears. The variable $\rho \in \mathbb{N}$ is used to represent the sum of the relative degrees of the system outputs such that $n_\chi > \rho \geq n_y$. If the zero dynamics are unstable then the system is called *non-minimum phase*. This is a generalization of linear system zeros. Indeed the poles of a linear system's zero dynamics are equivalent to the zeros of the full-order system. The zero dynamics are sometimes called the *internal dynamics* and the output dynamics are sometimes called the *external dynamics*. The majority of adaptive control literature assumes that within the domain of interest, the zero dynamics are stable about some equilibrium (i.e. minimum phase) (e.g. [65, 24, 35]). This chapter demonstrates how KAMS can be used to relax that assumption.

This chapter proceeds as follows. Section 3.2 describes a diffeomorphism that is used to manifest the timescales of the system and separate the internal and external dynamics. Section 3.3 gives an example of KAMS on a nonlinear non-minium phase system. This example demonstrates how methods common in the literature - ANDI in this case - can be used on non-minimum phase systems within the framework of KAMS even though these methods assume the plant is minimum phase.

3.2 Diffeomorphism

The first step is to apply a transformation to the system called R. The purpose of R is to accomplish the following two tasks which enable the analysis and control:

1. To effectively control a non-minimum phase system with KAMS the internal and external dynamics must be identified. R separates the internal dynamics from the external dynamics using a change of variables.

2. For this method to be valid, the internal dynamics must evolve on a timescale that is different

from the external dynamics. R identifies the relative timescales of the internal dynamics and the external dynamics. The stability analysis later in this chapter will specify how much timescale separation is necessary for KAMS to be applicable.

This section formally defines R by describing the form of the system after the transformation. An example of R is then given.

Let the transformation R be set of three diffeomorphisms - one on the states, one on the input, and one on the time

$$R(\boldsymbol{\chi}, \boldsymbol{\mu}, t) : \mathbb{D}_{\chi}^{n_\chi} \times \mathbb{R}^{n_u} \times \mathbb{R}_+ \to \mathbb{D}_x^{\rho} \times \mathbb{D}_z^{n_\chi - \rho} \times \mathbb{R}^{n_u} \times \mathbb{R}_+ \tag{3.2}$$

The variables $\boldsymbol{x} \in \mathbb{D}_x^{\rho}$ and $\boldsymbol{z} \in \mathbb{D}_z^{n_\chi - \rho}$ are the state variables after the transformation R. The variable $\boldsymbol{u} \in \mathbb{R}^{n_u}$ represents the input after this transformation. The variable $t_s \in \mathbb{R}_+$ represents the time after this transformation. Let R be defined such that it transforms Eq. (3.1) into the following format :

$$\acute{\boldsymbol{x}} = f_x(\boldsymbol{x}, \boldsymbol{z}, \boldsymbol{u}) \tag{3.3a}$$

$$\epsilon \acute{\boldsymbol{z}} = f_z(\boldsymbol{x}, \boldsymbol{z}, \boldsymbol{u}, \epsilon) \tag{3.3b}$$

$$\boldsymbol{y} = C_x \boldsymbol{x} + C_z \boldsymbol{z} \tag{3.3c}$$

The output is a linear combination of the states through the matrices $C_x \in \mathbb{R}^{g \times \rho}$ and $C_z \in \mathbb{R}^{g \times (n_\chi - \rho)}$. By definition, either $C_x = 0$ or $C_z = 0$ but not both. The small positive constant $0 < \epsilon \ll 1$ is the timescale separation parameter as defined in previous chapters. The notation $\acute{(\cdot)}$ is the derivative with respect to the new time variable t_s as defined in previous chapters. Lastly, by definition $\mathcal{O}(f_x) = \mathcal{O}(f_z) = \mathcal{O}(1)$ for the variable ϵ. The following example is provided to further clarify the diffeomorphism R. Consider a linear time-invariant (LTI) single-input single-output

(SISO) plant in the Laplace domain

$$y(s) = \frac{s - 49}{s^2 - 248 - 49} u(s) \tag{3.4}$$

This system is non-minimum phase because the zero is in the right-half plane. In controllable canonical form, this plant is

$$\dot{\boldsymbol{\chi}} = \begin{bmatrix} 0 & 1 \\ 49 & 248 \end{bmatrix} \boldsymbol{\chi} + \begin{bmatrix} 0 \\ 1 \end{bmatrix} \mu \tag{3.5a}$$

$$y = \begin{bmatrix} -49 & 1 \end{bmatrix} \boldsymbol{\chi} \tag{3.5b}$$

This matches the form of Eq. (3.1). Let the new state variables x and z be defined as a linear transformation of $\boldsymbol{\chi}$. Let the new input u be identically equal to the original input μ. Let the slow timescale t_s be defined as identically equal to the original timescale t. These three transformations are the diffeomorphism R

$$R \begin{cases} \begin{bmatrix} x \\ z \end{bmatrix} & \triangleq \begin{bmatrix} -49 & 1 \\ 0 & 100 \end{bmatrix} \boldsymbol{\chi} \\ u & \triangleq \mu \\ t_s & \triangleq t \end{cases} \tag{3.6}$$

Applying R to the original system from Eq. (3.5) gives

$$\begin{bmatrix} \acute{x} \\ \epsilon \acute{z} \end{bmatrix} = \begin{bmatrix} -1 & 2 \\ -1 & 2.49 \end{bmatrix} \begin{bmatrix} x \\ z \end{bmatrix} + \begin{bmatrix} 1 \\ 1 \end{bmatrix} u \tag{3.7a}$$

$$y = x \tag{3.7b}$$

where $\epsilon = 0.01$. This form now matches Eq (3.3) and Assumption 3.1 is meet.

In summary, the first step of this approach is to use a diffeomorphism (R) to reformat the

system so that it matches the form of Eq. (3.3). The two primary characterizing features of this form are:

1. The timescale properties as indicated by the appearance of the timescale separation parameter ϵ and the order of the functions f_x and f_z.

2. The output is linearly dependent upon $\boldsymbol{x}$ or $\boldsymbol{z}$ but not both.

The transformation R, by definition, must be a diffeomorphism on the states and time such that these two properties are met. The following assumption is now made:

Assumption 3.1 - *The diffeomorphism R as defined above exists and is known.*

Now that the timescales of the system have been identified theorem 2.1 is applicable and KAMS can be used to stabilize the system. The control input to the original system can be found by selecting u and then inverting R. This works because KAMS applies the adaptive control to the reduced subsystems, not the full-order system. Thus the minimum phase assumption is imposed upon the subsystems and not the full-order system.

Remark 3.1 - *There is currently no systematic method to find the diffeomorphism R. However, transformations that are similar to R have been studied in several other contexts. For example, R is related to the diffeomorphism used to separate the internal and external dynamics when implementing input-output feedback linearization [18, Section 12.2]. R is also related to timescale identification which is an open area of research (e.g. [11]). These other transformations can be informative and even serve as building blocks for R. The author of this work has found success by applying the input-output feedback linearization diffeomorphism and then nondimensionalizing, but other approaches may be valid.*

Remark 3.2 - *The existence and uniqueness of R are worth considering. Existence: If f is affine and the timescale separation is ignored then the transformation R is guaranteed to exist [18, p. 566]. This work is not limited to affine systems, but affine systems are common in adaptive control applications. Thus the existence of R is likely. The applicability of KAMS will depend upon how*

large the timescale separation is. Uniqueness: R is not typically unique. Unlike [18] no constraints are placed upon $\boldsymbol{z}$. Thus it is possible for $\epsilon\acute{\boldsymbol{z}}$ to be dependent upon the input.

Remark 3.3 - *Consider the case when the output is solely dependent upon $\boldsymbol{x}$. This implies that $\boldsymbol{y} = C_x\boldsymbol{x}$ and $C_z = 0$. Referring to Eq.* (3.3) *it can be seen that the internal dynamics are analogous to the reduced fast subsystem and the external dynamics are analogous to the reduced slow subsystem. The zero dynamics are analogous to the manifold. This realization is the linchpin that makes this approach possible.*

3.3 Numerical Demonstration

Consider the nonlinear system

$$\acute{x} = \theta_1 \left[\arctan(x) + \pi\right] z + \theta_2 \left(\cos(x) + 1\right) u \tag{3.8a}$$

$$\epsilon\acute{z} = x^2 z - u \tag{3.8b}$$

$$y = x \tag{3.8c}$$

where $\theta_1, \theta_2 \in \mathbb{R}_+$ are uncertain model parameters. The zero dynamics are:

$$\acute{z} = \frac{\theta_1 \pi}{2\theta_2 \epsilon} z \tag{3.9}$$

which are unstable because ${}^{\theta_1\pi}/_{2\theta_2\epsilon} > 0$. Thus the system is non-minimum phase. The control objective is for the slow states to track the following reference model

$$\acute{x}_m = -a_{x_m} x_m \tag{3.10}$$

where $a_{x_m} \in \mathbb{R}_+$. The transformation R is an automorphism. The reduced slow subsystem is

$$\acute{x} = \theta_1 \left[\arctan(x) + \pi\right] z_s + \theta_2 \left(\cos(x) + 1\right) u_s \tag{3.11}$$

and the reduced fast subsystem is

$$\acute{x} = 0 \tag{3.12a}$$

$$\epsilon \acute{z} = x^2 z - u \tag{3.12b}$$

Sequential Control is selected to fuse the control signals for the reduced subsystems. Accordingly, z is treated as the input to the reduced slow subsystem. The manifold z_s is selected such that the reduced slow subsystem converges to a reference model. ANDI is selected for this purpose [65, p. 6-12]. Now u must be selected to make the reduced fast subsystem track z_s. The input is selected by inspection to ensure the fast subsystem is Lyapunov sense stable. This yields the following manifold and control signal

$$z_s = \frac{-a_{x_m} x_m - \hat{\theta}_2 \left(\cos(x) + 1\right) u - k_x e_x}{\hat{\theta}_1 \left(\arctan(x) + \pi\right)} \tag{3.13a}$$

$$u = x^2 z + k_z e_z \tag{3.13b}$$

where $k_x, k_z \in \mathbb{R}_+$ are control gains. By definition $z_m \triangleq z_s$ for all time. Note that the manifold is an asymptotically stable equilibrium of the fast subsystem, but not the full-order subsystem. z_s appears on both sides of Eq. (3.13a) so it must be solved. Recall that in the reduced slow subsystem $z = z_s$. Substituting Eq. (3.13b) into Eq. (3.13a) and solving for z_s gives

$$z_s = \frac{-a_{x_m} x_m - k_x e_x}{\hat{\theta}_1 \left(\arctan(x) + \pi\right) + \hat{\theta}_2 \left(\cos(x) + 1\right) x^2} \tag{3.14}$$

The adaptation laws are

$$\acute{\hat{\theta}}_1 = \gamma_1 \text{Proj}\left(\hat{\theta}_1, \left(\arctan(x) + \pi\right) z_s e_x\right) \tag{3.15a}$$

$$\acute{\hat{\theta}}_2 = \gamma_2 \text{Proj}\left(\hat{\theta}_2, \left(\cos(x) + 1\right) u_s e_x\right) \tag{3.15b}$$

where $u_s = x^2 z_s$ is the input when $z = z_s$ and $\gamma_1, \gamma_2 \in \mathbb{R}_+$ are gains for the adaptation laws.

Consider the following Lyapunov functions for the reduced slow subsystems:

$$V_{e_x} = \frac{1}{2}\left(e_x^2 + \gamma_1^{-1}\tilde{\theta}_1^2 + \gamma_2^{-1}\tilde{\theta}_2^2\right) \tag{3.16a}$$

$$V_{e_z} = \frac{1}{2}e_z^2 \tag{3.16b}$$

Per [65, Eq. 1.23] the time derivatives are

$$\acute{V}_{e_x} \leq -k_x e_x^2 \tag{3.17a}$$

$$\grave{V}_{e_z} = -k_z e_z^2 \tag{3.17b}$$

Now that the reduced subsystems have been proven independently stable, the interconnection condition must be checked. From Eq. (2.28b)

$$\mathcal{L}(f_x - f_{x,s})V_{e_x} = \left(\theta_1\left[\arctan(x) + \pi\right]\tilde{z}_s + \theta_2\left(\cos(x) + 1\right)\left(u - u_s\right)\right)e_x \tag{3.18}$$

Substituting in for the input gives

$$\mathcal{L}(f_x - f_{x,s})V_{e_x} = \left(\theta_1\left[\arctan(x) + \pi\right]\tilde{z}_s + \theta_2\left(\cos(x) + 1\right)\left(x^2 z + k_z e_z - x^2 z_s\right)\right)e_x \tag{3.19}$$

rearranging and using the fact that $z_m = z_s$

$$\mathcal{L}(f_x - f_{x,s})V_{e_x} = \left(\theta_1\left[\arctan(x) + \pi\right] + \theta_2\left(\cos(x) + 1\right)\left(x^2 + k_z\right)\right)\tilde{z}e_x \tag{3.20}$$

Assume that the domain is limited to $|x| < x_{max}$ for some $x_{max} \in \mathbb{R}_+$ and x is initialized within this region. Note that due to the projection operator, θ_1 and θ_2 are bounded. Let $\theta_{1,max}$ and $\theta_{2,max}$ respectively be those bounds. Using these facts it can be shown that

$$\mathcal{L}(f_x - f_{x,s})V_{e_x} \leq \left[\theta_{1,max}\frac{3}{2}\pi + \theta_{2,max}2\left(x_{max}^2 + k_z\right)\right]\tilde{z}e_x \tag{3.21}$$

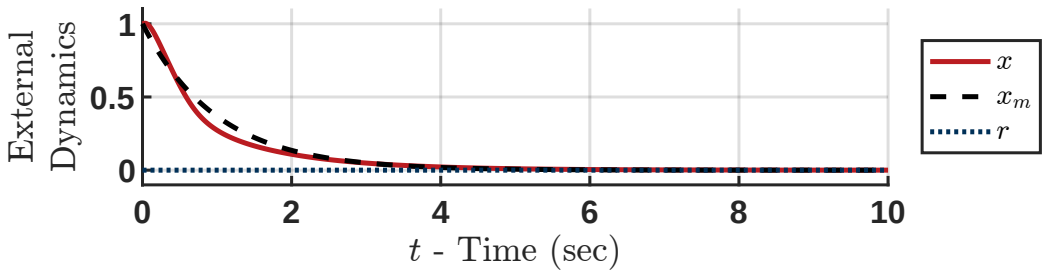

Figure 3.1: Evolution of the external dynamics for a non-minimum phase system.

Thus there exists some constant parameter

$$\beta = \theta_{1,max}\frac{3}{2}\pi + \theta_{2,max}2\left(x_{max}^2 + k_z\right) \tag{3.22}$$

such that Eq. (2.28b) is satisfied. Thus the conditions of Corollary 2.2 are satisfied. By Corollary 2.2 $e_z, e_x \to 0$ as $t_s \to \infty$.

The values used in this simulation are $\epsilon = 0.1$, $\theta_1 = \theta_2 = 1$, $\gamma_1 = 10$, and $\gamma_2 = 10$. The initial conditions are $x = x_m = 1$ and $z = 0$. The initial error of the adapting parameters $\tilde{\boldsymbol{\theta}}$ is randomly selected from a 0 mean normal distribution with a standard deviation of 10% their true value. The timescale separation parameter ϵ is also simulated to be uncertain. As such its error is sampled from the same distribution. Note that the estimate of the timescale separation parameter is not an adapting parameter. The parameter for the reference model is $a_x = 1$. The control gains are $k_x = 1$ and $k_z = 10$. Figure 3.1 shows the time evolution of the external dynamics. Figure 3.2 shows the time evolution of the internal dynamics. Figure 3.3 shows the time evolution of the adapting parameters. It is worth noting that ANDI alone is incapable of stabilizing this system because it non-minimum phase. Thus KAMS is a significant improvement.

3.4 Chapter Summary

This chapter presents a method of adaptive control for a wide class of systems which may be both nonlinear and non-minimum phase. The method requires some timescale separation between the internal and the external dynamics. Further, it does not matter if the internal dynamics are faster

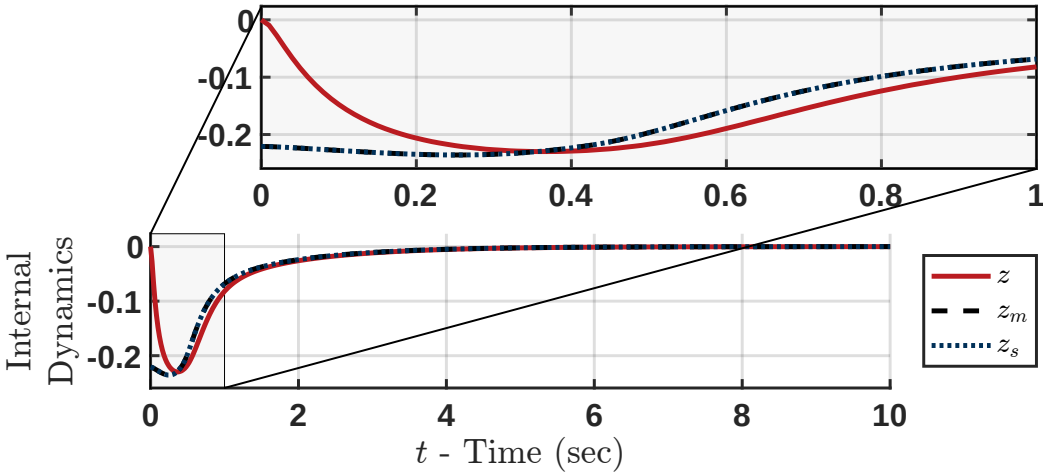

Figure 3.2: Evolution of the internal dynamics for a non-minimum phase system.

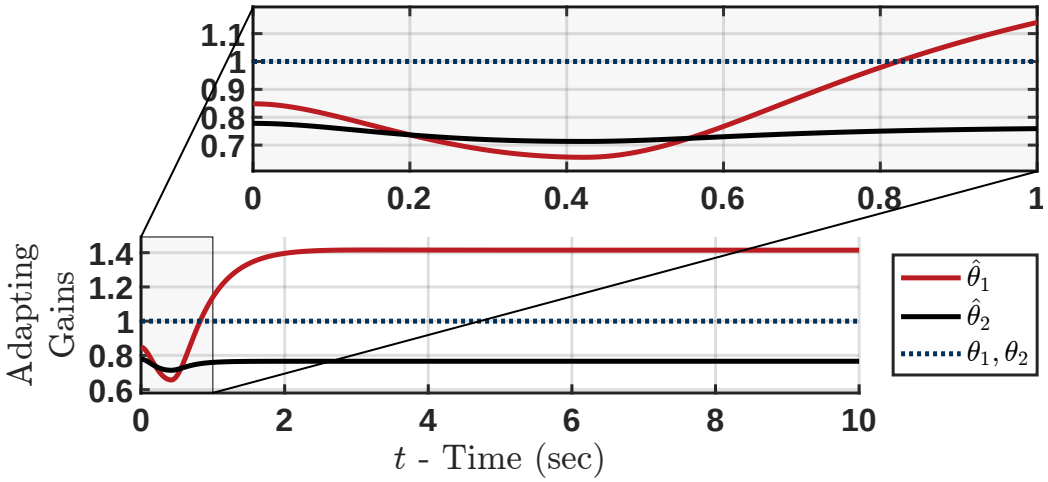

Figure 3.3: Evolution of the adapting parameters for a non-minimum phase system.

or the external dynamics are faster. In both cases, the system has been converted into a singularly perturbed system suitable for multiple-timescale control. This was done using a simple diffeomorphism that is shown to be likely to exist. KAMS is then used to control the system. Finally, a validating example was presented. From this chapter, it can be concluded that KAMS allows adaptive control to be effectively applied to non-minimum phase systems provided there is at least some timescale separation. Non-minimum phase systems have been a challenging problem for adaptive control since its inception. The conclusions of this chapter bring the scientific community one step closer to solving this problem.

4. COMPARISONS WITH OTHER APPROACHES *

In this chapter, Reduced-Order Adaptive Control (ROAC) and Full-Order Adaptive Control (FOAC) are formally defined and generalized for the first time. ROAC and FOAC are both alternatives to KAMS. ROAC and FOAC have been used but not formalized in prior work. Both ROAC and FOAC use elements of adaptive control and multiple-timescale control. On the other hand, KAMS fully and rigorously merges these two fields. Section 4.1 describes FOAC. Section 4.2 describes ROAC. Section 4.4 directly compares ROAC, FOAC, KAMS, and Composite Control using a numerical analysis of the multiple-timescale pitch rate dynamics of a Boeing 747-100/200 with actuator dynamics. This example highlights the similarities and differences between the four methods. As will be seen, KAMS performs better than the alternatives and demonstrates increased robust to uncertainties in the timescale separation. However, all three multiple-timescale adaptive control methodologies are effective, and each method has its benefits and detriments. Composite Control on the other hand fails to converge to the reference model due to model uncertainty

4.1 Full-Order Adaptive Control

The most intuitive solution to multiple-timescale adaptive control is to treat multiple-timescale systems like other systems. Equation (1.1) can be rewritten as

$$\acute{\boldsymbol{x}} = f_x(\boldsymbol{x}, \boldsymbol{z}, \boldsymbol{u}) \tag{4.1a}$$

$$\acute{\boldsymbol{z}} = \frac{1}{\epsilon} f_z(\boldsymbol{x}, \boldsymbol{z}, \boldsymbol{u}, \epsilon) \tag{4.1b}$$

Now $\boldsymbol{x}$ and $\boldsymbol{z}$ can be concatenated into a single state vector. If a valid adaptive control methodology exists for the resulting system then there is no reason that the adaptive control algorithm won't work. However, proving that a given adaptive control methodology is valid can be problematic and will depend on the given system. Figure 4.1 shows a bloack diagram for FOAC. The following

*This chapter is reprinted with permission from "Introduction to Adaptive Control for Multiple Time Scale Systems" by Kameron Eves and John Valasek, 2023. Scitech Conference and Exposition, Copyright 2023 by American Institute of Aeronautics and Astronautics, Inc. [53].

theorem formalizes this conceptual definition of FOAC.

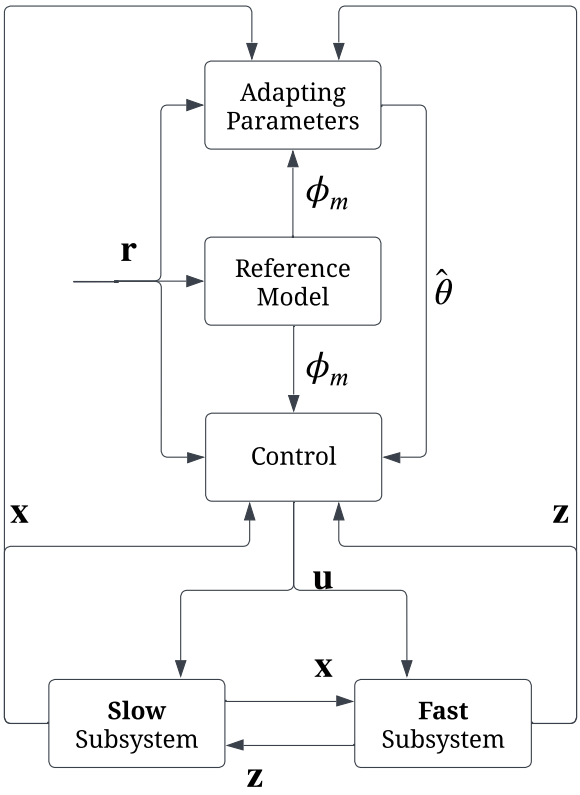

Figure 4.1: A block diagram of FOAC.

Theorem 4.1 - *Consider the system in Eq.* (1.1)*. If there exists an adaptive controller which accomplishes the control objective for the equivalent system in Eq.* (4.1) *and assuming said adaptive control problem is well posed, then the adaptive controller for Eq.* (4.1) *is also valid for Eq.* (1.1)*.*

Proof. The timescale separation parameter, whereas often unknown, is simply a fixed scalar value. Additionally, the timescale separation parameter is very small, but not zero. Thus dividing by the timescale separation parameter is valid. Further, dividing by the timescale separation parameter does not affect the time evolution the system states $\boldsymbol{x}$ and $\boldsymbol{z}$. □

Theorem 4.1 seems simple and obvious, but the results are significant to FOAC. Effectively, Theorem 4.1 states that the singularly perturbed nature of Eq. (1.1) does not inhibit the use of the normal adaptive control techniques. Theorem 4.1 seems to imply that multiple-timescale systems are no different from traditional systems and can be controlled in the same manner. However, the application of Theorem 4.1 can lack robustness to uncertainties in the timescale separation parameter. The timescale separation parameter is frequently unknown. This is particularly true for systems with model uncertainties because the timescale separation parameter is a function of system parameters and is related to the form of the dynamics. In other words, multiple-timescale systems which require adaptive control are even more likely to have large uncertainty bounds on the timescale separation parameter. This problem is exacerbated by the ϵ^{-1} term in Eq. (4.1). Small inaccuracies in an estimate of the timescale separation parameter can cause large discrepancies between the predicted and actual system response because $0 < \epsilon \ll 1$. Traditional multiple-timescale control methodologies account for this problem by giving a range of valid timescale separation parameters. However, Theorem 4.1 does not give rise to any such valid range. A valid range might be found by application of the assumptions from the chosen adaptive control methodology, but this must be determined on a case-by-case basis.

Consider the following parametrically uncertain multiple-timescale system

$$\acute{x} = a_1 x + a_2 z + b_1 u \tag{4.2a}$$

$$\epsilon \acute{z} = a_3 x + a_4 z - a_5 \epsilon z + b_2 u \tag{4.2b}$$

where a_1, a_2, a_3, a_4, a_5, b_1, and b_2 are uncertain system parameters. Converting to the format of Eq. (4.1) gives

$$\acute{x} = a_1 x + a_2 z + b_1 u \tag{4.3a}$$

$$\acute{z} = \frac{a_3}{\epsilon} x + \left(\frac{a_4}{\epsilon} - a_5 \right) z + \frac{b_2}{\epsilon} u \tag{4.3b}$$

where x and z can be concatenated into a combined state vector. Adaptive laws and control laws

can then be derived by following a standard MRAC methodology (e.g. [24, Table 6.4]). This is FOAC. Figure 4.2 shows the closed-loop response of Eq. (4.2) under FOAC. The reference model is $\acute{x}_m = -a_m \tilde{x}_m$ with a constant input of $r = 1$. The parameters used in the creation of Fig. 4.2 are $a_1 = a_3 = a_m = -1$, $a_2 = 2$, $a_4 = 2.1$, and $a_5 = b_1 = b_2 = 1$. To highlight the effect of the timescale separation parameter, the initial values for the gains are chosen to be the true Model Reference Control value. The adaptation gains are all identity. Several different timescale separation parameters are shown for comparison. As can be seen, small changes in the timescale separation parameter can have a large effect on the system performance and can even incite instability.

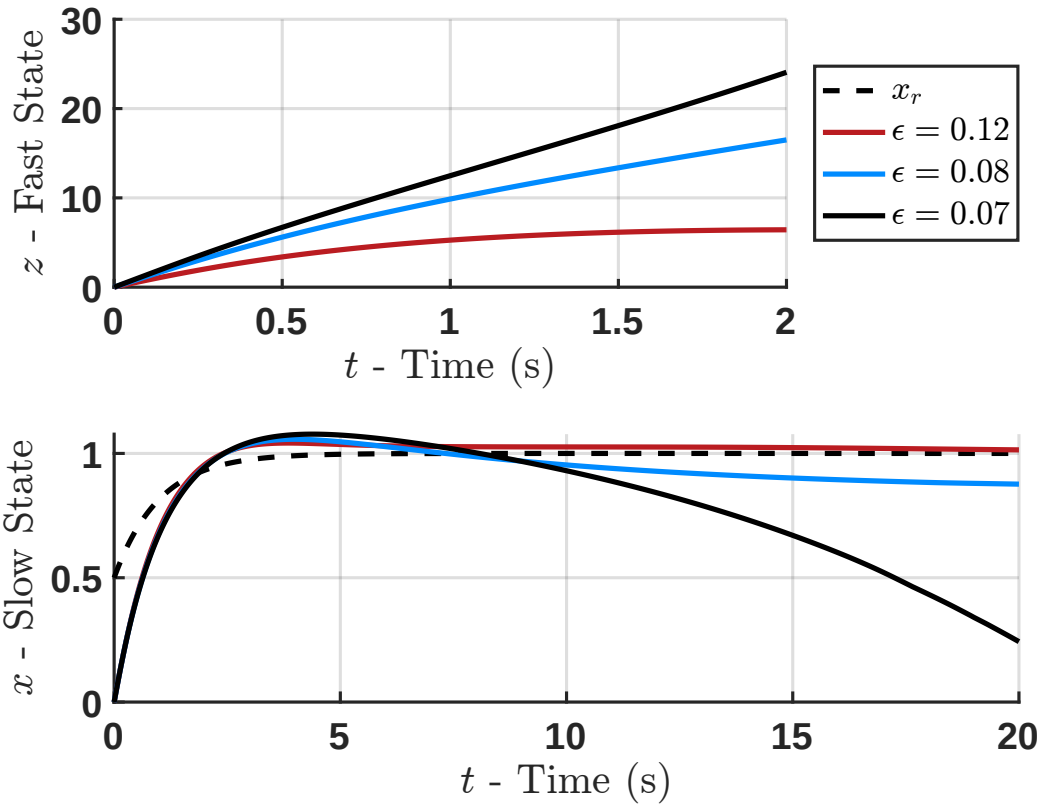

Figure 4.2: Evolution of a simple linear system under FOAC for several different timescale separation parameters.

Because this system is linear, a brief analytical analysis clearly explains why adjusting the

timescale separation parameter induced instability. The input-output transfer function for this system is

$$\frac{x(s)}{u(s)} = b_1 \frac{s + \left(-\frac{a_4}{\epsilon} + a_5 + \frac{b_2 a_2}{b_1 \epsilon}\right)}{s^2 + \left(-a_1 - \frac{a_4}{\epsilon} + a_5\right) s + \left(\frac{a_1 a_2}{\epsilon} - a_1 a_5 - \frac{a_2 a_3}{\epsilon}\right)} \tag{4.4}$$

Thus the system is minimum phase if

$$-\frac{a_4}{\epsilon} + a_5 + \frac{b_2 a_2}{b_1 \epsilon} > 0 \tag{4.5}$$

Substituting the parameters and solving for the timescale separation parameter gives

$$\epsilon > 0.1 \tag{4.6}$$

Thus, when the timescale separation parameter is decreased below 0.1 then the system becomes non-minimum phase. This violates assumption P1 of [24, p. 332]. Therefore, to apply FOAC, the assumptions of the chosen control method must be carefully observed. This can be difficult to guarantee if the timescale separation parameter is unknown. $\epsilon > 0.1$ gives a valid range for the timescale separation but such a range is not usually readily apparent when using FOAC. Notably, this range is somewhat constrictive because by definition $0 < \epsilon \ll 1$.

4.2 Reduced-Order Adaptive Control

If either the reduced fast model or the reduced slow model is stable, then one intuitive approach to adaptive multiple-timescale control is to apply adaptive control to the other reduced-order model and rely on the inherent stability of the discounted dynamics to assure convergence. This technique is ROAC. All models which discount fast actuator dynamics inherently apply ROAC. Figure 4.3 shows a bloack diagram for ROAC.

The problems incurred by reducing a model have been studied in the adaptive control literature. Discounted dynamics are often treated as a time delay (e.g. [62]) or unmodeled dynamics (e.g. [31]). The primary challenge is that inputs to one reduced-order model can excite dynamic modes in the other reduced-order model. It has been shown that even stable discounted dynamics can be

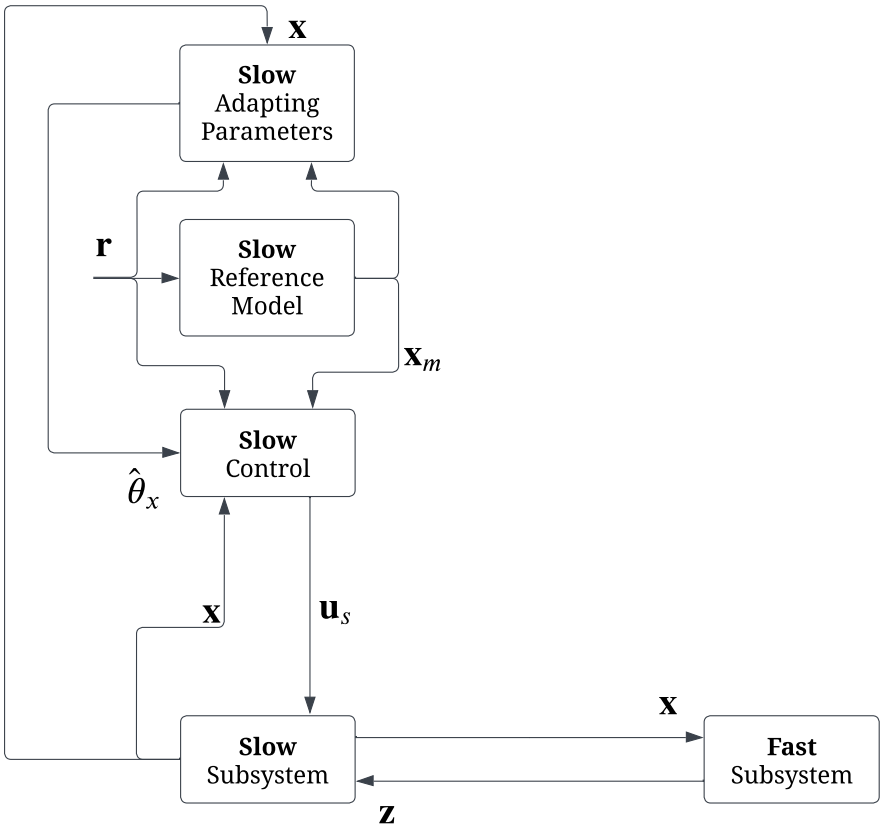

Figure 4.3: A block diagram of ROAC.

driven unstable in this manner [24, p. 549-552] [55]. Narang-Siddarth and Valasek demonstrated this problem with multiple-timescale systems [9, p. 46].

Theorem 4.2 - *Consider the singularly perturbed system as defined in Chapter 2. Let* $\boldsymbol{u}_f = 0$*. Assume that in the context of the closed-loop full-order dynamics, the manifold* $\boldsymbol{z}_s$ *is an asymptotically stable equilibrium of the fast states and the initial conditions are within the region of attraction for that equilibrium. Under these conditions,* $\exists$ *a timescale separation parameter* $0 < \epsilon^* \ll 1$ *and* $\exists$ *a time after the initial time* $t_0 < t^*(\epsilon^*)$ *such that* $\forall \epsilon < \epsilon^*$ *the difference between the closed-loop full-order system and the closed-loop reduced slow subsystem is on the order of* ϵ^* *after* t^**.*

Proof. As described in Chapter 2 the system can be written as a time-varying vector field (see Eq. (2.17)). Note that the manifold for this new multiple-timescale system representing the closed-

loop dynamics is the same as the manifold for the open-loop dynamics. All of the conditions of Tikhonov's Theorem [9, Theorem 1] are satisfied. Thus, via Tikhonov's Theorem, $\exists$ a timescale separation parameter $0 < \epsilon^* \ll 1$ and $\exists$ a time after the initial time $t_0 < t^*(\epsilon^*)$ such that $\forall \epsilon < \epsilon^*$ the difference between the closed-loop full-order system and the closed-loop reduced slow subsystem is on the order of ϵ^* after t^*. □

Two corollaries follow directly from Theorem 4.2

Corollary 4.1 - *If the conditions of Theorem 4.2 are met and the closed-loop reduced slow system is bounded, then the closed-loop full-order system is also bounded.*

Corollary 4.2 - *If the conditions of Theorem 4.2 are met and the reference model is an asymptotically stable equilibrium of the closed-loop reduced slow system with the initial conditions being in the region of attraction for this equilibrium, then after time t^* the error between the reference model and the slow states of the closed-loop full-order system is on the order of the timescale separation. Succinctly the system is stable about the reference model in the sense of Lyapunov.*

In a general sense, Theorem 4.2 and its associated corollaries state that an adaptive controller designed for the reduced slow model also stabilizes the full-order model if the system can be rewritten such that Tikonov's Theorem applies. Theorem 4.2 as written only applies to systems with adaptive control in the reduced slow system. Applying a similar derivation to adaptive control for the reduced fast model makes the closed-loop system nonstandard and as a result, Tikonov's Theorem does not apply. However, some researchers have managed to use a similar process to prove boundedness for specific systems with adaptive control on the reduced fast model (e.g. [5, 70, 72]).

Notably, Tikhonov's Theorem, and by association Theorem 4.2, implies stability in the sense of Lyapunov, but not convergence. This is interesting to consider in the common case of discounted actuator dynamics. Recall from Theorem 4.2 that the bound on the slow state tracking is of the order of the timescale separation parameter. This means that speeding up the actuators (effectively

increasing the timescale separation by decreasing the timescale separation parameter) can improve tracking performance. This formalizes the common wisdom that faster actuators are preferable.

The most difficult condition to satisfy in Theorem 4.2 is usually that the closed-loop manifold is an asymptotically stable equilibrium of the fast states. This gets back to the heart of the problem discussed at the beginning of this section. That is that controlling a subset of the dynamics can drive the discounted dynamics unstable. Sometimes, a Lyapunov function can be found for the system which proves the manifold is asymptotically stable (see [24, Theorem 3.4.1 Statment iii]). However, valid Lyapunov functions can prove evasive for some systems.

4.3 [K]control of Adaptive Multiple-Timescale Systems

ROAC requires that the discounted reduced model be stable. Further, the difficulty of applying ROAC stems from proving that the closed-loop manifold is an asymptotically stable equilibrium of the fast dynamics. If some method could be found to increase the stability of the discounted dynamics without affecting the primary reduced-order model it could simplify and expand the applicability of ROAC. This was the original motivation behind KAMS. If the fast control is selected to be a non-adaptive controller then Theorem 4.2 still applies. More formally

Theorem 4.3 - *Let all of the conditions of Theorem 4.2 be satisfied except let* $\mathbf{u}_f$ *be a non-adaptive control method. Then the conclusions of Theorem 4.2 and its associated corollaries 4.1 and 4.2 are still valid.*

Proof. The proof is identical to Theorem 4.2. The logic of Corollaries 4.1 and 4.2 are not affected. □

Because KAMS specifically designs a controller for the dynamics of both reduced systems, the assumption that one of the two reduced subsystems is inherently stable is relaxed. Another benefit of KAMS is that the stability of the reduced fast subsystem is asserted instead of assumed. Therefore it is easier to prove that the manifold of the closed-loop system is an asymptotically stable equilibrium. In fact, for some forms of nonlinear control, a valid Lyapunov function could

be directly implied by the control design. The third benefit of KAMS is that the range of valid timescale separation parameters is often larger.

The conclusions of Theorem 2.1 are equivalent to Theorem 4.2 except Theorem 2.1 implies asymptotic stability instead of stability in the sense of Lyapunov. However, Theorem 2.1 offers a few other unique benefits. First, Theorem 2.1 gives a bound on the timescale separation parameter. This gives a measure of the robustness to timescale separation uncertainties. Second, the conditions of Theorem 2.1 are more practical. Note that the condition in Eq. (2.27c) is the same condition that was difficult to address in Theorems 4.2 and 4.3, namely that the manifold of the closed-loop model be an asymptotically stable equilibrium of the fast states. However, in the case of Theorem 2.1 there is a simple way to verify this condition is met. A third benefit is that in some cases Barbalat's Lemma [39] can be used to show convergence. The following Corollary to Theorem 2.1 is also notable.

Corollary 4.3 - *Theorem 2.1 also applies to ROAC.*

Proof. ROAC is equivalent to KAMS when the fast control is selected to be $u_f = 0$. Thus, Theorem 2.1 can be used to find a valid range for the timescale separation parameter of a system under ROAC. □

4.4 Numerical Comparision

Consider the pitch dynamics of a fixed-wing aircraft. The actuator dynamics of the elevator can be modeled as a first-order low-pass filter [108]. The time evolution of the pitch rate can be found in [109, p. 84]. Thus the dynamics are described by the following system of equations

$$\dot{q} = M_q q + M_{\delta_e}\delta_e \tag{4.7a}$$

$$\dot{\delta}_e = -\tau\delta_e + \tau\delta_{e,c} \tag{4.7b}$$

The dimensional stability and control derivatives M_q, M_{δ_e}, and τ are uncertain system parameters. q is the body-axis pitch rate. δ_e is the elevator deflection and $\delta_{e,c}$ is the commanded elevator

deflection. q and δ_e are taken to be 0 at trim. As an abstract system of equations, Eq. (4.7) does not obviously exhibit multiple-timescale characteristics since the timescale separation parameter is not apparent. However, with an understanding of actuator dynamics, it is clear that the system can be multiple-timescale. This behavior can be made explicit by non-dimensionalizing Eq. (4.7). Three-dimensional parameters must be chosen for this purpose: M_q has units of s^{-1} and will be the first of these three values. The magnitude of the other two-dimensional parameters is arbitrary and will not affect the outcome of the following development so long as their units match q and δ_e. As such arbitrary positive reference values q_{ref} and $\delta_{e,ref}$ are used. The non-dimensional variables are, therefore:

$$\bar{q} \triangleq \frac{q}{q_{ref}} \qquad \bar{\delta}_e \triangleq \frac{\delta_e}{\delta_{e,ref}} \qquad \bar{\delta}_{e,c} \triangleq \frac{\delta_{e,c}}{\delta_{e,ref}} \qquad \bar{t} \triangleq t|M_q| \tag{4.8}$$

Substituting into Eq. (4.7) and simplifying gives

$$\frac{\mathrm{d}\bar{q}}{\mathrm{d}\bar{t}} = \mathrm{sign}(M_q)\bar{q} + \mathrm{sign}(M_{\delta_e})\frac{|M_{\delta_e}|\delta_{e,ref}}{|M_q|q_{ref}}\bar{\delta}_e \tag{4.9a}$$

$$\frac{|M_q|}{|\tau|}\frac{\mathrm{d}\bar{\delta}_e}{\mathrm{d}\bar{t}} = -\mathrm{sign}(\tau)\bar{\delta}_e + \mathrm{sign}(\tau)\bar{\delta}_{e,c} \tag{4.9b}$$

Assuming that $|M_q| \ll |\tau|$ then this system exhibits multiple-timescale characteristics. Let $\epsilon = \frac{|M_q|}{|\tau|}$ and $t_s = \bar{t}$

$$\acute{\bar{q}} = \mathrm{sign}(M_q)\bar{q} + \mathrm{sign}(M_{\delta_e})\frac{|M_{\delta_e}|\delta_{e,ref}}{|M_q|q_{ref}}\bar{\delta}_e \tag{4.10a}$$

$$\epsilon\acute{\bar{\delta}}_e = -\mathrm{sign}(\tau)\bar{\delta}_e + \mathrm{sign}(\tau)\bar{\delta}_{e,c} \tag{4.10b}$$

This is the full-order multiple-timescale system. The reduced slow model is

$$\acute{\bar{q}} = \mathrm{sign}(M_q)\bar{q} + \mathrm{sign}(M_{\delta_e})\frac{|M_{\delta_e}|\delta_{e,ref}}{|M_q|q_{ref}}\bar{\delta}_{e,c} \tag{4.11a}$$

$$\bar{\delta}_{e,s} = \bar{\delta}_{e,c} \tag{4.11b}$$

and the reduced fast model is

$$\grave{\bar{q}} = 0 \tag{4.12a}$$

$$\grave{\bar{\delta}}_e = -\text{sign}(\tau)\bar{\delta}_e + \text{sign}(\tau)\bar{\delta}_{e,c} \tag{4.12b}$$

with the fast timescale being $t_f = t|\tau|$. It is useful to redimensionalize these equations. The dimensional reduced slow model

$$\dot{q} = M_q q + M_{\delta_e}\delta_{e,c} \tag{4.13a}$$

$$\delta_{e,s} = \delta_{e,c} \tag{4.13b}$$

and the dimensional reduced fast model

$$\dot{q} = 0 \tag{4.14a}$$

$$\dot{\delta}_e = -\tau\delta_e + \tau\delta_{e,c} \tag{4.14b}$$

4.4.1 Control Synthesis

In this section, a FOAC, a ROAC, and a KAMS adaptive controller are designed. The reference model is

$$\dot{q}_m = -a_m\tilde{q}_m \tag{4.15}$$

where $a_m \in \mathbb{R}_+$. The reference model transfer function is strictly positive real (SPR). MRAC is used. For KAMS Composite Control will be used to fuse the control signals.

4.4.1.1 Full-Order Adaptive Control

The full-order system from Eq. (4.7) has a transfer function of

$$\frac{q(s)}{\delta_{e,c}(s)} = \frac{\tau M_{\delta_e}}{s^2 + (\tau - M_q)\, s + (-M_q\tau)} \tag{4.16}$$

This is minimum phase and satisfies assumptions P1-P4 of [24, page 332]. The reference model given in Eq. (4.15) is not valid here because the transfer function in Eq. (4.16) has a relative degree of 2. Therefore, a new reference model is selected to be

$$\ddot{q}_m = -2a_m\dot{q}_m - a_m^2\tilde{q}_m \tag{4.17}$$

This satisfies assumptions M1 and M2 of [24, page 332]. Therefore, an adaptive controller can be selected directly from [24, Table 6.2]. Defining $\boldsymbol{\omega} \triangleq \begin{bmatrix} \boldsymbol{\omega}_1^T & \boldsymbol{\omega}_2^T & q & r \end{bmatrix}^T$

$$\dot{\boldsymbol{\omega}}_1 = -\boldsymbol{\omega}_1 + \hat{\boldsymbol{\theta}}^T\boldsymbol{\omega} + \boldsymbol{\phi}^T\dot{\hat{\boldsymbol{\theta}}} \tag{4.18a}$$

$$\dot{\boldsymbol{\omega}}_2 = -\boldsymbol{\omega}_2 + q \tag{4.18b}$$

$$\dot{\boldsymbol{\phi}} = a_m\boldsymbol{\phi} + \boldsymbol{\omega} \tag{4.18c}$$

$$\dot{\hat{\boldsymbol{\theta}}} = -\Gamma e_q\boldsymbol{\phi}\,\mathrm{sign}\left(\tau M_{\delta_e}\right) \tag{4.18d}$$

$$\delta_{e,c} = \hat{\boldsymbol{\theta}}^T\boldsymbol{\omega} + \boldsymbol{\phi}^T\dot{\hat{\boldsymbol{\theta}}} \tag{4.18e}$$

where $\boldsymbol{\omega}_1(t=0) = 0$, $\boldsymbol{\omega}_2(t=0) = 0$, and $\boldsymbol{\phi}(t=0) = \begin{bmatrix} 0 & 0 & 0 & 0 \end{bmatrix}^T$. The initial conditions of $\hat{\boldsymbol{\theta}}$ can be chosen to take advantage of prior knowledge (i.e. an initial guess of the optimal gains). Γ is the adaptive gain. The assumptions in [24, Table 6.2] are not affected by the timescale separation parameter. Thus, by Theorem 4.1, the error e_q converges to 0 and the system is bounded. Further, again by Theorem 4.1, all timescale separation parameters are valid for this system under FOAC.

4.4.1.2 Reduced-Order Adaptive Control

The dimensional reduced slow model from Eq. (4.13) has a transfer function of

$$\frac{q(s)}{\delta_{e,c}(s)} = \frac{M_{\delta_e}}{s - M_q} \tag{4.19}$$

This is minimum phase and satisfies assumptions P1-P4 of [24, page 332]. The relative degree is 1 so the first-order reference model is valid. This satisfies assumptions M1 and M2 of [24, page

332]. Therefore, an adaptive controller can be selected directly from [24, Table 6.1].

$$\acute{\boldsymbol{\omega}}_1 = -\boldsymbol{\omega}_1 + \hat{\boldsymbol{\theta}}^T \boldsymbol{\omega} \tag{4.20a}$$

$$\acute{\boldsymbol{\omega}}_2 = -\boldsymbol{\omega}_2 + q \tag{4.20b}$$

$$\acute{\hat{\boldsymbol{\theta}}} = -\Gamma e_q \boldsymbol{\omega} \operatorname{sign}(M_{\delta_e}) \tag{4.20c}$$

$$\delta_{e,c} = \boldsymbol{\theta}^T \boldsymbol{\omega} \tag{4.20d}$$

where $\boldsymbol{\omega}_1(t=0) = 0$ and $\boldsymbol{\omega}_2(t=0) = 0$. The initial conditions of $\hat{\boldsymbol{\theta}}$ can be chosen to take advantage of prior knowledge (i.e. an initial guess of the optimal gains). Γ is the adaptive gain. By Theorem 4.2 and Corollary 4.2, there exists a set of timescale separation parameters such that the closed-loop tracking error e_q is bounded by a bound on the order of the timescale separation parameter. The set of valid timescale separation parameters for ROAC will be discussed in the next section. However, the following Lyapunov function for the reduced slow subsystem will be useful

$$V_{e_{\bar{q}}} = \frac{1}{2a_m q_{ref}^2} e_q^2 + \frac{1}{2q_{ref}^2} \tilde{\boldsymbol{\theta}}^T \Gamma^{-1} \tilde{\boldsymbol{\theta}} \frac{|M_{\delta_e}|}{a_m} \tag{4.21}$$

By [24, equation 6.4.8] the error dynamics for the reduced slow system (i.e. not considering the fast states) are

$$f_{e_q,s} = -a_m e_q + a_m \frac{M_{\delta_e}}{a_m} \tilde{\boldsymbol{\theta}}^T \boldsymbol{\omega} \tag{4.22}$$

Differentiating Eq. (4.21) and substituting in Eqs. (4.20c) and (4.22) gives

$$\begin{aligned} \mathcal{L}(f_{e_q,s}) V_{e_{\bar{q}}} = & \frac{1}{a_m q_{ref}^2} e_q \left(-a_m e_q + a_m \frac{M_{\delta_e}}{a_m} \tilde{\boldsymbol{\theta}}^T \boldsymbol{\omega} \right) \\ & + \frac{1}{q_{ref}^2} \tilde{\boldsymbol{\theta}}^T \Gamma^{-1} \left(-\Gamma e_q \boldsymbol{\omega} \operatorname{sign}(M_{\delta_e}) \right) \frac{|M_{\delta_e}|}{a_m} \end{aligned} \tag{4.23}$$

Using $e_{\bar{q}} \triangleq \frac{e_q}{q_{ref}}$ this simplifies to

$$\mathcal{L}(f_{e_q,s}) V_{e_{\bar{q}}} = -e_{\bar{q}}^2 \tag{4.24}$$

4.4.1.3 KAMS

The adaptive controller designed in the previous section can be extended to be a KAMS controller by selecting the slow control $\delta_{e,c,s}$ to be the control from ROAC (Eq. (4.20)) and designing an additional controller for the fast states. Consider the following candidate Lyapunov function for the reduced fast system in Eq. (4.12)

$$V_{e_{\delta_e}} = \frac{1}{2}\tilde{\bar{\delta}}_e^2 \tag{4.25}$$

Differentiating

$$\mathcal{L}(f_{e_{\delta_e},f})V_{e_{\delta_e}} = \tilde{\bar{\delta}}_e\dot{\tilde{\bar{\delta}}}_e \tag{4.26}$$

Substituting Eq. (4.12b) and recalling that in the fast timescale the manifold is constant with respect to time gives

$$\mathcal{L}(f_{e_{\delta_e},f})V_{e_{\delta_e}} = \tilde{\bar{\delta}}_e\left(-\text{sign}(\tau)\bar{\delta}_e + \text{sign}(\tau)\bar{\delta}_{e,c}\right) \tag{4.27}$$

By definition of Composite Control

$$\mathcal{L}(f_{e_{\delta_e},f})V_{e_{\delta_e}} = \tilde{\bar{\delta}}_e\left(-\text{sign}(\tau)\bar{\delta}_e + \text{sign}(\tau)\left[\bar{\delta}_{e,c,s} + \bar{\delta}_{e,c,f}\right]\right) \tag{4.28}$$

Some algebra gives

$$\mathcal{L}(f_{e_{\delta_e},f})V_{e_{\delta_e}} = -\text{sign}(\tau)\tilde{\bar{\delta}}_e\left(\bar{\delta}_e - \bar{\delta}_{e,c,s}\right) + \text{sign}(\tau)\tilde{\bar{\delta}}_e\bar{\delta}_{e,c,f} \tag{4.29}$$

Because the manifold is $\bar{\delta}_{e,c,s}$ so $\tilde{\bar{\delta}}_e = \left(\bar{\delta}_e - \bar{\delta}_{e,c,s}\right)$ can be substituted. Therefore

$$\mathcal{L}(f_{e_{\delta_e},f})V_{e_{\delta_e}} = -\text{sign}(\tau)\tilde{\bar{\delta}}_e^2 + \text{sign}(\tau)\tilde{\bar{\delta}}_e\bar{\delta}_{e,c,f} \tag{4.30}$$

The left side of this equation is negative definite if the fast control is selected to be

$$\bar{\delta}_{e,c,f} = \left(1 - \text{sign}(\tau)k_f\right)\tilde{\bar{\delta}}_e \tag{4.31}$$

where $k_f > 0$ is a non-adaptive gain. Notably, this meets the condition that $\bar{\delta}_{e,c,f}(\bar{\delta}_e = \bar{\delta}_{e,c}) = 0$. Substituting this fast control into Eq. (4.30) gives

$$\mathcal{L}(f_{e_{\delta_e},f})V_{e_{\delta_e}} = -k_f\tilde{\bar{\delta}}_e^2 \tag{4.32}$$

Applying the definition of Composite Control:

$$\delta_{e,c} = \delta_{e,c,s} + \delta_{e,c,f} \tag{4.33}$$

Substituting Eq. (4.20) and the dimensional version of Eq. (4.31) gives:

$$\acute{\boldsymbol{\omega}}_1 = -\boldsymbol{\omega}_1 + \hat{\boldsymbol{\theta}}^T\boldsymbol{\omega} \tag{4.34a}$$

$$\acute{\boldsymbol{\omega}}_2 = -\boldsymbol{\omega}_2 + q \tag{4.34b}$$

$$\acute{\hat{\boldsymbol{\theta}}} = -\Gamma e_q\boldsymbol{\omega}\,\mathrm{sign}\,(M_{\delta_e}) \tag{4.34c}$$

$$\delta_{e,c} = \hat{\boldsymbol{\theta}}^T\boldsymbol{\omega} + (1 - \mathrm{sign}(\tau)k_f)\,\tilde{\delta}_e \tag{4.34d}$$

By Theorem 4.3 there exists a set of timescale separation parameters such that the closed-loop tracking error e_q is bounded by a bound on the order of the timescale separation parameter. The set of valid timescale separation parameters will now be found by applying Corollary 2.2. By Eq. (4.24)

$$\alpha_1 = 1 \tag{4.35}$$

By Eq. (4.32)

$$\alpha_3 = k_f \tag{4.36}$$

Now consider the interconnection condition Eq. (2.28b). Substituting Eq. (4.10a), Eq. (4.11a), and the partial of Eq. (4.21) gives

$$\mathcal{L}(f_{\bar{q}} - f_{\bar{q},s})V_{e_{\bar{q}}} = \frac{1}{a_m} e_{\bar{q}} \left[\left(\text{sign}(M_q)\bar{q} + \text{sign}(M_{\delta_e}) \frac{|M_{\delta_e}|\delta_{e,ref}}{|M_q|q_{ref}} \bar{\delta}_e \right) - \left(\text{sign}(M_q)\bar{q} + \text{sign}(M_{\delta_e}) \frac{|M_{\delta_e}|\delta_{e,ref}}{|M_q|q_{ref}} \bar{\delta}_{e,c,s} \right) \right]$$

Simplifying gives

$$\mathcal{L}(f_{\bar{q}} - f_{\bar{q},s})V_{e_{\bar{q}}} = \frac{1}{a_m} \text{sign}(M_{\delta_e}) \frac{|M_{\delta_e}|\delta_{e,ref}}{|M_q|q_{ref}} e_{\bar{q}} \left[\bar{\delta}_e - \bar{\delta}_{e,c,s} \right] \tag{4.37}$$

Using $\tilde{\bar{\delta}}_e = \bar{\delta}_e - \bar{\delta}_{e,c,s}$

$$\mathcal{L}(f_{\bar{q}} - f_{\bar{q},s})V_{e_{\bar{q}}} = \frac{1}{a_m} \text{sign}(M_{\delta_e}) \frac{|M_{\delta_e}|\delta_{e,ref}}{|M_q|q_{ref}} e_{\bar{q}} \tilde{\bar{\delta}}_e \tag{4.38}$$

Because β is the upper bound

$$\beta = \frac{|M_{\delta_e}|\delta_{e,ref}}{a_m |M_q| q_{ref}} \tag{4.39}$$

Thus $\exists \alpha_1, \alpha_3, \beta$ such that the conditions of Corollary 2.2 are satisfied. By Corollary 2.2, the closed-loop system under KAMS is asymptotically stable for all values of the timescale separation parameter.

Now consider Corollary 4.3 for ROAC. KAMS is equivalent to ROAC when $k_f = \text{sign}(\tau)$ (i.e. the fast control is always zero). Thus, there are two cases. First, if $\text{sign}(\tau) > 0$ then all of the logic for the KAMS stability analysis holds. In this case, ROAC is also asymptotically stable for all values of the timescale separation parameter. The second case is when $\text{sign}(\tau) < 0$. In this case, Eq. (4.32) becomes positive definite. Thus the conditions of Corollary 4.3 are not satisfied. Thus the boundedness of the closed-loop system can not be guaranteed by Theorem 2.1. This makes sense because $\text{sign}(\tau) < 0$ is the case where the neglected fast dynamics are unstable. Intuitively, ROAC can not account for this. In this case, the manifold is not an asymptotically

stable equilibrium of the fast states, so Theorem 4.2 is also not valid. Because the theorems in Chapter 2 only give sufficient conditions, no conclusions about the stability of the system when $\text{sign}(\tau) < 0$ can be drawn. However, because the fast subsystem is unstable and left unregulated the full-order system would likely be unstable as well.

4.4.1.4 Summary of Control Laws

The adaptive control equations for FOAC, ROAC, and KAMS are summarized and compared in Table 4.1. The equations for ROAC and KAMS have been converted to the original timescale t. This is done using the previously defined relationship $t_s = t|M_q|$. This adds $|M_q|$ to the differential equations for the extra states and the adaptive law. However, M_q is an unknown and constant parameter so it must be eliminated from the control. This is done by absorbing the extra $|M_q|$ terms into the adaptive law gains. Notably, Γ must be chosen to ensure the adaptation occurs in the slow timescale.

Table 4.1 allows the three methods to be directly compared. The significant differences are highlighted in red. The most notable difference between FOAC and ROAC is that FOAC is a second-order method. This makes sense because ROAC is a reduced-order method. Thus FOAC has a second-order reference model and additional terms in the extra states, adaptive law, and control law. See [24] for more details. The other notable difference between FOAC and ROAC is that ROAC can not guarantee the stability of the system when $\tau \leq 0$ (i.e. the fast dynamics are unstable). ROAC assumes that the fast dynamics are stable. Finally, Table 4.1 makes it clear that KAMS is an extension of ROAC. The only difference between the two is the addition of a fast control term in the control law. This one change allows the fast dynamics to be inherently unstable without destabilizing the closed-loop system. Thus KAMS is found to be simpler than FOAC and more capable than ROAC.

4.4.2 Numerical Results

In this section, the performance of FOAC, ROAC, KAMS, and Composite Control are compared (i.e. rise time and overshoot). To that end, a numerical simulation of the linearized pitch

Table 4.1: Comparison of ROAC, FOAC, and KAMS control methodologies.

	FOAC	**ROAC**	**KAMS**
Model	$\ddot{q}_m = 2a_m\dot{q}_m - a_m^2\tilde{q}_m$	$\dot{q}_m = a_m\tilde{q}_m$	$\dot{q}_m = a_m\tilde{q}_m$
Extra States	$\dot{\boldsymbol{\omega}}_1 = -\boldsymbol{\omega}_1 + \hat{\boldsymbol{\theta}}^T\boldsymbol{\omega} + \boldsymbol{\phi}^T\dot{\hat{\boldsymbol{\theta}}}$ $\dot{\boldsymbol{\omega}}_2 = -\boldsymbol{\omega}_2 + q$ $\dot{\boldsymbol{\phi}} = a_m\boldsymbol{\phi} + \boldsymbol{\omega}$	$\dot{\boldsymbol{\omega}}_1 = -\boldsymbol{\omega}_1 + \hat{\boldsymbol{\theta}}^T\boldsymbol{\omega}$ $\dot{\boldsymbol{\omega}}_2 = -\boldsymbol{\omega}_2 + q$	$\dot{\boldsymbol{\omega}}_1 = -\boldsymbol{\omega}_1 + \hat{\boldsymbol{\theta}}^T\boldsymbol{\omega}$ $\dot{\boldsymbol{\omega}}_2 = -\boldsymbol{\omega}_2 + q$
Adaptive Law	$\dot{\hat{\boldsymbol{\theta}}} = -\Gamma e_q\boldsymbol{\phi}\,\mathrm{sign}\,(\tau M_{\delta_e})$	$\dot{\hat{\boldsymbol{\theta}}} = -\Gamma e_q\boldsymbol{\omega}\,\mathrm{sign}\,(M_{\delta_e})$	$\dot{\hat{\boldsymbol{\theta}}} = -\Gamma e_q\boldsymbol{\omega}\,\mathrm{sign}\,(M_{\delta_e})$
Control Law	$\delta_{e,c} = \hat{\boldsymbol{\theta}}^T\boldsymbol{\omega} + \boldsymbol{\phi}^T\dot{\hat{\boldsymbol{\theta}}}$	$\delta_{e,c} = \hat{\boldsymbol{\theta}}^T\boldsymbol{\omega}$	$\delta_{e,c} = \hat{\boldsymbol{\theta}}^T\boldsymbol{\omega}$ $+\,(1 - \mathrm{sign}(\tau)k_f)\,\tilde{\delta}_e$
Stability	Asymptotically Stable	Asymptotically Stable	Asymptotically Stable
Valid ϵ	$\forall\epsilon \in (0,1)$	$\tau > 0 \implies \forall\epsilon \in (0,1)$	$\forall\epsilon \in (0,1)$

dynamics is performed using parameters from a Boeing 747-100/200. The system is linearized about trim during an approach for landing (0 ft altitude, 131 knots true airspeed, 8.5° angle of attack, and a standard atmosphere). An analysis of a Boeing 747-100/200 on approach can be found in [110, Appendix B Airplane J]. Using this information, the parameters needed in Section 4.4 can be found

$$M_q = \frac{\rho V_a^* S c^2 C_{m_q}}{2J_y} \tag{4.40a}$$

$$M_{\delta_e} = \frac{\rho V_a^{*2} S c C_{m_{\delta_e}}}{J_y} \tag{4.40b}$$

where ρ is the air density, V_a^* is the aircraft airspeed, S is the wing area, c is the mean aerodynamic chord (mac), C_{m_q} the nondimensional pitch damping stability derivative, $C_{m_{\delta_e}}$ nondimensional elevator effectiveness control derivative and J_y is the mass moment of inertia of the aircraft about the body frame right axis. The time constant $\frac{1}{\tau}$ for the actuator dynamics is not known. However, it has been published that the elevator rate saturates at $\dot{\delta}_e = 37^\circ\ s^{-1}$ [111]. Therefore, $\tau = 80\ s^{-1}$ is chosen so that the elevator moves quickly but does not saturate. $\hat{\boldsymbol{\theta}}$ is initialized at the Model Reference Control gains. However, uncertainty is added to the system parameters before calculating the Model Reference Control gains. Uncertainty is created by sampling the estimated parameter values from a normal distribution with a mean of the true value and a standard deviation of 20% of the true value. All other states are initialized at 0. a_m is chosen to be -1 and 1 respectively. Γ and k_f are each tuned for optimal performance. The diagonal entries of Γ are found to be 0.05 deg^{-2}. k_f is found to be 4. The reference model input is chosen to be $r = sin(0.1 * t) + 2$ degrees per second.

Figure 4.4 shows the evolution of the body axis pitch rate, Fig. 4.5 shows the evolution of the elevator deflection, and Figs. 4.6, 4.7, 4.8, and 4.9 show the time histories of the adapting parameters. All three multiple-timescale adaptive control methodologies - FOAC, ROAC, and KAMS - are shown for comparison. All three methodologies converge to the reference model. KAMS drives the fast actuator dynamics to the manifold the quickest and with the least overshoot of the

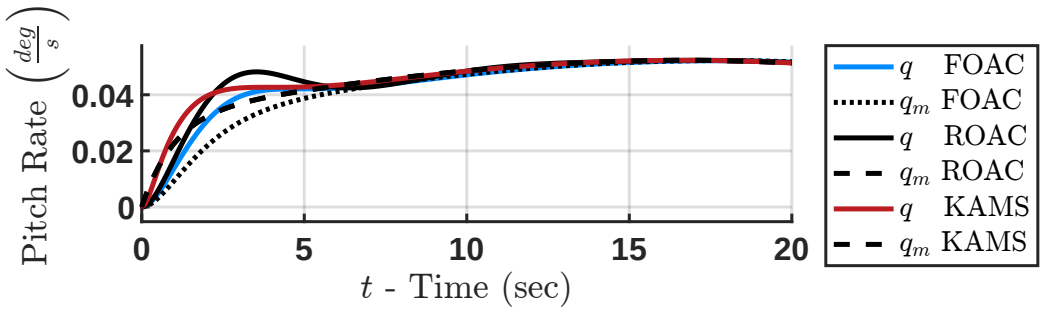

Figure 4.4: Slow state evolution comparison of FOAC, ROAC, and KAMS.

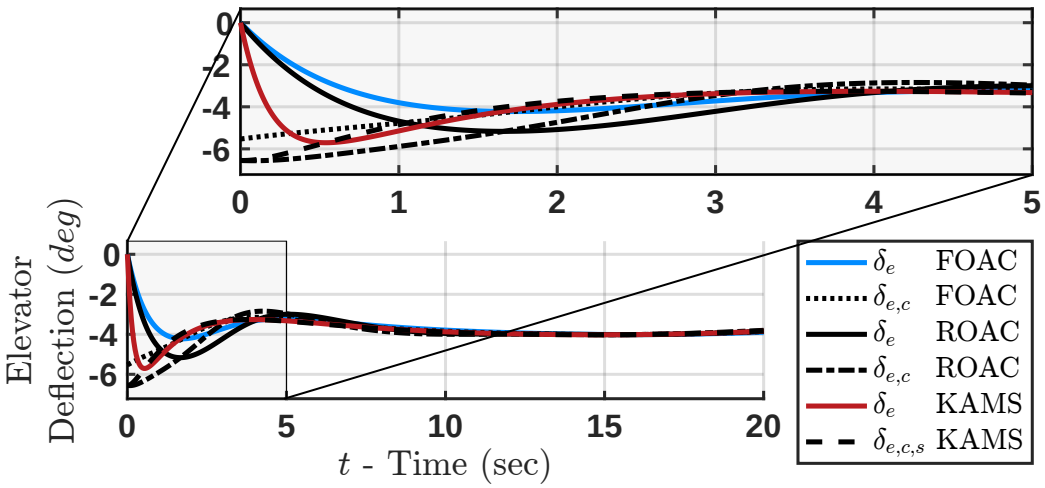

Figure 4.5: Fast state evolution comparison of FOAC, ROAC, and KAMS.

three methodologies. This leads to improved accuracy in tracking the slow state reference model. The KAMS adapting gains do not overshoot their steady-state value because KAMS converges more quickly to the manifold. Effectively, this means that the evolution of the gains relies more on q and is not misled by the actuator dynamics. See specifically $\hat{\theta}_2$ in Fig. 4.7 where this effect is especially clear. For completeness, Figs. 4.10 and 4.11 show the slow state evolution and fast state evolution of this system under Composite Control. The Composite Control control laws used here are the same as KAMS except the parameters are constant with respect to time. As can be seen, Composite Control has steady-state error in the slow states.

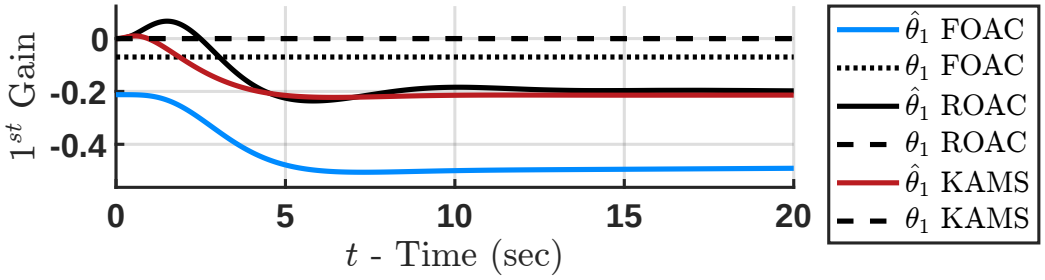

Figure 4.6: First adapting gain evolution comparison of FOAC, ROAC, and KAMS.

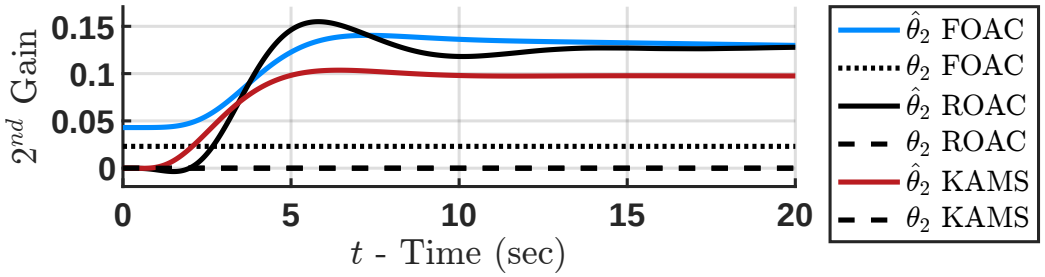

Figure 4.7: Second adapting gain evolution comparison of FOAC, ROAC, and KAMS.

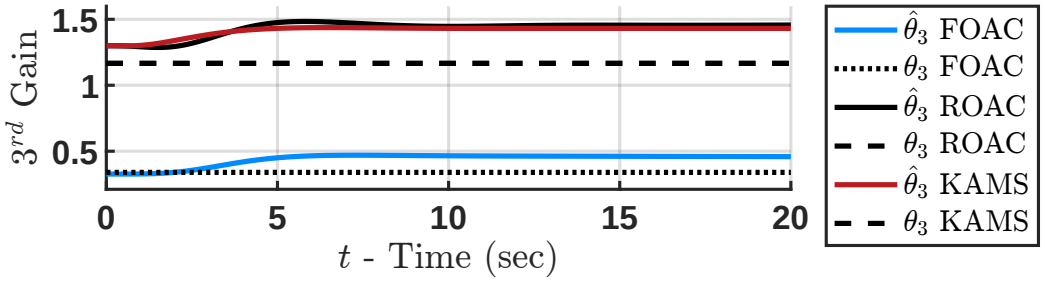

Figure 4.8: Third adapting gain evolution comparison of FOAC, ROAC, and KAMS.

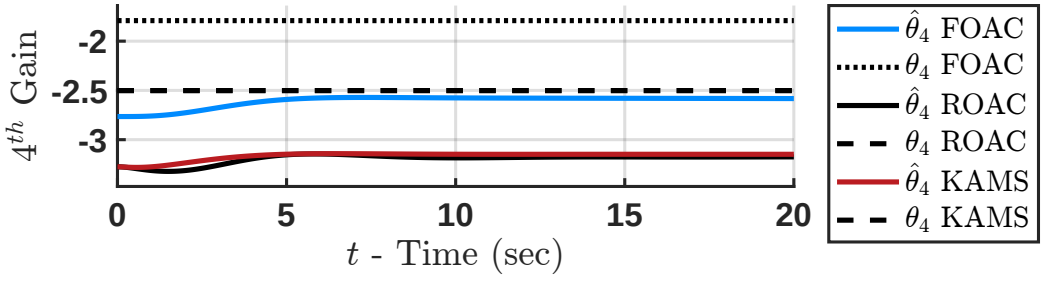

Figure 4.9: Fourth adapting gain evolution comparison of FOAC, ROAC, and KAMS.

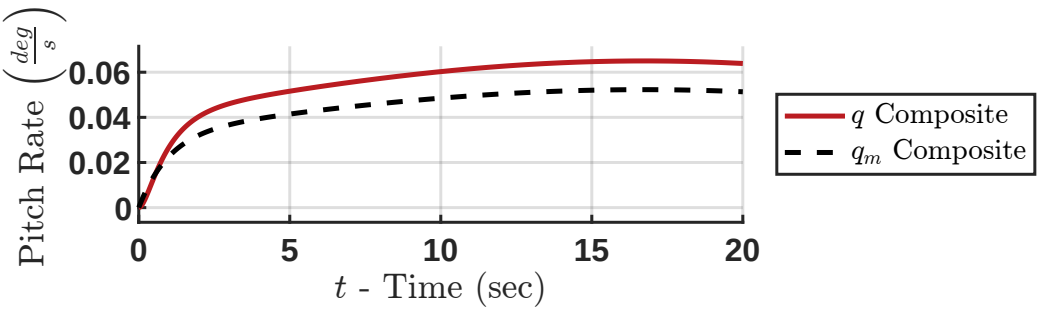

Figure 4.10: Slow state evolution of Composite Control on a parametrically uncertain plant.

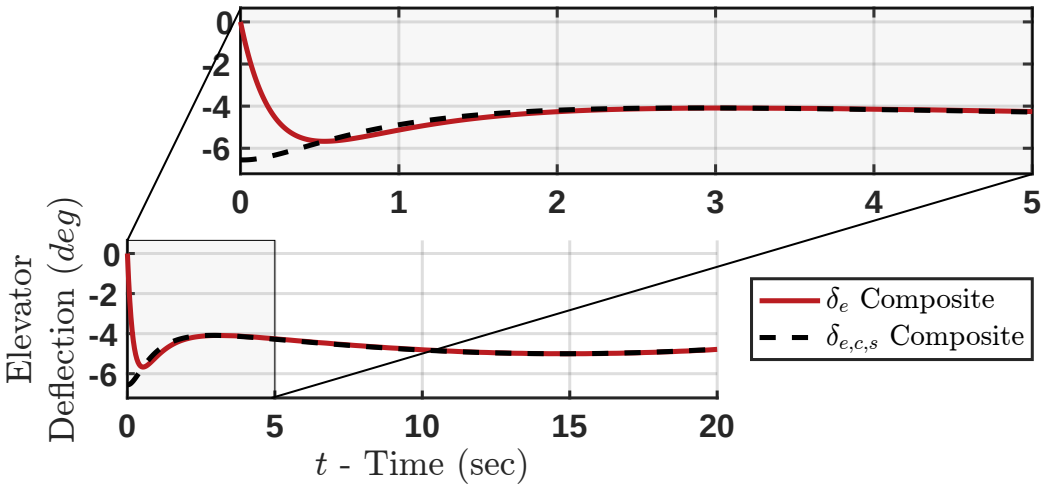

Figure 4.11: Fast state evolution of Composite Control on a parametrically uncertain plant.

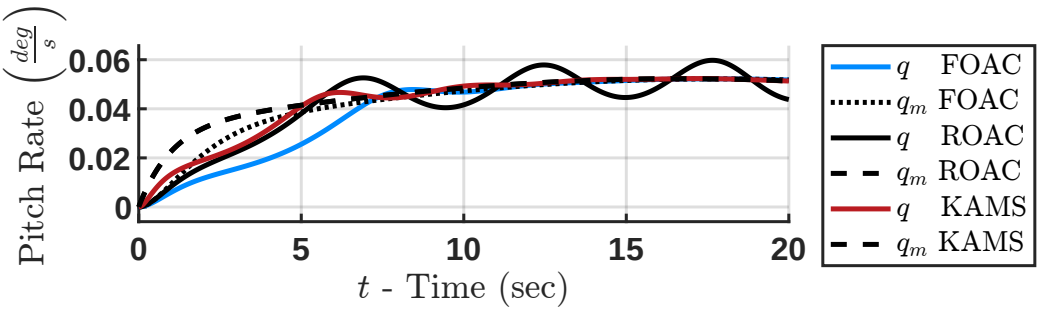

Figure 4.12: Slow state evolution comparison with large timescale uncertainty.

4.4.3 Robustness Test

In this subsection, the robustness of FOAC, ROAC, and KAMS is compared. This is done by performing the same numerical simulation as the previous section but changing the timescale separation. In the previous section, the timescale separation parameter was $\epsilon = 0.38$. In this section, the nondimensional pitch damping stability derivative is increased to $C_{m_q} = 51.4$ per radian (as opposed to $C_{m_q} = 21.4$). This increases the timescale separation parameter to $\epsilon = 0.92$. To allow for slightly more precision, the initial estimate of the adapting parameters is set to be exactly 80% of the Model Reference Control value (instead of being drawn from a normal distribution with a standard deviation of 20% away from the Model Reference Control value as was done in the previous section). Figure 4.12 shows the evolution of the body axis pitch rate, Fig. 4.13 shows the evolution of the elevator deflection, and Figs. 4.14, 4.15, 4.16, and 4.17 shows the time histories of the adapting parameters. All three multiple-timescale adaptive control methodologies - FOAC, ROAC, and KAMS - are shown for comparison. As can be seen, ROAC fails to converge to the reference model (or at least converges slowly with significant transient oscillations). This is because the timescale separation is small enough to induce a time delay between a commanded input and the actual response. Both FOAC and KAMS converge to their reference models, but the transient response of KAMS deviates the least from the performance in the prior section. This demonstrates robustness to uncertainties in the timescale separation. Again KAMS demonstrates the best rise time.

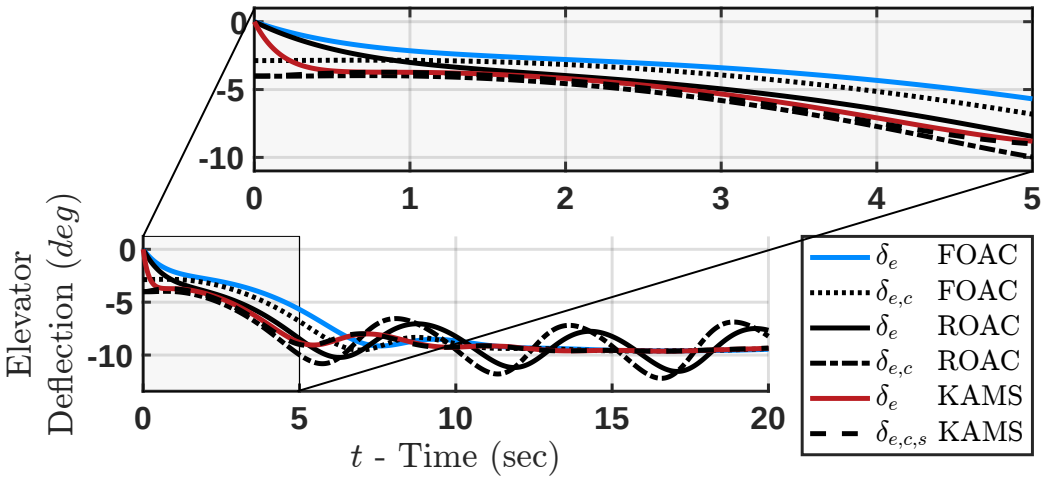

Figure 4.13: Fast state evolution comparison of FOAC, ROAC, and KAMS.

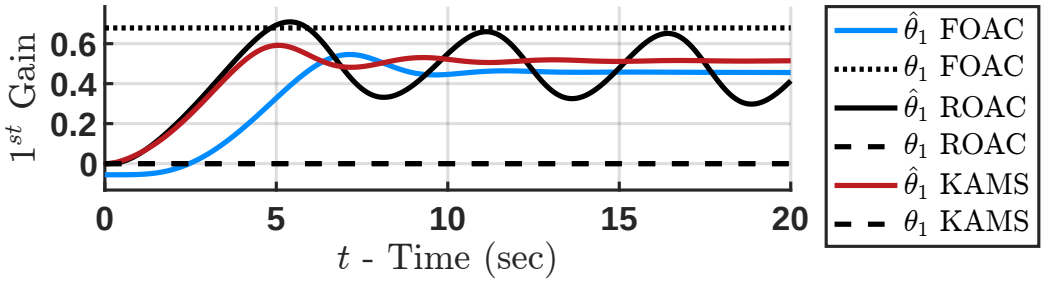

Figure 4.14: First adapting gain evolution comparison of FOAC, ROAC, and KAMS.

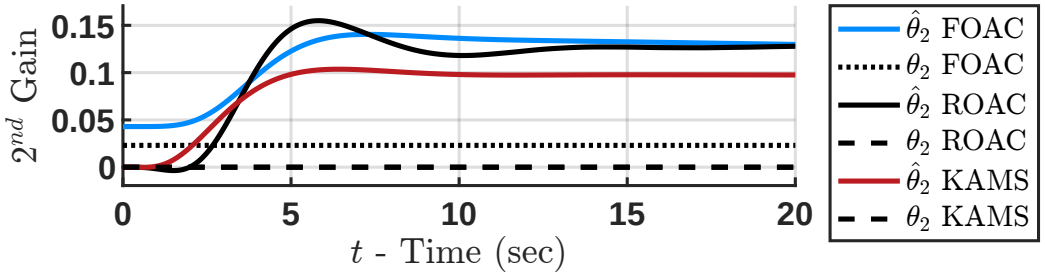

Figure 4.15: Second adapting gain evolution comparison of FOAC, ROAC, and KAMS.

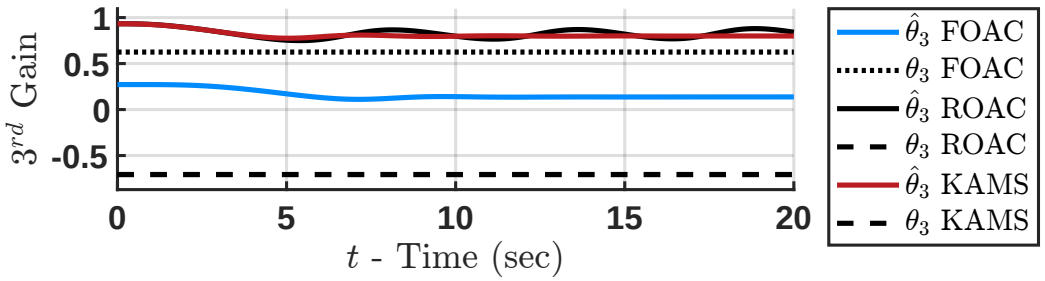

Figure 4.16: Third adapting gain evolution comparison of FOAC, ROAC, and KAMS.

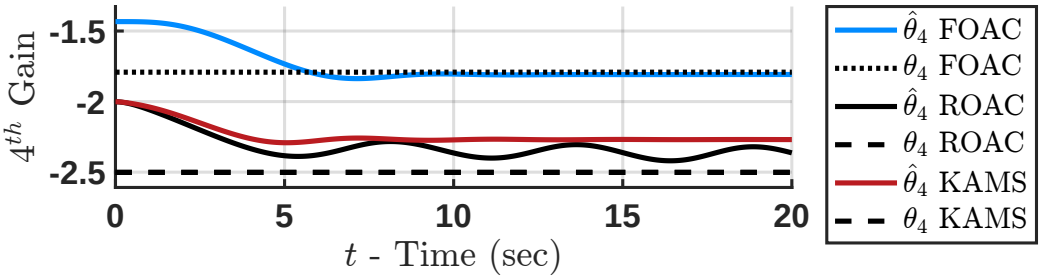

Figure 4.17: Fourth adapting gain evolution comparison of FOAC, ROAC, and KAMS.

4.5 Chapter Summary

This chapter presented and developed two additional adaptive control methodologies for multiple-timescale systems. Full-Order Adaptive Control (FOAC) uses traditional adaptive control on the full-order model. Reduced-Order Adaptive Control (ROAC) uses adaptive control on one of the reduced-order models. Both methods were shown to be asymptotically stable under the conditions described by Theorem 2.1, Theorem 4.1, Theorem 4.2, and Theorem 4.3 respectively. An example with numerical results was given to demonstrate and compare these methods to KAMS. Two conclusions can be drawn from the theoretical and numerical results of this chapter.

1. Small changes in the timescale separation parameter can have a large effect on the system response. Thus, a method of adaptive control tailored specifically for multiple-timescale systems is needed.

2. FOAC, ROAC, and KAMS are all valid adaptive multiple-timescale control methodologies.

   (a) FOAC is the most straightforward because little to no additional work is needed to reformat the plant. However, FOAC is also the most sensitive to uncertainties in the timescale separation parameter and one must be careful to ensure that none of the stability criteria for the chosen adaptive control method are violated.

   (b) ROAC allows the designer to take advantage of model reduction. The reduced-order model simplifies the control synthesis, but ROAC requires that the discounted dynam-

ics be asymptotically stable. Because of this ROAC often has the most stringent stability criteria of the three.

(c) KAMS also takes advantage of model reduction but does not require the fast dynamics to be stable (unlike ROAC). KAMS also tends to have the best performance because each reduced-order model is stabilized separately and the fast dynamics converge to the manifold more quickly than other methods. This can also lead to improved robustness. KAMS tends to have a more complicated design process because two separate controllers must be designed.

While all three methods are valid, KAMS is judged to provide the best balance between performance and robustness.

5. QUADROTOR ATTITUDE STABILIZATION USING ADAPTIVE REGULATION OF A LINEAR MULTIPLE-TIMESCALE MODEL

From military [112] to industry [113] and from competitive racing [28] to recreation [114] - quadrotor UAV are becoming more and more essential to the future. UAVs must operate in increasingly complex and dynamic environments. At the same time, the drive for low development costs can lead to large uncertainties in system parameters. From the author's experience, many UAV manufacturers don't even bother finding stability and control derivatives for their products. Adaptive control is well suited for these parametric uncertainties. UAVs are excellent testbeds for adaptive control because they are cheap, uncertain, and carry less risk than crewed vehicles. The stabilization of a quadrotor is not a new challenge. Several commercial and open-source solutions exist (e.g. [109, 115]). The most common approach is Proportional-Integral-Derivative (PID) control with sequential loop closure. This chapter proposes and validates a novel method of adaptive attitude stabilization for quadrotors using KAMS. This is the first evaluation of KAMS on a multiple-input multiple-output (MIMO) system. Adaptive control has a long history in aerospace [25] and has been frequently evaluated on quadrotor (e.g. [26, 28, 40]). However, these works did not consider the timescales of the system. Multiple-timescale control has also been evaluated on quadrotor [10], but adaptive control for multiple-timescale systems has not been applied to quadrotors. This chapter fills that gap in the literature. This is done in three stages. First, a multiple-timescale model of a quadrotor is developed in section 5.1. Second, the control architecture is synthesized in section 5.2. Finally, the control is numerically validated in section 5.3.

5.1 Multiple-Timescale Model

The dynamics of a rigid body quadrotor have been published in several sources (e.g. [116]). These differential equations differ from a fixed-wing aircraft primarily in the aerodynamic and control forces. The present work will address the dynamics of a quadrotor linearized about hover.

The state space form is

$$\begin{bmatrix} \acute{h} \\ \acute{u} \\ \acute{v} \\ \acute{w} \\ \acute{p} \\ \acute{q} \\ \acute{r} \\ \acute{\phi} \\ \acute{\theta} \\ \acute{\psi} \end{bmatrix} = \begin{bmatrix} 0 & 0 & 0 & -1 & 0 & 0 & 0 & 0 & 0 & 0 \\ 0 & 0 & 0 & 0 & 0 & 0 & 0 & 0 & -g & 0 \\ 0 & 0 & 0 & 0 & 0 & 0 & 0 & g & 0 & 0 \\ 0 & 0 & 0 & 0 & 0 & 0 & 0 & 0 & 0 & 0 \\ 0 & 0 & 0 & 0 & 0 & 0 & 0 & 0 & 0 & 0 \\ 0 & 0 & 0 & 0 & 0 & 0 & 0 & 0 & 0 & 0 \\ 0 & 0 & 0 & 0 & 0 & 0 & 0 & 0 & 0 & 0 \\ 0 & 0 & 0 & 0 & 1 & 0 & 0 & 0 & 0 & 0 \\ 0 & 0 & 0 & 0 & 0 & 1 & 0 & 0 & 0 & 0 \\ 0 & 0 & 0 & 0 & 0 & 0 & 1 & 0 & 0 & 0 \end{bmatrix} \begin{bmatrix} h \\ u \\ v \\ w \\ p \\ q \\ r \\ \phi \\ \theta \\ \psi \end{bmatrix} + \begin{bmatrix} 0 & 0 & 0 & 0 \\ 0 & 0 & 0 & 0 \\ 0 & 0 & 0 & 0 \\ -\frac{2b\omega_t}{m} & -\frac{2b\omega_t}{m} & -\frac{2b\omega_t}{m} & -\frac{2b\omega_t}{m} \\ -\frac{\sqrt{2}bl\omega_t}{J_{xx}} & -\frac{\sqrt{2}bl\omega_t}{J_{xx}} & \frac{\sqrt{2}bl\omega_t}{J_{xx}} & \frac{\sqrt{2}bl\omega_t}{J_{xx}} \\ \frac{\sqrt{2}bl\omega_t}{J_{yy}} & -\frac{\sqrt{2}bl\omega_t}{J_{yy}} & -\frac{\sqrt{2}bl\omega_t}{J_{yy}} & \frac{\sqrt{2}bl\omega_t}{J_{yy}} \\ \frac{2d\omega_t}{J_{zz}} & -\frac{2d\omega_t}{J_{zz}} & \frac{2d\omega_t}{J_{zz}} & -\frac{2d\omega_t}{J_{zz}} \\ 0 & 0 & 0 & 0 \\ 0 & 0 & 0 & 0 \\ 0 & 0 & 0 & 0 \end{bmatrix} \begin{bmatrix} \omega_1 \\ \omega_2 \\ \omega_3 \\ \omega_4 \end{bmatrix} \tag{5.1a}$$

$$\boldsymbol{y} \triangleq \begin{bmatrix} h & \phi & \theta & \psi \end{bmatrix}^T \tag{5.1b}$$

A traditional body-fixed forward-right-down (1,2,3) coordinate frame is used with the origin at the center of mass. the quadrotor is assumed to be in the X configuration (i.e the x axis is in-between two motors). u, v, and w are the body frame velocities in the 1, 2, and 3 directions respectively. p, q, and r are the body frame angular velocities about the 1, 2, and 3 axes respectively. ϕ, θ, and ψ are the Euler angles for a 3-2-1 rotation sequence about the 1, 2, and 3 axes respectively. h is the vehicle's altitude. ω_i is the angular velocity of the i^{th} motor. The motor indexes begin at 1 in the top right corner and increase clockwise around the vehicle. The front-right motor is assumed to spin counter-clockwise and the direction of rotation alternates for each motor in the sequence.

b and d are motor parameters describing the thrust and torque respectively of each motor through the following relationships

$$T_i = b\omega_i^2 \tag{5.2a}$$

$$\tau_i = d\omega_i^2 \tag{5.2b}$$

where T is thrust and τ is torque. ω_t is the angular velocity of the motors at hover. $l > 0$ is the distance between the center of gravity and each motor. It is assumed that the motors are radially symmetric across the x and y axes. g is the acceleration due to gravity. m is the mass of the quadrotor. Finally, J_{xx}, J_{yy}, and J_{zz} are the body frame mass moments of inertia about the 1, 2, and 3 axes respectively. This system can be rewritten as individual equations (i.e. not in vector-matrix form)

$$\acute{h} = -w \tag{5.3a}$$

$$\acute{\phi} = p \tag{5.3b}$$

$$\acute{\theta} = q \tag{5.3c}$$

$$\acute{\psi} = r \tag{5.3d}$$

$$\acute{w} = -\frac{2b\omega_t}{m}\left(\omega_1 + \omega_2 + \omega_3 + \omega_4\right) \tag{5.3e}$$

$$\acute{p} = \frac{\sqrt{2}bl\omega_t}{J_{xx}}\left(-\omega_1 - \omega_2 + \omega_3 + \omega_4\right) \tag{5.3f}$$

$$\acute{q} = \frac{\sqrt{2}bl\omega_t}{J_{yy}}\left(\omega_1 - \omega_2 - \omega_3 + \omega_4\right) \tag{5.3g}$$

$$\acute{r} = \frac{2d\omega_t}{J_{zz}}\left(\omega_1 - \omega_2 + \omega_3 - \omega_4\right) \tag{5.3h}$$

u and v have been dropped because they are internal dynamics.

The goal is to write these differential equations as a set of singularly perturbed differential equations where the timescales of the system have been made evident. Syrcos and Sannuti suggested one way to do this [117]. Ren, Jaing, and Yang used a variation of Syrcos and Sannuti's

method [7]. In this chapter the timescale separation parameter is choosen to be

$$\epsilon = \text{mean}_{i,j} \left(\frac{z_{j,max} - z_{j,min}}{x_{i,max} - x_{i,min}} \frac{\dot{x}_{i,max}}{\dot{z}_{j,max}} \right) \tag{5.4}$$

where x_i and z_j are the i^{th} and j^{th} components of $\boldsymbol{x}$ and $\boldsymbol{z}$ respectively. Max and min here indicate the maximum and minimum possible values over the system's domain. This is a slight variation on Ren, Jaing, and Yang's method (mean is used instead of max). Intuitively, this is the average value of the ratio between the time rate of change of the fast states and the time rate of change of the slow states normalized by the size of the range across which the respective states are allowed to vary. For this chapter, it is assumed that the mission and system inputs are tuned such that the slow states are h, ϕ, θ, and ψ and the fast states are w, p, q, and r. Multiplying both sides by ϵ gives

$$\acute{h} = -w \tag{5.5a}$$

$$\acute{\phi} = p \tag{5.5b}$$

$$\acute{\theta} = q \tag{5.5c}$$

$$\acute{\psi} = r \tag{5.5d}$$

$$\epsilon\acute{w} = -\epsilon\frac{2b\omega_t}{m}\left(\omega_1 + \omega_2 + \omega_3 + \omega_4\right) \tag{5.5e}$$

$$\epsilon\acute{p} = \epsilon\frac{\sqrt{2}bl\omega_t}{J_{xx}}\left(-\omega_1 - \omega_2 + \omega_3 + \omega_4\right) \tag{5.5f}$$

$$\epsilon\acute{q} = \epsilon\frac{\sqrt{2}bl\omega_t}{J_{yy}}\left(\omega_1 - \omega_2 - \omega_3 + \omega_4\right) \tag{5.5g}$$

$$\epsilon\acute{r} = \epsilon\frac{2d\omega_t}{J_{zz}}\left(\omega_1 - \omega_2 + \omega_3 - \omega_4\right) \tag{5.5h}$$

Because the inputs and the domain are tuned so that there is a timescale separation between the fast and slow states it can be concluded that

$$\mathcal{O}\left(f_w\right) = \mathcal{O}\left(f_p\right) = \mathcal{O}\left(f_q\right) = \mathcal{O}\left(f_r\right) = \mathcal{O}\left(1\right) \tag{5.6}$$

This is now a singularly perturbed set of differential equations. To simplify notation, let $\boldsymbol{x} \triangleq [h\ \phi\ \theta\ \psi]^T$, $\boldsymbol{z} \triangleq [w\ p\ q\ r]^T$, and $\boldsymbol{u} \triangleq [\omega_1\ \omega_2\ \omega_3\ \omega_4]^T$. Therefore

$$\acute{\boldsymbol{x}} = B_x \boldsymbol{z} \tag{5.7a}$$

$$\epsilon \acute{\boldsymbol{z}} = B_z \boldsymbol{u} \tag{5.7b}$$

where

$$B_x = \begin{bmatrix} -1 & 0 & 0 & 0 \\ 0 & 1 & 0 & 0 \\ 0 & 0 & 1 & 0 \\ 0 & 0 & 0 & 1 \end{bmatrix} \tag{5.8a}$$

$$B_z = \epsilon\omega_t \begin{bmatrix} -\frac{2b}{m} & -\frac{2b}{m} & -\frac{2b}{m} & -\frac{2b}{m} \\ -\frac{\sqrt{2}bl}{J_{xx}} & -\frac{\sqrt{2}bl}{J_{xx}} & \frac{\sqrt{2}bl}{J_{xx}} & \frac{\sqrt{2}bl}{J_{xx}} \\ \frac{\sqrt{2}bl}{J_{yy}} & -\frac{\sqrt{2}bl}{J_{yy}} & -\frac{\sqrt{2}bl}{J_{yy}} & \frac{\sqrt{2}bl}{J_{yy}} \\ \frac{2d}{J_{zz}} & -\frac{2d}{J_{zz}} & \frac{2d}{J_{zz}} & -\frac{2d}{J_{zz}} \end{bmatrix} \tag{5.8b}$$

The system is now in the proper format for the application of KAMS.

5.2 Control Synthesis

The control objective is for the slow states to track a reference model. The reduced slow subsystem is

$$\acute{\boldsymbol{x}} = B_x \boldsymbol{z}_s \tag{5.9}$$

The reduced fast subsystem is

$$\grave{\boldsymbol{x}} = 0 \tag{5.10a}$$

$$\grave{\boldsymbol{z}} = B_z \boldsymbol{u} \tag{5.10b}$$

The inertias and engine parameters (i.e. b and d) are uncertain. Note that the slow dynamics are deterministic. In the following sections Adaptive Nonlinear Dynamic Inversion (ANDI) will be used to stabilize the reduced slow subsystems and Sequential Control will be used to fuse the control signals. The pilot will be given influence over the system by allowing them to control the input signal for the slow subsystem. Finally, the error between the reference models and the full-order systems will be shown to asymptotically converge to zero using Theorem 2.1 from KAMS.

5.2.1 Control and Adaptation Laws

The reference model for the slow subsystem is

$$\acute{\boldsymbol{x}}_m = A_{x_m} \tilde{\boldsymbol{x}}_m \tag{5.11}$$

where $A_{x_m} \in \mathbb{R}^{4\times4}$ is hurwitz. The pilot is given control over the system through $\boldsymbol{r}$. This slow reference model can also be written as

$$\acute{\tilde{\boldsymbol{x}}}_m = A_{x_m} \tilde{\boldsymbol{x}}_m - \acute{\boldsymbol{r}} \tag{5.12}$$

Only Nonlinear Dynamic Inversion (NDI) is needed for the slow subsystem because B_x is known perfectly. The manifold is selected to be

$$\boldsymbol{z}_s = B_x^{-1}(A_{x_m} \tilde{\boldsymbol{x}}_m + K_x \boldsymbol{e}_x) \tag{5.13}$$

where $K_x \in \mathbb{R}^{4\times4}$ is hurwitz. The fast subsystem does require adaptive control because it is parametrically uncertain. The reference model for the fast subsystem is

$$\dot{\tilde{\boldsymbol{z}}}_m = A_{z,m}\tilde{\boldsymbol{z}}_m \tag{5.14}$$

where $A_{z_m} \in \mathbb{R}^{4\times4}$ is hurwitz. The input is selected to be

$$\boldsymbol{u} = \hat{B}_z^{-1}(A_{z,m}\tilde{\boldsymbol{z}}_m + K_z\boldsymbol{e}_z) \tag{5.15}$$

where $K_z \in \mathbb{R}^{4\times4}$ is hurwitz. The adaptation law is

$$\dot{\hat{B}}_z = \Gamma\mathrm{Proj}\left(\hat{B}_z, \boldsymbol{e}_z\boldsymbol{u}^T\right) \tag{5.16}$$

where $\Gamma \in \mathbb{R}^{4\times4}$ is a symmetric positive definite adaptation rate gain matrix.

5.2.2 Stability Analysis

Consider the following Lyapunov functions

$$V_{e_x} = \frac{1}{2}\boldsymbol{e}_x^T P_x \boldsymbol{e}_x \tag{5.17a}$$

$$V_{\tilde{x}_m} = \frac{1}{2}\tilde{\boldsymbol{x}}_m^T P_{x_m} \tilde{\boldsymbol{x}}_m \tag{5.17b}$$

$$V_{e_z} = \frac{1}{2}\left(\boldsymbol{e}_z^T P_z \boldsymbol{e}_z + \mathrm{tr}\left(\tilde{B}_z\Gamma^{-1}\tilde{B}_z^T\right)\right) \tag{5.17c}$$

$$V_{\tilde{z}_m} = \frac{1}{2}\tilde{\boldsymbol{z}}_m^T P_{z_m} \tilde{\boldsymbol{z}}_m \tag{5.17d}$$

where $0 < P_x, P_{x_m}, P_z, P_{z_m} \in \mathbb{R}_+^{4\times4}$ are symmetric positive definite matrices and the solutions to the Lyapunov equations $K_x^T P_x + P_x K_x = -Q_x$, $A_x^T P_{x_m} + P_{x_m} A_x = -Q_{x_m}$, $K_z^T P_z + P_z K_z = -Q_z$, and $A_z^T P_{z_m} + P_{z_m} A_z = -Q_{z_m}$ for some symmetric positive matrices $0 < Q_x, Q_{x_m}, Q_z, Q_{z_m} \in$

$\mathbb{R}_{+}^{4\times4}$. Differentiating along the trajectories of the subsystems

$$\mathcal{L}(f_{e_\xi,s})V_{e_x} \leq -\boldsymbol{e}_x^T Q_x \boldsymbol{e}_x \tag{5.18a}$$

$$\mathcal{L}(f_{\tilde{x}_m})V_{\tilde{x}_m} = -\tilde{\boldsymbol{x}}_m^T Q_{x_m} \tilde{\boldsymbol{x}}_m - \left[\tilde{\boldsymbol{x}}_m^T P_{x_m} \acute{\boldsymbol{r}}\right] \tag{5.18b}$$

$$\mathcal{L}(f_{e_\eta,f})V_{e_z} \leq -\boldsymbol{e}_z^T Q_z \boldsymbol{e}_z \tag{5.18c}$$

$$\mathcal{L}(f_{z_m,f})V_{\tilde{z}_m} = -\tilde{\boldsymbol{z}}_m^T Q_{z_m} \tilde{\boldsymbol{z}}_m \tag{5.18d}$$

Eqs. (5.18a) and (5.18c) are derived in [65, Eqs. 1.20 to 1.23]. Taking the 2-norm gives

$$\mathcal{L}(f_{e_\xi,s})V_{e_x} \leq -\lambda_{min}(Q_x) \left|\boldsymbol{e}_x\right|_2^2 \tag{5.19a}$$

$$\mathcal{L}(f_{\tilde{x}_m})V_{\tilde{x}_m} \leq -\lambda_{min}(Q_{x_m}) \left|\tilde{\boldsymbol{x}}_m\right|_2^2 + \left[\sigma_{max}\left(P_{x_m}\right) \left|\tilde{\boldsymbol{x}}_m\right|_2 \left|\acute{\boldsymbol{r}}\right|_2\right] \tag{5.19b}$$

$$\mathcal{L}(f_{e_\eta,f})V_{e_z} \leq -\lambda_{min}(Q_z) \left|\boldsymbol{e}_z\right|_2^2 \tag{5.19c}$$

$$\mathcal{L}(f_{z_m,f})V_{\tilde{z}_m} \leq -\lambda_{min}(Q_{z_m}) \left|\tilde{\boldsymbol{z}}_m\right|_2^2 \tag{5.19d}$$

where $\lambda_{min}(\cdot)$ is the minimum eigenvalue of the matrix in the parentheses and $\sigma_{max}(\cdot)$ is the maximum singular value of the matrix in the parentheses. The time derivative of the manifold is needed to evaluate the interconnection conditions

$$\acute{\boldsymbol{z}}_s = B_x^{-1}\left(A_{x_m}^2 \tilde{\boldsymbol{x}}_m - A_{x_m} \acute{\boldsymbol{r}} + K_x^2 \boldsymbol{e}_x\right) \tag{5.20}$$

Evaluating the left side of the interconnection conditions (Eq. (2.28)) gives

$$\mathcal{L}(f_x - f_{x,s})V_{e_x} = \boldsymbol{e}_x^T P_x B_x \tilde{\boldsymbol{z}} \tag{5.21a}$$

$$\mathcal{L}(f_z - f_{z,f})V_{e_z} = 0 \tag{5.21b}$$

$$-\mathcal{L}(f_{z_s})V_{\tilde{z}_m} = -\tilde{\boldsymbol{z}}_m^T P_{z_m} B_x^{-1}\left(A_{x_m}^2 \tilde{\boldsymbol{x}}_m - A_{x_m} \acute{\boldsymbol{r}} + K_x^2 \boldsymbol{e}_x\right) \tag{5.21c}$$

Again taking the 2-norm and rearranging slightly gives

$$\mathcal{L}(f_x - f_{x,s})V_{e_x} \leq \sigma_{max}\left(P_x B_x\right)|\boldsymbol{e}_x|_2\,|\tilde{\boldsymbol{z}}|_2 \tag{5.22a}$$

$$\mathcal{L}(f_z - f_{z,f})V_{e_z} \leq 0 \tag{5.22b}$$

$$\begin{aligned}-\mathcal{L}(f_{z_s})V_{\tilde{z}_m} \leq\ & \sigma_{max}\left(P_{z_m}B_x^{-1}K_x^2\right)|\boldsymbol{e}_x|_2\,|\tilde{\boldsymbol{z}}_m|_2 + \sigma_{max}\left(P_{z_m}B_x^{-1}A_{x_m}^2\right)|\tilde{\boldsymbol{x}}_m|_2\,|\tilde{\boldsymbol{z}}_m|_2 \\ & + \left[\sigma_{max}\left(P_{z_m}B_x^{-1}A_{x_m}\right)|\tilde{\boldsymbol{z}}_m|_2\,|\acute{\boldsymbol{r}}|_2\right]\end{aligned} \tag{5.22c}$$

These functions are in the proper format for the application of Theorem 2.1 except for the terms that are proportional to $\acute{\boldsymbol{r}}$ (i.e. the terms in square brackets in Eqs. (5.18b) and (5.22c)). Two cases will be considered. If $\acute{\boldsymbol{r}} = 0$ then Theorem 2.1 may be applied as is. In this case, by Theorem 2.1, the system is asymptotically stable if K is positive definite. If $\acute{\boldsymbol{r}} \neq 0$ then additional work is necessary. It can be seen by referring back to the proof for Theorem 2.1 that for the quadrotor under consideration, the final form of the composite Lyapunov function (V) at the end of the proof for Theorem 2.1 is

$$\acute{V} \leq -\boldsymbol{v}^T K \boldsymbol{v} + \left[\sigma_{max}\left(P_{x_m}\right)|\tilde{\boldsymbol{x}}_m|_2\,|\acute{\boldsymbol{r}}|_2 + \sigma_{max}\left(P_{z_m}B_x^{-1}A_{x_m}\right)|\tilde{\boldsymbol{z}}_m|_2\,|\acute{\boldsymbol{r}}|_2\right] \tag{5.23}$$

Let

$$\boldsymbol{v}^* \triangleq \begin{bmatrix}\boldsymbol{v}^T & \left|\tilde{\boldsymbol{B}}_{z,1}\right|_2 & \left|\tilde{\boldsymbol{B}}_{z,2}\right|_2 & \dots & \left|\tilde{\boldsymbol{B}}_{z,n_z}\right|_2\end{bmatrix}^T \tag{5.24a}$$

$$K^* \triangleq \begin{bmatrix}K & 0 \\ 0 & I_{n_z}\end{bmatrix} \tag{5.24b}$$

where $\tilde{B}_z \triangleq [\tilde{\boldsymbol{B}}_{z,1}\ \tilde{\boldsymbol{B}}_{z,2}\ \dots\ \tilde{\boldsymbol{B}}_{z,n_z}]$ and n_z is the dimension of $\boldsymbol{z}$. Note that K is positive definite if and only if K^* is positive definite. Adding and subtracting $\left|\tilde{B}_z\right|_2^2$ to Eq. (5.23) gives

$$\acute{V} \leq -\boldsymbol{v}^{*T}K^*\boldsymbol{v}^* + \left|\tilde{B}_z\right|_2^2 + \left[\sigma_{max}\left(P_{x_m}\right)|\tilde{\boldsymbol{x}}_m|_2\,|\acute{\boldsymbol{r}}|_2 + \sigma_{max}\left(P_{z_m}B_x^{-1}A_{x_m}\right)|\tilde{\boldsymbol{z}}_m|_2\,|\acute{\boldsymbol{r}}|_2\right] \tag{5.25}$$

The 2-norm of the adapting parameters $|B_z|_2$ is bounded by the projection operator. Let $|B_{z,max}|_2$ be this bound. It is now assumed that the pilot flies in such a way that $\boldsymbol{r}$ and $\acute{\boldsymbol{r}}$ are bounded. Let $\boldsymbol{r}_{max}$ and $\acute{\boldsymbol{r}}_{max}$ be those bounds. Finally, the objective is to show that the system is stable within a subset of the domain. Let the input $\boldsymbol{r}$ be choosen so that $|\boldsymbol{x}|_2 \leq |\boldsymbol{r}_{max}|_2$ and $|\boldsymbol{x}_m|_2 \leq |\boldsymbol{r}_{max}|_2$. This implies that $|\boldsymbol{e}_x|_2 \leq 2|\boldsymbol{r}_{max}|_2$ and $|\tilde{\boldsymbol{x}}_m|_2 \leq 2|\boldsymbol{r}_{max}|_2$. From Eq. (5.13)

$$|\boldsymbol{z}_s|_2 \leq 2|B_x^{-1}|_2 \left(|A_{x_m}|_2 + |K_x|_2\right) |\boldsymbol{r}_{max}|_2 \tag{5.26}$$

The fast states $\boldsymbol{z}$ and $\boldsymbol{z}_m$ are constrained to the same domain. In summary, the following limits on the domain are imposed

$$|\boldsymbol{e}_x|_2 \leq 2|\boldsymbol{r}_{max}|_2 \tag{5.27a}$$

$$|\tilde{\boldsymbol{x}}_m|_2 \leq 2|\boldsymbol{r}_{max}|_2 \tag{5.27b}$$

$$|\boldsymbol{e}_z|_2 \leq 4|B_x^{-1}|_2(|A_{x_m}|_2 + |K_x|_2)|\boldsymbol{r}_{max}|_2 \tag{5.27c}$$

$$|\tilde{\boldsymbol{z}}_m|_2 \leq 4|B_x^{-1}|_2(|A_{x_m}|_2 + |K_x|_2)|\boldsymbol{r}_{max}|_2 \tag{5.27d}$$

$$|\tilde{B}_z|_2 \leq 2|B_{z,max}|_2 \tag{5.27e}$$

Substituting these bounds into Eq. (5.25)

$$\begin{aligned}\acute{V} \leq & -\boldsymbol{v}^{*T} K^* \boldsymbol{v}^* + \left[2\,|B_{z,max}|_2\right. \\ & + \left.\left(\sigma_{max}\left(P_{x_m}\right) + \sigma_{max}\left(P_{z_m} B_x^{-1} A_{x_m}\right) 2\left|B_x^{-1}\right|_2 \left(|A_{x_m}|_2 + |K_x|_2\right)\right) 2\,|\boldsymbol{r}_{max}|_2\,|\acute{\boldsymbol{r}}_{max}|_2\right]\end{aligned} \tag{5.28}$$

Again, everything in the square brackets is constant. Let this constant be defined as L. Let $\lambda_3 = \lambda_{max}(K^*)$. Note that $|\boldsymbol{v}^*|_2^2 = |\boldsymbol{e}_\phi|_2^2$. Therefore

$$\acute{V} \leq -\lambda_3\,|\boldsymbol{e}_\phi|_2^2 + L \tag{5.29}$$

Let Γ be restricted to diagonal matrices. The initial composite Lyapunov function from the proof of Theorem 2.1 can be written as

$$\lambda_1 \left|\boldsymbol{e}_\phi\right|_2^2 \leq V \leq \lambda_2 \left|\boldsymbol{e}_\phi\right|_2^2 \tag{5.30}$$

where

$$\lambda_1 \triangleq \frac{1}{2} \min \left(d^* \lambda_{min}(P_x), d^* \lambda_{min}(P_{x_m}), d\lambda_{min}(P_z), d\lambda_{min}(P_{z_m}), d \min_{i \in \{1,2,\ldots,n_z\}} \left(|\Gamma_{ii}^{-1}| \right) \right) \tag{5.31a}$$

$$\lambda_2 \triangleq \frac{1}{2} \max \left(d^* \lambda_{max}(P_x), d^* \lambda_{max}(P_{x_m}), d\lambda_{max}(P_z), d\lambda_{max}(P_{z_m}), d \max_{i \in \{1,2,\ldots,n_z\}} \left(|\Gamma_{ii}^{-1}| \right) \right) \tag{5.31b}$$

Recall that $d \in (0,1)$ and $d^* \triangleq 1 - d$ as defined in Theorem 2.1. Lyapunov-like functions of the form described by Eqs. (5.29) and (5.30) were studied by Raffoul. Theorem 2.2 of [118] concludes that

$$|\boldsymbol{e}_\phi|_2 \leq \sqrt{\frac{1}{\lambda_1} \left(\lambda_2 \left|\boldsymbol{e}_\phi(t=0)\right|_2^2 + \frac{L\lambda_2}{\lambda_3} \right)} \tag{5.32}$$

If this bound is within the domain previously specified then the system is stable in the sense of Lyapunov.

In summary, using Theorem 2.1 it has been shown that when $\acute{\boldsymbol{r}} = 0$ the system is asymptotically stable if K is positive definite. It has also been shown that when $\acute{\boldsymbol{r}} \neq 0$ the system is Lyapunov sense stable if K is positive definite and Eq. (5.32) is satisfied. In the next section, it will be shown that these conditions are satisfied for the numerical values of the test aircraft. To do so, the

following parameters of K will be needed

$$\boldsymbol{\alpha} = \begin{bmatrix} \lambda_{min}(Q_x) & \lambda_{min}(Q_{x_m}) & \lambda_{min}(Q_z) & \lambda_{min}(Q_{z_m}) \end{bmatrix}^T \tag{5.33a}$$

$$\beta = \sigma_{max}\left(P_x B_x\right) \tag{5.33b}$$

$$\boldsymbol{\gamma} = 0 \tag{5.33c}$$

$$\boldsymbol{\delta} = \begin{bmatrix} \sigma_{max}(P_{z_m} B_x^{-1} K_x^2) & \sigma_{max}(P_{z_m} B_x^{-1} A_{x_m} x^2) & 0 & 0 \end{bmatrix}^T \tag{5.33d}$$

These paramters are obtained from Eqs. (5.19) and (5.22).

Remark 5.1 - *If the steady-state error of the reference models is known then more precise bounds on the domain may be available. This system is linear and the slow subsystem is deterministic. So several conclusions can be drawn about the steady-state error. The transfer functions from the reference model inputs to the reference model errors are*

$$\tilde{\boldsymbol{x}}_m(s) = (sI - A_{x_m})^{-1} s\boldsymbol{r}(s) \tag{5.34a}$$

$$\tilde{\boldsymbol{z}}_m(s) = (sI - A_{z_m})^{-1} s\boldsymbol{z}_s(s) \tag{5.34b}$$

Assuming that the slow error is asymptotically stable then the steady state value is $\boldsymbol{e}_x = 0$ *(this assumption is only applicable to the analysis of this remark). The Laplace Transform of Eq.* (5.13) *is*

$$\boldsymbol{z}_s(s) = B_x^{-1} A_{x_m} \tilde{\boldsymbol{x}}_m(s) \tag{5.35}$$

Solving for $\tilde{\boldsymbol{z}}_m(s)$ *in terms of* $\boldsymbol{r}(s)$ *gives*

$$\tilde{\boldsymbol{x}}_m(s) = (sI - A_{x_m})^{-1} s\boldsymbol{r}(s) \tag{5.36a}$$

$$\tilde{\boldsymbol{z}}_m(s) = (sI - A_{z_m})^{-1} s B_x^{-1} A_{x_m} (sI - A_{x_m})^{-1} s\boldsymbol{r}(s) \tag{5.36b}$$

For this remark, let the zeros be in the open left half plane and let all of the components of $\boldsymbol{r}(s)$

be equivalent. Define $\boldsymbol{r}_1 \triangleq [1\ 1\ 1\ 1]^T$. *Using the final value Theorem the steady-state error can be determined for several different input types. Table 5.1 shows this. Note that the steady-state error of* ∞ *will never actually come to fruition because* $\boldsymbol{r}$ *is bounded. However, as the order of the input increases the maximum error will approach* $2|\boldsymbol{r}_{max}|_2$. *Similar conclusions can be drawn for a sinusoidal input. The maximum steady-state error can be calculated from the phase lag. Again, the maximum error will approach* $2|\boldsymbol{r}_{max}|_2$.

Table 5.1: Reference model steady state error.

Input	**Slow Steady State Error**	**Fast Steady State Error**
Step	$\tilde{\boldsymbol{x}}_m(s) = 0$	$\tilde{\boldsymbol{z}}_m(s) = 0$
Ramp	$\tilde{\boldsymbol{x}}_m(s) = -A_{x_m}^{-1}\boldsymbol{r}_1$	$\tilde{\boldsymbol{z}}_m(s) = 0$
Parabola	$\tilde{\boldsymbol{x}}_m(s) = -\infty$	$\tilde{\boldsymbol{z}}_m(s) = -A_{x_m}^{-1}B_x^{-1}\boldsymbol{r}_1$
Cubic	$\tilde{\boldsymbol{x}}_m(s) = -\infty$	$\tilde{\boldsymbol{z}}_m(s) = -\infty$

Remark 5.2 - *This system does not require adaptive control in the slow subsystem. Corollary 2.1 is intended for just such a case. However, Corollary 2.1 is not applicable because there is a slow state reference model. Thus the full-strength Theorem 2.1 is used instead.*

5.3 Numerical Results

A numerical simulation was performed with the parameters for a Da-Jiang Innovations (DJI) F450 quadrotor [119, 116]. The objective of this simulation is to validate the control architecture that is presented above. The effects of a MIMO system on KAMS are also studied. Consistent with the stability analysis above, asymptotic stability is achieved for constant pilot commands and bounded tracking is achieved for time-varying pilot commands. One representative test case is given. The trim condition is hover at sea level and in a standard atmosphere. The parameters for this vehicle are summerized in table 5.2. Table 5.3 gives the control gains which were chosen

Table 5.2: Quadrotor vehicle parameters.

Variable	Value	Units	Name
b	$1.6 * 10^{-5}$	$kg\ m$	Motor Thrust Coefficent
d	$1.6731 * 10^{-6}$	$kg\ m^2$	Motor Torque Coefficient
l	0.32	m	Motor Position Radius
m	2.5	kg	Vehicle Mass
J_{xx}	$1.6 * 10^{-2}$	$kg\ m^2$	Mass Moment of Inertia About Bodyframe x Axis
J_{yy}	$1.6 * 10^{-2}$	$kg\ m^2$	Mass Moment of Inertia About Bodyframe y Axis
J_{zz}	$1.7 * 10^{-2}$	$kg\ m^2$	Mass Moment of Inertia About Bodyframe z Axis

through tuning. The slow reference model input was chosen to be a set of sinusoids with a phase offset

$$\boldsymbol{r} = \frac{\pi}{8} \begin{bmatrix} 0 \\ \sin\left(\frac{t}{10} + \frac{2}{5}\pi\right) \\ \sin\left(\frac{t}{10} + \frac{3}{5}\pi\right) \\ \sin\left(\frac{t}{10} + \frac{4}{5}\pi\right) \end{bmatrix} \tag{5.37}$$

The motor paramters (b and d) and the mass moment of inertias (J_{xx}, J_{yy}, and J_{zz}) are assumed to be uncertian. The estimates for these parameters are drawn from a normal distribution with the mean being the true value and the standard deviation being 20% of the true value. These values are used to initialize the estimates of B_z and ϵ which are uncertain by implication. Note that $\hat{\epsilon}$ is not an adapting parameter. It is only used to ensure the timescales of the control states are correct. The system states are initialized at hover. The fast reference model is also initialized at 0. The initial conditions for the slow reference model are randomly initialized from a normal distribution with a mean of zero and a standard deviation of 20% of $2|\boldsymbol{r}_{max}|_2$ (see Eq. (5.27)).

Using these parameters and Eq. (5.4) the timescale separation parameter is found to be $\epsilon = 0.46$.

Table 5.3: Quadrotor vehicle control gains.

Variable	Value	Name
A_{x_m}	$-0.7I_4$	Slow Reference Model State Matrix
K_x	$-2I_4$	Slow Subsystem Closed-Loop State Matrix
A_{z_m}	$-10I_4$	Fast Reference Model State Matrix
K_z	$-500I_4$	Fast Subsystem Closed-Loop State Matrix
Γ	$10I_4$	Adaptation Rate Gain

The LPM of K are shown in Fig. 5.1 for a range of d. The solid dark blue line indicates values of d where all LPM are positive and Eq. (5.32) is satisfied. Notably, there is a region where the LPMs are positive but Eq. (5.32) is not satisfied. The size of this region is influenced by the control gains. For example, Q_z and its magnitude compared to K_z were found to have a significant effect. The system was not tuned for optimal performance, but instead, so that the trends are visible in each of the following plots. Regardless, it is known that KAMS is a valid approach because $\exists d \in (0, 1)$ such that the sufficient conditions are satisfied. Because the slow reference model input is time-varying the system is Lyapunov sense stable (as opposed to asymptotically stable which occurs when the slow reference model input is constant).

The results of the numerical simulation are displayed in the following time histories. First Figs. 5.2, 5.3, 5.4, and 5.5 show the time histories of the slow states. There are a few interesting trends. First, note the phase lag. This is expected. Recall that $\tilde{\boldsymbol{x}}_m$ is only guaranteed to be bounded (as opposed to asymptotically stable) when $\boldsymbol{r}$ is time-varying as is the case here. More powerful results may be avaliable if $\tilde{\boldsymbol{x}}_m$ and $\tilde{\boldsymbol{z}}_m$ could be removed. However, this would require prior knowledge about the time derivative of the slow reference model input which is not available when a pilot is operating the vehicle. See remark 5.1 for more information related to the steady state error of the slow reference model. The second interesting trend in the slow states is that the altitude briefly diverges from 0 despite the commanded value of 0. This occurs because of incorrect

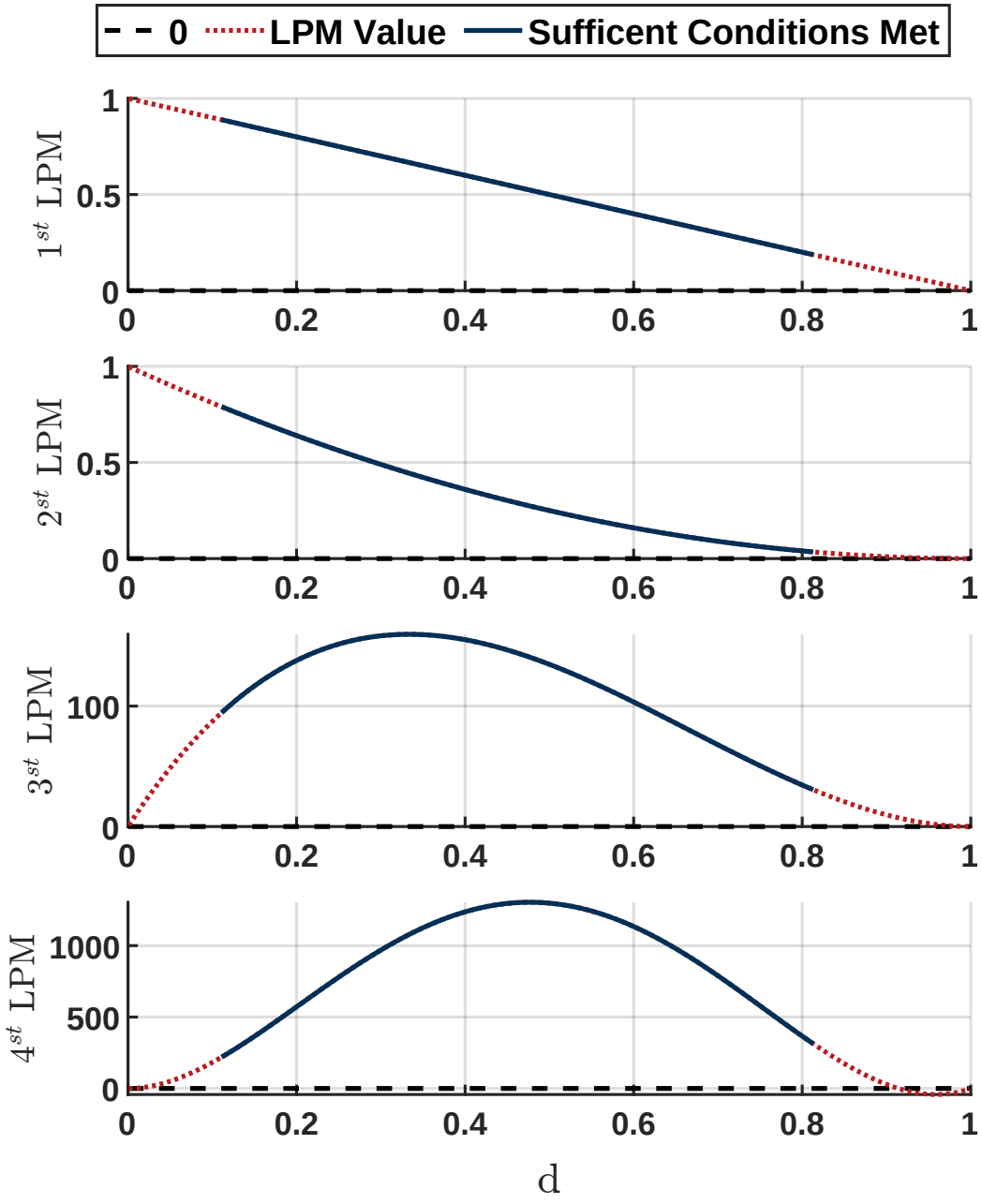

Figure 5.1: LPM over a range of possible d.

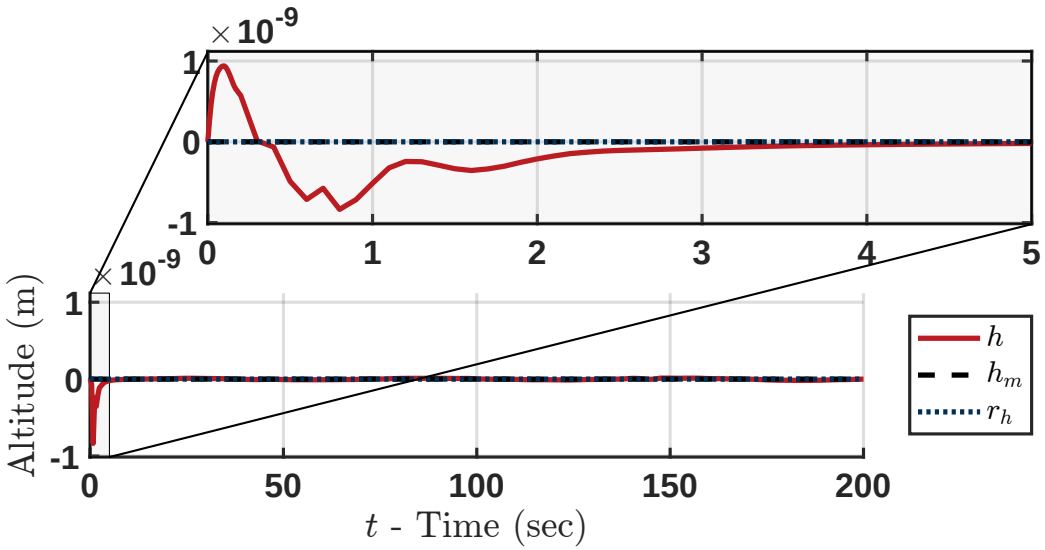

Figure 5.2: Evolution of the altitude.

mixing due to an incorrect estimate of the control influence matrix. However, the adaptive control rectifies the problem over time. Figures. 5.6, 5.7, 5.8, and 5.9 show the time histories of the fast states. For both the fast and slow states note that the system converges to the reference model. Figure 5.10 shows the evolution of the various components of $\tilde{B}_z$. The parameters adapt in the fast timescale. Figure 5.11 shows the evolution of the control inputs.

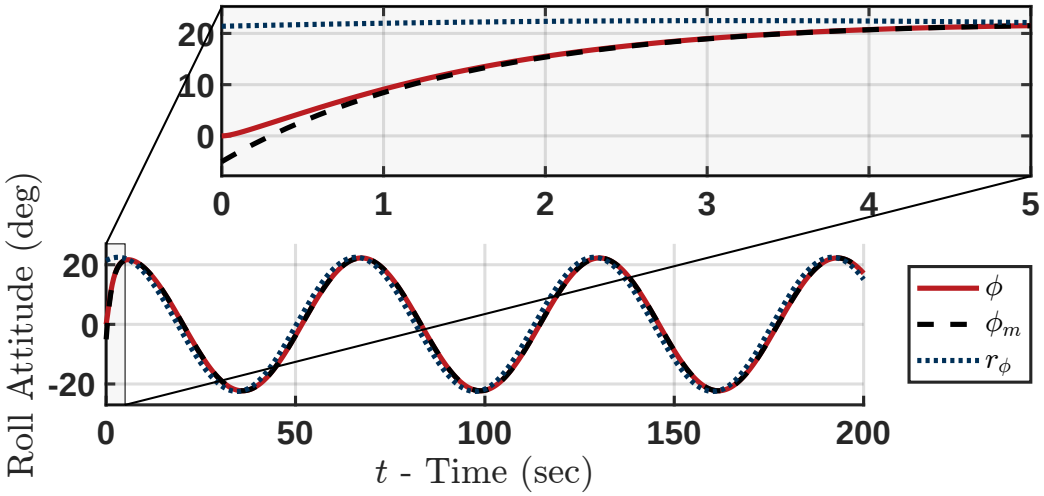

Figure 5.3: Evolution of the roll attitude angle.

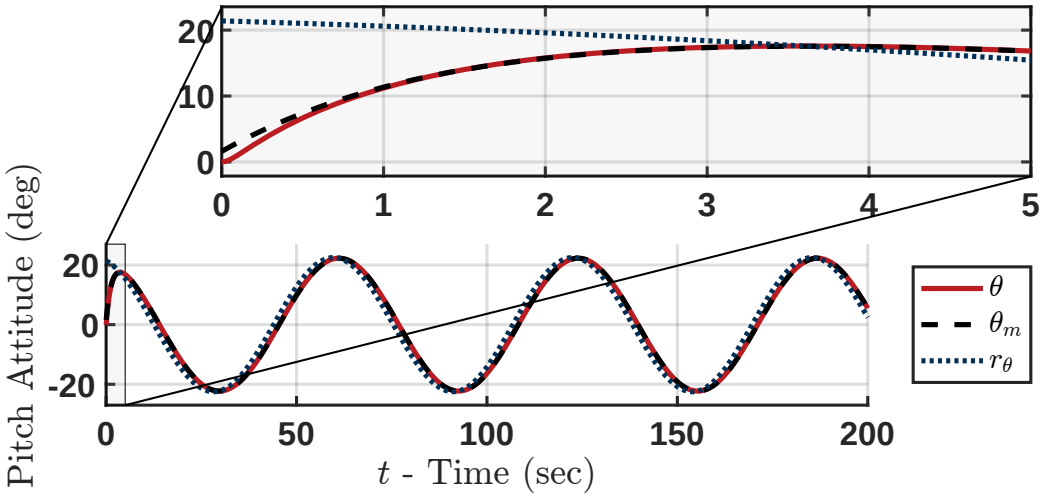

Figure 5.4: Evolution of the pitch attitude angle.

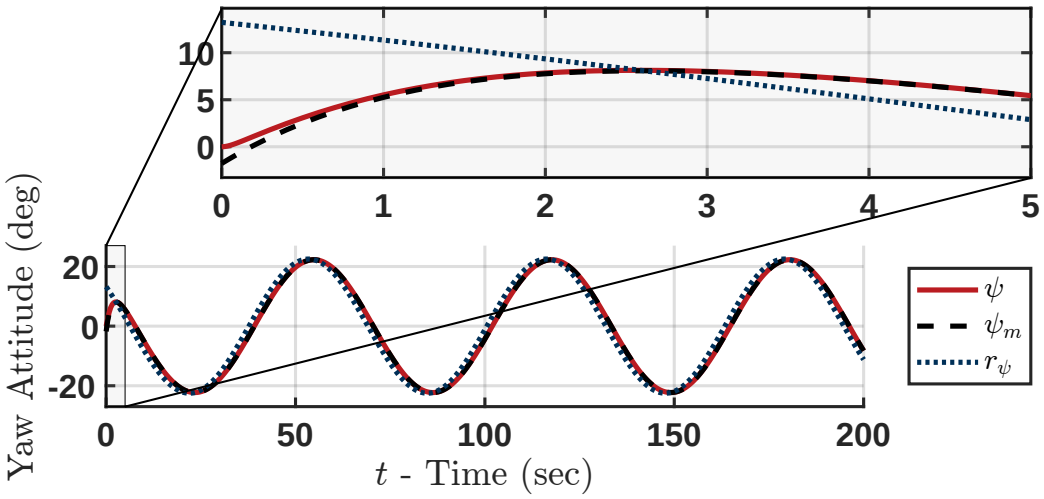

Figure 5.5: Evolution of the yaw attitude angle.

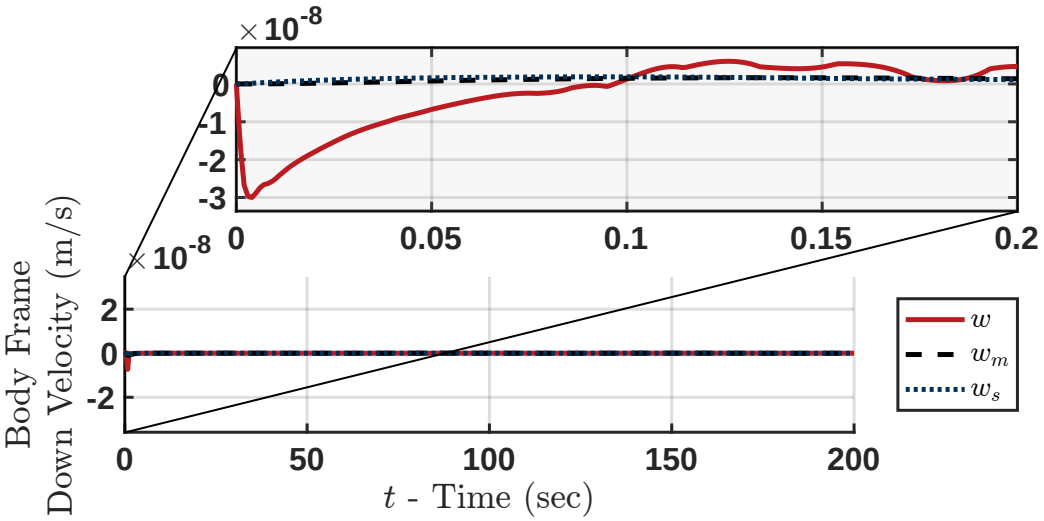

Figure 5.6: Evolution of body axis down velocity.

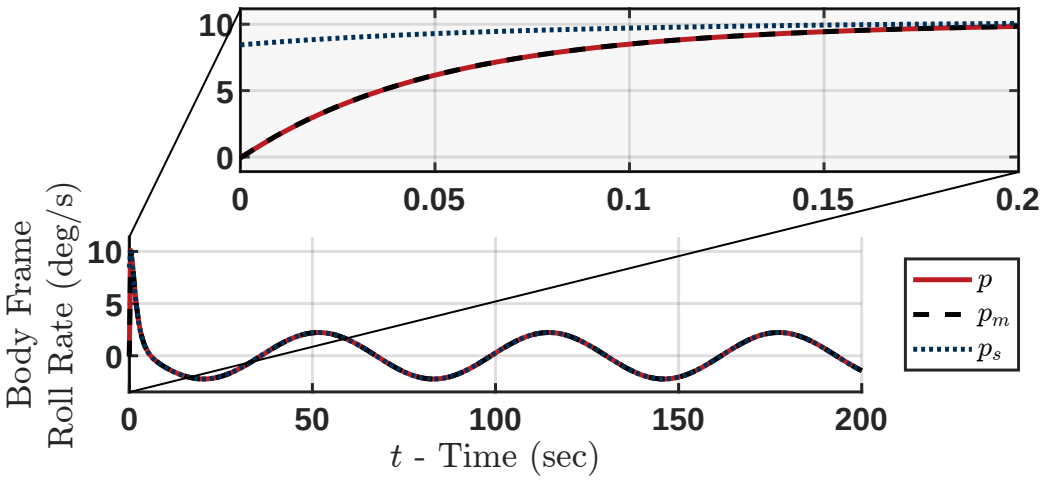

Figure 5.7: Evolution of body axis roll rate.

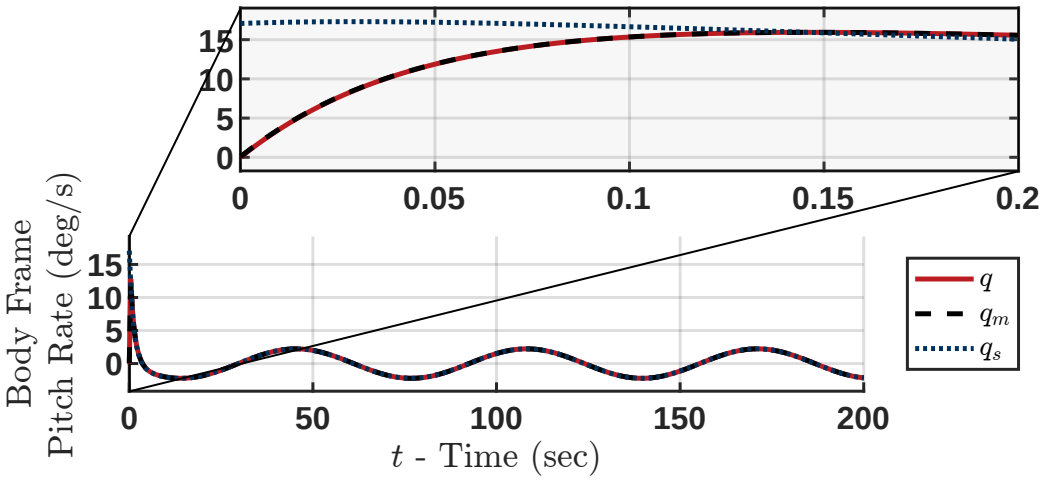

Figure 5.8: Evolution of body axis pitch rate.

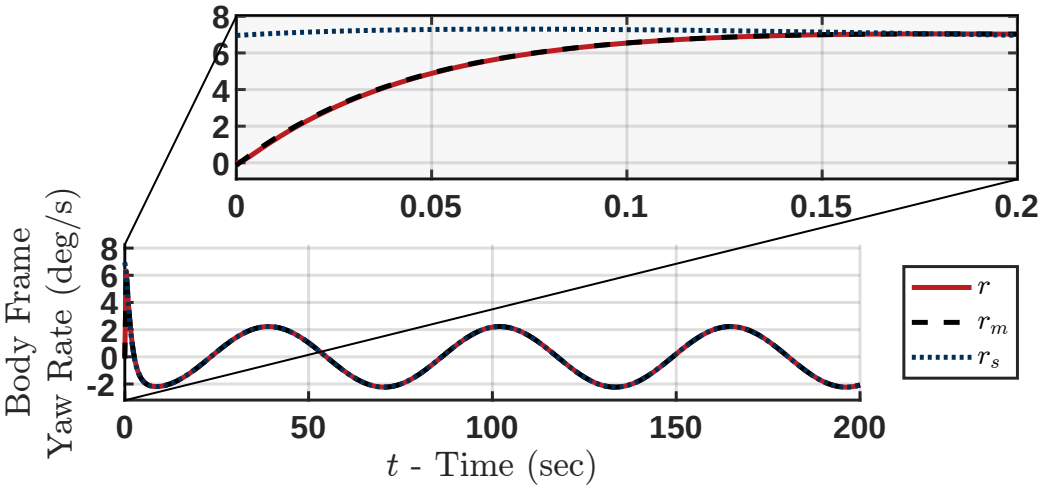

Figure 5.9: Evolution of body axis yaw rate.

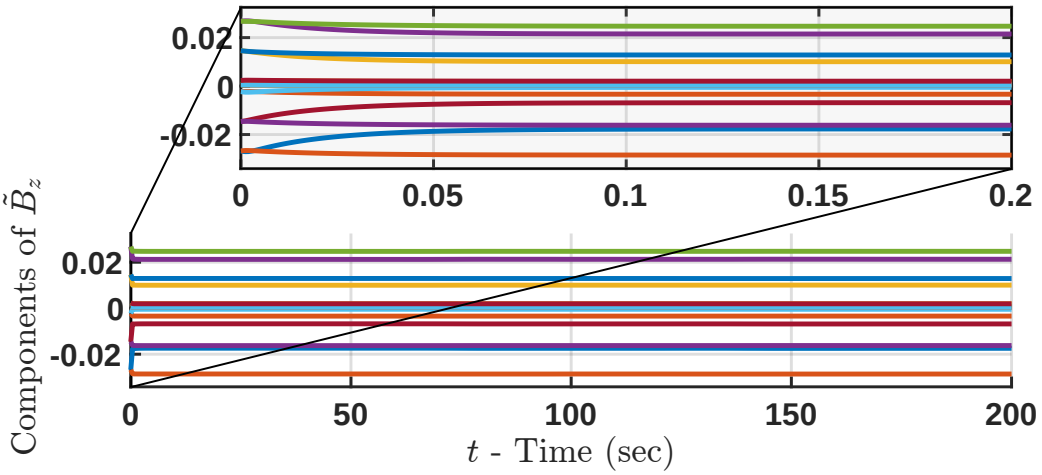

Figure 5.10: Evolution of the components of the adapting parameters' error.

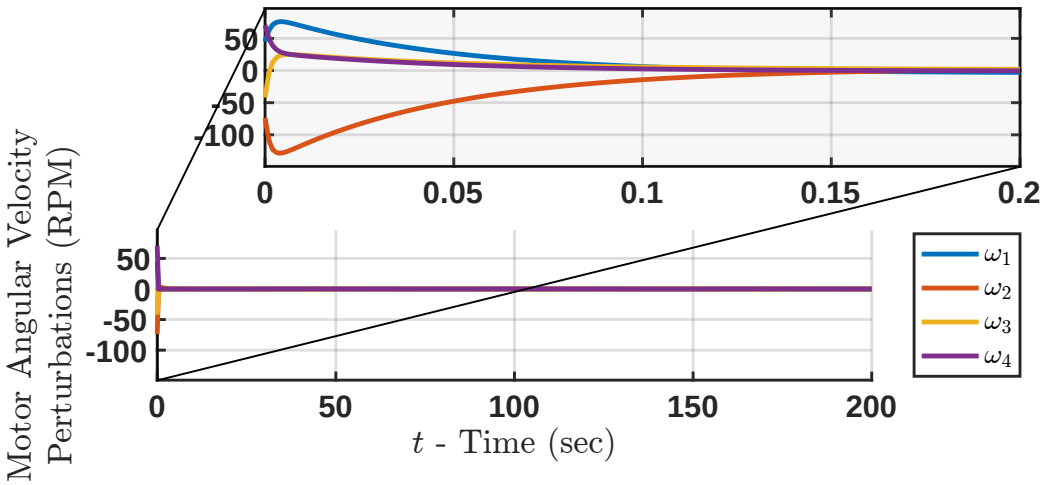

Figure 5.11: Evolution of the motor angular velocities.

5.4 Chapter Summary

The control objective of this chapter is to provide attitude stabilization for a quadrotor. A secondary objective was for the pilot to be given influence over the system. These objectives were both accomplished using KAMS. KAMS was recently proposed as a method of adaptive control for multiple-timescale systems. First, a multiple-timescale model of a quadrotor was developed. Second, the system was separated into two subsystems using singular perturbation theory. Third, two separate control laws were developed for the subsystems. Fourth, these control signals were fused using Sequential Control. Fifth, the system was shown to be asymptotically stable when the input to the slow state reference model is constant and Lyapunov sense stable otherwise. Sixth and finally, the control was validated using a numerical simulation. The inertia and motor parameters were allowed to be uncertain. Based on the results presented in this chapter, two conclusions are drawn.

1. KAMS is a promising approach to attitude stabilization for quadrotors. The system was shown to be asymptotically stable for constant inputs and bounded for time-varying inputs. The numerical example demonstrated how the system is dynamically well-behaved and can asymptotically track a reference model. Controller performance can be improved if the

pilot selects slow smooth commands because the magnitude of the bound on the closed-loop trajectory is a function of the time derivative of the slow subsystem input. This further constrains the range of d which satisfies the sufficient conditions of KAMS.

2. KAMS is shown to be an effective approach for multiple-input multiple-output systems. The numerical example demonstrated this. The coupling between the multiple inputs and outputs caused some small ($< 10^{-9}$ m) deviations in the altitude due to parametric uncertainty, but the adaptive elements of the control were able to recover quickly.

6. ORBITAL TRANSFER MANEUVERS USING ADAPTIVE CONTROL OF A MULTIPLE-TIMESCALE MODEL

Few environments are as challenging to engineering as outer space. Spacecraft are required to operate at the very edge of physical limits. For example, launch vehicle capabilities require reduced mass, vibration hardening, and compact form factors. The uninhibited solar effects require computational power concessions, reduced electrical power, and thermodynamic extremes. From a guidance, control, and dynamics perspective space systems are frequently highly coupled nonlinear systems with limited fuel. Furthermore, the distances make repair infeasible and communication slow. In such an environment autonomy and redundancy are essential. Adaptive control is well suited for uncertain and time-varying environments like space [24]. This chapter presents a novel method of orbital transfer using adaptive control for multiple-timescale systems. First, a multiple-timescale model of orbital dynamics is developed. Then KAMS is presented as a potential solution.

Orbital transfers are essential components of almost all space missions (e.g. [120]). Many different control architectures have been proposed for orbital transfers (e.g. [121, 122]). Fuel and time requirements have frequently necessitated some form of optimal control in this application. For example, Wiesel and Alfano studied an optimal low thrust minimum time transfer maneuver [123]. Kechichain studied an optimal minimum time transfer maneuver to geostationary orbit with an intermediate control input [124]. Avendaño *et al.* studied minimum-cost multi-impulse orbit transfers [125]. The Hohmann transfer has been proven to be the minimum impulse transfer maneuver [126, 127, 128]. Instantaneous impulses are not possible in physical systems. However, they are commonly assumed because of the large timescale separation between the angular velocity and radial velocity of spacecraft. The present work derives a multiple-timescale model of orbital dynamics which rigorously models the timescale separation and also allows for finite time continuous inputs. The timescale model is similar to the one proposed by Saha and Valasek [8]. However, this chapter analytically derives the timescale behavior instead of assuming it. Zhong and Zhu derived a similar timescale model and also used nondimensionalization, but they studied

the timescales of tethered dynamics instead of the actual orbital maneuver [129]. Williams developed a numerical method of optimal control in the presence of timescales and applied it to orbital dynamics [130]. In a more general sense, perturbation theory has a rich history in orbital mechanics. For example, Muñoa and Scheeres studied perturbation of Hamiltonian's [131]. McGrath and Macdonald used a perturbation technique to reconfigure satellite constellations [132]. These studies look at the effects of small perturbations on the forces and do not study the singularly perturbed differential equations that are addressed by multiple-timescale control [9]. A few researchers have applied adaptive control to space systems. Ma *et al.* proposed a form of MRAC as a method of accounting for actuator faults of spacecraft [133]. McInnes proposed a method of adaptive control for gravity turns during reentry [134]. Junkins, Akella, and Robinett also used adaptive control for orbital transfer maneuvers but did not consider the timescales of the system [135].

This chapter presents the first application of Simultaneous Slow and Fast Tracking within the framework of KAMS. This chapter is organized as follows. Section 6.1 derives the multiple-timescale model used in this work. Section 6.2 proves stability for the control and guidance laws using the KAMS framework. Section 6.3 demonstrates the control using a numerical simulation of an orbital transfer from medium earth orbit to geostationary orbit.

6.1 Multiple-Timescale Model

The dynamics of an orbital craft are well known

$$\ddot{r} = r\omega^2 - G\frac{M}{r^2} + \frac{\Lambda_r}{m}F_r \tag{6.1a}$$

$$\dot{\theta} = \omega \tag{6.1b}$$

$$\dot{\omega} = -\frac{2}{r}\dot{r}\omega + \frac{\Lambda_\theta}{mr}F_\theta \tag{6.1c}$$

r is the radius from the planetary body, ω is the angular velocity of the satellite around the planetary body, and θ is the true anomaly. M is the mass of the planetary body and m is the mass of the satellite. G is the universal gravitational constant. F_θ is the force of a thruster that is tangential to the vehicle's orbit and F_r is the force of a thruster that is pointed radially away from the planetary

body. Finally, $\Lambda_r \in \mathbb{R}_+$ and $\Lambda_\theta \in \mathbb{R}_+$ are control effectiveness parameters. All parameters are assumed to be known or perfectly measured except Λ_r, Λ_θ, and the satellite mass m. These parameters are uncertain justifying the use of adaptive control.

The first step in developing a timescale model is to nondimensionalize the system. This is the same tactic as the one used by [9]. The following nondimensional parameters are chosen using Buckingham Pi Theorem [136]

$$\bar{r} \triangleq \frac{r - r_2}{r_2} \qquad \bar{\omega} \triangleq \omega\sqrt{\frac{r_2^3}{GM}} \qquad t_s \triangleq t\sqrt{\frac{GM}{r_2^3}} \qquad \bar{F}_r \triangleq \frac{F_r r_2^2}{GM^2} \qquad \bar{F}_\theta \triangleq \frac{F_\theta r_2^2}{GM^2} \tag{6.2}$$

where r_2 is the new desired orbital radius. So the control objective is to drive $\bar{r}$ to zero. Note that $\bar{\omega}$ is always positive. Substituting these into the equations of motion gives

$$\frac{GM}{r_2^2}\frac{d^2\bar{r}}{dt_s^2} = (\bar{r}r_2 + r_2)\frac{GM}{r_2^3}\bar{\omega}^2 - \frac{GM}{(\bar{r}r_2 + r_2)^2} + \frac{GM^2}{r_2^2 m}\Lambda_r \bar{F}_r \tag{6.3a}$$

$$\sqrt{\frac{GM}{r_2^3}}\acute{\theta} = \sqrt{\frac{GM}{r_2^3}}\bar{\omega} \tag{6.3b}$$

$$\frac{GM}{r_2^3}\acute{\omega} = -\frac{2}{(\bar{r}r_2 + r_2)}\sqrt{\frac{GM}{r_2}}\acute{\bar{r}}\sqrt{\frac{GM}{r_2^3}}\bar{\omega} + \frac{1}{m(\bar{r}r_2 + r_2)}\frac{GM^2}{r_2^2}\Lambda_\theta \bar{F}_\theta \tag{6.3c}$$

Simplifying

$$\frac{d^2\bar{r}}{dt_s^2} = (\bar{r} + 1)\bar{\omega}^2 - \frac{1}{(\bar{r} + 1)^2} + \Lambda_r\frac{\bar{F}_r}{\epsilon} \tag{6.4a}$$

$$\acute{\theta} = \bar{\omega} \tag{6.4b}$$

$$\epsilon\acute{\bar{\omega}} = -\frac{2\epsilon\acute{\bar{r}}\bar{\omega}}{(\bar{r} + 1)} + \frac{\Lambda_\theta \bar{F}_\theta}{(\bar{r} + 1)} \tag{6.4c}$$

where $\epsilon = \frac{m}{M}$ is the timescale separation parameter. Intuitively it is a ratio of the mass of the satellite and the mass of the planetary body. If the satellite's mass is much smaller than the planetary body's mass then the system exhibits multiple-timescale behavior. One final adjustment is now made. The appearance of ϵ on the right side of Eq. (6.4a) implies that $\bar{F}_r$ plays a disproportionately

large role in the evolution of r. However, F_r is an input so it can be scaled up or down as necessary. F_r is an inefficient method to change the orbital radius. So it is valid to assume $\bar{F}_r$ is small. Let $\bar{F}_{r\epsilon} \triangleq \frac{\bar{F}_r}{\epsilon}$. Another way to state this assumption is that $\mathcal{O}(\epsilon^{-1}\bar{F}_r) = \mathcal{O}(1)$. Using this change the system becomes

$$\frac{d^2\bar{r}}{dt_s^2} = (\bar{r}+1)\,\bar{\omega}^2 - \frac{1}{(\bar{r}+1)^2} + \Lambda_r \bar{F}_{r\epsilon} \tag{6.5a}$$

$$\acute{\theta} = \bar{\omega} \tag{6.5b}$$

$$\epsilon\acute{\bar{\omega}} = -\frac{2\epsilon\acute{\bar{r}}\bar{\omega}}{(\bar{r}+1)} + \frac{\Lambda_\theta \bar{F}_\theta}{(\bar{r}+1)} \tag{6.5c}$$

6.2 Control Synthesis

The system model is now suitable for KAMS control synthesis. The system is nonstandard and the timescale separation parameter appears on the right-hand side of Eq. (6.5). Adaptive Nonlinear Dynamic Inversion (ANDI) is used to stabilize the subsystems. The multiple-timescale technique of Simultaneous Slow and Fast Tracking is used to fuse the subsystem control signals. The reduced slow subsystem is

$$\frac{d^2\bar{r}}{dt_s^2} = (\bar{r}+1)\,\bar{\omega}_s^2 - \frac{1}{(\bar{r}+1)^2} + \Lambda_r \bar{F}_{r\epsilon} \tag{6.6a}$$

$$\acute{\theta} = \bar{\omega}_s \tag{6.6b}$$

The reduced fast subsystem is

$$\frac{d^2 r}{dt_f^2} = 0 \tag{6.7a}$$

$$\grave{\theta} = 0 \tag{6.7b}$$

$$\grave{\bar{\omega}} = \frac{\Lambda_\theta \bar{F}_\theta}{(\bar{r}+1)} \tag{6.7c}$$

Note that the fast subsystem does not include the $-\frac{2\epsilon\acute{\bar{r}}\bar{\omega}}{(\bar{r}+1)}$ term. KAMS allows a control law to be designed without this term because it is of order $\mathcal{O}(\epsilon)$. The stability analysis to follow will show that the full-order system is stable even though this term is neglected. Define

$$\tilde{\bar{r}} \triangleq \bar{r} - \bar{r}_c \quad \tilde{\bar{r}}_m \triangleq \bar{r}_m - \bar{r}_c \quad e_{\bar{r}} \triangleq \bar{r} - \bar{r}_m \quad \tilde{\bar{\omega}} \triangleq \bar{\omega} - \bar{\omega}_c \quad \tilde{\bar{\omega}}_m \triangleq \bar{\omega}_m - \bar{\omega}_c \quad e_{\bar{\omega}} \triangleq \bar{\omega} - \bar{\omega}_m \tag{6.8}$$

where the subscript m indicates a reference model state and the subscript c indicates a commanded value.

6.2.1 Control and Adaptation Laws

Let $\boldsymbol{x} \triangleq [\bar{r} \quad \acute{\bar{r}}]^T$ and $C \triangleq [0 \quad 1]$. In previous chapters $\boldsymbol{r}$ has been used for the reference model input. In this chapter, the subscript c is used to indicate the reference model input to avoid confusion with the orbital radius r. The reference models are

$$\acute{\boldsymbol{x}}_m = A_x \tilde{\boldsymbol{x}}_m + \acute{\boldsymbol{x}}_c \tag{6.9a}$$

$$\grave{\tilde{\omega}}_m = -a_{\bar{\omega}} \tilde{\bar{\omega}}_m + \grave{\tilde{\omega}}_c \tag{6.9b}$$

where $A_x \in \mathbb{R}^{2\times 2}$ is hurwitz and $a_{\bar{\omega}} \in \mathbb{R}_+$. From ANDI the inputs are

$$\bar{F}_{r\epsilon} = \hat{\Lambda}_r^{-1} \left(C\left(A_x \tilde{\boldsymbol{x}}_m + \acute{\boldsymbol{x}}_c\right) - \left(\bar{r}+1\right)\bar{\omega}_s^2 + \frac{1}{\left(\bar{r}+1\right)^2} + C K_x \boldsymbol{e}_x \right) \tag{6.10a}$$

$$\bar{F}_\theta = \left(\frac{2\bar{\omega}}{(\bar{r}+1)} \hat{\Lambda}_\theta \right)^{-1} \left(-a_{\bar{\omega}} \tilde{\bar{\omega}}_m + \grave{\tilde{\omega}}_c - k_{\bar{\omega}} e_{\bar{\omega}} \right) \tag{6.10b}$$

where $K_x \in \mathbb{R}^{2\times 2}$ is hurwitz and $k_{\bar{\omega}} \in \mathbb{R}_+$ are design variables. Furthermore, let the top row of A_x and K_x be $[0 \; 1]$. Note that Eq. (6.10a) is more precisely a form of adaptive feedback linearization. The adaptation laws are

$$\acute{\hat{\Lambda}}_r = \gamma_r \text{Proj}\left(\hat{\Lambda}_r, \bar{F}_{r\epsilon} e_{\bar{r}} \right) \tag{6.11a}$$

$$\grave{\hat{\Lambda}}_\theta = \gamma_\theta \text{Proj}\left(\hat{\Lambda}_\theta, \frac{1}{(\bar{r}+1)} \bar{F}_\theta e_{\bar{\omega}} \right) \tag{6.11b}$$

where $\gamma_r, \gamma_\theta \in \mathbb{R}_+$ are adaption gains.

6.2.2 Guidance

The trajectory ($\bar{r}_c$ and $\bar{\omega}_c$) is chosen to be an orbital transfer between two circular orbits. Let r_1 and ω_1 be respectively the radius and angular velocity for the initial orbit and r_2 and ω_2 be the same for the final orbit. It is out of the scope of this work to minimize fuel usage. However, a Hohmann transfer is used to ensure the control inputs remained feasible. Let t_1 be the time when the transfer is initiated and let t_2 be the time when the transfer ends. The Hohmann transfer is a constant energy maneuver (other than the impulses at the beginning and end). So the sum of the kinetic and potential energy is always equal to one-half of the potential energy at $r = a$ where a is the transfer orbit's semi-major axis

$$\frac{m r_c^2 \omega_c^2}{2} + \frac{m \dot{r}_c^2}{2} - \frac{GMm}{r_c} = -\frac{GMm}{2a} \tag{6.12}$$

The boundary conditions are found by solving for the angular velocity at apsis

$$\bar{\omega}_c(t_1^+) = \frac{1}{r_1}\sqrt{\frac{2GM}{r_1} - \frac{GM}{a}} \tag{6.13a}$$

$$\bar{\omega}_c(t_2^-) = \frac{1}{r_2}\sqrt{\frac{2GM}{r_2} - \frac{GM}{a}} \tag{6.13b}$$

where t_1^+ is the time immediately after the Hohmann transfer begins and t_2^- is the time immediately before the Hohmann transfer ends. After t_1^+, the commanded values follow a trajectory along the

unforced equations of motion. In summary, the guidance law is

$$r_c = \begin{cases} r_1 & t \leq t_1 \\ \ddot{r}_c = r_c\omega_c^2 - G\frac{M}{r_c^2} & t_1 < t < t_2 \\ r_2 & t_2 \leq t \end{cases} \tag{6.14a}$$

$$\omega_c = \begin{cases} \omega_1 & t < t_1 \\ \frac{1}{r_1}\sqrt{\frac{2GM}{r_1} - \frac{GM}{a}} & t = t_1^+ \\ \dot{\omega}_c = -\frac{2}{r_c}\dot{r}_c\omega_c & t_1 < t < t_2 \\ \frac{1}{r_2}\sqrt{\frac{2GM}{r_2} - \frac{GM}{a}} & t = t_2^- \\ \omega_2 & t_2 < t \end{cases} \tag{6.14b}$$

Note that there is a discrete step change in the commanded angular velocity at t_1 and t_2, but the commanded radius is a continuous function.

6.2.3 Stability Analysis

In the previous sections, control was designed for the reduced subsystems. In this section, it is shown that the full-order system is also stable under this control. Consider the following Lyapunov functions

$$V_{e_x} = \frac{1}{2}\left(\boldsymbol{e}_x^T P_x \boldsymbol{e}_x + \frac{1}{\gamma_r}\tilde{\Lambda}_r^2\right) \tag{6.15a}$$

$$V_{\tilde{x}_m} = \frac{1}{2}\tilde{\boldsymbol{x}}_m^T P_{x_m} \tilde{\boldsymbol{x}}_m \tag{6.15b}$$

$$V_{e_{\tilde{\omega}}} = \frac{1}{2}\left(e_{\tilde{\omega}}^2 + \frac{1}{\gamma_\theta}\tilde{\Lambda}_\theta^2\right) \tag{6.15c}$$

$$V_{\tilde{\tilde{\omega}}_m} = \frac{1}{2}\tilde{\tilde{\omega}}_m^2 \tag{6.15d}$$

where $0 < P_x = P_x^T \in \mathbb{R}_+^{2\times 2}$ and $0 < P_{x_m} = P_{x_m}^T \in \mathbb{R}_+^{2\times 2}$ are solutions to $K_x^T P_x + P_x K_x = -Q_x$ and $A_x^T P_{x_m} + P_{x_m} A_x = -Q_{x_m}$ respectively for some $0 < Q_x = Q_x^T \in \mathbb{R}_+^{2\times 2}$ and $0 < Q_{x_m} =$

$Q_{x_m}^T \in \mathbb{R}_+^{2\times 2}$. Differentiating along the subsystems' trajectories

$$\mathcal{L}(f_{e_\xi,s})V_{e_x} \leq -\boldsymbol{e}_x^T Q_x \boldsymbol{e}_x \tag{6.16a}$$

$$\mathcal{L}(f_{\tilde{x}_m})V_{\tilde{x}_m} = -\tilde{\boldsymbol{x}}_m^T Q_{x_m} \tilde{\boldsymbol{x}}_m \tag{6.16b}$$

$$\mathcal{L}(f_{e_\eta,f})V_{e_{\bar{\omega}}} \leq -k_{\bar{\omega}} e_{\bar{\omega}}^2 \tag{6.16c}$$

$$\mathcal{L}(f_{\bar{\omega}_m,f})V_{\tilde{\bar{\omega}}_m} = -a_{\bar{\omega}} \tilde{\bar{\omega}}_m^2 \tag{6.16d}$$

Eqs. (6.16a) and (6.16c) are derived in [65, Eqs. 1.20 to 1.23]. The interconnection conditions are

$$\mathcal{L}(f_x - f_{x,s})V_{e_x} = \boldsymbol{e}_x^T P_x \begin{bmatrix} 0 \\ (\bar{r}+1)\left(\bar{\omega}^2 - \bar{\omega}_s^2\right) \end{bmatrix} \tag{6.17a}$$

$$\mathcal{L}(f_{\bar{\omega}} - f_{\bar{\omega},f})V_{e_{\bar{\omega}}} = -\frac{2\epsilon \acute{\bar{r}} \bar{\omega}}{(\bar{r}+1)} e_{\bar{\omega}} \tag{6.17b}$$

Rearranging gives

$$\mathcal{L}(f_{\bar{r}} - f_{\bar{r},s})V_{e_{\bar{r}}} = \begin{bmatrix} 0 & (\bar{r}+1)\left(\bar{\omega} + \bar{\omega}_s\right) \end{bmatrix} P_x \boldsymbol{e}_x \tilde{\bar{\omega}} \tag{6.18a}$$

$$\mathcal{L}(f_{\bar{\omega}} - f_{\bar{\omega},f})V_{e_{\bar{\omega}}} = -\epsilon \frac{2\bar{\omega}}{(\bar{r}+1)} \left(e_{\acute{\bar{r}}} + \acute{\tilde{\bar{r}}}_m + \acute{\bar{r}}_c \right) e_{\bar{\omega}} \tag{6.18b}$$

Taking the 2-norm gives

$$\mathcal{L}(f_{\bar{r}} - f_{\bar{r},s})V_{e_{\bar{r}}} \leq |\bar{r}+1| \left(|\bar{\omega}| + |\bar{\omega}_s|\right) |P_x|_2 |\boldsymbol{e}_x|_2 |\tilde{\bar{\omega}}| \tag{6.19a}$$

$$\mathcal{L}(f_{\bar{\omega}} - f_{\bar{\omega},f})V_{e_{\bar{\omega}}} \leq \epsilon \frac{2|\bar{\omega}|}{|\bar{r}+1|} \left(|e_{\acute{\bar{r}}}| + |\acute{\tilde{\bar{r}}}_m| + |\acute{\bar{r}}_c| \right) |e_{\bar{\omega}}| \tag{6.19b}$$

The desire is to show asymptotic stability within a subset of the domain. So it is sufficient to limit the domain and show that the time evolution of the Lyapunov function is negative definite within

those bounds. For this purpose assume that the domain is

$$|r - r_c| < \mu_r r_c \tag{6.20a}$$

$$|\omega - \omega_c| < \mu_\omega \omega_c \tag{6.20b}$$

where $\mu_r, \mu_\omega \in (0, 1)$ are arbitrary constants. Nondimentionalizing

$$|\bar{r} - \bar{r}_c| < \mu_r \bar{r}_c + \mu_r \tag{6.21a}$$

$$|\bar{\omega} - \bar{\omega}_c| < \mu_\omega \bar{\omega}_c \tag{6.21b}$$

Another way to write these inequalities is

$$(1 - \mu_r)\bar{r}_c - \mu_r \ < \ \bar{r} \ < \ (1 + \mu_r)\bar{r}_c + \mu_r \tag{6.22a}$$

$$(1 - \mu_\omega)\bar{\omega}_c \ < \ \bar{\omega} \ < \ (1 + \mu_\omega)\bar{\omega}_c \tag{6.22b}$$

Therefore

$$(1 - \mu_r)(\bar{r}_c + 1) \ < \ (\bar{r} + 1) \ < \ (1 + \mu_r)(\bar{r}_c + 1) \tag{6.23a}$$

$$(1 - \mu_\omega)\bar{\omega}_c \ < \ \bar{\omega} \ < \ (1 + \mu_\omega)\bar{\omega}_c \tag{6.23b}$$

Assuming that the reference models are bounded by the same bounds as the system states

$$(1 - \mu_\omega)\bar{\omega}_c \ < \ \bar{\omega}_m \ < \ (1 + \mu_\omega)\bar{\omega}_c \tag{6.24}$$

Combining Eqs. (6.23) and (6.24)

$$(1-\mu_r)(\bar{r}_c+1) \;<\; (\bar{r}+1) \;<\; (1+\mu_r)(\bar{r}_c+1) \tag{6.25a}$$

$$(1-\mu_\omega)\bar{\omega}_c \;<\; \bar{\omega} \;<\; (1+\mu_\omega)\bar{\omega}_c \tag{6.25b}$$

$$2\mu_\omega\bar{\omega}_c \;<\; e_{\bar{\omega}} \;<\; 2\mu_\omega\bar{\omega}_c \tag{6.25c}$$

The commanded angular velocity is at a maximum when $t = t_1^+$ and minimum when $t = t_2^-$. Similarly, the maximum commanded radius is r_2 and the minimum is r_1. Recall that $\bar{r}_2 = 0$.

$$(1-\mu_r)(\bar{r}_1+1) \;<\; (\bar{r}+1) \;<\; (1+\mu_r) \tag{6.26a}$$

$$(1-\mu_\omega)\bar{\omega}_c(t_2^-) \;<\; \bar{\omega} \;<\; (1+\mu_\omega)\bar{\omega}_c(t_1^+) \tag{6.26b}$$

$$2\mu_\omega\bar{\omega}_c(t_2^-) \;<\; e_{\bar{\omega}} \;<\; 2\mu_\omega\bar{\omega}_c(t_1^+) \tag{6.26c}$$

$$\bar{\omega}_c(t_2^-) \;<\; \bar{\omega}_s \triangleq \bar{\omega}_c \;<\; \bar{\omega}_c(t_1^+) \tag{6.26d}$$

$$\bar{r}_1 \;<\; \bar{r}_s \triangleq \bar{r}_c \;<\; 0 \tag{6.26e}$$

Substituting these relationships into Eq. (6.19) gives

$$\mathcal{L}(f_{\bar{r}} - f_{\bar{r},s})V_{e_{\bar{r}}} \leq \left[(1+\mu_r)\,(2+\mu_\omega)\,\bar{\omega}_c(t_1^+)\sigma_{max}(P_x)\right]|\boldsymbol{e}_x|_2|\tilde{\bar{\omega}}| \tag{6.27a}$$

$$\mathcal{L}(f_{\bar{\omega}} - f_{\bar{\omega},f})V_{e_{\bar{\omega}}} \leq \left[\epsilon\frac{2(1+\mu_\omega)\bar{\omega}_c(t_1^+)}{(1-\mu_r)(\bar{r}_1+1)}\right](|\boldsymbol{e}_x|_2 + |\tilde{\boldsymbol{x}}_m|_2)\,|e_{\bar{\omega}}| + \left[\frac{4\epsilon\mu_\omega(1+\mu_\omega)\bar{\omega}_c^2(t_1^+)}{(1-\mu_r)(\bar{r}_1+1)}\right]|\dot{\bar{r}}_c| \tag{6.27b}$$

where $\sigma_{max}(P_x)$ is the maximum singular value of P_x and it has been used that $|e_{\dot{\bar{r}}}| \leq |\boldsymbol{e}_x|_2$ and $|\dot{\tilde{\bar{r}}}_m| \leq |\tilde{\boldsymbol{x}}_m|_2$. All of the values in square brackets are constants. The second inequality is almost in the format required by theorem 2.1. However, the second term must be eliminated. This is done one of two ways depending on the value of $\dot{\bar{r}}_c$. If $\dot{\bar{r}}_c = 0$ then the troublesome term is eliminated. In this case, the conditions of theorem 2.1 are met if K is positive definite. If $\dot{\bar{r}}_c \neq 0$ then the

composite Lyapunov function, V, becomes

$$\acute{V}(\boldsymbol{e_\phi}) \leq -\boldsymbol{v}^T K \boldsymbol{v} + \left[\frac{4\epsilon\mu_\omega(1+\mu_\omega)\bar{\omega}_c^2(t_1^+)}{(1-\mu_r)(\bar{r}_1+1)}\right]|\acute{\bar{r}}_c| \tag{6.28}$$

Adding and subtracting $|\tilde{\Lambda}_r|^2 + |\tilde{\Lambda}_\theta|^2$

$$\acute{V}(\boldsymbol{e_\phi}) \leq -\boldsymbol{v}^{*T} K^* \boldsymbol{v}^* + |\tilde{\Lambda}_r|^2 + |\tilde{\Lambda}_\theta|^2 + \left[\frac{4\epsilon\mu_\omega(1+\mu_\omega)\bar{\omega}_c^2(t_1^+)}{(1-\mu_r)(\bar{r}_1+1)}\right]|\acute{\bar{r}}_c| \tag{6.29}$$

where $\boldsymbol{v}^* = [\boldsymbol{v}^T \ |\tilde{\Lambda}_r| \ |\tilde{\Lambda}_\theta|]^T$ and $K^* \in \mathbb{R}^{6\times6}$ is $K \in \mathbb{R}^{4\times4}$ after being augmented with rows and columns for $\tilde{\Lambda}_r$ and $\tilde{\Lambda}_\theta$. Note that the only entries in these additional rows and columns are ones on the diagonal. So this operation doesn't change the positive definiteness. K is positive definite if and only if K^* is positive definite. The errors of the adapting parameters are bounded by the projection operator. Let the subscript "max" indicate the upper bound. $\acute{\bar{r}}_c$ is also upper bounded. This fact is demonstrated now. The radius as a function of θ is known from the geometry of conic sections

$$\bar{r}_c = \frac{a}{r_2}\frac{(1-e^2)}{(1+e\cos(\theta))} - 1 \tag{6.30}$$

where e is the eccentricity and a is the semi major axis. Differentiating gives

$$\acute{\bar{r}}_c = \frac{a}{r_2}\frac{(1-e^2)}{(1+e\cos(\theta))^2} e\sin(\theta)\bar{\omega}_c \tag{6.31}$$

An upper bound is

$$\acute{\bar{r}}_c \leq \frac{a}{r_2}(1-e^2)e\bar{\omega}_c(t_1^+) \tag{6.32}$$

Substituting these bounds into Eq. (6.29) gives

$$\acute{V}(\boldsymbol{e_\phi}) \leq -\boldsymbol{v}^{*T} K^* \boldsymbol{v}^* + \left[\tilde{\Lambda}_{r,max}^2 + \tilde{\Lambda}_{\theta,max}^2 + \frac{4\epsilon\mu_\omega(1+\mu_\omega)\bar{\omega}_c^3(t_1^+)a(1-e^2)e}{(1-\mu_r)(\bar{r}_1+1)r_2}\right] \tag{6.33}$$

Again everything in the square bracket is a constant. Let

$$L \triangleq \left[\tilde{\Lambda}_{r,max}^2 + \tilde{\Lambda}_{\theta,max}^2 + \frac{4\epsilon\mu_\omega(1+\mu_\omega)\bar{\omega}_c^3(t_1^+)a(1-e^2)e}{(1-\mu_r)(\bar{r}_1+1)r_2}\right] \tag{6.34}$$

Assuming that K is positive definite (note that this will be proven later and is the same condition that is required when $\acute{\bar{r}}_c = 0$) then Eq. (6.33) becomes

$$\acute{V}(\boldsymbol{e_\phi}) \leq -\lambda_3 |\boldsymbol{e}_\phi|_2^2 + L \tag{6.35}$$

where $\lambda_3 = \lambda_{max}(K^*)$ is the maximum eigenvalue of K^*. Also the fact that $|\boldsymbol{v}^*|_2^2 = |\boldsymbol{e}_\phi|_2^2$ has been used. Let $\lambda_1 \triangleq \frac{1}{2}\min(d^*\lambda_{min}(P_x), d^*\gamma_r^{-1}, d^*\lambda_{min}(P_{x_m}), d, d\gamma_r^{-1})$ and $\lambda_2 \triangleq \frac{1}{2}\max(d^*\lambda_{max}(P_x), d^*\gamma_r^{-1}, d^*\lambda_{max}(P_{x_m}), d, d\gamma_r^{-1})$ (recall from theorem 2.1 that $d \in (0,1)$ and $d^* \triangleq 1-d$). From the definition of V

$$\lambda_1 |\boldsymbol{e}_\phi|_2^2 \leq V \leq \lambda_2 |\boldsymbol{e}_\phi|_2^2 \tag{6.36}$$

Raffoul studied Lyapunov functions which are of the form described by Eqs. (6.35) and (6.36). By theorem 2.5 of [118], it is known that $\boldsymbol{e}_\phi$ is bounded. If that bound is less than the bounds on the domain (i.e. the state remains within the domain) then the transfer is well-behaved. In summary, the following results are obtained

$$\left(K = K^T > 0\right) \implies \begin{cases} \boldsymbol{e}_x, e_{\bar{\omega}} \in L_\infty & 0 \leq \theta \leq \pi \\ \boldsymbol{e}_x, e_{\bar{\omega}} \to 0 \text{ as } t \to \infty & \text{Otherwise} \end{cases} \tag{6.37}$$

This is sufficient to show that the new orbit at radius r_2 is asymptotically stable and the transfer maneuver is well-behaved. The following constants related to theorem 2.1 have been obtained (see

Eqs. (6.16) and (6.27))

$$\boldsymbol{\alpha} = \begin{bmatrix} \lambda_{min}(Q_x) & \lambda_{min}(Q_{x_m}) & k_{\bar{\omega}} & a_{\bar{\omega}} \end{bmatrix}^T \tag{6.38a}$$

$$\beta = (1+\mu_r)\,(2+\mu_\omega)\,\bar{\omega}_c(t_1^+)\sigma_{max}(P_x) \tag{6.38b}$$

$$\boldsymbol{\gamma} = \begin{bmatrix} 1 & 1 & 0 & 0 \end{bmatrix}^T \frac{2(1+\mu_\omega)\bar{\omega}_c(t_1^+)}{(1-\mu_r)(\bar{r}_1+1)} \tag{6.38c}$$

Finally, $\delta = 0$ by the same arguments as those used in Corollary 2.3. In the next section, it will be shown numerically that these parameters make K positive definite.

6.3 Numerical Results

In this section, the KAMS control designed above is numerically validated. A 26,520 kg spacecraft is transferred from a 10,000 km earth orbit to a geostationary orbit in numerical simulation. The effects of Simultaneous Slow and Fast Tracking are identified and the efficiency is examined by comparing the magnitude of the radial and tangential inputs. One transfer is performed but this one transfer has 5 distinct segments which were each simulated. First, a coast phase at the initial orbit r_2 is used to show asymptotic stability when r_c is constant. Second, the vehicle transitions to tracking a Hohmann transfer. This allows the control to be examined under a discrete change in the guidance signal. Third, the system coasts along the Hohmann transfer trajectory. This allows the system to be studied under a time-varying guidance signal. Fourth, the system transitions to a constant radius orbit at r_2. This is another opportunity to study the control after a discrete change in the guidance signal. Finally, another coast phase is used to show that the system is asymptotically stable at this new orbital radius. The vehicle is allowed to complete a quarter of an orbit before and after the maneuver. Figure 6.1 shows an overview of the maneuver. As can be seen, the vehicle tracks a Hohmann transfer well. The earth can be seen in the center of the figure. The x and the star mark the beginning and end of the Hohmann transfer respectively. The time histories for the first and last coast phases are neglected for brevity, but the trends can be seen in the time histories describing the transition phases.

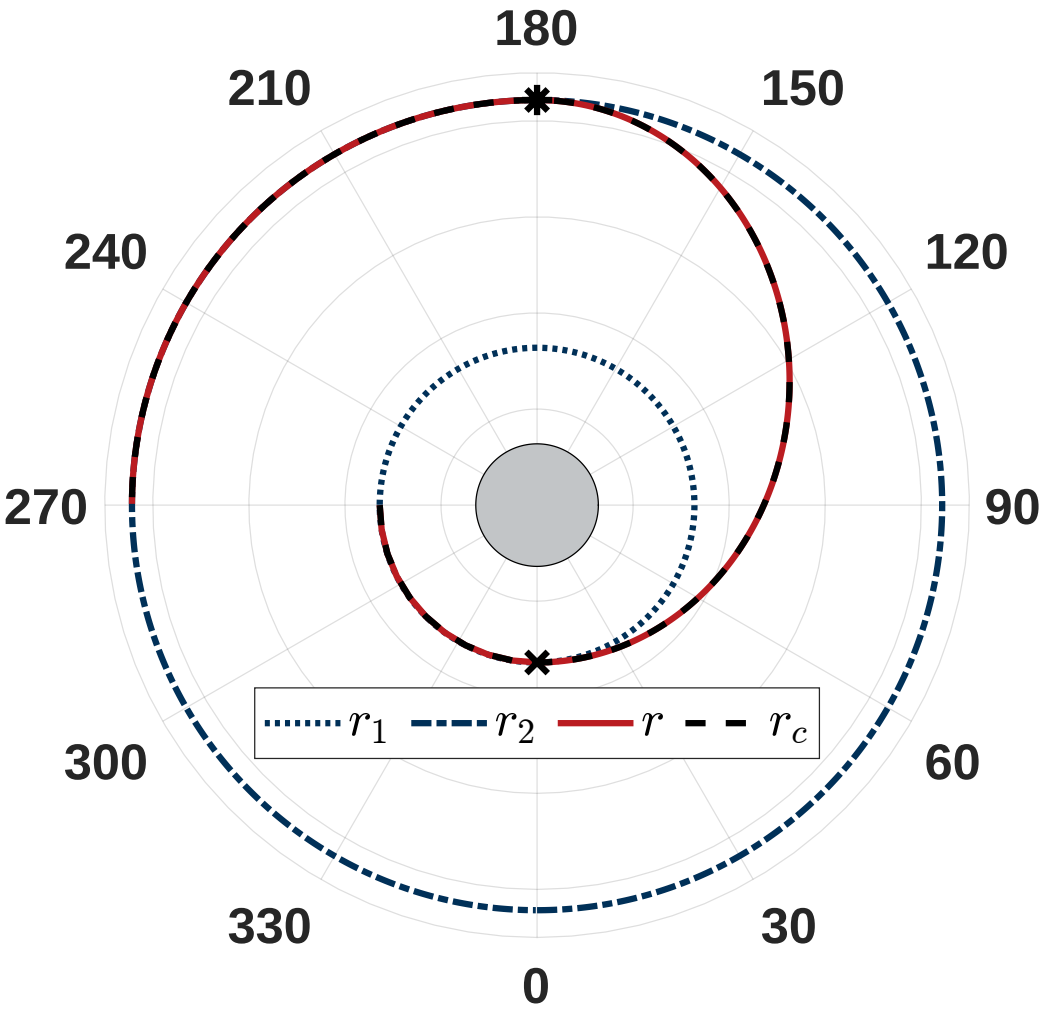

Figure 6.1: Numerical simulation of the system trajectory.

The timescale separation is found to be $\epsilon = 4.4 * 10^{-21}$. The control effectiveness parameters Λ_r and Λ_θ are set to 1. The uncertain estimates of control effectiveness parameters are initialized by sampling from a normal distribution with a mean of the true value and a standard deviation of 20% of the true value. The estimated value of the spacecraft's mass is also drawn from a similarly defined normal distribution. Notably, this means that the timescale separation is uncertain. The reference model is initialized as $\boldsymbol{x}_m(t=0) = \boldsymbol{x}(t=0)$ and $\boldsymbol{\omega}_m(t=0) = \boldsymbol{\omega}(t=0)$. The control gains are tuned to maximize performance. The final gains are

$$A_x = \begin{bmatrix} 0 & 1 \\ -100 & -20 \end{bmatrix} \tag{6.39a}$$

$$K_x = \begin{bmatrix} 0 & 1 \\ -100 & -20 \end{bmatrix} \tag{6.39b}$$

$$a_{\bar{\omega}} = 10^{-17} \tag{6.39c}$$

$$k_{\bar{\omega}} = 5 * 10^{-16} \tag{6.39d}$$

$$\gamma_r = 10 \tag{6.39e}$$

$$\gamma_\theta = 10 \tag{6.39f}$$

The matrix K can be found using these parameters. Let $d = 0.75$

$$K = \begin{bmatrix} 0.25 & 0 & -45 & -16 \\ 0 & 2.5 & -29 & 0 \\ -45 & -29 & 8.4 * 10^4 & 0 \\ -16 & 0 & 0 & 1.7 * 10^3 \end{bmatrix} \tag{6.40}$$

The LPMs of K are found to be

$$1^{st}LPM = 0.25 \tag{6.41a}$$

$$2^{nd}LPM = 0.63 \tag{6.41b}$$

$$3^{rd}LPM = 4.7 * 10^4 \tag{6.41c}$$

$$4^{th}LPM = 2.9 * 10^7 \tag{6.41d}$$

Thus, by Sylvester's Criterion, K is positive definite [95]. This implies that the conditions of Theorem 2.1 are satisfied. Therefore, the system is asymptotically stable to a circular orbit (i.e. before and after the transfer).

6.3.1 Geostationary Transfer

At the time t_1 a trans-geostationary injection (TGI) burn is performed. If the guidance law wasn't in place then the adaptive controller would implement the step change in radius using the radial thrusts. This is a very inefficient way to change orbits. However, because the vehicle is commanded to track a Hohmann transfer the primary change during the TGI burn is angular velocity. Figure 6.2 shows a evolution of the angular velocity. The cutout in this figure gives a zoomed-in view of the angular velocity during the TGI burn. The guidance law has a step change in angular velocity at time t_1 but the vehicle must follow a continuous trajectory. Thus there is some initial error in angular velocity and an initial build-up of radial position error. The radial position error is corrected with the radial thrusters while the angular velocity is given time to catch up. The net result is asymptotic stability to a Hohmann transfer. Figure 6.3 gives a evolution for the orbital radius. Time histories of the tangential and radial inputs are given in Figs. 6.4 and 6.5 respectively. Note that the radial thrust is significantly smaller than the tangential thrust. Figures 6.6 and 6.7 show the time evolution of the uncertain parameters. Finally, Fig. 6.8 shows a evolution of the true anomaly during the transfer.

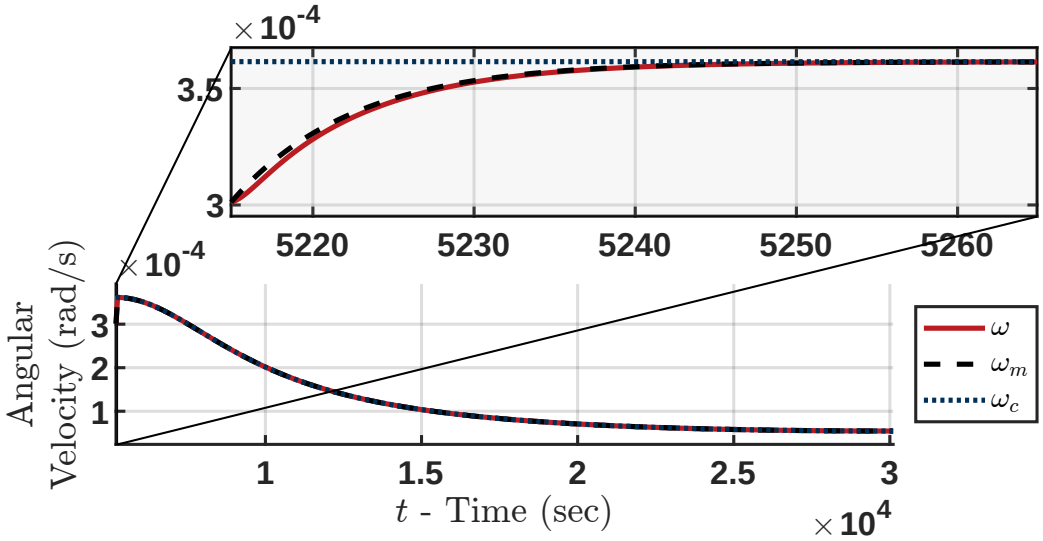

Figure 6.2: Evolution of the angular velocity during the Hohmann transfer.

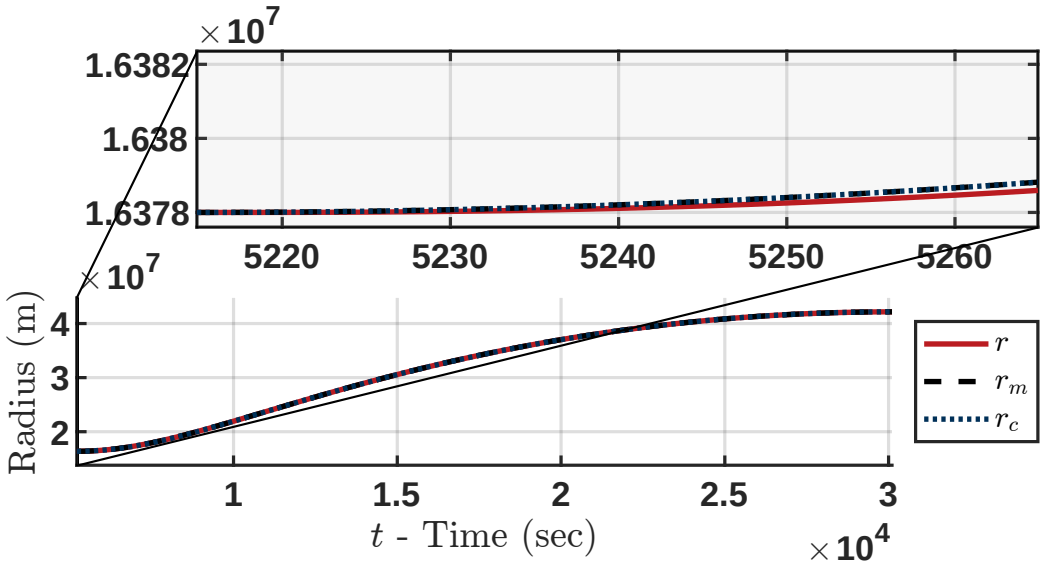

Figure 6.3: Evolution of the radius during the Hohmann transfer.

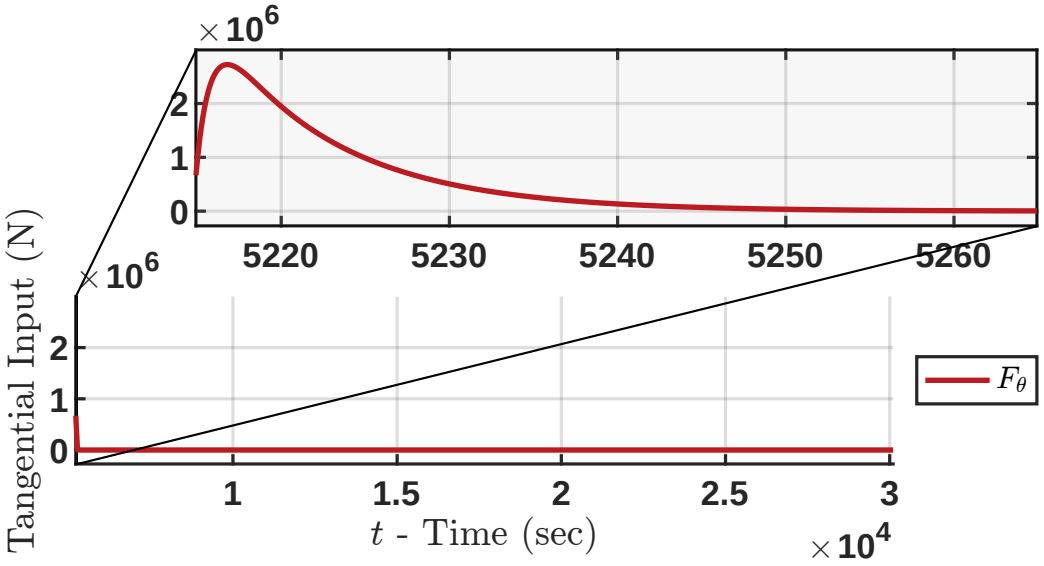

Figure 6.4: Evolution of the tangential thrust during the TGI burn.

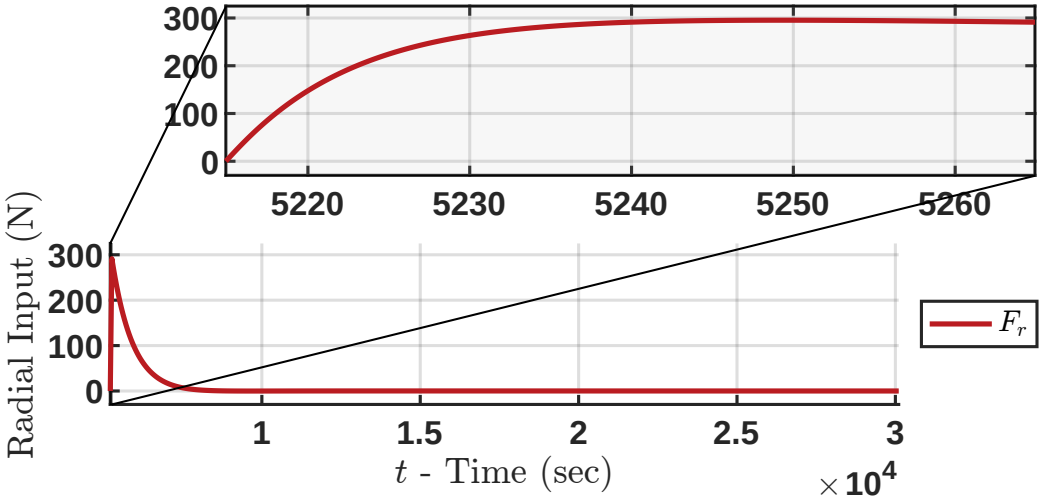

Figure 6.5: Evolution of the radial thrust during the TGI burn.

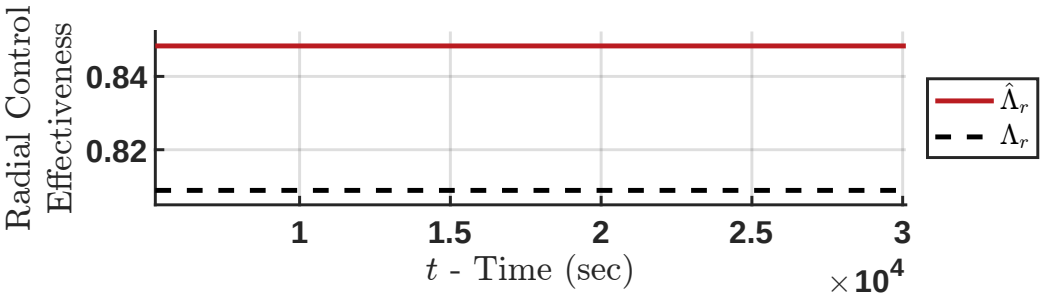

Figure 6.6: Evolution of the radial control effectiveness parameter during the Hohmann transfer.

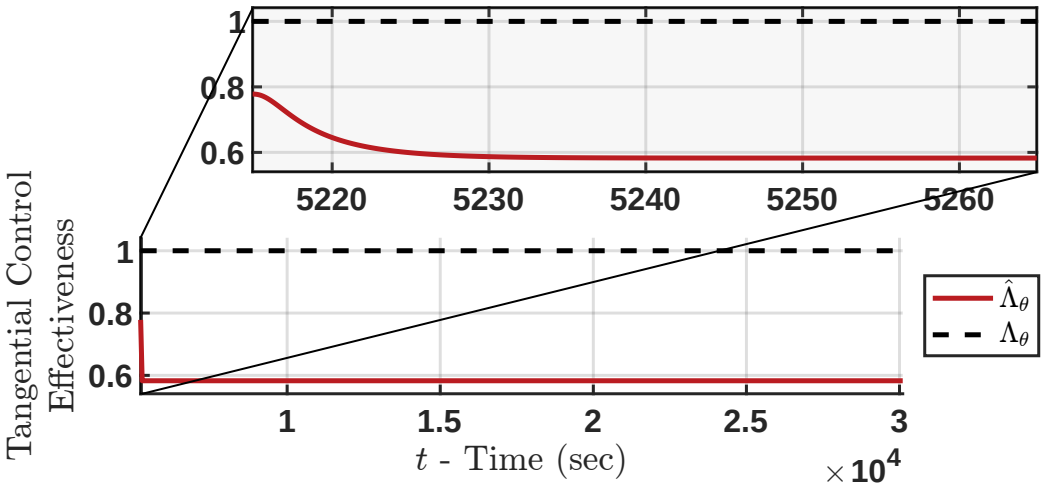

Figure 6.7: Evolution of the tangential control effectiveness parameter during the Hohmann transfer.

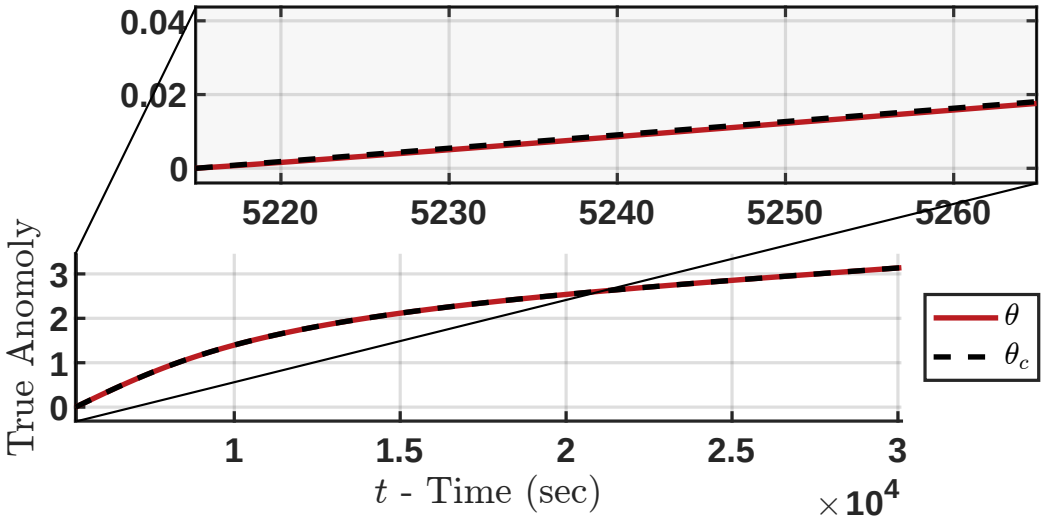

Figure 6.8: Evolution of the true anomaly during the Hohmann transfer.

6.3.2 Geostationary Orbit Insertion

At the time t_2 a geostationary orbit insertion (GOI) burn is performed. A process occurs that is similar to the TGI burn. A step change in the commanded angular velocity circularizes the orbit while radial thrusts keep the radius at r_2. Figure 6.9 shows a evolution of the angular velocity. Similar to the TGI burn there is some initial error in angular velocity and an initial build-up of radial position error. The radial position error is corrected with the radial thrusters while the angular velocity is given time to catch up. The net result is asymptotic stability to a circular geostationary orbit. Figure 6.10 gives a evolution for the orbital radius. Time histories of the tangential and radial inputs are given in Figs. 6.11 and 6.12 respectively. Note that the radial thrust is significantly smaller than the tangential thrust. Figures 6.13 and 6.14 show the time evolution of the uncertain parameters. Finally, Fig. 6.15 shows a evolution of the true anomaly during the circularization.

Notice the steady state error between the commanded and actual true anomaly. This is expected. The control and guidance laws drive the angular velocity and radius to match the reference signal from the commanded system. However, no guarantees are made about the phase angle between the actual and the reference system. As previously discussed, the continuous system is unable to track the instantaneous step change which occurs in the reference system angular velocity. This leads to the use of radial thrusters. It also causes the phase lag in the true anomaly. As the system accelerates to the reference angular velocity it begins to lag behind the reference system which has already reached the reference angular velocity. The radial thrusters correct the radial error, but not the phase lag. Thus the system arrives at geostationary orbit at the same time, but not at the same place (i.e. true anomaly) as the reference system. This may or may not be problematic depending upon the use case. For example, the phase lag would need to be accounted for in rendezvous operations.

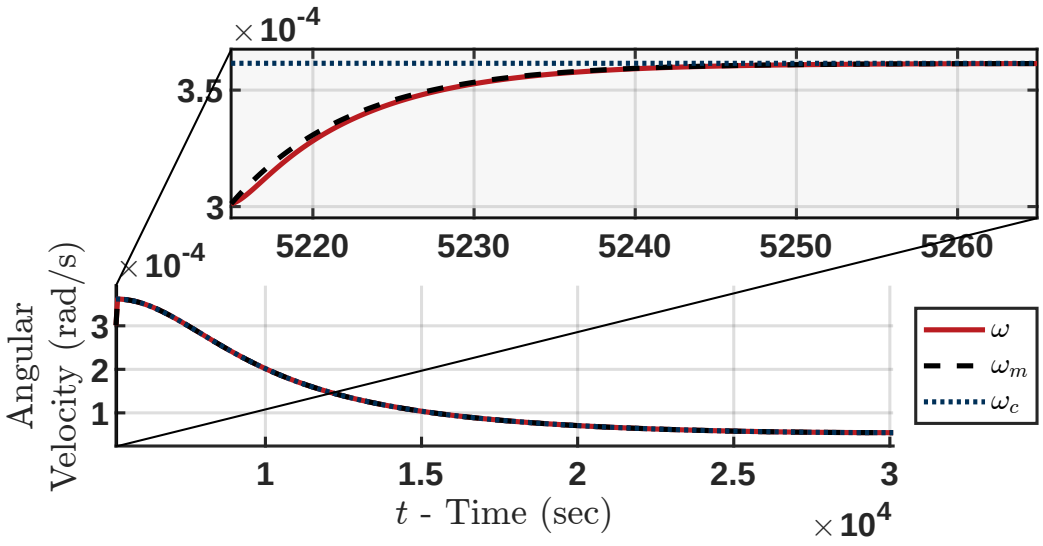

Figure 6.9: Evolution of the angular velocity after reaching geostationary orbit.

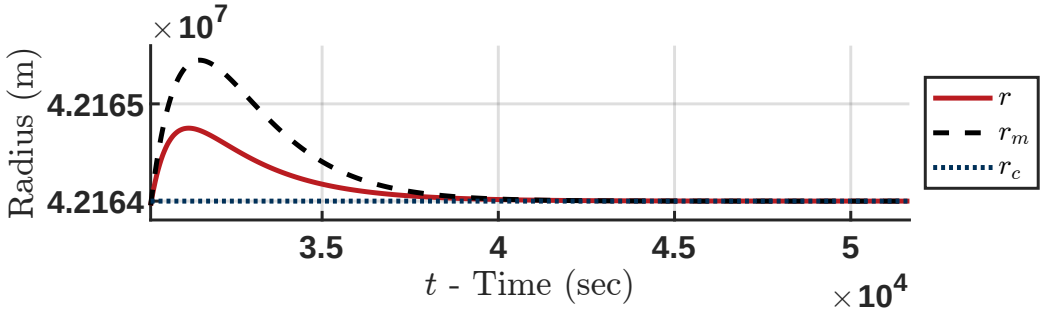

Figure 6.10: Evolution of the radius after reaching geostationary orbit.

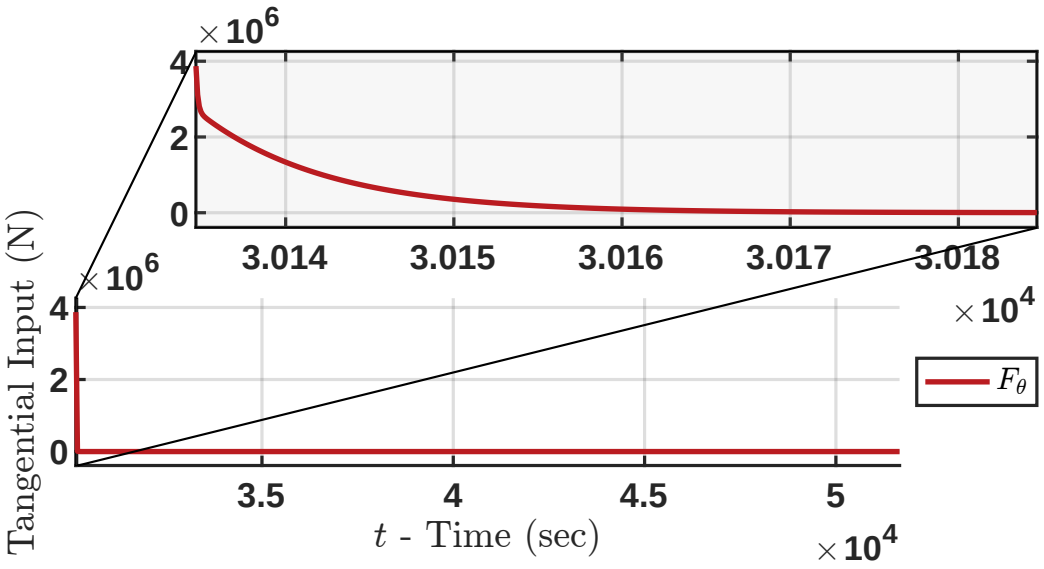

Figure 6.11: Evolution of the tangential thrust during the GOI burn.

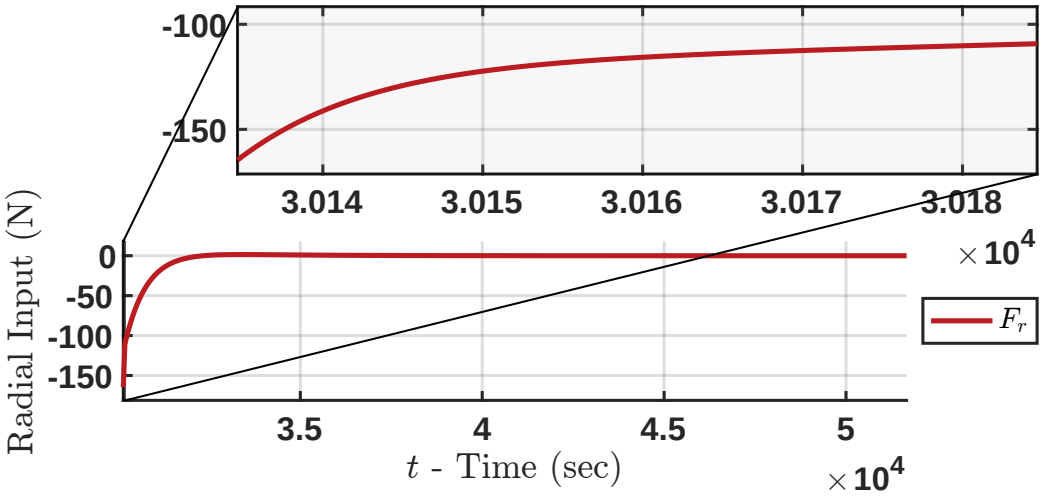

Figure 6.12: Evolution of the radial thrust during the GOI burn.

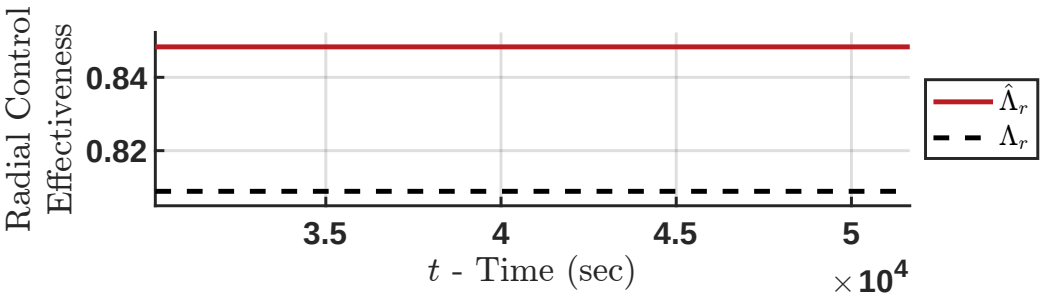

Figure 6.13: Evolution of the radial control effectiveness parameter after reaching geostationary orbit.

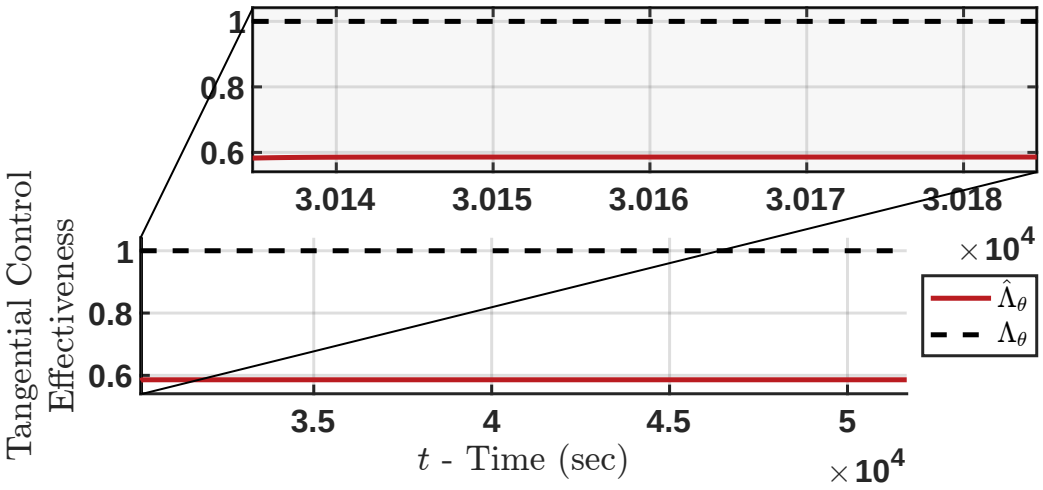

Figure 6.14: Evolution of the tangential control effectiveness parameter after reaching geostationary orbit.

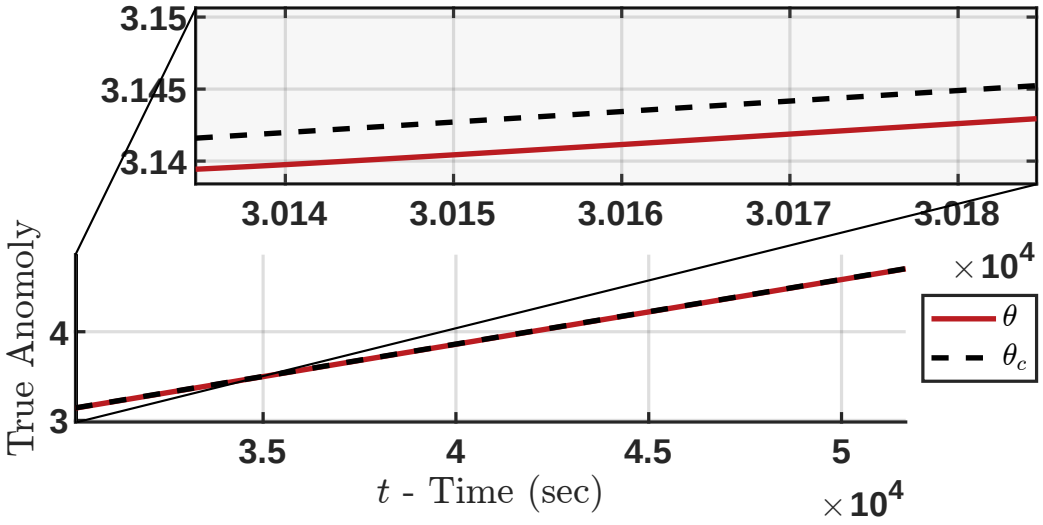

Figure 6.15: Evolution of the true anomaly after reaching geostationary orbit.

6.3.3 Efficiency Analysis

The Delta-v (Δv) for the ideal Hohmann transfer (the optimal two-impulse maneuver) when applied to the system described above is $1,762$ m/s. The Δv using the control architecture described above is $3,519$ m/s. During the primary burns (entering and exiting the maneuver) the total thrust required is on on the order of 10^6 newton. During the coast phases, the thrust is on the order of 1 newton. The Δv for the control architecture described above becomes numerically indistinguishable (within 0.25%) from the ideal Hohmann transfer if the integration is limited to 400-second windows around the primary burns. The remaining Δv occurs during the coast phase. This suggests that one possible way to improve fuel efficiency would be to swap from a traditional rocket engine to a more efficient low-thrust Hall-effect thruster during the coast phase.

6.4 Chapter Summary

This chapter derived and validated a novel method of orbital transfer using a multiple-timescale model of a satellite. It demonstrated the first example of the method KAMS on a system with the timescale separation parameter appearing on the right side of the fast state differential equation. It also demonstrated the first example of KAMS applied with Simultaneous Slow and Fast Tracking fusion. This control architecture was proven to be asymptotically stable during station-keeping operations and bounded during an orbital transfer maneuver. During the transfer, the angular velocity and radius are driven to a reference signal which is tracking a Hohmann transfer. Numerical simulations confirmed these results and also showed asymptotic stability during the transfer. Based on the results presented in this chapter, it is concluded that

1. KAMS is flexible. This chapter showed that KAMS is effective when using Simultaneous Slow and Fast Tracking. Prior work relied upon Sequential Control, but in this work, both the slow and fast states are shown to converge to their respective trajectories. KAMS is also shown to be robust to systems where the timescale separation parameter appears on the right-hand side of the fast equations of motion. This complicated the stability analysis, but guarantees on stability and boundedness are still obtained. The numerical example demon-

strated the versatility of KAMS by showing how the fused control signal is effective even though the singularly perturbed terms are not considered during the fast subsystem control synthesis.

2. KAMS is a promising method of orbital transfer for satellites. It guarantees stability and boundedness, and it ensures that the system is reasonably efficient. The radial thrust was several orders of magnitude lower than the tangential thrust, and the vehicle asymptotically converges to a Hohmann transfer trajectory. The adaptive element ensures that the system is robust to model uncertainties. The closed-loop system was driven toward a precise time of arrival, but it was unable to guarantee the precise location (i.e. true anomaly) of the circularization burn because the true anomaly is allowed to drift.

7. INLET UNSTART PREVENTION BY ADAPTIVE REGULATION USING A NONLINEAR LONGITUDINAL TIMESCALE MODEL

Inlet unstart remains a challenging problem for supersonic and especially hypersonic aircraft. Inlet unstart occurs when the shock wave is expelled from the inlet of a supersonic engine. This can occur because of fluid dynamic effects but has also been linked to excessive angle-of-attack (AoA) [137, 138]. Various methods have been developed to mitigate the risk of AoA-induced inlet unstart. Rollins *et al.* demonstrated a method of Adaptive Nonlinear Dynamic Inversion (ANDI) for inlet unstart prevention [34]. Famularo *et al.* extended this method to include state observers [66] and state constraints [30]. Famularo also studied a sampled-data version of this control architecture [67]. Many inlet unstart prevention methods utilize adaptive control. High-speed aerodynamics and thermodynamics are particularly challenging to model. This means that the stability and control derivatives cannot be analytically determined due to uncertainties in the aerodynamics and thrust. The empirical models which do exist often have large uncertainty bounds. Thus adaptive control is a natural fit for hypersonic aircraft. Kuipers *et al.* applied adaptive linear quadratic control to a hypersonic aircraft [139]. Mooij performed a numerical study on MRAC for hypersonic aircraft [140]. Banerjee *et al.* studied $\mathcal{L}_1$ adaptive control on a hypersonic aircraft [141]. In a general sense adaptive control has seen extensive application in fixed-wing aircraft. For example, Tandale and Valasek studied adaptive model inversion control for an F-16 [50]. Chowdhary *et al.* demonstrated adaptive control on a UAV with extreme faults like loss of 50% of the right-wing [27]. High-speed aircraft also exhibit multiple-timescale behavior. The high velocity causes some states to evolve quickly. However, other states are constrained to evolve slowly to avoid damaging the aircraft. For example, later in this chapter, it is formally shown that the high-speed airflow induces high aerodynamic moments which result in high angular acceleration, but the AoA must be kept low to limit inlet unstart. Singularly perturbed differential equations can be used to model these multiple-timescale systems. Ren, Jiang, and Yang developed and used a timescale analysis of a hypersonic aircraft [7]. More generally, Khalil and Chen published a multiple-timescale model

of a generic fixed-wing aircraft [6]. Saha *et al.* studied multiple-timescale models of an F-16A [91] and Narang-Siddarth *et al.* studied multiple-timescale models of an F/A-18A [17]. Ardema and Rajan used a multiple-timescale model to perform trajectory optimization [11]. For more examples see [12].

This chapter's objective is to demonstrate how KAMS can be used for inlet unstart prevention on hypersonic aircraft. This work is novel because it is the first method that simultaneously considers the model uncertainties and system timescales. This work is the first time KAMS has been applied to systems that require adaptive control in both timescales. This work also contributes a new timescale model of a hypersonic aircraft. Ren, Jiang, and Yang also developed a timescale model of a hypersonic aircraft [7], but they imposed the timescale separation after a comparative analysis of the system's domain. In contrast, the timescale model is derived in this work. This chapter is organized as follows. Section 7.1 derives the multiple-timescale model of a hypersonic aircraft. Section 7.2 derives the KAMS control and adaptation laws and proves that the system is asymptotically stable. Section 7.3 reports the results of a numerical simulation that was used to validate this control.

7.1 Multiple-Timescale Model

The present work addresses the longitudinal dynamics of a rigid-body aircraft which have been published in numerous sources (e.g. [142, 109, 110, 143]) as

$$\dot{U} = -QW - g\sin(\theta) + \frac{1}{m}(T - D) \tag{7.1a}$$

$$\dot{W} = QU + g\cos(\theta) - \frac{1}{m}L \tag{7.1b}$$

$$\dot{\theta} = Q \tag{7.1c}$$

$$\dot{Q} = \frac{1}{J_{yy}}M \tag{7.1d}$$

Here U and W are the body frame 1 and 3 axes' translational velocities respectively. Q is the body axis pitch rate, θ is the pitch attitude angle, and α is the AoA. g is the acceleration due to gravity,

m is the vehicle's mass, and J_{yy} is its inertia about the body frame 2 axis. Finally, T is the engine thrust, L is the lift force, and D is the drag force. The model assumes that the thrust is colinear with the stability frame 1 axis and that the aerodynamic coupling between U and W is negligible (i.e. L doesn't appear in Eq. (7.1a) and D doesn't appear in Eq. (7.1b)). These are appropriate assumptions for a hypersonic aircraft trimmed in cruise flight.

This longitudinal model is rewritten as a multiple-timescale system. As recommended by [9] the timescales are identified by non-dimensionalizing using Buckingham Pi Theorem [136, p. 346-360]. First, the following non-dimensional parameters are defined

$$\bar{u} \triangleq \frac{U - U_1}{U_1} \qquad \alpha \triangleq \frac{W - W_1}{U_1} \qquad \bar{\theta} \triangleq \theta - \theta_1 \qquad \bar{q} \triangleq Q\frac{mU_1}{q_\infty S} \tag{7.2a}$$

$$t_s \triangleq t\frac{q_\infty S}{mU_1} \qquad C_T \triangleq \frac{T}{q_\infty S} \qquad C_L \triangleq \frac{L}{q_\infty S} \qquad C_M \triangleq \frac{M}{q_\infty S c_{mac}} \tag{7.2b}$$

where q_∞ is the free stream dynamic pressure, S is wing area, and c_{mac} is the mean aerodynamic chord. The subscript 1 indicates a variable that is evaluated at the trim condition. If the stability coordinate frame is used and the aircraft is trimmed about straight and level flight then $W_1 = 0$ and $\theta_1 = 0$. Substituting these non-dimensional parameters into Eq. (7.1) gives

$$\frac{q_\infty S}{m}\acute{\bar{u}} = -\frac{q_\infty S}{mU_1}\bar{q}\alpha U_1 - g\sin(\bar{\theta}) + \frac{q_\infty S}{m}(C_T - C_D) \tag{7.3a}$$

$$\frac{q_\infty S}{m}\acute{\alpha} = \frac{q_\infty S}{mU_1}\bar{q}\left(\bar{u}U_1 + U_1\right) + g\cos(\bar{\theta}) - \frac{q_\infty S}{m}C_L \tag{7.3b}$$

$$\frac{q_\infty S}{mU_1}\acute{\bar{\theta}} = \frac{q_\infty S}{mU_1}\bar{q} \tag{7.3c}$$

$$\left(\frac{q_\infty S}{mU_1}\right)^2\acute{\bar{q}} = \frac{mU_1^2}{mU_1^2}\frac{q_\infty S c_{mac}}{J_{yy}}C_M \tag{7.3d}$$

Simplifying gives

$$\acute{\bar{u}} = -\bar{q}\alpha - \frac{mg}{q_\infty S}\sin(\bar{\theta}) + (C_T - C_D) \tag{7.4a}$$

$$\acute{\alpha} = \bar{q}\,(\bar{u}+1) + \frac{mg}{q_\infty S}\cos(\bar{\theta}) - C_L \tag{7.4b}$$

$$\acute{\bar{\theta}} = \bar{q} \tag{7.4c}$$

$$\epsilon\acute{\bar{q}} = \frac{q_\infty S c_{mac}}{mU_1^2} C_M \tag{7.4d}$$

where

$$\epsilon \triangleq J_{yy}\frac{q_\infty^2 S^2}{m^3 U_1^4} \tag{7.5}$$

For notational simplicity let

$$C_G = \frac{mg}{q_\infty S} \tag{7.6a}$$

$$C_R = \frac{q_\infty S c_{mac}}{mU_1^2} \tag{7.6b}$$

When numerical values are substituted into these equations it will be seen that $\epsilon \ll C_R, C_G$. So ϵ can be treated as a singular perturbation parameter. The aerodynamic and thrust forces are derived from those recommended by [142]. They are

$$C_L = C_{L_1} + C_{L_\alpha}\alpha \tag{7.7a}$$

$$C_D = C_{D_1} + C_{D_\alpha}\alpha + C_{D_{\alpha^2}}\alpha^2 \tag{7.7b}$$

$$C_M = C_{M_1} + C_{M_\alpha}\alpha + C_{M_{\alpha^2}}\alpha^2 + C_{M_{\delta_e}}\delta_e \tag{7.7c}$$

$$C_T = C_{T_1} + C_{T_\alpha}\alpha + C_{T_{\alpha^2}}\alpha^2 + C_{T_{\alpha^3}}\alpha^3 \tag{7.7d}$$

Where variables of the form $C_{a_b} \triangleq \frac{\partial C_a}{\partial b}$ are non-dimensional stability and control derivatives. The throttle input is assumed to be constant, but the thrust is allowed to vary with AoA. Substituting

into Eq. (7.1) gives

$$\acute{\bar{u}} = -\bar{q}\alpha - C_G \sin(\bar{\theta}) + (C_{T_1} - C_{D_1}) + (C_{T_\alpha} - C_{D_\alpha})\alpha + (C_{T_{\alpha^2}} - C_{D_{\alpha^2}})\alpha^2 + C_{T_{\alpha^3}}\alpha^3 \quad (7.8a)$$

$$\acute{\alpha} = \bar{q}\,(\bar{u} + 1) + C_G \cos(\bar{\theta}) - C_{L_1} - C_{L_\alpha}\alpha \quad (7.8b)$$

$$\acute{\bar{\theta}} = \bar{q} \quad (7.8c)$$

$$\epsilon\acute{\bar{q}} = C_R(C_{M_1} + C_{M_\alpha}\alpha + C_{M_{\alpha^2}}\alpha^2 + C_{M_{\delta_e}}\delta_e) \quad (7.8d)$$

At the trim condition, these equations reduce down to

$$C_{D_1} = C_{T_1} \quad (7.9a)$$

$$C_{L_1} = C_G \quad (7.9b)$$

$$C_{M_1} = 0 \quad (7.9c)$$

This leads to the following simplification of Eq. (7.8):

$$\acute{\bar{u}} = -\bar{q}\alpha - C_G \sin(\bar{\theta}) + (C_{T_\alpha} - C_{D_\alpha})\alpha + (C_{T_{\alpha^2}} - C_{D_{\alpha^2}})\alpha^2 + C_{T_{\alpha^3}}\alpha^3 \quad (7.10a)$$

$$\acute{\alpha} = \bar{q}\,(\bar{u} + 1) - C_G(1 - \cos(\bar{\theta})) - C_{L_\alpha}\alpha \quad (7.10b)$$

$$\acute{\bar{\theta}} = \bar{q} \quad (7.10c)$$

$$\epsilon\acute{\bar{q}} = C_R(C_{M_\alpha}\alpha + C_{M_{\alpha^2}}\alpha^2 + C_{M_{\delta_e}}\delta_e) \quad (7.10d)$$

Using the trigonometric identity $1 - \cos(\alpha) = 2\sin^2(\alpha/2)$ gives

$$\acute{\bar{u}} = -\bar{q}\alpha - C_G \sin(\bar{\theta}) + (C_{T_\alpha} - C_{D_\alpha})\alpha + (C_{T_{\alpha^2}} - C_{D_{\alpha^2}})\alpha^2 + C_{T_{\alpha^3}}\alpha^3 \quad (7.11a)$$

$$\acute{\alpha} = \bar{q}\,(\bar{u} + 1) - 2C_G \sin^2\left(\frac{\bar{\theta}}{2}\right) - C_{L_\alpha}\alpha \quad (7.11b)$$

$$\acute{\bar{\theta}} = \bar{q} \quad (7.11c)$$

$$\epsilon\acute{\bar{q}} = C_R(C_{M_\alpha}\alpha + C_{M_{\alpha^2}}\alpha^2 + C_{M_{\delta_e}}\delta_e) \quad (7.11d)$$

This is the form of the equations of motion that is used for control synthesis. This form is beneficial for two reasons. First, the system is singularly perturbed because ϵ appears on the left side of Eq. (7.11d). This enables the application of KAMS. Second, there are no constant terms. While this is not strictly necessary, it will simplify the stability analysis.

7.2 Control Synthesis

The control objective is for the AoA to track a slow timescale reference model. This is done by designing a regulator using KAMS. All aerodynamic stability and control derivatives are taken to be uncertain. Note that C_G and C_R are not aerodynamic properties and are deterministic. ANDI [65] is used to control the subsystems and Sequential Control [9] is used to fuse the control signals. The reduced slow subsystem is

$$\acute{\bar{u}} = -\bar{q}_s\alpha - C_G\sin(\bar{\theta}) + (C_{T_\alpha} - C_{D_\alpha})\alpha + (C_{T_{\alpha^2}} - C_{D_{\alpha^2}})\alpha^2 + C_{T_{\alpha^3}}\alpha^3 \tag{7.12a}$$

$$\acute{\alpha} = \bar{q}_s\left(\bar{u}+1\right) - 2C_G\sin^2\left(\frac{\bar{\theta}}{2}\right) - C_{L_\alpha}\alpha \tag{7.12b}$$

$$\acute{\bar{\theta}} = \bar{q}_s \tag{7.12c}$$

The reduced fast subsystem is

$$\grave{\bar{u}} = 0 \tag{7.13a}$$

$$\grave{\alpha} = 0 \tag{7.13b}$$

$$\grave{\bar{\theta}} = 0 \tag{7.13c}$$

$$\grave{\bar{q}} = C_R(C_{M_\alpha}\alpha + C_{M_{\alpha^2}}\alpha^2 + C_{M_{\delta_e}}\delta_e) \tag{7.13d}$$

7.2.1 Zero Dynamics

One assumption of ANDI is that the zero dynamics are stable. Per Sequential Control design, the input to the fast subsystem is δ_e and the output is $\bar{q}$. Similarly, the input to the slow subsystem is $\bar{q}_s$ and the output is α. The zero dynamics of the fast subsystem are stable because the slow

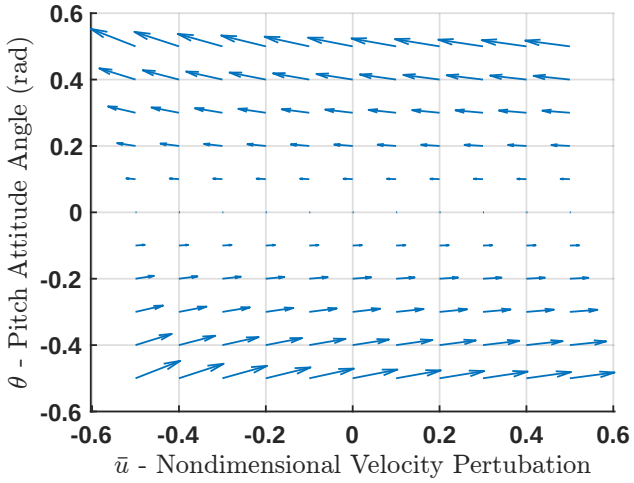

Figure 7.1: Phase diagram of the slow subsystem zero dynamics.

states are constant in time. However, the slow subsystem requires additional analysis. The zero dynamics can be found by setting $\alpha = \acute{\alpha} = 0$. This gives

$$\acute{\bar{u}} = -\frac{mg}{q_\infty S}\sin(\bar{\theta}) \tag{7.14a}$$

$$\acute{\bar{\theta}} = 2C_G \sin^2\left(\frac{\bar{\theta}}{2}\right)\frac{1}{\bar{u}+1} \tag{7.14b}$$

The phase diagram for the zero dynamics is given in Fig. 7.1 (numerical values as given in Section 7.3). The terms related to gravity make the system weakly non-minimum phase. The non-minimum phase effects are roughly proportional to the magnitude of the velocity and pitch perturbations. This implies that ANDI is not a valid approach. However, Hauser, Sastry, and Meyer showed that asymptotic stability can still be achieved for weakly non-minimum phase systems by neglecting the offending terms during the control synthesis [144]. Thus, the following reduced

slow subsystem will be used for the control synthesis

$$\acute{\bar{u}} = -\bar{q}_s\alpha + (C_{T_\alpha} - C_{D_\alpha})\alpha + (C_{T_{\alpha^2}} - C_{D_{\alpha^2}})\alpha^2 + C_{T_{\alpha^3}}\alpha^3 \tag{7.15a}$$

$$\acute{\alpha} = \bar{q}_s\,(\bar{u} + 1) - C_{L_\alpha}\alpha \tag{7.15b}$$

$$\acute{\bar{\theta}} = \bar{q}_s \tag{7.15c}$$

7.2.2 Control Synthesis

Following the design process for Sequential Control [9], the manifold is first selected so that the reduced slow subsystem is stable. The slow reference model is

$$\acute{\alpha}_m = -a_\alpha(\alpha_m - r) \tag{7.16}$$

where $a_\alpha, r \in \mathbb{R}_+$. The slow reference model input, r, will be set to 0 later but is included here for generality. Per ANDI the following manifold is sufficient to accomplish the control objective in the slow subsystem

$$\bar{q}_s = (\bar{u} + 1)^{-1}\left(-a_\alpha(\alpha_m - r) + \hat{C}_{L_\alpha}\alpha - k_\alpha(\alpha - \alpha_m)\right) \tag{7.17}$$

where $k_\alpha \in \mathbb{R}_+$ is a constant control gain. The adaptation law is

$$\acute{\hat{C}}_{L_\alpha} = \gamma_{L_\alpha}\mathrm{Proj}(\hat{C}_{L_\alpha}, -\alpha(\alpha - \alpha_m)) \tag{7.18}$$

where $\gamma_{L_\alpha} \in \mathbb{R}_+$ is an adaptation rate gain. A similar process is used to design the control for the reduced slow subsystem using the fast-state reference model

$$\grave{\bar{q}}_m = -a_{\bar{q}}(\bar{q}_m - \bar{q}_s) \tag{7.19}$$

where $a_{\bar{q}} \in \mathbb{R}_+$. The input is

$$\delta_e = \left(C_R \hat{C}_{M_{\delta_e}}\right)^{-1} \left(-a_{\bar{q}}(\bar{q}_m - \bar{q}_s) - C_R \left(\hat{C}_{M_\alpha}\alpha + \hat{C}_{M_{\alpha^2}}\alpha^2\right) - k_{\bar{q}}(\bar{q} - \bar{q}_m)\right) \tag{7.20}$$

where $k_{\bar{q}} \in \mathbb{R}_+$ is a constant control gain. The adaptation laws are thus

$$\dot{\hat{C}}_{M_\alpha} = \gamma_{M_\alpha} \mathrm{Proj}(\hat{C}_{M_\alpha}, C_R \alpha(\bar{q} - \bar{q}_m)) \tag{7.21a}$$

$$\dot{\hat{C}}_{M_{\alpha^2}} = \gamma_{M_{\alpha^2}} \mathrm{Proj}(\hat{C}_{M_{\alpha^2}}, C_R \alpha^2(\bar{q} - \bar{q}_m)) \tag{7.21b}$$

$$\dot{\hat{C}}_{M_{\delta_e}} = \gamma_{M_{\delta_e}} \mathrm{Proj}(\hat{C}_{M_{\delta_e}}, C_R \delta_e(\bar{q} - \bar{q}_m)) \tag{7.21c}$$

where $\gamma_{M_\alpha}, \gamma_{M_{\alpha^2}}, \gamma_{M_{\delta_e}} \in \mathbb{R}_+$ are adaptation rate gains.

To implement this control the control states (i.e. α_m, $\hat{C}_{L_\alpha}$, $\bar{q}_m$, $\hat{C}_{M_\alpha}$, $\hat{C}_{M_{\alpha^2}}$, and $\hat{C}_{M_{\delta_e}}$) must be integrated over time. This is easiest to do in the standard timescale t. Thus Eqs. (7.16), (7.18), (7.19), and (7.21) need to be converted to the correct timescale

$$\dot{\alpha}_m = \frac{q_\infty S}{m U_1} \left(-a_\alpha(\alpha_m - r)\right) \tag{7.22a}$$

$$\dot{\hat{C}}_{L_\alpha} = \frac{q_\infty S}{m U_1} \left(\gamma_{L_\alpha} \mathrm{Proj}(\hat{C}_{L_\alpha}, -\alpha(\alpha - \alpha_m))\right) \tag{7.22b}$$

$$\dot{\bar{q}}_m = \frac{1}{\epsilon} \frac{q_\infty S}{m U_1} \left(-a_{\bar{q}}(\bar{q}_m - \bar{q}_s)\right) \tag{7.22c}$$

$$\dot{\hat{C}}_{M_\alpha} = \frac{1}{\epsilon} \frac{q_\infty S}{m U_1} \left(\gamma_{M_\alpha} \mathrm{Proj}(\hat{C}_{M_\alpha}, C_R \alpha(\bar{q} - \bar{q}_m))\right) \tag{7.22d}$$

$$\dot{\hat{C}}_{M_{\alpha^2}} = \frac{1}{\epsilon} \frac{q_\infty S}{m U_1} \left(\gamma_{M_{\alpha^2}} \mathrm{Proj}(\hat{C}_{M_{\alpha^2}}, C_R \alpha^2(\bar{q} - \bar{q}_m))\right) \tag{7.22e}$$

$$\dot{\hat{C}}_{M_{\delta_e}} = \frac{1}{\epsilon} \frac{q_\infty S}{m U_1} \left(\gamma_{M_{\delta_e}} \mathrm{Proj}(\hat{C}_{M_{\delta_e}}, C_R \delta_e(\bar{q} - \bar{q}_m))\right) \tag{7.22f}$$

7.2.3 Full-Order Stability Analysis

In this section, it is shown that the full-order closed-loop system is asymptotically stable. The objective is to ensure that the conditions of Theorem 2.1 are met. This requires a bound on the time derivative of the manifold.

7.2.3.1 *Differentiation of the Manifold*

From Eq. (7.17)

$$f_{\bar{q}_s} \triangleq \frac{d}{dt_s}\left((\bar{u}+1)^{-1}\left(-a_\alpha(\alpha_m - r) + \hat{C}_{L_\alpha}\alpha - k_\alpha(\alpha - \alpha_m)\right)\right) \tag{7.23}$$

Evaluating

$$\begin{aligned} f_{\bar{q}_s} = &-(\bar{u}+1)^{-2}\left(-a_\alpha(\alpha_m - r) + \hat{C}_{L_\alpha}\alpha - k_\alpha(\alpha - \alpha_m)\right)\acute{\bar{u}} \\ &+ (\bar{u}+1)^{-1}\left((k_\alpha - a_\alpha)\acute{\alpha}_m + \acute{\hat{C}}_{L_\alpha}\alpha + \left(\hat{C}_{L_\alpha} - k_\alpha\right)\acute{\alpha}\right) \end{aligned} \tag{7.24}$$

Using the system dynamics

$$\begin{aligned} f_{\bar{q}_s} = &-(\bar{u}+1)^{-2}\left(-a_\alpha(\alpha_m - r) + \hat{C}_{L_\alpha}\alpha - k_\alpha(\alpha - \alpha_m)\right)\acute{\bar{u}} \\ &+ (\bar{u}+1)^{-1}\Big((a_\alpha - k_\alpha)a_\alpha(\alpha_m - r) + \gamma_{L_\alpha}\mathrm{Proj}(\hat{C}_{L_\alpha}, -\alpha(\alpha - \alpha_m))\alpha \\ &+ \left(\hat{C}_{L_\alpha} - k_\alpha\right)\left(\bar{q}\left(\bar{u}+1\right) - C_{L_\alpha}\alpha\right)\Big) \end{aligned} \tag{7.25}$$

Using the relationships from Eq. (2.10) it can be shown that

$$\alpha = e_\alpha + \tilde{\alpha}_m + r \tag{7.26a}$$

$$\bar{q} = e_{\bar{q}} + \tilde{\bar{q}}_m + \bar{q}_s \tag{7.26b}$$

$\bar{q}_s$ is known and a function of α (see Eq. (7.17)) so Eq. (7.26b) can be expanded further

$$\bar{q} = e_{\bar{q}} + \tilde{\bar{q}}_m + (\bar{u}+1)^{-1}\left(-a_\alpha\tilde{\alpha}_m + \hat{C}_{L_\alpha}(e_\alpha + \tilde{\alpha}_m + r) - k_\alpha e_\alpha\right) \tag{7.27}$$

Substituting these relationships into Eq. (7.25) produces

$$
\begin{aligned}
f_{\bar{q}_s} = & -(\bar{u}+1)^{-2}\left(-a_\alpha\tilde{\alpha}_m + \hat{C}_{L_\alpha}(e_\alpha+\tilde{\alpha}_m+r) - k_\alpha e_\alpha\right)\acute{u} \\
& + (\bar{u}+1)^{-1}\Big((a_\alpha-k_\alpha)a_\alpha\tilde{\alpha}_m + \gamma_{L_\alpha}\mathrm{Proj}(\hat{C}_{L_\alpha},-\alpha e_\alpha)\alpha \\
& + \left(\hat{C}_{L_\alpha}-k_\alpha\right)\left(\left(e_{\bar{q}}+\tilde{\tilde{q}}_m+(\bar{u}+1)^{-1}\left(-a_\alpha\tilde{\alpha}_m+\hat{C}_{L_\alpha}(e_\alpha+\tilde{\alpha}_m+r)-k_\alpha e_\alpha\right)\right)(\bar{u}+1)\right. \\
& \left. - C_{L_\alpha}(e_\alpha+\tilde{\alpha}_m+r)\right)\Big)
\end{aligned} \tag{7.28}
$$

Expanding and collecting like terms

$$
\begin{aligned}
f_{\bar{q}_s} = & (\bar{u}+1)^{-1}\left(\hat{C}_{L_\alpha}-k_\alpha\right)\left(\left(\hat{C}_{L_\alpha}-C_{L_\alpha}-k_\alpha\right)-(\bar{u}+1)^{-1}\acute{u}\right)e_\alpha \\
& + (\bar{u}+1)^{-1}\gamma_{L_\alpha}\mathrm{Proj}\left(\hat{C}_{L_\alpha},-\alpha e_\alpha\right)\alpha \\
& + (\bar{u}+1)^{-1}\left(\hat{C}_{L_\alpha}-k_\alpha\right)\left(\left(\hat{C}_{L_\alpha}-C_{L_\alpha}-a_\alpha\right)-(\bar{u}+1)^{-1}\acute{u}\right)\tilde{\alpha}_m \\
& + (\bar{u}+1)^{-1}(a_\alpha-k_\alpha)a_\alpha\tilde{\alpha}_m \\
& + (\bar{u}+1)^{-1}\left(\hat{C}_{L_\alpha}-k_\alpha\right)e_{\bar{q}} + (\bar{u}+1)^{-1}\left(\hat{C}_{L_\alpha}-k_\alpha\right)\tilde{\tilde{q}}_m \\
& + (\bar{u}+1)^{-1}\left(\left(\hat{C}_{L_\alpha}-k_\alpha\right)\left(\hat{C}_{L_\alpha}-C_{L_\alpha}\right)-(\bar{u}+1)^{-1}\hat{C}_{L_\alpha}\acute{u}\right)r
\end{aligned} \tag{7.29}
$$

Taking the 2-norm

$$
\begin{aligned}
f_{\bar{q}_s} \leq & |\bar{u}+1|^{-1}\left|\hat{C}_{L_\alpha}-k_\alpha\right|_2\left(\left|\hat{C}_{L_\alpha}-C_{L_\alpha}-k_\alpha\right|_2+|\bar{u}+1|^{-1}\left|\acute{u}\right|_2\right)|e_\alpha|_2 \\
& + |\bar{u}+1|^{-1}\gamma_{L_\alpha}\left|\mathrm{Proj}\left(\hat{C}_{L_\alpha},-\alpha e_\alpha\right)\right|_2|\alpha|_2 \\
& + |\bar{u}+1|^{-1}\left|\hat{C}_{L_\alpha}-k_\alpha\right|_2\left(\left|\hat{C}_{L_\alpha}-C_{L_\alpha}-a_\alpha\right|_2+|\bar{u}+1|^{-1}\left|\acute{u}\right|_2\right)|\tilde{\alpha}_m|_2 \\
& + |\bar{u}+1|^{-1}|a_\alpha-k_\alpha|_2\,a_\alpha\,|\tilde{\alpha}_m|_2 \\
& + |\bar{u}+1|^{-1}\left|\hat{C}_{L_\alpha}-k_\alpha\right|_2|e_{\bar{q}}|_2 + |\bar{u}+1|^{-1}\left|\hat{C}_{L_\alpha}-k_\alpha\right|_2|\tilde{\tilde{q}}_m|_2 \\
& + |\bar{u}+1|^{-1}\left(\left|\hat{C}_{L_\alpha}-k_\alpha\right|_2\left|\hat{C}_{L_\alpha}-C_{L_\alpha}\right|_2+|\bar{u}+1|^{-1}\left|\hat{C}_{L_\alpha}\right|_2\left|\acute{u}\right|_2\right)|r|_2
\end{aligned} \tag{7.30}
$$

Assuming that the domain is $|\bar{u}| < 0.5$, $\alpha, \alpha_m, \theta, \bar{q} < 1$ rad, and $r = 0$ (regulation)

$$\begin{aligned} f_{\bar{q}_s} \leq\ & 2\left|\hat{C}_{L_\alpha} - k_\alpha\right|_2 \left(\left|\hat{C}_{L_\alpha} - C_{L_\alpha} - k_\alpha\right|_2 + 2\left|\acute{\bar{u}}\right|_2\right)|e_\alpha|_2 \\ & + 2\gamma_{L_\alpha}\left|\text{Proj}\left(\hat{C}_{L_\alpha}, -\alpha e_\alpha\right)\right|_2 \\ & + 2\left|\hat{C}_{L_\alpha} - k_\alpha\right|_2 \left(\left|\hat{C}_{L_\alpha} - C_{L_\alpha} - a_\alpha\right|_2 + 2\left|\acute{\bar{u}}\right|_2\right)|\tilde{\alpha}_m|_2 \\ & + 2\left|a_\alpha - k_\alpha\right|_2 a_\alpha\,|\tilde{\alpha}_m|_2 \\ & + 2\left|\hat{C}_{L_\alpha} - k_\alpha\right|_2 |e_{\bar{q}}|_2 + 2\left|\hat{C}_{L_\alpha} - k_\alpha\right|_2 |\tilde{\bar{q}}_m|_2 \end{aligned} \tag{7.31}$$

Using the definition of the projection operator and recalling that $\alpha < 1$

$$\begin{aligned} f_{\bar{q}_s} \leq\ & 2\left(\left|\hat{C}_{L_\alpha} - k_\alpha\right|_2 \left(\left|\hat{C}_{L_\alpha} - C_{L_\alpha} - k_\alpha\right|_2 + 2\left|\acute{\bar{u}}\right|_2\right) + 2\gamma_{L_\alpha}\right)|e_\alpha|_2 \\ & + 2\left(\left|\hat{C}_{L_\alpha} - k_\alpha\right|_2 \left(\left|\hat{C}_{L_\alpha} - C_{L_\alpha} - a_\alpha\right|_2 + 2\left|\acute{\bar{u}}\right|_2\right) + 2\left|a_\alpha - k_\alpha\right|_2 a_\alpha\right)|\tilde{\alpha}_m|_2 \\ & + 2\left|\hat{C}_{L_\alpha} - k_\alpha\right|_2 |e_{\bar{q}}|_2 + 2\left|\hat{C}_{L_\alpha} - k_\alpha\right|_2 |\tilde{\bar{q}}_m|_2 \end{aligned} \tag{7.32}$$

Recall that the time derivative of $\bar{u}$ in the full-order system is

$$\acute{\bar{u}} = -\bar{q}\alpha + (C_{T_\alpha} - C_{D_\alpha})\alpha + (C_{T_{\alpha^2}} - C_{D_{\alpha^2}})\alpha^2 + C_{T_{\alpha^3}}\alpha^3 \tag{7.11a revisited}$$

Within the domain of interest ($|\bar{q}|, |\alpha| \leq 1$) this function is bounded

$$\acute{\bar{u}} \leq 1 + |(C_{T_\alpha} - C_{D_\alpha})| + |(C_{T_{\alpha^2}} - C_{D_{\alpha^2}})| + |C_{T_{\alpha^3}}| \tag{7.33}$$

Let $\acute{\bar{u}}_{max}$ be equal to the right side of this equation so that $\acute{\bar{u}} \leq \acute{\bar{u}}_{max}$. Similarly, the adapting parameter $\hat{C}_{L_\alpha}$ is bounded due to the use of the projection operator. Let $\hat{C}_{L_\alpha} \leq \hat{C}_{L_{\alpha,\max}}$ where

$\hat{C}_{L_{\alpha,\max}} > 0$. Substituting these inequalities into Eq. (7.32)

$$\begin{aligned} f_{\bar{q}_s} \leq\ & 2\left(\left|\hat{C}_{L_{\alpha,\max}} - k_\alpha\right|_2 \left(\left|\hat{C}_{L_{\alpha,\max}} - C_{L_\alpha} - k_\alpha\right|_2 + 2\acute{\bar{u}}_{max}\right) + 2\gamma_{L_\alpha}\right)|e_\alpha|_2 \\ & + 2\left(\left|\hat{C}_{L_{\alpha,\max}} - k_\alpha\right|_2 \left(\left|\hat{C}_{L_{\alpha,\max}} - C_{L_\alpha} - a_\alpha\right|_2 + 2\acute{\bar{u}}_{max}\right) + 2\left|a_\alpha - k_\alpha\right|_2 a_\alpha\right)|\tilde{\alpha}_m|_2 \\ & + 2\left|\hat{C}_{L_{\alpha,\max}} - k_\alpha\right|_2 |e_{\bar{q}}|_2 + 2\left|\hat{C}_{L_{\alpha,\max}} - k_\alpha\right|_2 |\tilde{\bar{q}}_m|_2 \end{aligned} \tag{7.34}$$

Define

$$\boldsymbol{\delta} \triangleq \begin{bmatrix} 2\left(\left|\hat{C}_{L_{\alpha,\max}} - k_\alpha\right|_2 \left(\left|\hat{C}_{L_{\alpha,\max}} - C_{L_\alpha} - k_\alpha\right|_2 + 2\acute{\bar{u}}_{max}\right) + 2\gamma_{L_\alpha}\right) \\ 2\left(\left|\hat{C}_{L_{\alpha,\max}} - k_\alpha\right|_2 \left(\left|\hat{C}_{L_{\alpha,\max}} - C_{L_\alpha} - a_\alpha\right|_2 + 2\acute{\bar{u}}_{max}\right) + 2\left|a_\alpha - k_\alpha\right|_2 a_\alpha\right) \\ 2\left|\hat{C}_{L_{\alpha,\max}} - k_\alpha\right|_2 \\ 2\left|\hat{C}_{L_{\alpha,\max}} - k_\alpha\right|_2 \end{bmatrix} \tag{7.35}$$

Thus

$$f_{\bar{q}_s} \leq \boldsymbol{\delta}^T \boldsymbol{v} \tag{7.36}$$

7.2.3.2 Application of Theorem 2.1

The tools have now been developed to check the conditions of Theorem 2.1. Consider the following Lyapunov functions for the reference models and subsystems

$$V_{e_\alpha} = \frac{1}{2}\left(e_\alpha^2 + \frac{1}{\gamma_{L_\alpha}}\tilde{C}_{L_\alpha}^2\right) \tag{7.37a}$$

$$V_{\tilde{\alpha}_m} = \frac{1}{2}\tilde{\alpha}_m^2 \tag{7.37b}$$

$$V_{e_{\bar{q}}} = \frac{1}{2}\left(e_{\bar{q}}^2 + \frac{1}{\gamma_{M_\alpha}}\tilde{C}_{M_\alpha}^2 + \frac{1}{\gamma_{M_{\alpha^2}}}\tilde{C}_{M_{\alpha^2}}^2 + \frac{1}{\gamma_{M_{\delta_e}}}\tilde{C}_{M_{\delta_e}}^2\right) \tag{7.37c}$$

$$V_{\tilde{\bar{q}}_m} = \frac{1}{2}\tilde{\bar{q}}_m^2 \tag{7.37d}$$

The time derivatives of these Lyapunov functions are

$$\mathcal{L}(f_{e_\xi,s})V_{e_\alpha} \leq -k_\alpha e_\alpha^2 \tag{7.38a}$$

$$\mathcal{L}(f_{\tilde{\alpha}_m})V_{\tilde{\alpha}_m} = -a_\alpha \tilde{\alpha}_m^2 \tag{7.38b}$$

$$\mathcal{L}(f_{e_\eta,f})V_{e_{\bar{q}}} \leq -k_{\bar{q}} e_{\bar{q}}^2 \tag{7.38c}$$

$$\mathcal{L}(f_{\bar{q}_m,f})V_{\tilde{\bar{q}}_m} = -a_{\bar{q}} \tilde{\bar{q}}_m^2 \tag{7.38d}$$

For proof of Eqs. (7.38a) and (7.38c) see [65, Eqs. 1.20 to 1.23]. Note that Eqs. (7.38b) and (7.38d) are derived using the fact that $\acute{r} = 0$ and in the slow subsystem $\acute{\bar{q}}_s = 0$. This implies that the reduced subsystems are stable, but additional work is necessary to extend these results to the full-order system. The final three conditions of Theorem 2.1 are

$$\mathcal{L}(f_\alpha - f_{\alpha,s})V_{e_\alpha} = 1.5\tilde{\bar{q}} e_\alpha \tag{7.39a}$$

$$\mathcal{L}(f_{\bar{q}} - f_{\bar{q},f})V_{e_{\bar{q}}} = 0 \tag{7.39b}$$

$$-\mathcal{L}(f_{\bar{q}_s})V_{\tilde{\bar{q}}_m} \leq \boldsymbol{\delta}^T \boldsymbol{v} |\tilde{\bar{q}}_m|_2 \tag{7.39c}$$

The matrix K is now found by comparing Eqs. (7.38) and (7.39) with Eqs. (2.27) and (2.28) and applying the results to Eq. (2.29):

$$K = \begin{bmatrix} d^* k_\alpha & 0 & -\frac{3}{4}d^* & -\frac{3}{4}d^* - \frac{1}{2}d\delta_1 \\ 0 & d^* a_\alpha & 0 & -\frac{1}{2}d\delta_2 \\ -\frac{3}{4}d^* & 0 & \frac{d}{\epsilon}k_{\bar{q}} & -\frac{1}{2}d\delta_3 \\ -\frac{3}{4}d^* - \frac{1}{2}d\delta_1 & -\frac{1}{2}d\delta_2 & -\frac{1}{2}d\delta_3 & \frac{d}{\epsilon}a_{\bar{q}} - d\delta_4 \end{bmatrix} \tag{7.40}$$

If K is positive definite then the full-order system is asymptotically stable under the KAMS controller. The positive definiteness of K is evaluated with the numerical example in the following

section.

7.3 Numerical Results

A numerical simulation is performed on the hypersonic aircraft from [142]. The objective of this numerical simulation is to show that Theorem 1 accurately predicts asymptotic stability. It is also shown that the system is stable despite the weak non-minimum phase behavior. This validates the KAMS control architecture presented above. One representative test case is given. The system has been tuned and the initial conditions have been selected to demonstrate relevant trends. Whereas the notation used herein is slightly different from [142] each of the system parameters used herein can be derived from [142] by solving for the stoichiometrically normalized fuel-to-air ratio at trim and non-dimensionalizing the engine parameters. Also, a change of variables is performed so that the trim conditions occur when $\alpha = \delta_e = 0$. The trim condition is $26,000$ m and Mach 8 with a standard atmosphere. These system parameters are given in table 7.1. Using these parameters the timescale separation parameter is found to be $\epsilon = 6 * 10^{-6}$. The large timescale separation and aerodynamic uncertainties make this hypersonic vehicle an ideal candidate for KAMS. The control gains are chosen through tuning and are given in table 7.2. The projection operator limits the range of the adapting parameters to be between -10 and 10. The initial conditions are given in table 7.3 The reference models are purposefully not initialized at the same locations as their respective states so that the convergence trends can be seen in the time histories. The initial conditions for the adapting parameters are randomly selected from a normal distribution with a mean of the true value and a standard deviation of 10% of the true value. Recall that $0 < d < 1$ is arbitrary. Let $d = 0.04$. The matrix K can now be found using the system parameters and

Table 7.1: Hypersonic vehicle parameters adapted from [142].

Variable	**Value**	**Units**	**Name**
m	136	kg	Vehicle Mass
J_{yy}	$21,000$	$kg\ m^2$	Mass Moment of Inertia
S	1.58	m^2	Reference Area
c_{mac}	0.52	m	Mean Aerodynamic Chord
C_{L_1}	0.0089	-	Trim Lift Coefficient
C_{L_α}	4.7	$\frac{1}{rad}$	Lift Curve Slope
C_{D_1}	0.010	-	Trim Drag Coefficient
C_{D_α}	0.023	$\frac{1}{rad}$	1^{st} Order AoA Contribution to the Drag Coefficient
$C_{D_{\alpha^2}}$	5.8	$\frac{1}{rad^2}$	2^{nd} Order AoA Contribution to the Drag Coefficient
C_{M_1}	0.0	-	Trim Pitching Moment Coefficient
C_{M_α}	2.2	$\frac{1}{rad}$	1^{st} Order AoA Contribution to the Moment Coefficient
$C_{M_{\alpha^2}}$	6.3	$\frac{1}{rad^2}$	2^{nd} Order AoA Contribution to the Moment Coefficient
$C_{M_{\delta_e}}$	-1.3	$\frac{1}{rad}$	Elevator Deflection Contribution to the Moment Coefficient
C_{T_1}	0.010	-	Trim Thrust Coefficient
C_{T_α}	-0.0043	$\frac{1}{rad}$	1^{st} Order AoA Contribution to the Thrust Coefficient
$C_{T_{\alpha^2}}$	-0.49	$\frac{1}{rad^2}$	2^{nd} Order AoA Contribution to the Thrust Coefficient
$C_{T_{\alpha^3}}$	-1.9	$\frac{1}{rad^3}$	3^{rd} Order AoA Contribution to the Thrust Coefficient

Table 7.2: Hypersonic vehicle control gains.

Variable	Value	Units	Name
k_α	5	$\frac{1}{rad}$	Rate of Convergence of e_α
a_α	2	$\frac{1}{rad}$	Rate of Convergence of $\tilde{\alpha}_m$
$k_{\bar{q}}$	0.1	$\frac{1}{rad}$	Rate of Convergence of $e_{\bar{q}}$
$a_{\bar{q}}$	0.01	$\frac{1}{rad}$	Rate of Convergence of $\tilde{\bar{q}}_m$
γ_{L_α}	100	$\frac{1}{rad^3}$	Adaptation Rate for $\hat{C}_{L_\alpha}$
γ_{M_α}	100	$\frac{1}{rad^3}$	Adaptation Rate for $\hat{C}_{M_\alpha}$
$\gamma_{M_{\alpha^2}}$	100	$\frac{1}{rad^4}$	Adaptation Rate for $\hat{C}_{M_{\alpha^2}}$
$\gamma_{M_{\delta_e}}$	100	$\frac{1}{rad^3}$	Adaptation Rate for $\hat{C}_{M_{\delta_e}}$

control gains

$$K = \begin{bmatrix} 4.8 & 0 & -0.72 & -12.5 \\ 0 & 1.92 & 0 & -4.83 \\ -0.72 & 0 & 684 & -0.2 \\ -12.5 & -4.83 & -0.2 & 68.0 \end{bmatrix} \tag{7.41}$$

The leading principal minors (LPM) of K are

$$1^{st}LPM = 4.8 \tag{7.42a}$$

$$2^{nd}LPM = 9.2 \tag{7.42b}$$

$$3^{rd}LPM = 6,300 \tag{7.42c}$$

$$4^{th}LPM = 150,000 \tag{7.42d}$$

Table 7.3: Hypersonic vehicle initial conditions.

Variable	Value	Units	Name
$U(t=0)$	$2,386$	$\frac{m}{s}$	Translational Velocity in the Body Axes 1 Direction
$\alpha(t=0)$	5	deg	Angle-of-Attack
$\alpha_m(t=0)$	4	deg	Angle-of-Attack Reference Model State
$\theta(t=0)$	0	deg	Pitch Attitude Angle
$Q(t=0)$	0	$\frac{deg}{s}$	Body Axis Pitch Rate
$\bar{q}_m(t=0)$	-4.3	deg	Non-dimensional Body Axis Pitch Rate Reference Model State

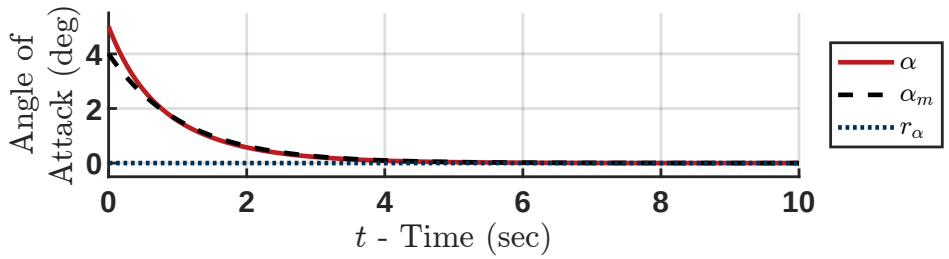

Figure 7.2: Evolution of the angle-of-attack.

Because the LPMs of K are positive Sylvester's Criterion [95] implies that K is positive definite. Thus all of the conditions of Theorem 2.1 are met. By Theorem 2.1 $\boldsymbol{e}_x, \boldsymbol{e}_z \to 0$ as $t \to \infty$.

Figure 7.2 shows the evolution of the AoA and Fig. 7.3 shows the evolution of the body axis pitch rate. As can be seen, the control objective is achieved since both AoA and body axis pitch rate converge asymptotically to their respective reference models. The adapting parameters are shown in Figs. 7.4 ($\hat{C}_{L_\alpha}$), 7.5 ($\hat{C}_{M_\alpha}$), 7.6 ($\hat{C}_{M_{\alpha^2}}$), and 7.7 ($\hat{C}_{M_{\delta_e}}$). Figure 7.8 shows the elevator control inputs. The KAMS control architecture is effective on the given system, but it is not recommended as the *sole* control technique for two reasons. First, the architecture as above is only designed for regulation whereas a typical mission would require tracking a commanded flight path angle. The architecture can be easily altered to allow for tracking a step input because the

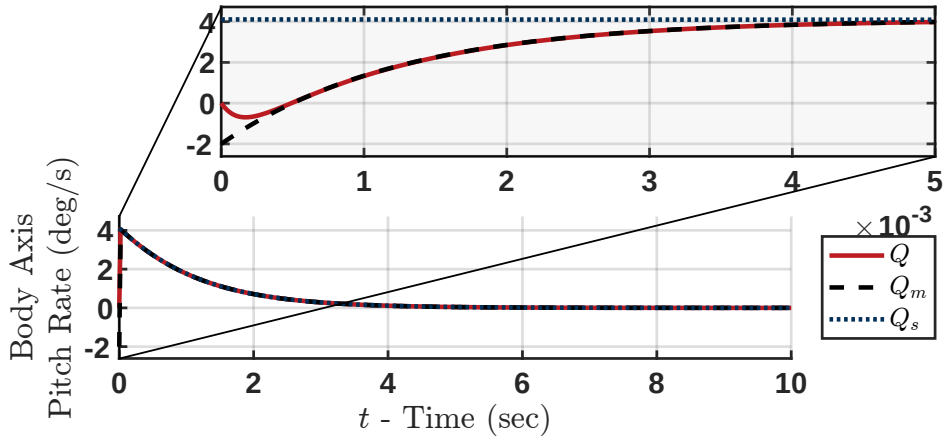

Figure 7.3: Evolution of the body axis pitch rate for a hypersonic aircraft.

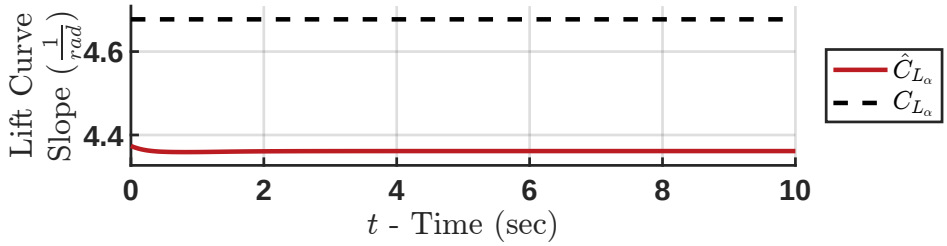

Figure 7.4: Evolution of the lift curve slope stability derivative estimate.

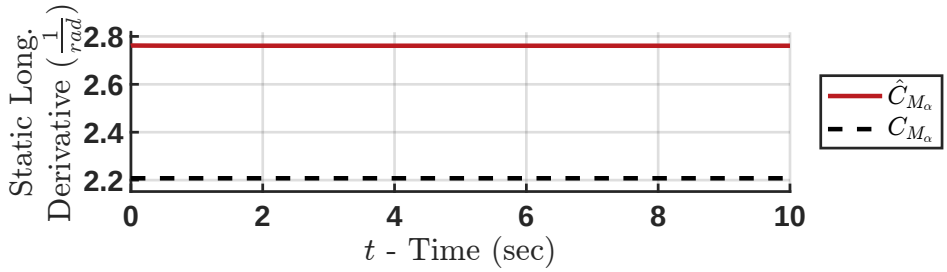

Figure 7.5: Evolution of the lift static longitudinal stability derivative estimate.

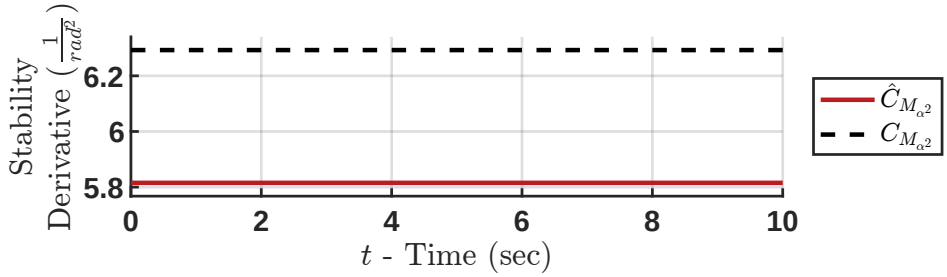

Figure 7.6: Evolution of the second order angle-of-attack stability derivative estimate.

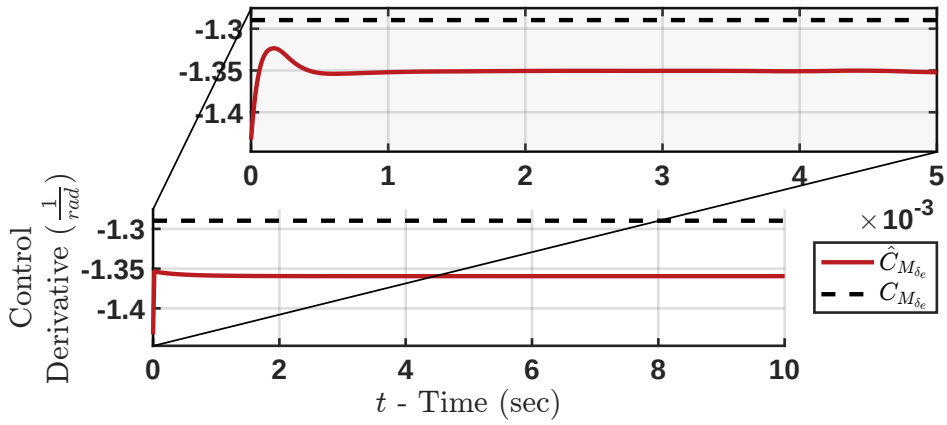

Figure 7.7: Evolution of the elevator effectiveness control derivative estimate.

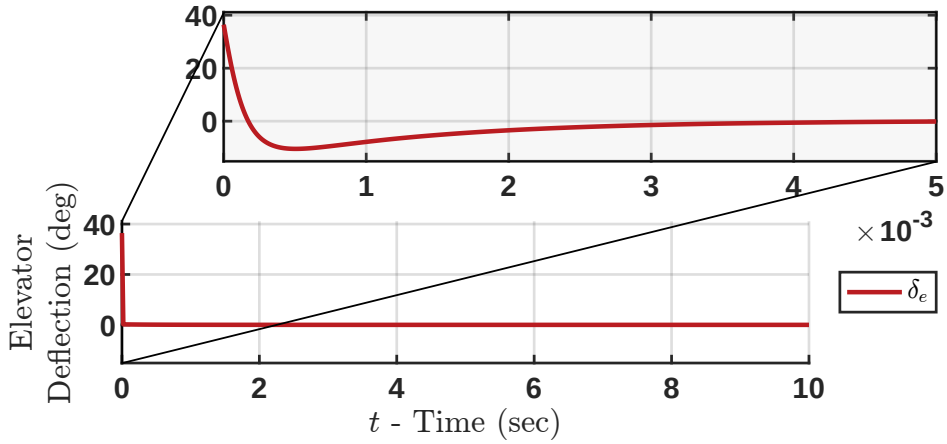

Figure 7.8: Evolution of the elevator control inputs.

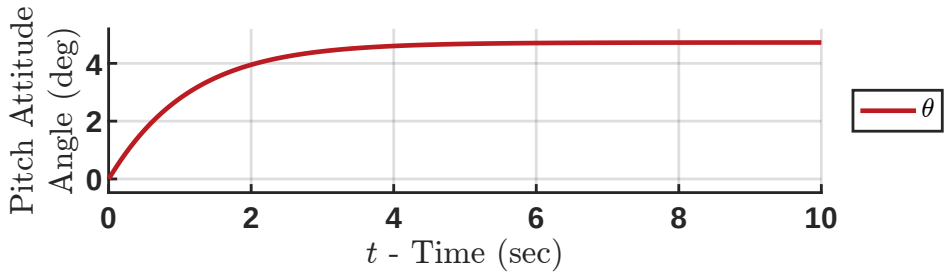

Figure 7.9: Evolution of the pitch attitude angle for a hypersonic aircraft.

only required change for this is to adjust the trim condition at a step change. Thus the control and adaptation laws would not change. However, a step input is likely to be insufficient for a complex mission. Second, as described previously the system is non-minimum phase. Famularo in [65] also encountered this problem while also attempting to prevent inlet unstart prevention with adaptive control, but it is important to note that Famularo did not consider the system timescales. Figs. 7.9 and 7.10 show the system's non-minimum phase behavior. It is a weak effect, so the external dynamics still converge but the internal dynamics diverge slowly. For these two reasons, long-term implementations of this method would be problematic. However, this method would work well as a backup control mode which is triggered when the AoA approaches or exceeds the point of concern for inlet unstart. The control in the present work is notably similar to Famularo's method, but Famularo used traditional Cascaded Control and did not account for the coupling between the subsystems. The singular perturbation analysis herein provides significant benefits. First, it provides formal proof that the sequential loop closure approach is valid. Second, it does not rely upon the rule of thumb that the inner loop is 10 times faster than the outer loop. The requirement that K be positive definite provides a precise bound on the allowed timescale separation. Numerical root-finding of the LPMs shows that KAMS is valid for all $\epsilon < 2.79 * 10^{-5}$. This limit is influenced by the adaptation gains (see Eq. (7.35)).

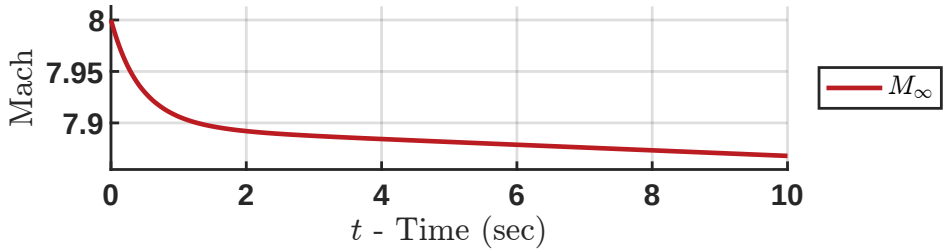

Figure 7.10: Evolution of the vehicle's Mach number.

7.4 Chapter Summary

This chapter presented a control architecture for the longitudinal dynamics of a hypersonic aircraft that accounts for the timescale behavior. First, a nonlinear multiple-timescale model was derived and used to design control and adaptation laws using the KAMS method. Adaptive Nonlinear Dynamic Inversion was used to regulate the reduced subsystems and Sequential Control was used to fuse the control signals for the reduced subsystems. A numerical example was proven to be asymptotically stable about the origin and simulated results supported the proof. Based upon the results presented in this chapter it is concluded that

1. KAMS is a good method of inlet unstart prevention for hypersonic aircraft. It is asymptotically stable and robust to weak non-minimum phase behavior in the subsystems. KAMS was shown to provide significant benefits over traditional methods. For example, unlike sequential loop closure, it provides a precise bound on the allowed timescale separation.

2. KAMS is effective for systems that require adaptive control in both subsystems. Prior work only considered adaptive control in one of the two subsystems. This validates the versatility of KAMS.

8. CONCLUSIONS

This dissertation introduced a novel method of adaptive control for multiple-timescale systems. This method is called [K]control of Adaptive Multiple-Timescale Systems (KAMS). KAMS begins with the first principles of adaptive control and multiple-timescale control and builds them up together. The general premise of KAMS is to separate the system into a fast and slow subsystem using singular perturbation theory, to use adaptive control to stabilize the reduced subsystems, and to use multiple-timescale control to fuse the separate control signals. KAMS can be used to extend adaptive control to non-minimum phase systems even though many adaptive control methods assume the system is the minimum phase. KAMS was compared to two other methods of adaptive control for multiple-timescale systems called Full-Order Adaptive Control (FOAC) and Reduced-Order Adaptive Control (ROAC). KAMS was demonstrated on quadrotor attitude stabilization, fuel-efficient orbital transfer maneuvers, and inlet unstart prevention for hypersonic aircraft. The results presented in this dissertation lead to the following conclusions:

1. KAMS is an effective and useful method of adaptive control for multiple-timescale systems. The work in this dissertation proved sufficient conditions for asymptotic stability and analytical results were validated using several numerical examples with practical significance. This is an improvement over prior work as it extends adaptive control to singularly perturbed systems and it extends multiple-timescale control to systems with model uncertainty.

2. The methodology and theorems proved in this dissertation are generalized to a wide class of plants. The plants used for demonstration in this dissertation included both linear and nonlinear; large and small timescale separation; Single-Input Single-Output (SISO) and Multiple-Input Multiple-Output (MIMO); and with and without the singular perturbation parameter appearing on the right-hand side of the fast states' equations of motion. In this dissertation, KAMS was demonstrated with Model Reference Adaptive Control (MRAC) and Adaptive Nonlinear Dynamic Inversion (ANDI). KAMS was also demonstrated with

Composite Control, Sequential Control, and Simultaneous Slow and Fast Tracking fusion techniques. The theorems in this dissertation are generalized to a wide class of adaptive algorithms and multiple-timescale fusion techniques. This collectively demonstrates the flexibility of KAMS and the generalized nature of the theorems proved in this dissertation.

3. KAMS provides insights into the underlying physics of the system in question. These insights are typically difficult to see in complex coupled models but become clear after the model reduction. For example, in Chapter 6 one term was eliminated from the equations of motion because the timescale analysis indicated it was insignificant. KAMS then uses these insights to work with the timescales of the system instead of fighting them. For example, this leads to fuel efficiency gains in Chapter 6.

4. In the context of uncertain multiple-timescale systems, KAMS is judged to be a better approach than FOAC, ROAC, and Composite Control. KAMS demonstrated better performance (i.e. rise time and overshoot) and improved robustness to variations in the timescale separation parameter. If the plant is deterministic or the timescale separation is negligible, then these other methods may yield similar results without requiring the additional step of checking the sufficient conditions. However, if the plant is uncertain and exhibits multiple-timescale behavior then KAMS is a good option compared to prior work.

5. KAMS is capable of extending common adaptive control methods to non-minimum phase systems even though these methods assume that the plant is minimum phase. This is because KAMS transfers the minimum phase requirement to the subsystems rather than the full-order system. If the external dynamics and internal dynamics evolve on a different timescale then these adaptive algorithms can still be used within the framework of KAMS. This capability was demonstrated in Chapter 3.

9. RECOMMENDATIONS

The work presented in this dissertation represents a significant step forward toward adaptive control for multiple-timescale systems. However, this is a new research field with many open questions for future research. The following list gives several recommended directions for future research:

1. This work used Lyapunov functions with quadratic first derivatives. However, this necessarily limits the theories to system and control which are capable of asymptotic stability. In this dissertation, additional theoretical tools [118] were used to show boundedness, but more general results may be available by considering more exotic Lyapunov functions. For example, Lyapunov functions with negative semidefinite time derivatives could be considered. Another option would be to consider Lyapunov functions of the type used in [20] by replacing the 2-norms with unspecified functions of the state variables. It is recommended that these possibilities be explored.

2. This work made no assumptions about the manifold for the fast adapting parameters. This was done because consistent with adaptive control generally, there are no guarantees that the fast adapting parameters converge to their true values. However, it is recommended that future work consider what would happen if their manifold was identified or specified. The manifold could be assumed to be the true value. This would create additional error terms in the full-order Lyapunov analysis, but it might also lead to additional cancellations as is seen in Model Reference Adaptive Control. It would also be interesting to study what would happen if the manifold for the fast adapting parameters was assigned to be some value that was beneficial for the slow subsystem. So the adapting parameters could transition between a value that was ideal for the fast subsystem and a value that is ideal for the slow subsystem. This would be an extension of KAMS with Sequential Control fusion.

3. In Chapter 2, an unconventional third feedback loop was identified. This was pointed out

to motivate the complexities inherent in multiple-timescale adaptive control, but it is recommended that future work study this phenomenon. It would be particularly interesting to determine if this unconventional feedback loop is parasitic or symbiotic to the other two primary feedback loops and the overall stability of the system.

4. This dissertation focused on nonlinear systems. More powerful results may be possible for linear systems. For example, see remark 5.1. It is therefore recommended that future work give particular attention to linear systems.

5. This dissertation did not consider estimation or output feedback. It is recommended that both of these be considered within the context of multiple-timescale adaptive control.

6. The analytical analysis and numerical demonstrations presented in this dissertation are promising. However, the ultimate test of any control algorithm is hardware experimentation. It is therefore recommended that future work include hardware demonstrations of KAMS. A good testbed for this would be to extend the quadrotor work given in Chapter 5.

REFERENCES

[1] A. Tavasoli, M. Eghtesad, and H. Jafarian, "Two-time scale control and observer design for trajectory tracking of two cooperating robot manipulators moving a flexible beam," *Robotics and Autonomous Systems*, vol. 57, no. 2, pp. 212–221, 2009. DOI: 10.1016/j.robot.2008.04.003.

[2] P. W. Sauer, "Time-scale features and their applications in electric power systems dynamic modeling and analysis," in *American Control Conference*. Institute of Electrical and Electronics Engineers, June 2011, pp. 4155–4159. DOI: 10.1109/ACC.2011.5991375.

[3] B. Mélykúti, J. ao P. Hespanha, and M. Khammash, "Equilibrium distributions of simple biochemical reaction systems for time scale separation in stochastic reaction networks," *Journal of the Royal Society Interface **11**: 20140054*, vol. 11, no. 97, 2014. DOI: 10.1098/rsif.2014.0054.

[4] H. M. Soner, "Singular perturbations in manufacturing," *Society for Industrial and Applied Mathematics Journal of Control and Optimization*, vol. 31, no. 1, pp. 132–146, 1993. DOI: 10.1137/0331010.

[5] M. A. Al-Radhawi, M. Sadeghi, , and E. D. Sontag, "Long-term regulation of prolonged epidemic outbreaks in large populations via adaptive control: A singular perturbation approach," *Control System Letters*, vol. 6, pp. 578–583, May 2021. DOI: 10.1109/LCSYS.2021.3083983.

[6] H. K. Khalil and F.-C. Chen, "Two-time-scale longitudinal conrol of airplanes using singular perturbation," *Journal of Guidance, Control, and Dynamics*, vol. 13, no. 6, pp. 952–960, 1990. DOI: 10.2514/3.20566.

[7] W. Ren, B. Jiang, and H. Yang, "Singular perturbation-based fault-tolerant control of the air-breathing hypersonic vehicle," *Transactions on Mechatronics*, vol. 24, no. 6, pp. 2562–2571, Dec 2019. DOI: 10.1109/TMECH.2019.2946645.

[8] D. Saha and J. Valasek, "Nonlinear multiple-time-scale attitude control of a rigid spacecraft with uncertain inertias," in *SciTech Forum*. American Institute of Aeronautics and Astronautics, 2019, pp. 1–20. DOI: 10.2514/6.2019-0932.

[9] A. Narang-Siddarth and J. Valasek, *Nonlinear Multiple Time Scale Systems in Standard and Non-Standard Forms: Analysis & Control*, 1st ed. Society for Industrial and Applied Mathematics, 2014. DOI: 10.1137/1.9781611973341.

[10] Z. Zhou, H. Wang, Z. Hu, Y. Wang, and H. Wang, "A multi-time-scale finite time controller for the quadrotor uavs with uncertainties," *Journal of Intelligent & Robotic Systems*, vol. 94, pp. 521–533, 2019. DOI: 10.1007/s10846-018-0837-1.

[11] M. D. Ardema and N. Rajan, "Separation of time scales in aircraft trajectory optimization," *Journal of Guidance, Control, and Dynamics*, vol. 8, no. 2, pp. 275–278, 1985. DOI: 10.2514/3.19972.

[12] D. S. Naidu and A. J. Calise, "Singular perturbations and time scales in guidance and control of aerospace systems: A survey," *Journal of Guidance, Control, and Dynamics*, vol. 24, no. 6, pp. 1057–1078, December 2001. DOI: 10.2514/2.4830.

[13] H. J. Wilson and J. M. Rallison, "Regular perturbation," 1997. [Online]. Available: https://www.ucl.ac.uk/~ucahhwi/LTCC/section2-3-perturb-regular.pdf

[14] N. Fenichel, "Geometric singular perturbation theory for ordinary differential equations," *Journal of Differential Equations*, vol. 31, pp. 53–98, 1979. DOI: 10.1016/0022-0396(79)90152-9.

[15] P. Kokotovic, H. K. Khalil, and J. O'Reilly, *Singular Perturbation Methods in Control Analysis and Design*, 2nd ed. Society for Industrial and Applied Mathematics, 1999.

[16] A. Narang-Siddarth and J. Valasek, "Global tracking control structures for nonlinear singularly perturbed aircraft systems," Proceedings of the 1st CEAS Specialist Conference on Guidance, Navigation and Control (Euro GNC 2011), Munchen, Germany, 13 April 2011, 2011. DOI: 10.1007/978-3-642-19817-5.

[17] ——, "Kinetic state tracking for a class of singularly perturbed systems," *Journal of Guidance, Control, and Dynamics*, vol. 34, no. 3, pp. 734–749, 2011. DOI: 10.2514/1.52127.

[18] H. K. Khalil, *Nonlinear Systems*, 3rd ed. Prentice Hall, 2002.

[19] A. Saberi and H. Khalil, "Quadratic-type lyapunov functions for singularly perturbed systems," *Transactions on Automatic Control*, vol. 29, pp. 542 – 550, June 1984. DOI: 10.1109/TAC.1984.1103586.

[20] ——, "Stabilization and regulation of nonlinear singularly perturbed systems–composite control," *Transactions on Automatic Control*, vol. 30, no. 8, pp. 739–747, August 1985. DOI: 10.1109/TAC.1985.1104064.

[21] D. Saha, J. Valasek, and D. Famularo, "Output feedback control using state observers of a class of nonlinear nonstandard two-time-scale systems," *International Journal of Control*, vol. 94, no. 7, pp. 1944–1958, 2021. DOI: 10.1080/00207179.2019.1687938.

[22] D. Saha and J. Valasek, "Observer-based sequential control of a nonlinear two-time-scale spring-mass-damper system with multiple slow and fast states," *IFAC-PapersOnLine*, vol. 49, no. 18, pp. 684–689, 2016. DOI: 10.1016/j.ifacol.2016.10.245.

[23] P. Li, L. Wang, B. Zhong, and M. Zhang, "Linear active disturbance rejection control for two-mass systems via singular perturbation approach," *Transactions on Industrial Informatics*, vol. 18, no. 5, pp. 3022–3032, May 2022. DOI: 10.1109/TII.2021.3108950.

[24] P. A. Ioannou and J. Sun, *Robust Adaptive Control*. Prentice Hall, 1996.

[25] E. Lavretsky, *Robust and Adaptive Control Methods for Aerial Vehicles*. Dordrecht: Springer, 2014. DOI: 10.1007/978-90-481-9707-1.

[26] S. K. Kannan, G. V. Chowdhary, and E. N. Johnson, *Adaptive Control of Unmanned Aerial Vehicles: Theory and Flight Tests*. Dordrecht: Springer, 2014, vol. Handbook of Unmanned Aerial Vehicles. DOI: 10.1007/978-90-481-9707-1.

[27] G. Chowdhary, E. N. Johnson, R. Chandramohan, M. S. Kimbrell, and A. Calise, "Guidance and control of airplanes under actuator failures and severe structural damage," *Journal of Guidance, Control, and Dynamics*, vol. 36, no. 4, pp. 1093–1104, July 2013. DOI: 10.2514/1.58028.

[28] J. Pravitra, K. A. Ackerman, C. Cao, N. Hovakimyan, and E. A. Theodorou, "L1-adaptive mppi architecture for robust and agile control of multirotors," in *International Conference on Intelligent Robots and Systems*. Institute of Electrical and Electronics Engineers/RSJ, October 2020, pp. 7661–7666. DOI: 10.1109/IROS45743.2020.9341154.

[29] N. Sun, D. Liang, Y. Wu, Y. Chen, Y. Qin, and Y. Fang, "Adaptive control for pneumatic artificial muscle systems with parametric uncertainties and unidirectional input constraints," *Transactions on Industrial Informatics*, vol. 16, no. 2, pp. 969–979, February 2020. DOI: 10.1109/TII.2019.2923715.

[30] D. Famularo, J. Valasek, J. A. Muse, and M. A. Bolender, "Enforcing state constraints on a model of a hypersonic vehicle," in *Guidance, Navigation, and Control Conference*. American Institute of Aeronautics and Astronautics, January 2016, pp. 1–13. DOI: 10.2514/6.2016-1865.

[31] H. S. Hussain, "Robust adaptive control in the presence of unmodeled dynamics," Ph.D. dissertation, Massachusetts Institute of Technology, 2017. DOI: 1721.1/111744.

[32] E. Lavretsky, "Combined/composite model reference adaptive control," *Transactions on Automatic Control*, vol. 54, no. 11, pp. 2692–2697, November 2009. DOI: 10.1109/TAC.2009.2031580.

[33] A. J. Koshkouei and A. S. I. Zinober, "Adaptive backstepping control of nonlinear systems with unmatched uncertainty," in *Conference on Decision and Control*. Institute of Electrical and Electronics Engineers, December 2000. DOI: 10.1109/CDC.2001.914681.

[34] E. Rollins, J. Valasek, J. A. Muse, and M. A. Bolender, "Nonlinear adaptive dynamic inversion applied to a generic hypersonic vehicle," in *Guidance, Navigation, and Control (GNC)*

Conference. American Institute of Aeronautics and Astronautics, August 2013, pp. 1–24. DOI: 10.2514/6.2013-5234.

[35] N. T. Nguyen, *Model-Reference Adaptive Control A Primer*, ser. Advanced Textbooks in Control and Signal Processing. Springer, 2018. DOI: 10.1007/978-3-319-56393-0.

[36] R. H. Middleton and G. C. Goodwin, "Adaptive control of time-varying linear systems," *Transactions on Automatic Control*, vol. 33, no. 2, pp. 150–155, February 1988. DOI: 10.1109/9.382.

[37] G. Kreisselmeier, "An approach to stable indirect adaptive control," *Automatica*, vol. 21, no. 4, pp. 425–431, 1985. DOI: 10.1016/0005-1098(85)90078-0.

[38] R. M. Sanner and J.-J. E. Slotine, "Gaussian networks for direct adaptive control," in *American Control Conference*. Institute of Electrical and Electronics Engineers, June 1991. DOI: 10.23919/ACC.1991.4791778.

[39] J.-J. E. Slotine and W. Li, *Applied Nonlinear Control*. Prentice Hall, 1991.

[40] H. Moncayo, M. G. Perhinschi, B. Wilburn, J. Wilburn, and O. Karas, "Uav adaptive control laws using non-linear dynamic inversion augmented with an immunity-based mechanism," in *Guidance, Navigation, and Control Conference*. American Institute of Aeronautics and Astronautics, August 2012, pp. 1–18. DOI: 10.2514/6.2012-4678.

[41] A. A. El-samahya and M. A. Shamseldin, "Brushless dc motor tracking control using self-tuning fuzzy pid control and model reference adaptive control," *Ain Shams Engineering Journal*, vol. 9, no. 3, pp. 341–352, September 2018. DOI: 10.1016/j.asej.2016.02.004.

[42] R. R. C. adn Liu Hsu, A. K. Imai, and P. Kokotović, "Lyapunov-based adaptive control of mimo systems," *Automatica*, vol. 39, no. 7, pp. 1251–1257, July 2003. DOI: 10.1016/S0005-1098(03)00085-2.

[43] K. Shojaei, A. M. Shahri, A. Tarakameh, and B. Tabibian, "Adaptive trajectory tracking control of a differential drive wheeled mobile robot," *Robotica*, vol. 29, pp. 391–402, 2011. DOI: 10.1017/S0263574710000202.

[44] J. Yang, J. Na, and G. Gao, "Robust adaptive control for unmatched systems with guaranteed parameter estimation convergence," *International Journal of Adaptive Control and Signal Processing*, vol. 33, no. 12, pp. 1868–1884, March 2019. DOI: 10.1002/acs.2982.

[45] P. R. Kumar, "Convergence of adaptive control schemes using least-squares parameter estimates," *Transactions on Automatic Control*, vol. 35, no. 4, pp. 416–424, April 1990. DOI: 10.1109/9.52293.

[46] N. Barabanov, R. Ortega, and A. Astolfi, "Is normalization necessary for stable model reference adaptive control?" *Transactions on Automatic Control*, vol. 50, no. 9, pp. 1384–1390, September 2005. DOI: 10.1109/TAC.2005.854625.

[47] E. Lavretsky and T. E. Gibson, "Projection operator in adaptive systems," Online, 2011. [Online]. Available: https://arxiv.org/abs/1112.4232v6. DOI: 10.48550/arXiv.1112.4232.

[48] E. Lavretsky and K. A. Wise, *Robust and Adaptive Control with Aerospace Applications*, ser. Advanced Textbooks in Control and Signal Processing. London: Springer, 2013. DOI: 10.1007/978-1-4471-4396-3.

[49] N. Hovakimyan and C. Cao, *L1 Adaptive Control Theory: Guaranteed Robustness with Fast Adaptation*, ser. Advances in Design and Control. Society for Industrial and Applied Mathematics, 2010.

[50] M. D. Tandale and J. Valasek, "Fault-tolerant structured adaptive model inversion control," *Journal of Guidance, Control, and Dynamics*, vol. 29, no. 3, pp. 635–642, June 2006. DOI: 10.2514/1.15244.

[51] R. Rysdyk, B. Leonhardt, and A. Calise, "Development of an intelligent flight propulsion and control system - nonlinear adaptive control," in *Guidance, Navigation, and Control Conference and Exhibit*. Denver, Colorado: American Institute of Aeronautics and Astronautics, August 2000. DOI: 10.2514/6.2000-3943.

[52] M. Benosman, "Model-based vs data-driven adaptive control: An overview," *International Journal of Adaptive Control and Signal Processing*, vol. 32, pp. 753–776, 2018. DOI: 10.1002/acs.2862.

[53] K. Eves and J. Valasek, "Introduction to adaptive control for multiple time scale systems," in *SciTech Forum*. American Institute of Aeronautics and Astronautics, 2023, pp. 1–15. DOI: 10.2514/6.2023-1444.

[54] D. Saha, "Full-state and output feedback control of uncertain nonlinear nonstandard multiple-time-scale systems," Ph.D. dissertation, Texas A&M University, College Station, Texas, December 2018.

[55] M. J. Balas, "Feedback control of flexible systems," *Transactions on Automatic Control*, vol. 23, no. 4, pp. 673–679, August 1978. DOI: 10.1109/TAC.1978.1101798.

[56] ——, "Enhanced modal control of flexible structures via innovations feedthrough," *International Journal of Control*, vol. 32, no. 6, pp. 983–1003, 1980. DOI: 10.1080/00207178008922903.

[57] A. M. Wahdan and A. Y. Tawfik, "Periodic resetting-mrac in control of a high-speed aircraft," in *International Conference on Control and Applications*. Institute of Electrical and Electronics Engineers, August 1994. DOI: 10.1109/CCA.1994.381352.

[58] C. Rohrs, L. Valavani, M. Athans, and G. Stein, "Robustness of continuous-time adaptive control algorithms in the presence of unmodeled dynamics," *Transactions on Automatic Control*, vol. 30, no. 9, pp. 881–889, September 1985. DOI: 10.1109/TAC.1985.1104070.

[59] C. E. Rohrs, L. Valavani, M. Athans, and G. Stein, "Robustness of adaptive control algorithms in the presence of unmodeled dynamics," in *Conference on Decision and Control*. Institute of Electrical and Electronics Engineers, Dec 1982, pp. 3–11. DOI: 10.1109/CDC.1982.268392.

[60] K. Astrom, "A commentary on the C.E. Rohrs et al. paper 'robustness of continuous-time adaptive control algorithms in the presence of unmodeled dynamics'," *Transactions on Automatic Control*, vol. 30, no. 9, pp. 889–889, Sep. 1985. DOI: 10.1109/TAC.1985.1104066.

[61] H. S. Hussain, A. M. Annaswamy, and E. Lavretsky, "Robust adaptive control in the presence of unmodeled dynamics: A counter to rohrs's counterexample," in *Guidance, Navigation, and Control (GNC) Conference*. American Institute of Aeronautics and Astronautics, 2013. DOI: 10.2514/6.2013-4753.

[62] B. C. Gruenwald, T. Yucelen, and J. A. Muse, "Model reference adaptive control in the presence of actuator dynamics with applications to the input time-delay problem," in *Guidance, Navigation, and Control Conference*. American Institute of Aeronautics and Astronautics, 2017, pp. 1–10. DOI: 10.2514/6.2017-1491.

[63] R. W. Beard, T. W. McLain, and C. Peterson, *Introduction to Feedback Control*. Independently Published, 2020. [Online]. Available: https://github.com/randybeard/controlbook_public

[64] E. Rollins, "Nonlinear adaptive dynamic inversion control for hypersonic vehicles," Ph.D. dissertation, Texas A&M University, College Station Texas, December 2013. DOI: 1969.1/151679.

[65] D. Famularo, "Observer-based nonlinear dynamic inversion adaptive control with state constraints," Ph.D. dissertation, Texas A&M University, 701 H. R. Bright Building, College Station, TX 77843, September 2017. DOI: 1969.1/169595.

[66] D. Famularo, J. Valasek, J. A. Muse, and M. A. Bolender, "Adaptive control of hypersonic vehicles using observer-based nonlinear dynamic inversion," in *SciTech Forum*. American Institute of Aeronautics and Astronautics, 2018, pp. 1–24. DOI: 10.2514/6.2018-0843.

[67] D. Famularo and J. Valasek, "A sampled-data approach to nonlinear dynamic inversion adaptive control," in *SciTech Forum*. American Institute of Aeronautics and Astronautics, 2018, pp. 1–17. DOI: 10.2514/6.2018-1131.

[68] A. N. Tikhonov, "On the dependence of the solutions of differential equations on a small parameter," *Matematicheskii Sbornik Novaya Seriya*, vol. 22, pp. 193–204, 1948. [Online]. Available: http://www.mathnet.ru/php/archive.phtml?wshow=paper&jrnid=sm&paperid=6075&option_lang=eng

[69] A. B. Vasil'eva, "Asymptotic behaviour of solutions to certain problems involving nonlinear differential equations containing a small parameter multiplying the highest derivatives," *Uspekhi Matematicheskikh Nauk*, vol. 18, no. 3, pp. 15–86, 1963. [Online]. Available: http://www.mathnet.ru/php/archive.phtml?wshow=paper&jrnid=rm&paperid=6350&option_lang=eng

[70] A. Macchelli, D. Barchi, L. Marconi, and G. Bosi, "Robust adaptive control of a hydraulic press," in *International Federation of Automatic Control World Congress*, vol. 53. International Federation of Automatic Control, July 2020, pp. 8790–8795. DOI: 10.1016/j.ifacol.2020.12.1384.

[71] N. Nguyen, K. Krishnakumar, and J. Boskovic, "An optimal control modification to model-reference adaptive control for fast adaptation," in *Guidance, Navigation and Control Conference and Exhibit*. American Institute of Aeronautics and Astronautics, August 2008, pp. 1–20. DOI: 10.2514/6.2008-7283.

[72] N. Nguyen, A. Ishihara, V. Stepanyan, and J. Boskovic, "Optimal control modification for robust adaptation of singularly perturbed systems with slow actuators," in *Guidance, Navigation, and Control Conference and Exhibit*. American Institute of Aeronautics and Astronautics, August 2009, pp. 1–21. DOI: 10.2514/6.2009-5615.

[73] N. Hovakimyan, E. Lavretsky, and A. Sasane, "Dynamic inversion for nonaffine-in-control systems via time-scale separation. part i," *Journal of Dynamical and Control Systems*, vol. 13, no. 4, pp. 451–465, October 2007. DOI: 10.1007/s10883-007-9029-1.

[74] E. Lavretsky and N. Hovakimyan, "Adaptive dynamic inversion for nonaffine-in-control uncertain systems via time-scale separation. part ii," *Journal of Dynamical and Control*

Systems, vol. 14, no. 1, pp. 33–41, January 2008. DOI: 10.1007/s10883-007-9033-5.

[75] N. Hovakimyan, E. Lavretsky, and C. Cao, "Dynamic inversion for multivariable non-affine-in- control systems via time-scale separation," *International Journal of Control*, vol. 81, no. 12, pp. 1960–1967, December 2008. DOI: 10.1080/00207170801961295.

[76] ——, "Adaptive dynamic inversion via time-scale separation," *Transactions on Neural Networks*, vol. 19, no. 10, pp. 1702–1711, October 2008. DOI: 10.1109/TNN.2008.2001221.

[77] S. Sastry and M. Bodson, *Adaptive Control: Stability, Convergence, and Robustness*, ser. Prentice Hall Informationn and System Sciences Series. Englewood Cliffs, New Jersey 07632: Prentice Hall, 1989.

[78] J. Deese and C. Vermillion, "Real-time experimental optimization of closed-loop crosswind flight of airborne wind energy systems via recursive gaussian process-based adaptive control," in *Conference on Control Technology and Applications (CCTA)*. Institute of Electrical and Electronics Engineers, August 2020. DOI: 10.1109/CCTA41146.2020.9206305.

[79] T. Sun, X. Zhang, H. Yang, and Y. Pan, "Singular perturbation-based saturated adaptive control for underactuated euler–lagrange systems," *International Society of Automation Transactions*, vol. 119, pp. 74–80, 2022. DOI: 10.1016/j.isatra.2021.02.036.

[80] M. M. Rayguru, B. Ramalingam, and M. R. Elara, "A singular perturbation based adaptive strategy for bounded controller design in feedback linearizable systems," *International Journal of Adaptive Control and Signal Processing*, vol. 36, no. 2, pp. 264–281, February 2021. DOI: 10.1002/acs.3360.

[81] Y. Yang, L. Tang, W. Zou, and D.-W. Ding, "Robust adaptive control of uncertain nonlinear systems with unmodeled dynamics using command filter," *International Journal of Robust and Nonlinear Control*, vol. 31, pp. 7746–7784, July 2021. DOI: 10.1002/rnc.5717.

[82] P. Krishnamurthy and F. Khorrami, "A singular perturbation based global dynamic high gain scaling control design for systems with nonlinear input uncertainties," *Transactions on Automatic Control*, vol. 58, no. 10, pp. 2686–2692, 2013. DOI: 10.1109/TAC.2013.2257968.

[83] M. Asadi and A. Khayatiyan, "Singular perturbation theory in control of nonlinear systems with uncertainties," in *Iranian Conference on Electrical Engineering*. Institute of Electrical and Electronics Engineers, May 2016, pp. 1908–1912. DOI: 10.1109/IranianCEE.2016.7585833.

[84] A. Chakrabortty and M. Arcak, "Time-scale separation redesign for stabilization and performance recovery for uncertain nonlinear systems," *Automatica*, vol. 45, pp. 34–44, 2009. DOI: 10.1016/j.automatica.2008.06.004.

[85] K. J. Astrom and B. Wittenmark, "On self tuning regulators," *Automatica*, vol. 9, pp. 185–199, 1973. DOI: 10.1016/0005-1098(73)90073-3.

[86] D. Saha and J. Valasek, "Observer-based sequential control of a nonlinear two-time-scale spring-mass-damper system," in *Guidance, Navigation, and Control Conference*. American Institute of Aeronautics and Astronautics, January 2016. DOI: 10.2514/6.2016-0361.

[87] C. Jing, H. Xu, and J. Jiang, "Practical torque tracking control of electro-hydraulic load simulator using singular perturbation theory," *International Society of Automation Transactions*, vol. 102, pp. 304–313, 2020. DOI: 10.1016/j.isatra.2020.02.035.

[88] P. A. Ioannou and P. Kokotovic, "Decentralized adaptive control of interconnected systems with reduced-order models," *Automatica*, vol. 21, no. 4, pp. 401–412, 1985. DOI: 10.1016/0005-1098(85)90076-7.

[89] L. Li and F. C. Sun, "An adaptive tracking controller design for non-linear singularly perturbed systems using fuzzy singularly perturbed model," *Journal of Mathematical Control and Information*, vol. 26, pp. 395–415, 2009. DOI: 10.1093/imamci/dnp020.

[90] D. Saha and J. Valasek, "Two-time-scale slow and fast state tracking of an f-16 using slow and fast controls," in *Guidance, Navigation, and Control Conference*. American Institute of Aeronautics and Astronautics, 2017, pp. 1–17. DOI: 10.2514/6.2017-1256.

[91] D. Saha, J. Valasek, C. Leshikar, and M. M. Reza, "Multiple-timescale nonlinear control of aircraft with model uncertainties," *Journal of Guidance, Control, and Dynamics*, vol. 43, no. 3, pp. 536–552, 2020. DOI: 10.2514/1.G004303.

[92] D. Saha, J. Valasek, and M. M. Reza, "Two-time-scale control of a low-order nonlinear, nonstandard system with uncertain dynamics," in *Annual American Control Conference*. Institute of Electrical and Electronics Engineers, 2018, pp. 3720–3725. DOI: 10.23919/ACC.2018.8431384.

[93] A. H. Nayfeh, *Perturbation Methods*. Wiley Verlag Chemie, 1973.

[94] A. Isidori, *Nonlinear Control Systems*. London: Springer, 1995. DOI: 10.1007/978-1-84628-615-5.

[95] G. T. Gilbert, "Positive definite matrices and Sylvester's criterion," *American Mathematical Monthly*, vol. 98, pp. 44–46, January 1991. DOI: 10.2307/2324036.

[96] K. Eves and J. Valasek, "Adaptive control for non-minimum phase systems via time scale separation," in *American Control Conference*. Institute of Electrical and Electronics Engineers, 2023, pp. 1–6.

[97] G. C. Goodwin and K. S. Sin, "Adaptive control of nonminimum phase systems," *Transactions on Automatic Control*, vol. 26, no. 2, pp. 478–483, 1981. DOI: 10.1109/TAC.1981.1102610.

[98] R. M. Johnstone, S. L. Shah, and D. G. Fisher, "An extension of hyperstable adaptive control to non-minimum phase systems," *International Journal of Control*, vol. 31, no. 3, pp. 539–545, 1980. DOI: 10.1080/00207178008961059.

[99] I. Barkana, "Classical and simple adaptive control for nonminimum phase autopilot design," *Journal of Guidance, Control, and Dynamics*, vol. 28, no. 4, pp. 631–638, 2005. DOI: 10.2514/1.9542.

[100] M. Makoudi and L. Radouane, "A robust model reference adaptive control for non-minimum phase systems with unknown or time-varying delay," *Automatica*, vol. 36, no. 7, pp. 1057–1065, 2000. DOI: 10.1016/S0005-1098(99)00223-X.

[101] D. A. Suarez and R. Lozano, "Adaptive control of nonminimum phase systems subject to unknown bounded disturbances," *Transactions on Automatic Control*, vol. 41, no. 12, pp. 1830–1836, 1996. DOI: 10.1109/9.545752.

[102] M. C. Campi, "Adaptive control of non-minimum phase systems," *International Journal of Adaptive Control and Signal Processing*, vol. 9, no. 2, pp. 137–149, 1995. DOI: 10.1002/acs.4480090203.

[103] M. A. Hersh and M. B. Zarrop, "Stochastic adaptive control of non-minimum phase systems," *Optimal Control Applications and Methods*, vol. 7, no. 2, pp. 153–161, 1986. DOI: 10.1002/oca.4660070205.

[104] L. Praly, S. T. Hung, and D. S. Rhode, "Towards a direct adaptive scheme for a discrete-time control of a minimum phase continuous-time system," in *Conference on Decision and Control*. Institute of Electrical and Electronics Engineers, 1985. DOI: 10.1109/CDC.1985.268690.

[105] J. B. Hoagg and D. S. Bernstein, "Retrospective cost model reference adaptive control for nonminimum-phase systems," *Journal of Guidance, Control, and Dynamics*, vol. 35, no. 6, pp. 1767–1786, 2012. DOI: 10.2514/1.57001.

[106] S. Dai, Z. Ren, and D. S. Bernstein, "Adaptive control of nonminimum-phase systems using shifted laurent series," *International Journal of Control*, vol. 90, no. 3, pp. 407–427, 2017. DOI: 10.1080/00207179.2016.1183173.

[107] D. W. Clarke, "Self-tuning control of nonminimum-phase systems," *Automatica*, vol. 20, no. 5, pp. 501–517, 1984. DOI: 10.1016/0005-1098(84)90003-7.

[108] S. Ganguli, A. Marcos, and G. Balas, "Reconfigurable lpv control design for boeing 747-100/200 longitudinal axis," in *American Control Conference*. Institute of Electrical and Electronics Engineers, 2002, pp. 3612–3617. DOI: 10.1109/ACC.2002.1024489.

[109] R. W. Beard and T. W. McLain, *Small Unmanned Aircraft Theory and Practice*, 2nd ed. Princeton University Press, 2019.

[110] J. Roskam, *Airplane Flight Dynamics and Automatic Flight Controls*. Design, Analysis, and Research Corporation, 1995, vol. 1.

[111] C. R. Hanke and D. R. Nordwall, "The simulation of a jumbo jet transport aircraft voume ii: Modeling data," The Boeing Company for NASA, Tech. Rep., 1970. [Online]. Available: https://ntrs.nasa.gov/citations/19730001300

[112] D. van Wijk, K. Eves, and J. Valasek, "Deep reinforcement learning controller for autonomous tracking of evasive ground target," in *SciTech Forum*. American Institute of Aeronautics and Astronautics, 2023, pp. 1–12. DOI: 10.2514/6.2023-0128.

[113] D. C. Schedl, I. Kurmi, and O. Bimber, "An autonomous drone for search and rescue in forests using airborne optical sectioning," *Science Robotics*, vol. 6, no. 55, p. eabg1188, 2021. DOI: 10.1126/scirobotics.abg1188.

[114] "Aerial and ground camera systems," Nov 2021. [Online]. Available: https://theaerialfilmingcompany.com/cinematography/

[115] "Arducopter," Online, 2023. [Online]. Available: https://ardupilot.org/copter/index.html

[116] C. Leshikar, K. Eves, N. Ninan, and J. Valasek, "Asymmetric quadrotor modeling and state-space system identification," in *International Conference on Unmanned Aircraft Systems (ICUAS)*. Institute of Electrical and Electronics Engineers, 2021, pp. 1422–1431. DOI: 10.1109/ICUAS51884.2021.9476871.

[117] G. P. Syrcos and P. Sannuti, "Singular perturbation modelling of continuous and discrete physical systems," *International Journal of Control*, vol. 37, no. 5, pp. 1007–1022, 1983. DOI: 10.1080/00207178308933025.

[118] Y. N. Raffoul, "Boundedness in nonlinear differential equations," Online, 1991. [Online]. Available: https://academic.udayton.edu/youssefraffoul/pdf/ExponentialBoundedness.pdf

[119] *FlameWheel 450 User Manual*, Da-Jiang Innovations, 2015.

[120] T. F. Dawn, J. Gutkowski, A. Batcha, J. Williams, and S. Pedrotty, "Trajectory design considerations for exploration mission 1," in *SciTech Forum*. American Institute of Aeronautics and Astronautics, 2018, pp. 1–14. DOI: 10.2514/6.2018-0968.

[121] M. M. Guelman and A. Shiryaev, "Closed-loop orbit transfer using solar electric propulsion," *Journal of Guidance, Control, and Dynamics*, vol. 39, no. 11, pp. 2563–2569, 2016. DOI: 10.2514/1.G000395.

[122] C. Han, Y. Wang, H. Chen, X. Sun, Y. Sun, and J. Li, "Practical low-thrust geostationary orbit transfer guidance via linearized state equations," *Journal of Guidance, Control, and Dynamics*, vol. 43, no. 3, pp. 620–627, 2020. DOI: 10.2514/1.G004692.

[123] W. E. Wiesel and S. Alfano, "Optimal many-revolution orbit transfer," *Journal of Guidance, Control, and Dynamics*, vol. 8, no. 1, pp. 155–157, 1985. DOI: 10.2514/3.19952.

[124] J. A. Kechichian, "Optimal low-earth-orbit-geostationary-earth-orbit intermediate acceleration orbit transfer," *Journal of Guidance, Control, and Dynamics*, vol. 20, no. 4, pp. 803–811, 1997. DOI: 10.2514/2.4116.

[125] M. Avendaño, V. Martín-Molina, J. Martín-Morales, and J. Ortigas-Galindo, "Algebraic approach to the minimum-cost multi-impulse orbit-transfer problem," *Journal of Guidance, Control, and Dynamics*, vol. 39, no. 8, pp. 1734–1743, 2016. DOI: 10.2514/1.G001598.

[126] J. Palmore, "An elementary proof of the optimality of hohmann transfers," *Journal of Guidance, Control, and Dynamics*, vol. 7, no. 5, pp. 629–630, 1984. DOI: 10.2514/3.56375.

[127] J. E. Prussing, "Simple proof of the global optimality of the hohmann transfer," *Journal of Guidance, Control, and Dynamics*, vol. 15, no. 4, pp. 1037–1038, 1992. DOI: 10.2514/3.20941.

[128] F. Yuan and K. Matsushima, "Strong hohmann transfer theorem," *Journal of Guidance, Control, and Dynamics*, vol. 18, no. 2, pp. 371–373, 1995. DOI: 10.2514/3.21394.

[129] R. Zhong and Z. H. Zhu, "Timescale separate optimal control of tethered space-tug systems for space-debris removal," *Journal of Guidance, Control, and Dynamics*, vol. 39, no. 11, pp. 2540–2545, 2016. DOI: 10.2514/1.G001867.

[130] P. Williams, "Optimal control of electrodynamic tether orbit transfers using timescale separation," *Journal of Guidance, Control, and Dynamics*, vol. 33, no. 1, pp. 88–98, 2010. DOI: 10.2514/1.45250.

[131] O. P. n. Muñoa and D. J. Scheeres, "Perturbation theory for hamilton's principal function," *Journal of Guidance, Control, and Dynamics*, vol. 34, no. 4, pp. 1129–1142, 2011. DOI: 10.2514/1.51524.

[132] C. N. McGrath and M. Macdonald, "General perturbation method for satellite constellation reconfiguration using low-thrust maneuvers," *Journal of Guidance, Control, and Dynamics*, vol. 42, no. 8, pp. 1676–1692, 2019. DOI: 10.2514/1.G003739.

[133] Y. Ma, G. Tao, B. Jiang, and Y. Cheng, "Multiple-model adaptive control for spacecraft under sign errors in actuator response," *Journal of Guidance, Control, and Dynamics*, vol. 39, no. 3, pp. 628–641, 2016. DOI: 10.2514/1.G001352.

[134] C. R. McInnes, "Direct adaptive control for gravity-turn descent," *Journal of Guidance, Control, and Dynamics*, vol. 22, no. 2, pp. 373–375, 1999. DOI: 10.2514/2.4392.

[135] J. L. Junkins, M. R. Akella, and R. D. Robinett, "Nonlinear adaptive control of spacecraft maneuvers," *Journal of Guidance, Control, and Dynamics*, vol. 20, no. 6, pp. 1104–1110, 1997. DOI: 10.2514/2.4192.

[136] P. M. Gerhart, A. L. Gerhart, and J. I. Hochstein, *Munson, Young, and Okiishi's Fundamentals of Fluid Mechanics*, 8th ed. John Wiley & Sons, 1990.

[137] A. C. Idris, M. R. Saad, H. Zare-Behtash, and K. Kontis, "Luminescent measurement systems for the investigation of a scramjet inlet-isolator," *Sensors*, vol. 14, no. 4, pp. 6606–6632, 2014. DOI: 10.3390/s140406606.

[138] J. Chang, N. Li, K. Xu, W. Bao, and D. Yu, "Recent research progress on unstart mechanism, detection and control of hypersonic inlet," *Progress in Aerospace Sciences*, vol. 89, pp. 1–122, 2017. DOI: 10.1016/j.paerosci.2016.12.001.

[139] M. Kuipers, M. Mirmirani, P. Ioannou, and Y. Huo, "Adaptive control of an aeroelastic airbreathing hypersonic cruise vehicle," in *Guidance, Navigation, and Control Conference*. American Institute of Aeronautics and Astronautics, 2007, pp. 1–12. DOI: 10.2514/2.4714.

[140] E. Mooij, "Numerical investigation of model reference adaptive control for hypersonic aircraft," *Journal of Guidance, Control, and Dynamics*, vol. 24, no. 2, pp. 315–323, 2001. DOI: 10.2514/2.4714.

[141] S. Banerjee, Z. Wang, B. Baur, F. Holzapfel, J. Che, and C. Cao, "L1 adaptive control augmentation for the longitudinal dynamics of a hypersonic glider," *Journal of Guidance, Control, and Dynamics*, vol. 39, no. 2, pp. 275–291, 2016. DOI: 10.2514/1.G001113.

[142] J. T. Parker, A. Serrani, S. Yurkovich, M. A. Bolender, and D. B. Doman, "Control-oriented modeling of an air-breathing hypersonic vehicle," *Journal of Guidance, Control, and Dynamics*, vol. 30, no. 3, pp. 856–869, 2007. DOI: 10.2514/1.27830.

[143] D. Schmidt, *Modern Flight Dynamics*, 1st ed. McGraw Hill, 20121.

[144] J. Hauser, S. Sastry, and G. Meyer, "Nonlinear control design for slightly non- minimum phase systems: Application to v/stol aircraft," *Automatica*, vol. 28, no. 4, pp. 665–679, 1992. DOI: 10.1016/0005-1098(92)90029-F.

APPENDIX A

PROOF OF LEMMAS *

A.1 Lemma 1

Lemma A.1 - *Given* $\acute{V}(t) : \mathbb{R}_{\geq 0} \to \mathbb{R}_{-}$, $\boldsymbol{x}(t) : \mathbb{R}_{\geq 0} \to \mathbb{R}^n$, *and* $\alpha \in \mathbb{R}_{+}$ *where* $\acute{V} \in L_1$ *and* $\boldsymbol{x} \in L_\infty$. *Then* $\forall p \in [1, \infty)$ *it is true that* $\acute{V} \leq -\alpha|\boldsymbol{x}|_p^p \implies \boldsymbol{x} \in L_p$

Proof. Begin with $\acute{V} \leq -\alpha|\boldsymbol{x}|_p^p$. The value $|\boldsymbol{x}|_p$ exists and is finite because $\boldsymbol{x} \in L_\infty \implies \boldsymbol{x} \in l_p$ for all p and t. Because both sides of the inequality are negative the following inequality also holds

$$\|\acute{V}\|_1 \geq \|\alpha|\boldsymbol{x}|_p^p\|_1 \tag{A.1}$$

$\|\acute{V}\|_1/\alpha$ exists and is finite because $\acute{V} \in L_1$. By Lemma A.2 $\boldsymbol{x} \in L_p$. □

A.2 Lemma 2

Lemma A.2 - *Let* $\boldsymbol{x}(t) : \mathbb{R}_{\geq 0} \to \mathbb{R}^n$. *Then* $\forall p \in [1, \infty)$ *it is true that* $\boldsymbol{x} \in L_p$ *if and only if* $|\boldsymbol{x}|_p^p \in L_1$.

Proof. Begin with $\boldsymbol{x} \in L_p$. By the definition of the L_p norm

$$\lim_{\tau \to \infty} \int_0^\tau |x_i|^p dt < \infty \tag{A.2}$$

Now note the following axiom: $(|x_i| < \infty \quad \forall i \in \{1, 2, 3, \dots n\}) \iff (\sum_{i=1}^n |x_i| < \infty)$. This leads to

$$\lim_{\tau \to \infty} \int_0^\tau \sum_{i=1}^n \left[|x_i|^p\right] dt < \infty \tag{A.3}$$

*This appendix is reprinted with permission from "Adaptive Control for Non-Minimum Phase Systems Via Time Scale Separation" by Kameron Eves and John Valasek, 2023. American Control Conference, Copyright 2023 by American Automatic Control Council [96].

Raising to the power of $1 = p/p$

$$\lim_{\tau\to\infty}\int_0^\tau \left(\left(\sum_{i=1}^{n}\left[|x_i|^p\right]\right)^{1/p}\right)^p dt < \infty \tag{A.4}$$

By the definition of l_p norms

$$\lim_{\tau\to\infty}\int_0^\tau |\boldsymbol{x}|_p^p dt < \infty \tag{A.5}$$

Thus $|\boldsymbol{x}|_p^p \in L_1$. Each of these logical steps can be inverted. So, by working backward, it is also true that $|\boldsymbol{x}|_p^p \in L_1 \implies \boldsymbol{x} \in L_p$ □